

**STRUCTURAL STUDIES OF AURIVILLIUS PHASE
FERROELECTRICS AND RELATED MATERIALS**

Charles H. Hervoches

**A Thesis Submitted for the Degree of PhD
at the
University of St Andrews**



2002

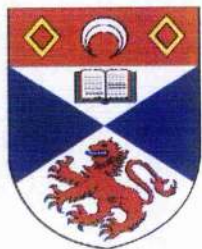
**Full metadata for this item is available in
St Andrews Research Repository
at:**

<http://research-repository.st-andrews.ac.uk/>

Please use this identifier to cite or link to this item:

<http://hdl.handle.net/10023/12926>

This item is protected by original copyright



Structural Studies of Aurivillius Phase Ferroelectrics and Related materials

A thesis submitted for the title of Ph.D. by

Charles H. Hervoches

In the Faculty of Science, Department of Chemistry,
University of St-Andrews, Scotland



December 2001

Supervisor: Dr P. Lightfoot

ProQuest Number: 10167034

All rights reserved

INFORMATION TO ALL USERS

The quality of this reproduction is dependent upon the quality of the copy submitted.

In the unlikely event that the author did not send a complete manuscript and there are missing pages, these will be noted. Also, if material had to be removed, a note will indicate the deletion.



ProQuest 10167034

Published by ProQuest LLC (2017). Copyright of the Dissertation is held by the Author.

All rights reserved.

This work is protected against unauthorized copying under Title 17, United States Code
Microform Edition © ProQuest LLC.

ProQuest LLC.
789 East Eisenhower Parkway
P.O. Box 1346
Ann Arbor, MI 48106 – 1346

Tu E 38

DECLARATION

I, Charles H. Hervoches, hereby certify that this thesis, which is approximately 30,000 words in length, has been written by me, that is the record of work carried out by me and that it has not been submitted in any previous application for a higher degree.

Date 13/12/01 Signature of Candidate

I was admitted as a research student in September 1998 and as a candidate for the degree of Doctor of Philosophy in September 1999, the higher study for which this is a record was carried out in the University of St. Andrews between 1998 and 2001.

Date 13/12/01 Signature of Candidate

I, hereby certify that the candidate has fulfilled the conditions of the Resolution and Regulations appropriate for the degree of Doctor of Philosophy in the University of St. Andrews and that the candidate is qualified to submit in application for that degree.

Date 13/12/01 Signature of Supervisor

In submitting this thesis to the University of St. Andrews, I understand that I am giving permission for it to be made available for use in accordance with the regulations of the University Library for the time being in force, subject to any copyright vested in the work not being affected thereby. I also understand that the title and abstract will be published, and that a copy of the work may be made and supplied by any *bona fide* library or research worker.

Date 13/12/01 Signature of Candidate

Acknowledgements

Thanks to the following people:

First of all, my supervisor, Phil Lightfoot, thanks for everything !

Also, all past and present members of the PL group: Dave Woodcock, Zoe Lethbridge, Chris Milne, Ardak Kusainova, and Alan Snedden for various help at one point or another.

David Flot, John Bradley and Angela Kruth for help with impedance measurements.

Humphrey Yiu and Sylvia Williamson for help with the DTA.

Ron Smith and Kevin Knight for help with the neutron experiments at ISIS.

EPSRC for funding.

Cheers !!!

ABSTRACT

The research carried out for this thesis has concentrated on Aurivillius bismuth oxide materials and the closely related Sillen and Bipox bismuth oxyhalides. X-ray and neutron powder diffraction techniques have been used to characterise precisely their structure and revealed several important features.

The unexpected presence of a double phase transition scheme has been discovered for the Aurivillius phases $\text{Sr}_{0.85}\text{Bi}_{2.1}\text{Ta}_2\text{O}_9$ and $\text{SrBi}_4\text{Ti}_4\text{O}_{15}$, both materials present the particularity of having an even number of perovskite layers n ($n = 2$ and $n = 4$ for $\text{Sr}_{0.85}\text{Bi}_{2.1}\text{Ta}_2\text{O}_9$ and $\text{SrBi}_4\text{Ti}_4\text{O}_{15}$ respectively).

The first transition from orthorhombic space group $A2_1am$ to $Amam$, occurs at T_c (375°C and 550°C for $\text{Sr}_{0.85}\text{Bi}_{2.1}\text{Ta}_2\text{O}_9$ and $\text{SrBi}_4\text{Ti}_4\text{O}_{15}$ respectively). The second transition from orthorhombic $Amam$ to tetragonal $I4/mmm$, occurs at higher temperature (550°C and 650°C for $\text{Sr}_{0.85}\text{Bi}_{2.1}\text{Ta}_2\text{O}_9$ and $\text{SrBi}_4\text{Ti}_4\text{O}_{15}$ respectively).

These phase transitions have been understood in terms of specific octahedral tilt and displacive modes.

In contrast, the $n = 2$ phase $\text{SrBi}_2\text{Nb}_2\text{O}_9$ and the $n = 3$ phase $\text{Bi}_4\text{Ti}_3\text{O}_{12}$ are shown to undergo a single-step transition from orthorhombic space group $A2_1am$ to tetragonal $I4/mmm$ at $T_c = 440^\circ\text{C}$ for $\text{SrBi}_2\text{Nb}_2\text{O}_9$, and from orthorhombic space group $B2cb$ to tetragonal $I4/mmm$ at $T_c = 675^\circ\text{C}$ for $\text{Bi}_4\text{Ti}_3\text{O}_{12}$.

The atomic disorder of the Bi and A cations in the fluorite and perovskite sites of the Aurivillius phases has been demonstrated and thoroughly studied for the solid solutions $\text{Bi}_{4-x}\text{Sr}_x\text{Ti}_{3-x}\text{Nb}_x\text{O}_{12}$ and $\text{Bi}_{4-x}\text{La}_x\text{Ti}_3\text{O}_{12}$, and "size-matching" between the fluorite and the perovskite site has been found to be the key to understanding this disorder phenomenon.

In the Sillen family, we extended the members of the $\text{Bi}_2\text{MO}_4\text{Cl}$ group, where $M =$ Lanthanide to the three following compounds: $\text{Bi}_2\text{ErO}_4\text{Cl}$, $\text{Bi}_2\text{YbO}_4\text{Cl}$, and

$\text{Bi}_2\text{LuO}_4\text{Cl}$. We have demonstrated that in the $\text{Bi}_2\text{MO}_4\text{Cl}$ group, the ionic radius of M must be greater than that of Sc^{3+} ($r(\text{Sc}^{3+}) = 0.87 \text{ \AA}$ for CN = 8).

Another new compound with a novel ordering scheme for this family has been studied, viz. $\text{Bi}_5\text{TeO}_{8.5}\text{I}_2$, crystallising in the orthorhombic space group Cmm2 . Te^{4+} is shown to adopt only one of the three available M sites, thus inducing a polar structure.

In the Bipox family, the crystal structures of two materials exhibiting ferroelectric properties, $\text{Bi}_4\text{NbO}_8\text{Cl}$ and $\text{Bi}_4\text{TaO}_8\text{Cl}$ have been determined to be orthorhombic, space group $\text{P2}_1\text{cn}$.

CONTENTS

CHAPTER 1 : INTRODUCTION.....	1
CHAPTER 2 : STRUCTURE OF THE SILLEN, AURIVILLIUS, AND BIPOX PHASES	3
2.1. SILLEN PHASES	3
2.2. AURIVILLIUS PHASES	5
2.3. BIPOX PHASES	8
REFERENCES:	9
CHAPTER 3 : PROPERTIES.....	10
3.1. FERROELECTRICITY	10
3.1.1. Dielectric materials	10
3.1.2. Ferroelectric materials	11
3.2. IONIC CONDUCTION	16
REFERENCES:	16
CHAPTER 4 : EXPERIMENTAL TECHNIQUES AND INSTRUMENTS.....	17
4.1 : X-RAY DIFFRACTION	17
4.1.1. Bragg's law.....	19
4.1.2. Diffraction theory	20
4.1.3. Temperature factor	21
4.2. INSTRUMENTS USED FOR X-RAY POWDER DIFFRACTION	22
4.2.1. STOE STADI/P powder diffractometer.....	22
4.2.2 High-resolution X-ray powder diffraction (Synchrotron) at CLRC Daresbury laboratory....	23
4.3. NEUTRON DIFFRACTION.....	25
4.4. ISIS-RAL.....	25
4.4.1. HRPD	27
4.4.2. POLARIS	28
4.5. CRYSTALLOGRAPHY/SYSTEMATIC ABSENCES	29
4.6. RIETVELD REFINEMENT	32
4.6.1. Theory.....	32
4.6.2. Constraints and damping.....	34
4.7. ALTERNATING CURRENT IMPEDANCE SPECTROSCOPY (A. C. IMPEDANCE).....	34
4.7.1. Theory.....	34
4.7.2. Experimental/Solartron for a.c. impedance measurements	37
4.8. DIFFERENTIAL THERMAL ANALYSIS (DTA).....	38
4.9. BOND VALENCE SUM ANALYSIS METHOD	38
4.10. SYNTHESIS OF THE SAMPLES.....	40
4.10.1. Preparation of Sillen phases.....	40
4.10.2. Preparation of Aurivillius phases.....	41
REFERENCES	42

CHAPTER 5 : AURIVILLIUS PHASES WITH AN EVEN NUMBER OF PEROVSKITE LAYERS.....43

INTRODUCTION.....	43
5.1. n=2 : Two perovskite layers.....	45
5.1.1. Variable temperature study of $Sr_{0.85}Bi_{2.1}Ta_2O_9$	48
5.1.2. Variable temperature study of $SrBi_2Nb_2O_9$	57
5.1.3. "solid solutions" $Bi_{2+2x/3}Sr_{1-x}Ta_2O_9$ and $Bi_2Sr_{1-x/2}Ta_{2-x}W_xO_9$	67
5.2. n=4 : Four perovskite layers: $SrBi_4Ti_4O_{15}$	69
5.2.1. Room temperature study.....	70
5.2.2. Variable temperature study.....	73
CONCLUSION.....	81
REFERENCES.....	81

CHAPTER 6 : AURIVILLIUS PHASES WITH AN ODD NUMBER OF PEROVSKITE LAYERS.....83

INTRODUCTION.....	83
6.1. Structure and phase transition in $Bi_4Ti_3O_{12}$	85
6.1.1. HRPD data.....	86
6.1.2. Polaris data.....	96
6.1.3. a.c. Impedance spectroscopy measurements.....	104
6.2. Solid solution $Bi_{4-x}Sr_xTi_{3-x}Nb_xO_{12}$	105
6.2.1. X-ray results of $Bi_{4-x}Sr_xTi_{3-x}Nb_xO_{12}$	106
6.2.2. Neutron results of $Bi_{1.8}Sr_{2.2}Ti_{0.8}Nb_{2.2}O_{12}$	114
6.3. Solid solution $Bi_{4-x}La_xTi_3O_{12}$ (x = 1 and 2).....	120
6.4. $Bi_2Ca_2TiNb_2O_{12}$	125
6.5. $Bi_2Ln_2Ti_3O_{12}$ (Ln = Eu, Nd).....	126
CONCLUSION.....	128
REFERENCES.....	128

CHAPTER 7 : SILLEN AND BIPOX PHASES.....130

7.1. SILLEN PHASES.....	130
7.1.1. Bi_2MO_4Cl (M = Er, Yb, Lu).....	130
7.1.2. $Bi_5TeO_{8.5}I_2$	137
7.2. Bipox phases: Bi_4MO_8Cl (M = Ta, Nb).....	140
CONCLUSION.....	148
REFERENCES:.....	148

CONCLUSION.....149

APPENDICES.....151

Appendix A: Final atomic coordinates for $SrBi_2Nb_2O_9$ at several temperatures (Polaris data).....	152
Appendix B: Final atomic coordinates for $SrBi_4Ti_4O_{15}$ at several temperatures (HRPD data).....	160
Appendix C.1: Final atomic coordinates for $Bi_4Ti_3O_{12}$ at several temperatures (Polaris data).....	169
Appendix C.2: Selected bondlengths and angles for $Bi_4Ti_3O_{12}$ (Polaris data).....	181
Appendix D: Final atomic coordinates for the solid solution $Bi_{4-x}Sr_xTi_{3-x}Nb_xO_{12}$ at room temperature (data obtained on the Stoe diffractometer).....	185
Appendix E: Neutron scattering lengths.....	194

Chapter 1 : INTRODUCTION

The aim of this project was to develop new bismuth oxide materials of potential use as ferroelectric materials or ionic conductors and to study the crystallographic structure of these new phases and its relation to their physical properties.

Applications envisaged for new ferroelectric materials are, for example, capacitors (which are the main commercial application of ferroelectrics), information storage devices (FERAMs) and high permittivity microwave resonators.

Ferroelectric random access memories (FERAMs) are a new emerging class of non-volatile memories. Because of their low-voltage/low-power operation, their fast write speed, and their excellent write endurance, they are becoming very attractive competitors for standard EEPROM (Electrically Erasable Programmable Read Only Memory). They are now entering embedded-memory markets e.g. for smartcards, but have the scaling potential to compete even with DRAM (Dynamic Random Access Memories) for stand-alone high-density non-volatile memories.

For new ionic conductors, the possible applications include solid oxide fuel cells and oxygen sensors.

The materials in which we are interested belong to the Sillen and Aurivillius families. These materials have a highly flexible chemical composition that affects the details of their crystal structure, which in turn is believed to play a critical role in their important electrical properties.

Our objective was systematically to explore the effects of chemical modification on crystal structure and physical properties and to understand the relationship of composition, structure and properties, in order to design improved materials.

The archetypal structure of these two families of products is described in the next chapter.

The aims of this work were therefore:

- To synthesise selected novel members of the Sillen and Aurivillius series.
- To characterise the structure as a function of composition by X-ray and neutron powder diffraction methods.
- To characterise the electrical properties of the materials.
- To rationalise the dependence of electrical properties on composition and structure and hence extrapolate to the design and synthesis of new improved analogues.

The work done can be broken down into two main parts:

- New variants of the Aurivillius family of layered bismuth oxides as potential ferroelectric materials.
- New variants of the Sillen family of layered oxyhalides and related materials as potential ferroelectric materials and oxide-ion conductors.

During this project, X-ray and neutron powder diffraction have been used to solve the crystal structure of both new and previously known materials.

The presentation of the results of our studies is divided into three chapters.

Chapter 5 presents our work on Aurivillius phases with an even number of perovskite layers, and particularly emphasis is given to the study of the phases transitions observed at different temperatures.

The results concerning Aurivillius phases with an odd number of perovskite layers are in Chapter 6. That chapter deals mostly with cations-ordering questions, and also with the phase transition behaviour, which contrasts with that of the “even-layer” materials.

Chapter 7 concerns the Sillen and Bipox families, oxyhalide materials that are both related to the Aurivillius phases.

Chapter 2 : Structure of the Sillen, Aurivillius, and Bipox phases

2.1. SILLEN PHASES	3
2.2. AURIVILLIUS PHASES	5
2.3. BIPOX PHASES	8
REFERENCES:	9

The Sillen and Aurivillius structure types are both constructed by the alternation of planar metal-oxygen (cationic) layers and anionic layers consisting of:

- Planar monoatomic layers in the Sillen phases
- Perovskite-like octahedral layers in the Aurivillius phases

A more precise description of both families follows, as well as the Bipox family, the structure of which is derived from the two others.

2.1. Sillen phases

The first members of this family were described in 1939 by L. Sillen¹.

The number of members of this family has since been greatly extended.

The structure of these phases can be described as intergrowths of double $[M_2O_2]$ or triple $[M_3O_{4+n}]$ planar fluorite-like metal-oxygen layers (examples of M in the literature include Bi^{3+} , Pb^{2+} , Ln^{3+} (lanthanides), Ca^{2+} , Sr^{2+} , Sb^{3+} , Li^+ , Na^+ , Cd^{2+} , but more classically Bi^{3+} or Pb^{2+})¹ separated by one or more planar monoatomic layer(s) X. Examples of X in the literature include halogen, chalcogen, or alkali-halogen planar layer(s) of formula $[X]$ and $[AX]_2$ ($X=Cl, Br, I, F, Se, Te$; $A=Na, K, Rb$)².

In this family, one structure differs from another in the number of the X layers. They are denoted by the symbols X_1, X_2, X_3 where the subscript indicates the number of X

layers, e.g. BaBiO_2Cl (X_1), BiOCl (X_2), $\text{Ca}_{1.25}\text{Bi}_{0.5}\text{O}_2\text{Cl}_3$ (X_3). It is also possible to have different combinations of these arrangements (X_1X_2 , X_2X_3 , $X_1X_1X_2, \dots$) within the same structure (e.g. $\text{SrBi}_3\text{O}_4\text{Cl}_3 - X_1X_2-$)².

A superscript notation n is also added to indicate the “thickness” of the fluorite layer (i.e. double $[\text{M}_2\text{O}_2]$ or triple $[\text{M}_3\text{O}_{4+n}]$).

Therefore the complete symbol to describe Sillen materials is : X_m^n ($m = X$ layer, $n =$ fluorite layer “thickness”).

Two simple examples belonging to this family are presented in Figure 2.1.

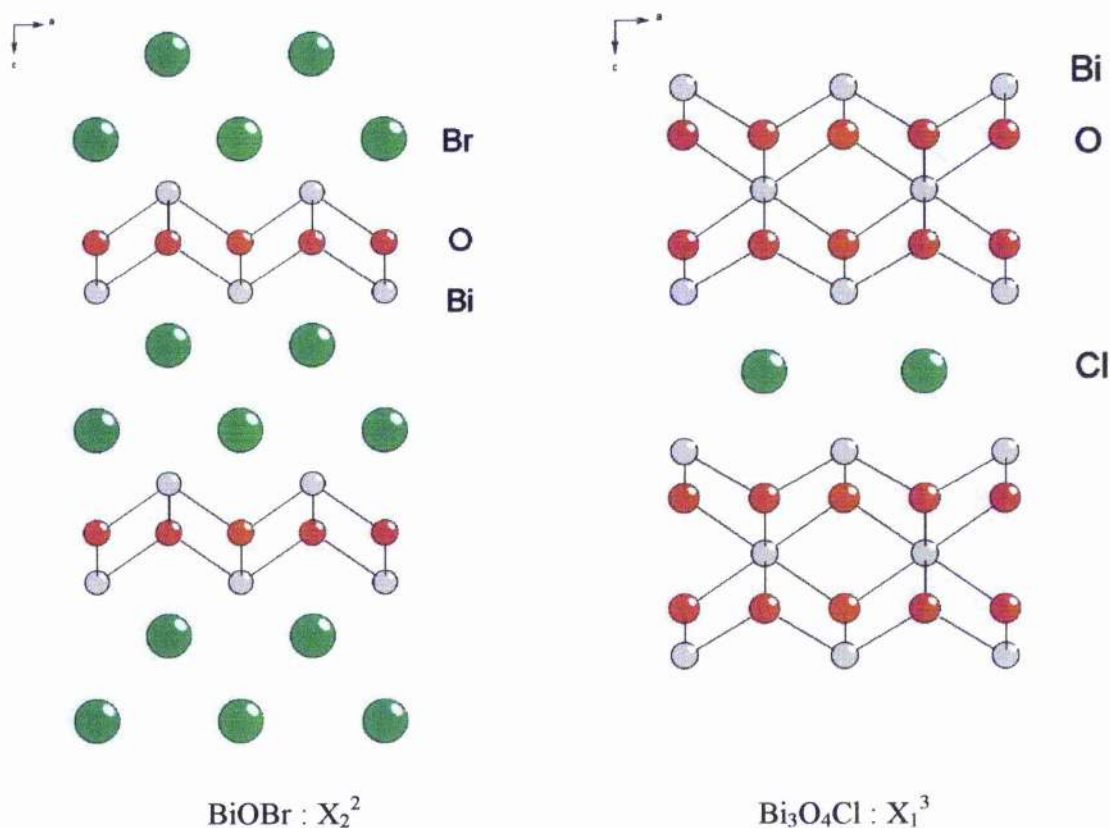


Figure 2.1 : Representation of the structure of two compounds belonging to the Sillen family

The unit cells of the “ideal” structures of these phases are approximately tetragonal with $a \approx 3.85 \text{ \AA}$ and c variable depending on the number of fluorite and X layers².

2.2. Aurivillius phases

Discovered in 1949 by B. Aurivillius when studying the $\text{Bi}_2\text{O}_3 - \text{TiO}_2$ system³, this family of layered bismuth oxides is generally formulated as $\text{M}_2\text{A}_{n-1}\text{B}_n\text{O}_{3n+3}$ or more conveniently $(\text{M}_2\text{O}_2)(\text{A}_{n-1}\text{B}_n\text{O}_{3n+1})^4$.

The possibility of ferroelectric behaviour for many of these materials has been known for about forty years since the work of Smolenskii⁵ and Subbarao⁶.

They can be described as $[\text{M}_2\text{O}_2]^{2+}$ layers interleaved by perovskite-like layers $[\text{A}_{n-1}\text{B}_n\text{O}_{3n+1}]^{2-}$, where :

- n is an integer,
- M and A are mono-, di- or trivalent ions or a mixture of each (literature examples of A include Bi, Ba, Sr, K, Ca, Na, Pb),
- B is a tri-, tetra-, penta- or hexavalent cation (e.g. B = Ti, Nb, Ta, Fe, W, Mo, Ga, Cr, etc...) singly or in combination.^{6,7}

Note: The substitution of O^{2-} by another anion has only been studied for the one-perovskite layer $\text{Bi}_2\text{NbO}_5\text{F}$ in 1952 by Aurivillius.⁸

Two possible representations of the perovskite structure of general formula ABX_3 are presented in Figure 2.2 (A = large cation, B = small cation, X = oxide or halide).

Its structure is based on a close packed array of oxide (or halide) ions with a cation (A) of similar size. The smaller cation (B) is located in the octahedral site formed by the oxide ions.

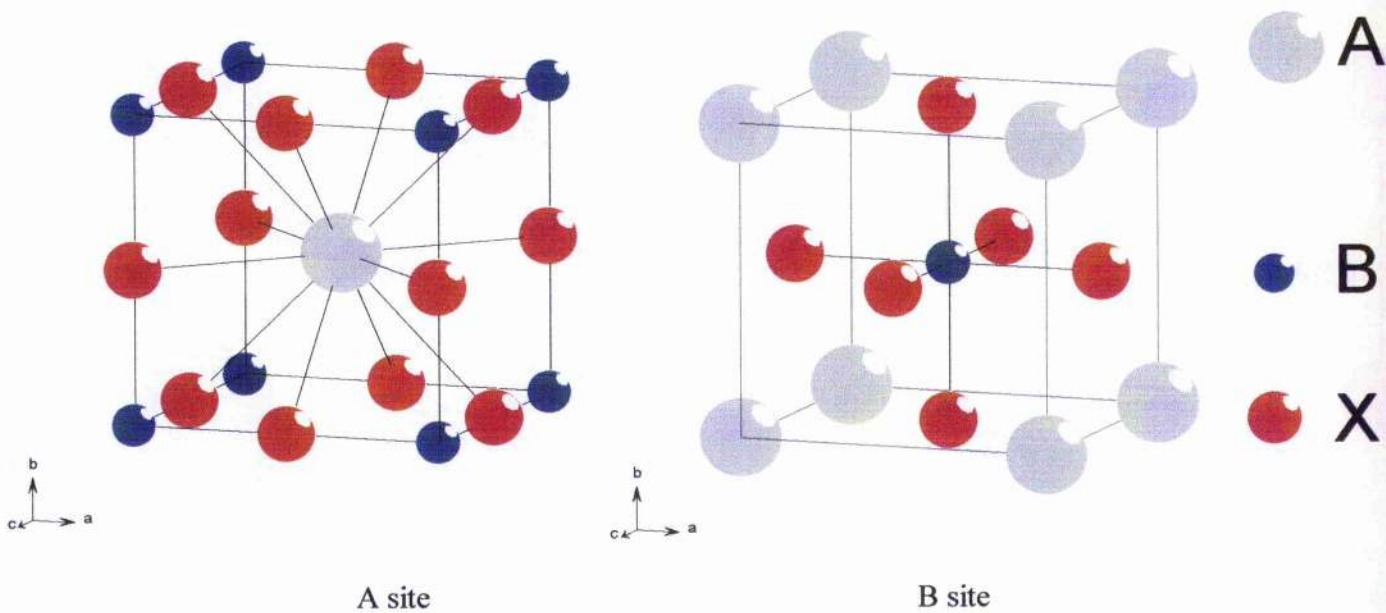


Figure 2.2: Two possible representations of the Perovskite structure

Until 1993 only structures with $[\text{Bi}_2\text{O}_2]^{2+}$ layers as $[\text{M}_2\text{O}_2]^{2+}$ had been synthesised. Later the possibility of replacing Bi^{3+} in these layers by Pb^{2+} , Sb^{3+} and Te^{4+} was demonstrated⁹ and the effects on the ferroelectric properties discussed¹⁰.

It has also been claimed that La could replace Bi in these layers¹¹.

It seems possible that thermal treatment could have an effect on the disorder between Bi^{3+} and other cations in the $[\text{Bi}_2\text{O}_2]^{2+}$ layers¹².

These ferroelectric Aurivillius phases have room-temperature structures which can be described in terms of small displacive perturbations away from a tetragonal $I4/mmm$ parent structure with the lattice parameters $a = b = 3.85 \text{ \AA}$ (Cf. Figure 2.3.)¹³.

The main cause of ferroelectricity is the structural distortion from this parent structure. It has been shown that the ferroelectricity in $\text{Bi}_4\text{Ti}_3\text{O}_{12}$ is due to the relative displacement of Bi atoms in the perovskite A site with respect to the chains of the corner shared TiO_6 octahedra¹⁴.

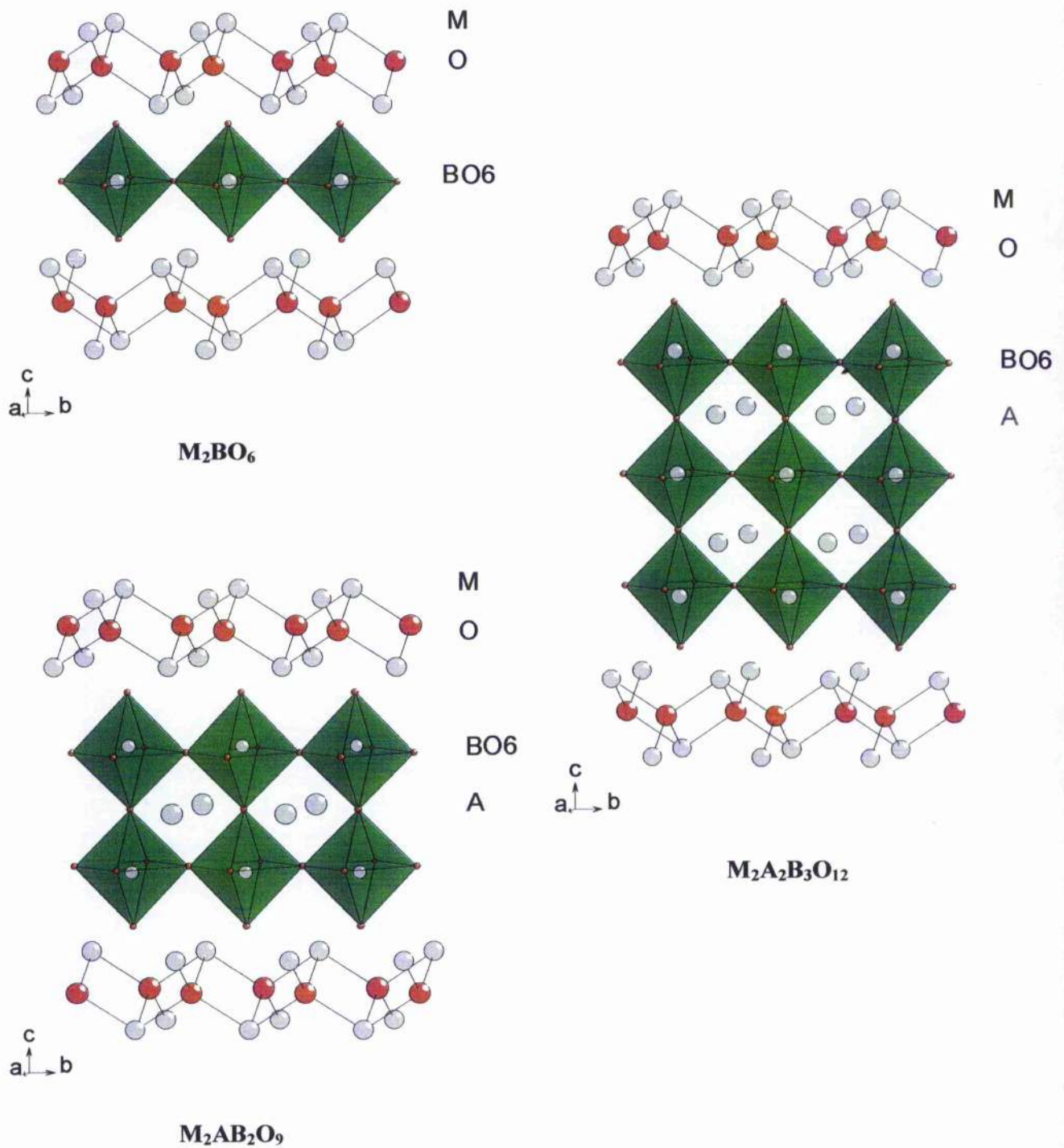


Figure 2.3: A perspective drawing of the undistorted $I4/mmm$ parent structures of three Aurivillius compounds. Only atoms between $1/4c$ and $3/4c$ are shown.

2.3. Bipox phases

This family of layered bismuth oxyhalides was first reported in the 1980's by J. F. Ackerman¹⁵ and B. Aurivillius¹⁶, and called "Bipox" for Bismuth-Perovskite-Oxyhalide.

It consists of a regular intergrowth of the Aurivillius and Sillen phases, i.e. $[\text{Bi}_2\text{O}_2]$ layers separated alternately by layers of type X (as in the Sillen phases) and perovskite-like layers (as in the Aurivillius phases) designated by the letter A.

This Bipox family includes compounds of different combinations: A_1X_1 , A_2X_1 , $A_1A_1X_1$, etc... synthesised and studied by Aurivillius and Ackerman.

A picture of one of the simplest member of this family ($\text{Bi}_4\text{NbO}_8\text{Cl}$) is shown in Figure 2.4. It can be described by the symbolism A_1X_1 , where "X₁" indicates that there is one X-layer (i.e. Cl here) and "A₁" indicates that there is one "Aurivillius-type" layer (i.e. NbO_4 in this case).

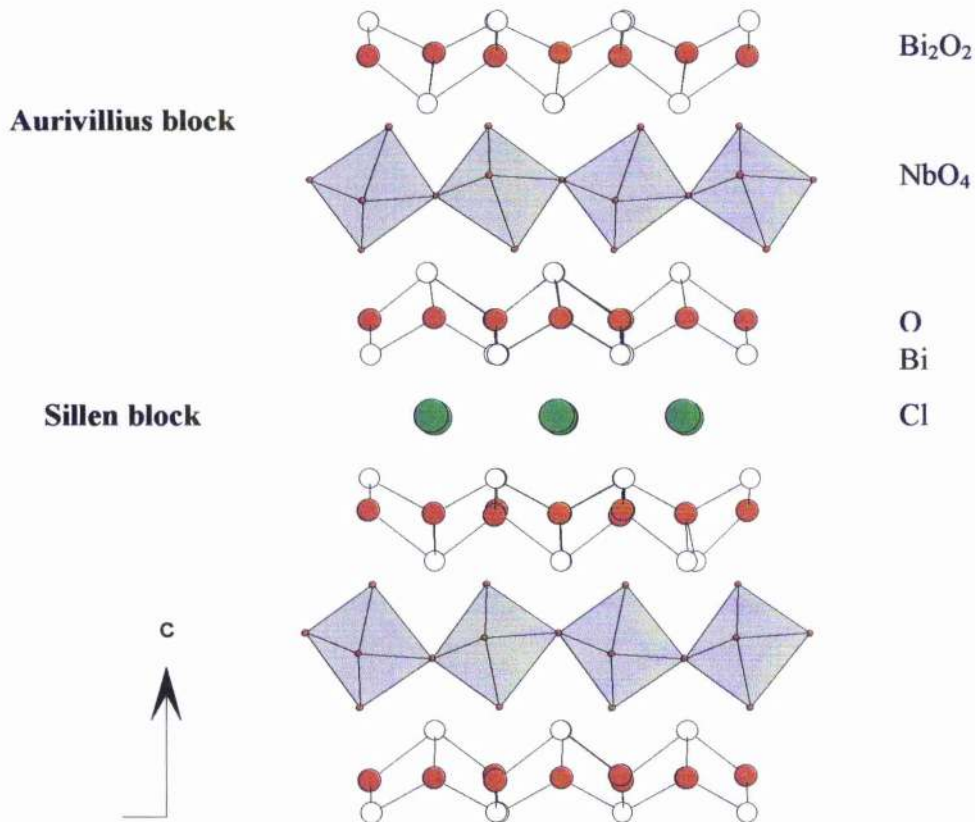


Figure 2.4: Schematic structure of the Bipox phase $\text{Bi}_4\text{NbO}_8\text{Cl}$

References:

- ¹ L. Sillen, *Z. Anorg. Allgem. Chem.*, 1939, **242**, 41
- ² V.A. Dolgikh and L.N. Kholodkovskaya, *Russ. J. Inorg. Chem.*, 1992, **37**, 488
- ³ B. Aurivillius, *Ark. Kemi*, 1949, **1**, 463
- ⁴ B. Frit, J.P. Mercurio, *J. Alloys and compounds*, 1992, **27**, 188
- ⁵ G. A. Smolenskii, V. A. Isupov and A. I. Agranovskaya, *Sov. Phys. Solid State (Engl. Transl.)*, 1959, **3**, 651
- ⁶ E.C. Subbarao, *J. Phys. Chem. Solids*, 1962, **23**, 665
- ⁷ R. E. Newnham, R. W. Wolfe and J. F. Dorrian, *Mat. Res. Bull.*, 1971, **6**, 1029
- ⁸ B. Aurivillius, *Ark. Kemi*, 1952, **5**, 39
- ⁹ A. Castro, P. Millan and M.J. Martinez-Lope, *Solid State Ionics*, 1993, **365**, 897
- ¹⁰ P. Duran-Martin, A. Castro, P. Millan and B. Jimenez, *J. Mater. Res.*, 1998, **13**, 2565
- ¹¹ T. Rentschler, *Mat. Res. Bull.*, 1997, **32**, 351
- ¹² Ismunandar, B.A. Hunter and B.J. Kennedy, *Solid State Ionics*, 1998, **112**, 281
- ¹³ A.D. Rae, J.G. Thompson, R.L. Withers and A.C. Willis, *Acta Cryst.*, 1990, **B 46**, 474
- ¹⁴ R.L. Withers, J.G. Thompson and A.D. Rae, *J. Solid State Chem.*, 1991, **94**, 404
- ¹⁵ J. F. Ackerman, *J. Solid State Chem.*, 1986, **62**, 92
- ¹⁶ B. Aurivillius, *Chem. Scr.*, 1984, **23**, 143

Chapter 3 : Properties

3.1. FERROELECTRICITY	10
3.1.1. Dielectric materials	10
3.1.2. Ferroelectric materials	11
REFERENCES:	16

3.1. Ferroelectricity

Before discussing ferroelectricity itself, it is necessary to introduce the notion of dielectric materials.

3.1.1. Dielectric materials

Dielectrics are a class of materials that, when submitted to an electric field, exhibit a polarisation of charge (P) that disappears when the voltage is switched off.

Application of a potential difference across a dielectric creates a dipole moment (μ), i.e. the centres of positive and negative charges are displaced from their equilibrium position.

$$\mu = \alpha E$$

where α is the polarizability of the dielectric and E is the local electric field.

The dipole moment per unit volume is called the polarisation (P).

$$P = \epsilon_0 \chi_e E$$

where ϵ_0 is the permittivity of free space ($\epsilon_0 = 8.854 \times 10^{-12} \text{ F}\cdot\text{m}^{-1}$), χ_e is the electric susceptibility and E is the applied electric field.

The polarizability α contains four different components that are described below.

$$\alpha = \alpha_e + \alpha_i + \alpha_d + \alpha_s$$

where :

- α_e is the electronic polarizability. It is present in all solids and is caused by a slight displacement of the electron cloud relatively to the nucleus of an atom.
- α_i is the ionic polarizability. It is the principal source of polarisation in ionic crystals and is caused by a slight relative displacement of anions and cations in the solid.
- α_d is the dipolar polarizability. It occurs in materials presenting permanent electric dipoles (such as ferroelectrics, or more generally polar materials).
- α_s is the space charge polarizability. It is present in materials that are not perfect ferroelectrics but in which some long range charge migration can nevertheless appear.

3.1.2. Ferroelectric materials

The differences between ferroelectric materials and ordinary dielectrics are :

- Their extremely large permittivities
- The possibility of retaining some residual electrical polarisation after an applied voltage has been switched off¹.
- The polarisation can be reversed by an applied electric field

They are characterised by the presence of spontaneous polarisation; i.e. they exhibit a polarisation in the absence of any applied field.

Submitted to external stimuli such as applied field, this spontaneous polarisation changes. Ferroelectrics also change their polarisation state when subjected to

temperature changes (this is the pyroelectric effect) or to pressure changes (this is the piezoelectric effect). These properties are of interest in engineering applications such as capacitors, information storage devices (FERAMs), high permittivity microwave resonators, personal sensors, sonar and ultrasonic medical imaging².

A hysteresis loop characteristic of these materials is observed instead of the simple linear relationship between P and V for ordinary dielectrics as shown in Figure 3.1.

For ferroelectrics with a perovskite-type structure, either cubic or distorted, the ferroelectricity is caused by the displacement of one type of cation relative to its anionic neighbours. This displacement gives rise to electric dipoles and the high dielectric constants characteristic of ferroelectric materials.

In ferroelectrics such as for example BaTiO₃, presenting a simple perovskite structure, domain structures forms because adjacent TiO₆ dipoles tend to align themselves parallel to each other.

The effect of applying an electric field is to persuade the individual dipoles to align themselves parallel to each other.

Ferroelectricity does not only occur in materials presenting a perovskite structure, it can also occur in oxides containing cations that are asymmetrically bonded because of the presence of a lone pair of electrons in their outer valence shell (e.g. Sn²⁺, Pb²⁺, Bi³⁺, etc...). Also, not all materials presenting a perovskite structure are ferroelectrics, e.g. BaTiO₃ and PbTiO₃ are whereas CaTiO₃ is not, which is probably related to the ionic radii of the cations involved (ionic radii : Ba²⁺ = 1.42 Å, Pb²⁺ = 1.29 Å, Ca²⁺ = 1.12 Å for a coordination number = 8).³

The ferroelectric state is usually a low temperature condition, as the increase of thermal movements gives enough energy to destroy the cooperative displacement in adjacent octahedra and therefore destroys the domain structure. Above the so-called Curie temperature T_c, the material is paraelectric (i.e. non-ferroelectric). The dielectric constant is still high but the polarisation is lost as soon as the field is removed (cf. Figure 3.2.).

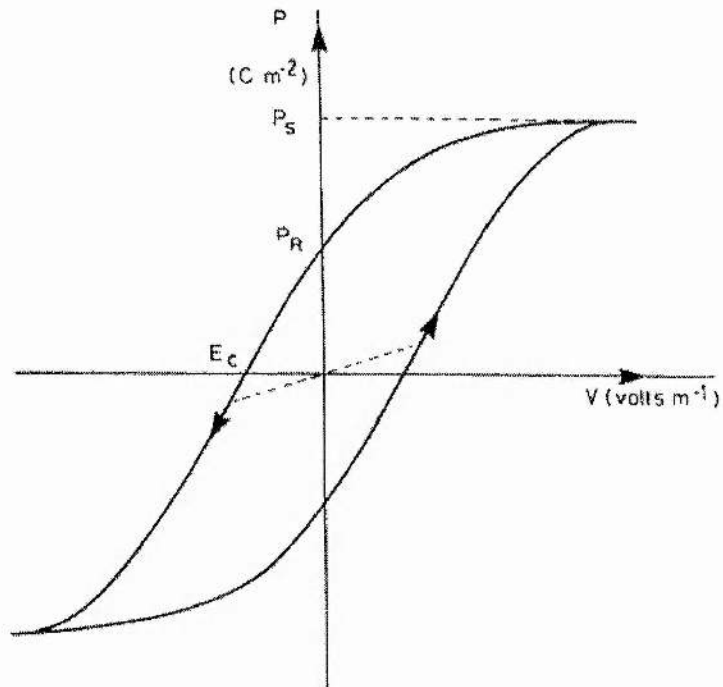


Figure 3.1: Hysteresis loop of a ferroelectric¹. The dashed line passing through the origin represents the behaviour of normal dielectric materials.

P_S is the saturation polarisation, P_R is the remanent polarisation when the electric field has been switched off after saturation, and E_C the coercive field, i.e. the reverse electric field needed to reduce P to zero.

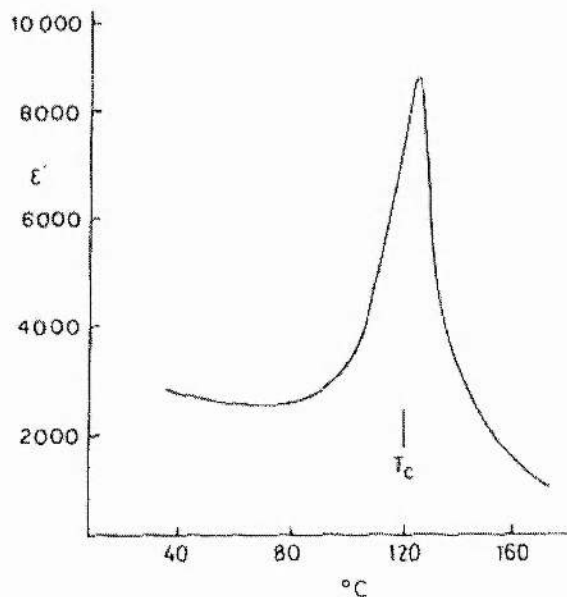


Figure 3.2: Temperature-dependence of dielectric constant of $BaTiO_3$ ceramic¹

Ferroelectricity is also related to the crystallographic point groups and space groups, as the fact that they present a spontaneous polarisation reduces the number of space groups they can belong to, i.e. the space group cannot present a centre of symmetry. Of the 32 point groups, 21 are non-centrosymmetric, 20 of them are piezoelectric. Amongst these 20 piezoelectric point groups, ten possess a unique polar axis (i.e. they are spontaneously polarised), they are the pyroelectrics. Only this latter class has the possibility to be ferroelectric.

This relationship between crystal classes and physical properties can be visualised in Figure 3.3.

Non-Centrosymmetric Crystal Classes

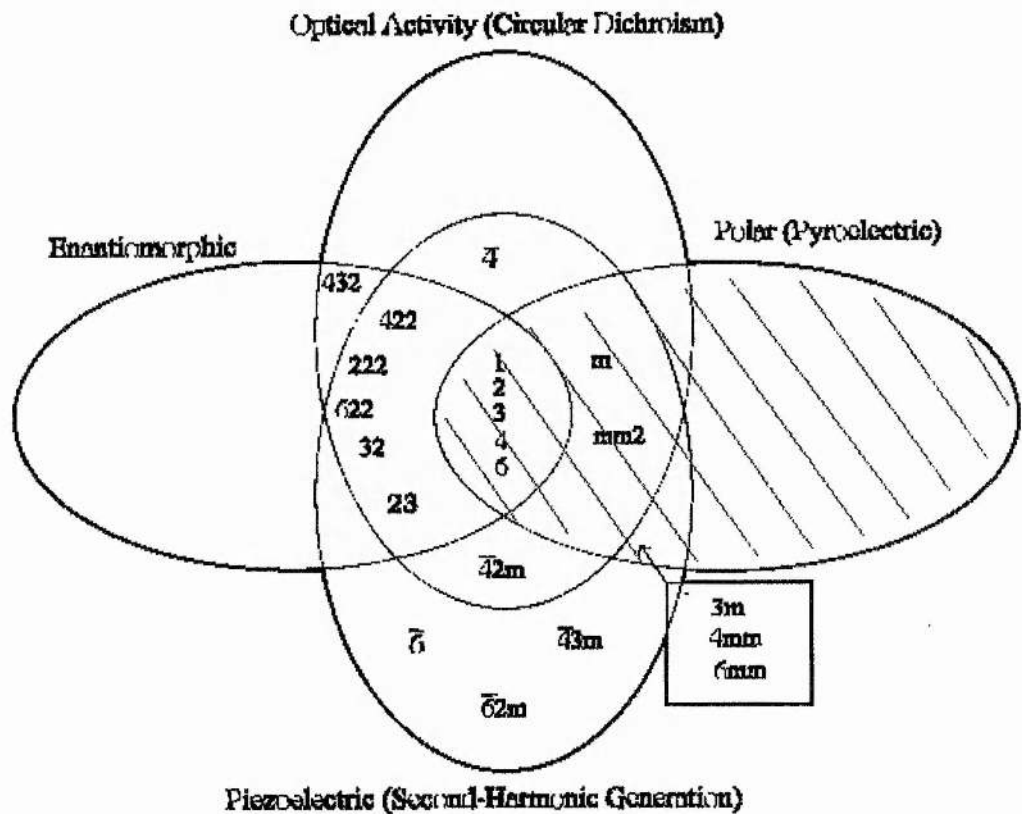


Fig. 3.3: Interrelationships of noncentrosymmetric crystal classes.⁴

The dashed area represents the potential ferroelectrics (i.e. the pyroelectrics)

Piezoelectric materials develop an electric charge when mechanically stressed (and inversely develop mechanical stress when submitted to an applied electric field).

$$P = d \sigma$$

Where P is the polarisation, σ the stress and d the piezoelectric coefficient.

Pyroelectric materials are piezoelectrics that exhibit a net spontaneous polarisation P_s that is temperature dependant.

$$\Delta P_s = \pi \Delta T$$

Where π is the pyroelectric coefficient and ΔT the difference in temperature.

The main use of pyroelectrics is in infrared radiation detectors.

Ferroelectrics are a sub-group of pyroelectrics, with the additional requirement that the polarisation is reversible in an electric field.

The knowledge of the crystal class is sufficient to establish the piezoelectric or pyroelectric properties of a solid, but ferroelectricity cannot be established only on a crystallographic basis, some kind of physical experiment is needed to establish this property.

References:

-
- ¹ A. R. West, "*Solid State Chemistry and its Applications*", John Wiley & Sons, Chichester, 1990
 - ² A. J. Bell and I.M. Reaney, *Electronic Materials*, 1994, **1**, 125
 - ³ R. D. Shannon, *Acta Cryst.*, 1976, **A32**, 751
 - ⁴ P. S. Halasyamani and K. R. Poeppelmeier, *Chem. Mater.*, 1998, **10**, 2753

Chapter 4 : Experimental techniques and instruments

4.1 : X-ray diffraction.....	17
4.1.1. Bragg's law.....	19
4.1.2. Diffraction theory.....	20
4.1.3. Temperature factor.....	21
4.2. Instruments used for X-ray powder diffraction.....	22
4.2.1. STOE STADI/P powder diffractometer.....	22
4.2.2 High-resolution X-ray powder diffraction (Synchrotron) at CLRC Daresbury laboratory.....	23
4.3. Neutron diffraction.....	25
4.4. ISIS-RAL.....	25
4.4.1. HRPD.....	27
4.4.2. POLARIS.....	28
4.5. Crystallography/Systematic absences.....	29
4.6. Rietveld refinement.....	32
4.6.1. Theory.....	32
4.6.2. Constraints and damping.....	34
4.7. Alternating current impedance spectroscopy (a. c. impedance).....	34
4.7.1. Theory.....	34
4.7.2. Experimental/Solartron for a.c. impedance measurements.....	37
4.8. Differential Thermal Analysis (DTA).....	38
4.9. Bond Valence Sum analysis method.....	38
4.10. Synthesis of the samples.....	40
4.10.1. Preparation of Sillen phases.....	40
4.10.2. Preparation of Aurivillius phases.....	41
References.....	42

4.1 : X-ray diffraction

For this work, X-ray powder diffraction is used as the main technique to determine phase purity as well as preliminary characterisation of the materials produced. Detailed crystallographic characterisation is carried out by a combination of X-ray and neutron powder diffraction as, for some reasons explained later, they are both essential for studying precisely these systems. Neutron powder diffraction is essential in particular to provide information on oxygen atom positions, which cannot be precisely determined from X-ray data in the presence of heavy atoms.

X-rays, like other forms of electromagnetic radiation, can undergo diffraction. The principle is that crystals, with their regularly repeating structures, are capable of diffracting radiation that has a wavelength similar to the interatomic separation, $\sim 1\text{\AA}$. The diffractogram produced is a characteristic pattern of the crystal structure.

X-rays for diffraction are normally produced by bombarding a metal target, often Cu or Mo, with a beam of electrons emitted from a heated filament of tungsten. The incident electron beam will ionise electrons from the K-shell (1 s) of the target atoms, and X-rays are emitted as the resultant vacancies are filled by electrons from the L (2 p) or M (3 p) levels. This gives rise to the intense $K\alpha$ and $K\beta$ lines:

- $L \rightarrow K : K\alpha_1, K\alpha_2$
- $M \rightarrow K : K\beta_1, K\beta_2$

A filter of elements (Z-1) or (Z-2) will normally absorb the $K\beta$ emission for an element of atomic number Z; a Ni filter is used for Cu radiation and a Zr filter for Mo radiation.

An alternative method, which produces $K\alpha_1$ only, is to use a monochromator. This method is used by the Stoe powder diffractometer (Cf § 4.2.1.)

During the powder diffraction process, an X-ray beam of fixed wavelength is fired through the sample powder. The beam is scattered through various angles. A detector moves around the sample and records the intensities of the scattered X-rays and gives a diffraction pattern, which can be used in identification of the structure.

X-rays are scattered by their interactions with atomic electrons and interference take place between X-rays scattered from different parts of the atom. As more interference occur at higher 2θ angles, scattering power or scattering factor f_x decreases with increasing scattering angle 2θ .

f_x is proportional to atomic number (at $(\sin \theta)/\lambda = 0$, $f_x = Z$) and is therefore very small for light atoms such as hydrogen or lithium. The diffraction pattern will tend to be dominated by heavy atoms, which are more powerful scatterers.

This makes it difficult to make precise interpretation of the positions of lighter atoms such as oxygen in the presence of heavy atoms in the structure such as bismuth.

4.1.1. Bragg's law

The Bragg approach to diffraction is to regard crystals as built up in layers or planes that each acts as a semi-transparent mirror. Some of the X-rays (or neutrons), are reflected off a plane with the angle of reflection equal to the angle of incidence, but the rest are transmitted to be subsequently reflected by succeeding planes.

Bragg's law can be written as follows:

$$2d \sin \theta = n\lambda$$

where:

- d is the d-spacing i.e. the perpendicular distance between pairs of adjacent planes.
- θ is the Bragg angle i.e. the angle of incidence of the X-ray (or neutron) beam.
- λ is the wavelength of the X-ray (or neutron) beam.

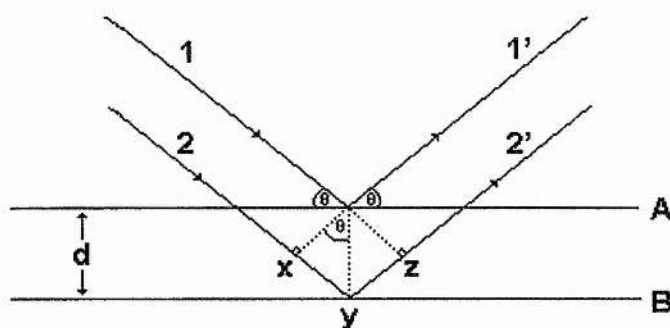


Figure 4.1: Derivation of Bragg's Law

When Bragg's law is satisfied, the reflected beams are in phase and interfere constructively. At angles of incidence other than the Bragg angle, reflected beams are out of phase and destructive interference or cancellation occurs.

In crystals, which contains thousands of planes, Bragg's law imposes a stringent condition on the angles at which reflection may occur. Away from these angles, cancellation of the reflected beams is usually complete.

It is these observations which can be used in the analysis of crystals which have regular packing and long range order.

4.1.2. Diffraction theory

For the determination of an unknown structure, it is important to understand the relationship between the atomic arrangement and the intensity I_{hkl} of an X-ray reflection from the planes hkl

For an arrangement of several atoms, we have to consider interference between waves scattered by different atoms. For example, the scattering by a unit cell for a reflection hkl :

$$\text{scattering amplitude} = \sum (f_n \times \text{phase factor})$$

for n atoms in the unit cell. This is the structure factor F_{hkl} and takes the form:

$$F_{hkl} = \sum f_n \exp[2\pi i(hx_n + ky_n + lz_n)]$$

where x_n, y_n, z_n are the fractional coordinates of the n^{th} atom.

The intensity of a reflection is something that can be measured, and it is related to the structure factor according to:

$$I_{hkl} = sLpF_{hkl}^2$$

where s is a scale factor, L is the Lorentz (geometrical) correction and p is a polarisation correction. Essentially:

$$I_{hkl} \propto F_{hkl}^2$$

Once the structure factor F_{hkl} is known for a complete set of X-ray reflections, it is possible to calculate the electron density ρ at any position xyz in the unit cell and, therefore, the atomic positions:

$$\rho(xyz) = 1/V \times \sum_h \sum_k \sum_l F_{hkl} \exp [2\pi i(hx + ky + lz)]$$

This is a Fourier summation; the electron density is the Fourier transform of the X-ray diffraction pattern.

4.1.3. Temperature factor

In a crystal structure, the arrangements of the atoms correspond to an energy minimum. When disturbed, they will oscillate as they tend to return to the position of minimal energy. These oscillations modify the electron density function of each atom and hence their scattering capacity.

The atomic temperature factor B permits to correct the measured scattering for these oscillations; it is dependent on the temperature and is defined as follows:

$$B = 8\pi^2U$$

Where U is the mean square shift of the atom from the position of equilibrium.

Generally, the order of value of \sqrt{U} is in many inorganic crystals between 0.05 and 0.20 Å (B lying between 0.20 and 3.16 Å²).¹

If we consider that the atom vibrates equally in all directions then only one parameter is needed to characterise the thermal motion: U_{iso} (iso stands for isotropic).

But generally, this is not the case. The movement of an atom in the three dimensions of space is anisotropic and can be described by vibrational or thermal ellipsoids. Six parameters are then needed: U^*_{11} , U^*_{22} , U^*_{33} , U^*_{12} , U^*_{13} and U^*_{23} , that define the orientation of the ellipsoid according to the crystallographic axes and the lengths of the three ellipsoid axes.

4.2. Instruments used for X-ray powder diffraction

All products were analysed on a Philips X-Ray powder diffractometer using Cu $K\alpha_1$ and $K\alpha_2$ radiation of wavelength respectively 1.54056 Å and 1.54439 Å. Intensity readings were taken every $2\theta = 0.02^\circ$ and recorded for 0.5 seconds at each point between 5° and 70° .

For more precise data, overnights runs were recorded on a Stoe X-Ray powder diffractometer described in the next paragraph.

4.2.1. STOE STADI/P powder diffractometer

The STOE STADI/P is the in-house powder diffractometer used for crystallographic characterisations. It uses Cu $K\alpha_1$ radiation of wavelength 1.54056 Å in transmission mode with a moving detector, covering about 6° in 2θ .

The powder sample is placed in a "sandwich" between two thin films of Mylar. Vaseline is used to fix the sample between these films. The sample is then placed in the transmission sample holder.

For data collection, intensity readings were taken between 2θ values of 4° and 120° with each recording lasting 145 seconds at each point. The diffraction patterns obtained were then used in the Rietveld refinement program GSAS³.

4.2.2 High-resolution X-ray powder diffraction (Synchrotron) at CLRC Daresbury laboratory

A synchrotron accelerates charged particles, such as electrons, to speeds close to that of light. A series of magnets is used to bend the path of the electrons into a circular shape. As they pass these "bending" magnets, the path of the electrons is deflected and they emit intense beams of light, known as synchrotron radiation. The beam is in the form of a cone in front of the electron, rather like a searchlight. The spectrum of synchrotron radiation covers part of the electromagnetic spectrum, from infra-red through to gamma-rays. It is used to investigate the structure and properties of all forms of matter.

Synchrotron X-rays are much more intense than those from a conventional laboratory source.

For data collection, the sample is enclosed in a thin walled glass capillary of 0.5mm diameter, and data collected on the beamline 9.1 over the range $3^\circ < 2\theta < 70^\circ$ at a wavelength of 1.00 Å.

4.2.2.1. Station 9.1

Station 9.1 is a high energy, monochromatic, diffraction station for structure solution, time resolved, and high pressure studies using a conventional two-circle diffractometer or image-plates for crystalline, amorphous and liquid materials. For our purpose, we used the two-circle diffractometer.

9.1 Schematic Diagram

Two-Circle Diffractometer

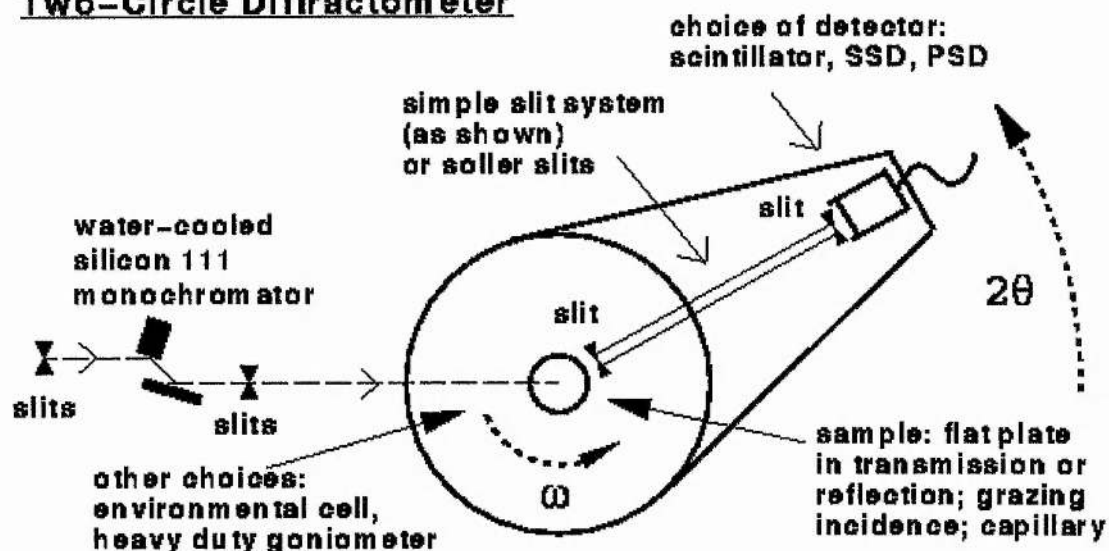


Figure 4.2: Schematic diagram of Station 9.1 at CLRC Daresbury laboratory

4.3. Neutron diffraction

Neutron diffraction differs from X-ray in a number of ways.

Firstly and most importantly, the neutrons are scattered by interaction with the atomic nuclei whereas the X-rays are by the electrons. Hence, there is no dependence on atomic number and better information can be obtained (i) on the position of lighter atoms such as oxygen and (ii) on the positions of two atoms with close atomic numbers (e.g. N and O) as, contrarily to X-rays, neutrons have no coherent variation of scattering factor versus Z .

Also, there is a continuous spectrum of radiation (i.e. no peaks K_α and K_β).

In the time-of-flight (TOF) method, instead of having a fixed wavelength and a moving detector, fixed detector and variable neutron wavelengths are used. In a simple case, the counter is placed at a fixed 2θ angle, and the different d -spacings are sampled by measuring the time that neutrons with different wavelengths take to reach the counter.

4.4. ISIS-RAL²

Neutron diffraction studies were performed at the Rutherford Appleton Laboratory (RAL) 200 μ A ISIS pulsed spallation source either on the HRPD station or the Polaris one.

In the case of a spallation (or pulsed) neutron source such as the one used in ISIS, pulses of high-energy (about 800 MeV) protons from a synchrotron are directed on to a heavy-metal target (Ta).

The acceleration chain begins with an H^- ion source. The extracted H^- beam is accelerated and injected into a linear accelerator.

On entry to the synchrotron, the H^- ion beam is passed through a 0.3 mm thick aluminium oxide stripping foil that removes both electrons from the H^- ions in the beam converting them to protons. The proton beam is then accelerated in the synchrotron for approximately 10 000 revolutions before being deflected in a single turn into the extracted proton beam line (EPB).

Protons hitting nuclei in the target material trigger an intranuclear cascade, placing individual nuclei into a highly excited state. The nuclei then release energy by evaporating nucleons (mainly neutrons). Each high energy proton delivered to the target results in the production of approximately 15 neutrons².

As a result, a high flux of neutrons is produced.

The amount of neutrons produced is related to the current of the H^- ion beam measured in micro-Amperes (μA).

The amount of neutrons received in each instrument is measured in μA hrs.

The neutrons produced in this process generally have very high energies and velocities and must be slowed down for materials studies. This is achieved by an array of small hydrogenous moderators around the target. After moderation to increase the proportion of thermal neutrons, the neutron beam is available for scattering experiments.

A plan of the instruments available at ISIS is shown on the next page.

The long path length for HRPD, which has significant resolution, can be clearly seen in Figure 4.3.

Note: Because of this long path, the faster neutrons of a pulse should be able to join the slowest ones of the previous pulse. In order to prevent this, only a portion (a fifth) of the beam is collected on HRPD.

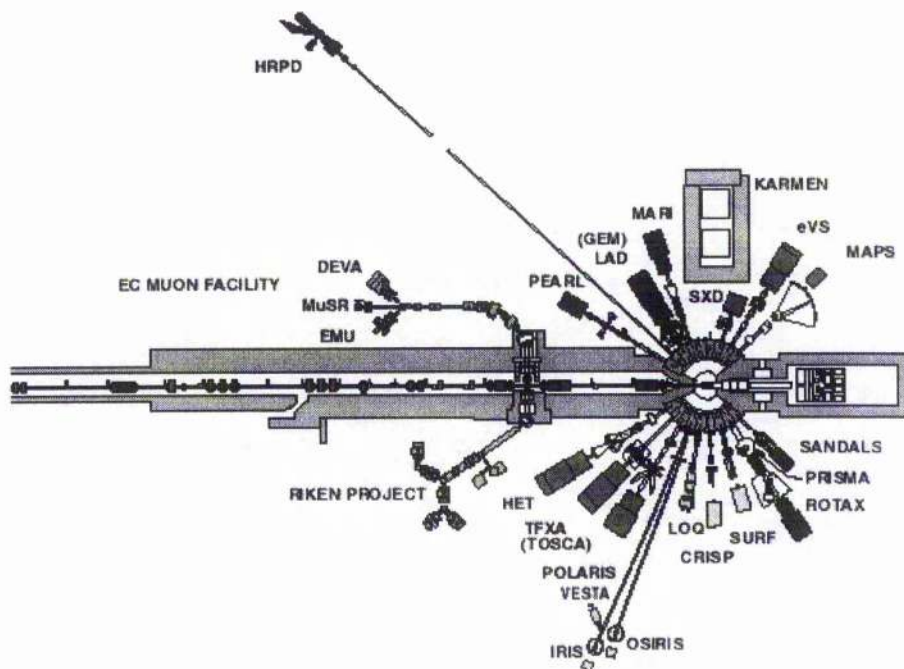


Figure 4.3: Plan of the instruments at the Rutherford Appleton Laboratory

For data collection on both diffractometers (HRPD or Polaris), the sample (generally about 10 g) is placed in a cylindrical vanadium can and held under vacuum.

4.4.1. HRPD

HRPD (High Resolution Powder Diffractometer) is placed nearly 100 m from the ISIS target and is able to achieve extremely high resolution in the back scattering detector bank. It has a $\Delta d/d$ resolution of 5×10^{-4} (resolution limit set by powder particle size) which is effectively constant over a wide d-spacing range.

The detector is fixed and the diffraction pattern collected by a time-of-flight (energy-dispersive) method. For a given reflection the Bragg condition is satisfied at a given wavelength rather than an angle. Results from successive pulses are accumulated and summed until the quantity is sufficient for analysis.

The resolution for a given d-spacing is defined by the value of $\Delta d/d$:

$$\Delta d/d = [\Delta\theta^2 \cot(\theta^2) + (\Delta t/t)^2 + (\Delta L/L)^2]^{1/2}$$

Where Δt is the timing uncertainty, $\Delta\theta$ the angular uncertainty, and ΔL the flight-path uncertainty.

The timing and flight-path uncertainty are minimised by the long path-length for HRPD.

In HRPD, the scattered neutrons are being detected at fixed detector banks centred at $2\theta = 90^\circ$ and 168° . As the use of the backscattering factor at $2\theta = 168^\circ$ minimises the $[\Delta\theta^2 \cot(\theta^2)]$ term, only the data from the 168° (high resolution) banks were used for Rietveld refinement.

4.4.2. POLARIS

POLARIS is a medium resolution, high intensity powder diffractometer and is an ideal complement to HRPD. The advantage of Polaris lies in collection of data in more rapid time than HRPD. It also allows the study of very small amounts of materials (as little as $\sim 1 \text{ mm}^3$).

POLARIS contains four different detectors: Very low angle (2θ range = $13^\circ - 15^\circ$), Low angle (2θ range = $28^\circ - 42^\circ$), 90 degrees (2θ range = $85^\circ - 95^\circ$) and Back scattering (2θ

range = $130^\circ - 160^\circ$). For the same reason as for HRPD, only the data from the Back scattering banks were used for Rietveld refinement.

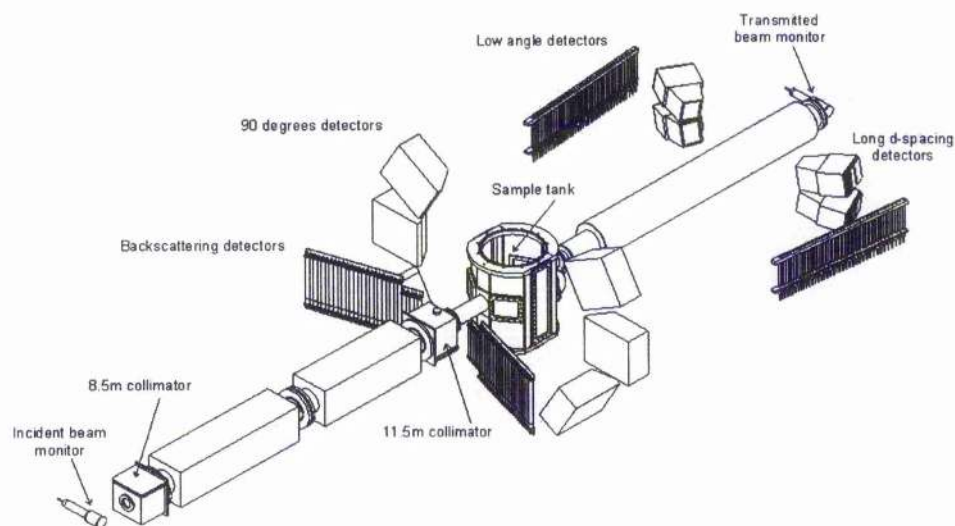


Figure 4.4: Schematic drawing of the POLARIS powder diffractometer.

4.5. Crystallography/Systematic absences

The basics of crystallography can be summed-up as follows:

There are seven crystal systems, they are written below from the lowest symmetry (triclinic) to the highest one (cubic).

Table IV-I: The seven crystal systems

Crystal system	Unit cell shape	Space lattice type
Triclinic	$a \neq b \neq c, \alpha \neq \beta \neq \gamma$	P
Monoclinic	$a \neq b \neq c, \alpha = \gamma = 90^\circ, \beta \neq 90^\circ$	P, C
Orthorhombic	$a \neq b \neq c, \alpha = \gamma = \beta = 90^\circ$	P, F, I, A (or B, or C)
Tetragonal	$a = b \neq c, \alpha = \gamma = \beta = 90^\circ$	P, I
Hexagonal	$a = b \neq c, \alpha = \beta = 90^\circ, \gamma = 120^\circ$	P
Trigonal (a)	$a = b \neq c, \alpha = \beta = 90^\circ, \gamma = 120^\circ$	P
(b)	$a = b = c, \alpha = \gamma = \beta \neq 90^\circ$	R
cubic	$a = b = c, \alpha = \gamma = \beta = 90^\circ$	P, F, I

There are seven lattice centring types (Bravais systems): Primitive (P), side-centred (C), etc..., depending on the equivalent positions for an atom in the unit cell. The combination of crystal system and lattice type gives 14 possible Bravais lattices.

The possible combinations of the different point symmetry elements (mirror plane (m), rotation axis (n), inversion axis (-n), and centre of symmetry (-1)) than can occur in a crystal give a total of 32 point groups.

By adding the possible point symmetry and space symmetry elements (glide planes (n, d, a, b, c) and screw axes (2₁, 3₁, etc...)) to the Bravais lattices, we obtain 230 possible crystallographic space groups.

The type of unit cell and the presence of some symmetry elements in the unit cell are linked with some "systematic absences" of peaks corresponding to some particular values of the Miller indices h, k, l. These indices are related to the d-spacing and the lattice parameters.

For the orthorhombic, tetragonal and cubic space groups:

$$d = 1/\sqrt{(h^2/a^2 + k^2/b^2 + l^2/c^2)}$$

where a, b and c are the lattice parameters.

The relations between the systematic absences and their interpretation is summed-up in the following table.

Table IV-II: Rules of systematic extinctions

Miller indices	Reflections to be observed	interpretation
Extinctions on the three indices are due to the tridimensional lattice		
hkl	$h + k + l = 2n$	I-centred
	$h + k = 2n$	C-centred
	$h + l = 2n$	B-centred
	$k + l = 2n$	A-centred
	$h + k, k + l, h + l = 2n$	F-centred
	$-h + k + l = 3n$	R-centred
Extinctions on two indices are due to bidimensional glide-planes		
0kl	$k = 2n$	b-plane // (100) ($t = b/2$)
	$l = 2n$	c-plane // (100) ($t = c/2$)
	$k + l = 2n$	n-plane // (100) ($t = (b + c)/2$)
	$k + l = 4n$	d-plane // (100) ($t = (b + c)/4$)
h0l	$h = 2n$	a-plane // (010) ($t = a/2$)
	$l = 2n$	c-plane // (010) ($t = c/2$)
	$h + l = 2n$	n-plane // (010) ($t = (a + c)/2$)
	$h + l = 4n$	d-plane // (010) ($t = (a + c)/4$)
hk0	$h = 2n$	a-plane // (001) ($t = a/2$)
	$k = 2n$	c-plane // (001) ($t = b/2$)
	$h + k = 2n$	n-plane // (001) ($t = (a + b)/2$)
	$h + k = 4n$	d-plane // (001) ($t = (a + b)/4$)
Extinctions on one index are due to monodimensional screw-axis		
h00	$h = 2n$	[100]-axis, $t = a/2, 2_1$ or 4_2
	$h = 4n$	[100]-axis, $t = ka/4, 4_1$ or 4_3
0k0	$k = 2n$	[010]-axis, $t = kb/2, 2_1$ or 4_2
	$k = 4n$	[010]-axis, $t = kb/4, 4_1$ or 4_3
00l	$l = 2n$	[001]-axis, $t = c/2, 2_1$ or 4_2
	$l = 3n$	[001]-axis, $t = kc/3, 3_1, 3_2, 6_2$, or 6_4
	$l = 4n$	[001]-axis, $t = kc/4, 4_1$ or 4_3
	$l = 6n$	[001]-axis, $t = kc/6, 6_1$ or 6_5

(t is the translation induced by the space symmetry elements)

4.6. Rietveld refinement

4.6.1. Theory

Rietveld refinement involves the fitting of the X-ray or neutron powder patterns to model structures of a particular space group symmetry to give accurate atomic co-ordinates and unit cell parameters. This is done by a least squares technique using the GSAS program.³ In that curve-fitting procedure, the least squares refinement minimises the difference between the observed and calculated profiles. This means varying the numerical parameters describing the structure to produce the best agreement between the diffraction pattern calculated from it by a Fourier transform and the observed diffraction pattern. Two models are refined at the same time: The structural model (x,y,z of the atoms, the thermal parameters and unit cell parameters $a,b,c,\alpha,\beta,\gamma$) and the instrumental model (zero point, background and $(FWHM)^2$, where FWHM is the “Full Width at Half Maximum” of a peak).

Several other factors are also considered such as thermal factors, scale factors, crystallite size and microstrain, to name but a few. These can all be varied depending on the observed data.

N.B: For our work, the most significant parameters to be determined are the atoms parameters and positions (and hence bond lengths) and site occupancies.

The comparison of observed and calculated diffraction patterns: The least square analysis define the “best fit” of two sets of data to be that which minimises the least square sum:

$$S_y = \sum_i w_i [y_i(\text{obs}) - y_i(\text{calc})]^2$$

where S_y is the weighted difference between the observed $y_i(\text{obs})$ and calculated $y_i(\text{calc})$ diffraction pattern.

The fit of the calculated pattern to the observed data can be given numerically. This is done in terms of agreement indices or R values. The weighted-profile R value, R_{wp} , is defined as:

$$R_{wp} = \{ \sum_i w_i [y_i(\text{obs}) - y_i(\text{calc})]^2 / \sum_i w_i [y_i(\text{obs})]^2 \}^{1/2}$$

where $y_i(\text{obs})$ is the intensity of the observed pattern at step i , $y_i(\text{calc})$ the intensity of the calculated pattern, and w_i the weight, with:

$$(w_i)^{-1} = \sigma_i^2 = \sigma_{ip}^2 + \sigma_{ib}^2$$

where σ_{ip} is the standard deviation associated with the peak, and σ_{ib} is the standard deviation associated with the background.

Ideally, the final R_{wp} should approach the statistically expected R value, R_{exp} :

$$R_{exp} = [(N - P) / \sum_i w_i y_i(\text{obs})^2]^{1/2}$$

where N is the number of observed data points and P the numbers of parameters.

R_{exp} reflects the quality of the data.

χ^2 is the ratio between the two and should approach the value of 1:

$$\chi^2 = R_{wp} / R_{exp}$$

The least square program calculates the best fit (lowest χ^2) based on all the variables included. A good fit is obtained when χ^2 is less than 5.⁴

4.6.2. Constraints and damping

Two processes are described here:

- Damping a particular unstable parameter, i.e. allowing it to vary in smaller steps during the Rietveld refinement process.
- Constrain similar atoms or sites to have identical displacement parameters (e.g. constrain the relative occupancies to maintain a sensible chemical formula).

These are two ways of allowing successful refinement of some structure whose refinement would not otherwise progress satisfactorily.

4.7. Alternating current impedance spectroscopy (a. c. impedance)

4.7.1. Theory

a. c. impedance is a powerful technique for unravelling the complexities of ferroelectric materials. Impedances usually have both resistive and reactive (capacities/inductive) components, both of which must be determined. The standard method of measurement involves the heating of the sample to the desired temperature and applying an alternating voltage across the sample and a standard resistor in series.

The impedance is measured over a wide range of frequencies (normally 10^{-2} to 10^7 Hertz)⁵.

A ferroelectric pellet has two main regions of interest: The bulk (the main part of the pellet) and the grain boundary. The impedance Z^* is defined as follows:

$$Z^* = Z' - j Z''$$

with $j = \sqrt{-1}$

Impedance data are normally presented in the form of imaginary, Z'' (capacitive) against real, Z' (resistive) impedances.

The RC element gives rise ideally to a semicircle for the plot of Z'' versus Z' , from which the component R and C values may be extracted. A typical semi-circle as obtained for our compounds is presented below in Figure 4.5.

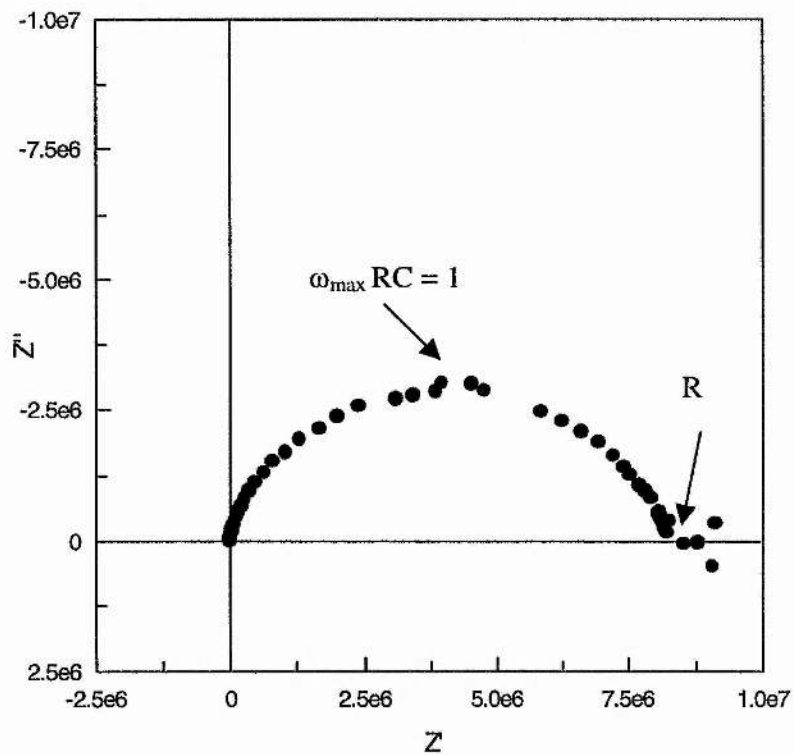


Figure 4.5: Typical semi-circle obtained with the Z'' versus Z' plot from which the values of R and C values can be extracted from the two points shown

The electric modulus M^* is related to Z^* by the following equation:

$$M^* = j \omega C_0 Z'$$

where ω is the angular frequency, $\omega = 2 \pi f$, and $C_0 = \epsilon_0 A/l$

A spectroscopic plot of the imaginary component M'' versus $\log f$ is shown in Figure 4.6.

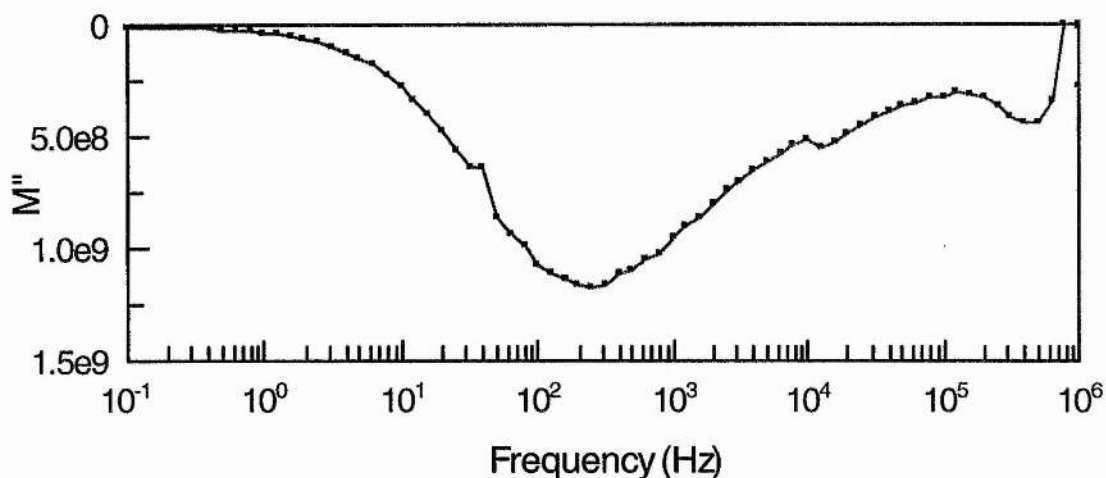


Figure 4.6: Plot of the maginary component of the modulus M'' versus the frequency

In this plot, the higher frequency M'' peak represents a bulk component of the sample. The capacitance C can be estimated from this value as they are related as follows:

$$M''_{\max} = \epsilon_0 / (2 C)$$

In our case, the dielectric constant ϵ' is the value of major interest. This can be calculated from the capacitance value C using the formula:

$$C = \epsilon' \epsilon_0 A/l$$

where ϵ_0 is the permittivity of free space ($8.854 \times 10^{-12} \text{ F m}^{-1}$), A is the area of the pellet and l its thickness.

A plot of the dielectric constant versus the temperature gives an indication of the Curie temperature T_c that occurs at the change from ferroelectric to paraelectric domains.

For ferroelectric phenomenon of the bulk material, the value of the capacitance should be in the range 10^{-10} to 10^{-9} F.

4.7.2. Experimental/Solartron for a.c. impedance measurements

Pellets were needed in order to study the possible ferroelectricity of some compounds.

The powder was ground using a pestle and mortar. The sample was pelleted using a press at 5 tonnes pressure, and the pellet sintered at 850°C for approximately 24 hours. Then both sides of the pellet were smoothly plated with gold paste and heated for a few hours at about 650°C to completely dry the paste.

After these operations, the plated pellet, ready for measurements, is connected to Pt electrodes and placed in a tube furnace.

The impedance is measured at different temperatures in air using an a.c. amplitude of 20 mV over the frequency range 100 mHz – 1MHz.

Dielectric data are collected by a.c. impedance spectroscopy using a Solartron 1255 Frequency Response Analyser with a 1287 Electrochemical Interface connected to a PC with the Z-Plot/Z-View software.

4.8. Differential Thermal Analysis (DTA)

This technique is based on the comparison between the temperature of a sample with that of an inert reference (generally α Al₂O₃) during a programmed change of temperature. The sample and the reference are placed in different alumina crucibles in a programmable furnace with thermocouples measuring the temperature of both of them. A temperature difference ΔT between the sample and the reference appears when an endo- or exothermic event occurs in the sample (e.g. phase transition).

$$\Delta T = T_S - T_R$$

Where T_S is the temperature of the sample, and T_R the temperature of the reference.

The results are presented as ΔT against the temperature.

DTA measurements were collected using a TA instruments SDT 2960 Simultaneous DTA-TGA, with N₂ inputs.

4.9. Bond Valence Sum analysis method

The valence of a bond, S , is a quantity whose sum around each atom is equal to the oxidation state of the atom, V .⁶

$$V = \sum_{ij} S(ij)$$

It correlates inversely with bond length, which allows it to be calculated if the bond length has been measured (which is the case with the GSAS program).

Bond valences, S , are calculated from the bond lengths, R , using the function:

$$S = \exp((R_0 - R)/B)$$

where R_0 is the length of a bond of unit valence, and B the slope of the correlation curve⁶, which has a value not significantly different from 0.37 Å for most bonds⁷.

For optimum bonding satisfaction the BVS for a metal site would be equal to its oxidation state, i.e. 4 for Ti and 3 for Bi, in $\text{Bi}_4\text{Ti}_3\text{O}_{12}$.

The model is restricted to compounds which can, in a formal sense, be described as ionic, i.e. all atoms can be labelled as anions or cations in such a way that the compound contains no cation-cation or anion-anion bonds.

Bond valences have a number of uses. In addition to providing a quantitative measure of bond strength, indicating which bonds are the most important in defining the structure, bond valences can also be used, for example, for detecting the presence of the lattice induced strains that give rise to displacive phase transitions and the unusual properties shown, for example, by perovskite related crystals. This is of importance for the compounds we study here.

The bonds in some compounds are strained as a result of the geometric constraints imposed by the 3-dimensional geometry and the space group symmetry. Because of these constraints some bonds are stretched and others are compressed, a condition indicated by some cations having bond valence sums that are too large (cation under compression) and others having bond valence sums that are too small (cation under tension). Strains will tend to relax and would result in lower crystallographic symmetry.

4.10. Synthesis of the samples

All the products were synthesised by traditional solid state reaction of stoichiometric mixtures of the appropriate oxides, carbonates and BiOCl (for the preparation of the Sillen phases) of purity > 98% from Aldrich. These powders were ground together in an agate mortar and heated in an alumina crucible at elevated temperature until the phase is pure.

A more precise description of each experiment is described later.

4.10.1. Preparation of Sillen phases

Three phases of the series of layered oxyhalides $\text{Bi}_2\text{MO}_4\text{Cl}$ (previously characterised with $\text{M} = \text{La, Nb, and Y}$)⁸ have been synthesised: $\text{Bi}_2\text{ErO}_4\text{Cl}$, $\text{Bi}_2\text{LuO}_4\text{Cl}$ and $\text{Bi}_2\text{YbO}_4\text{Cl}$.

Attempts to prepare $\text{Bi}_2\text{ScO}_4\text{Cl}$ failed, instead a mixture of $\text{Bi}_3\text{O}_4\text{Cl}$ and Sc_2O_3 was obtained. This was probably due to the small size of the Sc^{3+} cation for this kind of structure (Cf. in Figure 4.7 the structure of $\text{Bi}_2\text{LaO}_4\text{Cl}$).

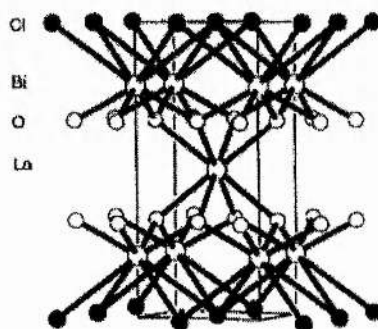


Figure 4.7: Structure of $\text{Bi}_2\text{LaO}_4\text{Cl}$

For each of these products, stoichiometric quantities of BiOCl, Bi₂O₃ and Ln₂O₃ (Ln = Er, Yb, Lu) were ground together and heated at 675°C for 48 hours. Then, after control of the product obtained by X-ray diffraction on the Philips diffractometer, they were reground and reheated at 725°C for a further 24 hours time.

4.10.2. Preparation of Aurivillius phases

Several compounds of this family containing 2, 3 or 4 perovskite-like layers (n=2, 3 or 4 respectively) have been successfully prepared. They are listed below.

n=2 :

- Bi₂CaNb₂O₉
- Bi₂CaTa₂O₉
- Bi₂SrTa₂O₉
- Bi_{2.1}Sr_{0.85}Ta₂O₉

n=3 :

- Bi₄Ti₃O₁₂
- Bi₂Eu₂Ti₃O₁₂
- Bi₂Nd₂Ti₃O₁₂
- Bi₂Ca₂TiNb₂O₁₂
- The solid solution Bi_{4-x}Sr_xTi_{3-x}Nb_xO₁₂ (0 ≤ x ≤ 2.8)
- The solid solution Bi_{4-x}La_xTi₃O₁₂ (x = 1 and 2)

n=4 :

- Bi₄SrTi₄O₁₅

All these products were prepared by mixing and grinding together stoichiometric quantities of Bi_2O_3 and the appropriate oxides or carboxides needed for the synthesis, i.e. TiO_2 , Ta_2O_5 , La_2O_5 , Nb_2O_5 , SrCO_3 , WO_3 , Eu_2O_3 , Nd_2O_3 alone or in combination. All powders were of purity > 98% from Aldrich. These powders were ground together in an agate mortar and heated in an alumina crucible.

After the first heat treatment, the phase purity is not complete. A second or third heat treatment is always required to give phase purity and to take the reaction to completion with intermediate regrinding between each stage.

The mixed powders were heated in air in an alumina crucible for 24 hours at 850°C (700°C for $\text{Bi}_4\text{Ti}_3\text{O}_{12}$) and a further 24 hours at the final temperature, which is 1000°C for all samples except for $\text{Bi}_4\text{Ti}_3\text{O}_{12}$: 850°C.

References

- ¹ C. Giacovazzo et al., "*Fundamentals of Crystallography*", IUCr Oxford Science Publications, 1992
- ² <http://www.isis.rl.ac.uk>
- ³ A.C. Larson and R.B. VonDreele, Los Alamos National Laboratory, report n° La-UR-86-748, 1987
- ⁴ R.A. Young, "*The Rietveld method*", 1993, New York, Oxford University Press.
- ⁵ J.T.S. Irvine, D.C. Sinclair and A.R. West, *Adv. Mater.*, 1990, **3**, 132
- ⁶ I. D. Brown and D. Altermatt, *Acta Cryst.*, 1985, **B41**, 244
- ⁷ R. L. Withers, J. G. Thompson and A. D. Rae, *J. Solid State Chem.*, 1991, **94**, 404
- ⁸ C.J. Milne, P. Lightfoot, J.D. Jorgensen, S. Short, *J. Mater. Chem*, 1995, **5**, 1419

Chapter 5 : Aurivillius phases with an even number of perovskite layers

Introduction	43
5.1. n=2 : Two perovskite layers	45
5.1.1. Variable temperature study of $\text{Sr}_{0.85}\text{Bi}_{2.1}\text{Ta}_2\text{O}_9$	48
5.1.2. Variable temperature study of $\text{SrBi}_2\text{Nb}_2\text{O}_9$	57
5.1.3. "Solid solutions" $\text{Bi}_{2+2x/3}\text{Sr}_{1-x}\text{Ta}_2\text{O}_9$ and $\text{Bi}_2\text{Sr}_{1-x/2}\text{Ta}_{2-x}\text{W}_x\text{O}_9$	67
5.2. n=4 : Four perovskite layers: $\text{SrBi}_4\text{Ti}_4\text{O}_{15}$	69
5.2.1. Room temperature study	70
5.2.2. Variable temperature study	73
Conclusion.....	81
References	81

Introduction

The results on Aurivillius phases have been split in two chapters, as some kind of systematics regarding the crystallographic behaviour can be seen depending on the fact that the Aurivillius compound contains either an even or odd number of perovskite layers. This observation follows earlier suggestions by Newnham et al. for "all even layered" structures, i.e. all Aurivillius phases of general formula $(\text{M}_2\text{O}_2)(\text{A}_{n-1}\text{B}_n\text{O}_{3n+1})$, — where M is usually Bi, A is a mono-, di- or trivalent cation and B a tri-, tetra-, penta- or hexavalent cation —, containing an even number n of perovskite layers should crystallise in the same space group ($\text{A2}_1\text{am}$)¹.

The M cation is coordinated to eight oxygens: four from the $[\text{M}_2\text{O}_2]$ block and four from the apices of the octahedra, the A cation in the perovskite site is coordinated to twelve oxygens, and the B cation is coordinated to the six oxygens forming the octahedra (cf. Figure 2.2: The representation of the perovskite structure in Chapter 2 and Figure 5.2).

The reason for the preference of Aurivillius compounds containing an even number of perovskite layers for the space group $\text{A2}_1\text{am}$ and the preference of Aurivillius compounds containing an odd number of perovskite layers for space group B2cb is well explained in reference 1. It lies in a strain energy argument which is related to the

non-distortion of the AO_6 octahedra ($A = Nb, Ta$) as the distortion of those octahedra would lead to energetically unfavorable short O-O distances.

From the ideal undistorted structure, space group $I4/mmm$, always observed at high temperature (and previously thought to appear just above T_c) whatever the number of perovskite-type layers, the important thing for the structure when going to the distorted space group $A2_1am$ or $B2cb$ is the loss of symmetry elements.

The space group $I4/mmm$ presents three mirror planes parallel to (ab) , (ac) and (bc) . For “odd-layers”, keeping the mirror plane $// (ab)$, i.e. adopting the space group $A2_1am$ would distort the octahedra, which is not the case when adopting the space group $B2cb$. The inverse is true for “even-layers” materials: keeping the mirror plane $// (ab)$ doesn’t distort the octahedra whereas the loss of the mirror plane in favour of a two-fold axis along a would.

The loss of symmetry when going from space group $I4/mmm$ to $A2_1am$ (or $B2cb$) also leads to a “ $\sqrt{2} \times \sqrt{2}$ ” distortion, i.e. in the lower orthorhombic symmetry $A2_1am$ (or $B2cb$) the lattice parameters $a_0 \approx b_0 \approx a_T\sqrt{2}$.

This is represented in the figure below.

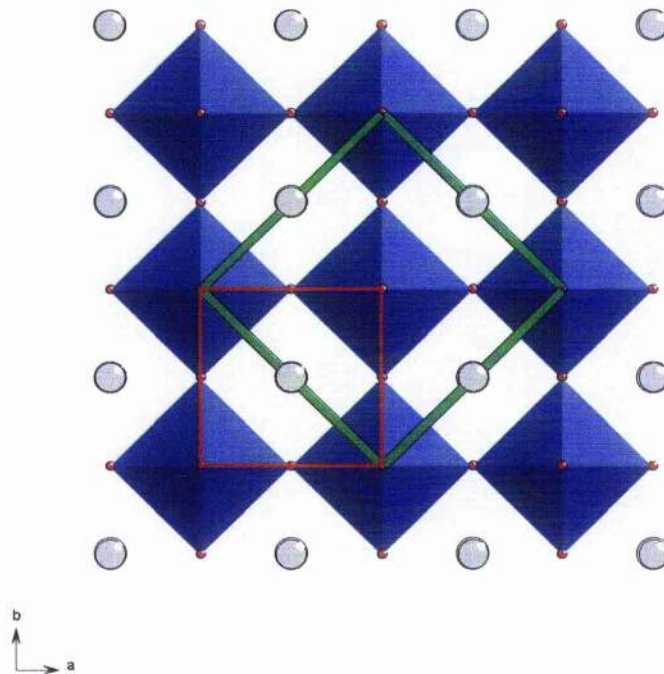


Figure 5.1: Distortion “ $\sqrt{2} \times \sqrt{2}$ ” ; The cell edge in red represents the tetragonal symmetry with $a_T = b_T$, the cell edge in green represents the orthorhombic symmetry with $a_0 \approx b_0 \approx a_T\sqrt{2}$

These distortions in the low temperature phase are correlated with the ferroelectric behaviour observed at low temperature for these materials.

5.1. $n=2$: Two perovskite layers

Several compounds with this type of structure, of general formula $ABi_2B_2O_9$ (where A is a monovalent, divalent or trivalent cation and B a tri-, tetra-, penta- or hexavalent cation) have been studied by different research groups in recent years, especially since it was discovered that $SrBi_2Ta_2O_9$ (SBT) was a promising material for ferroelectric devices due to its “fatigue-free” nature, i.e. the non-degradation of its remanent polarization (P_r) after many switching cycles².

Materials structurally related to SBT and studied in recent years include: $CaBi_2Ta_2O_9$ and $BaBi_2Ta_2O_9$ ^{3,4}, and $ABi_2Nb_2O_9$ (with A = Sr, Ca and Ba).⁵

All the crystal structures of type $Bi_2AB_2O_9$ with A = Sr or Ca are orthorhombic at room temperature, crystallising in the non-centrosymmetric space group $A2_1am$, and were assumed to transform to the tetragonal space group $I4/mmm$ above the Curie temperature T_c , as shown in Figure 5.2. In this report, we demonstrate that in fact for at least two of these compounds, another crystal symmetry (space group $Amam$) occurs above T_c , but still transforms to $I4/mmm$ at high temperature

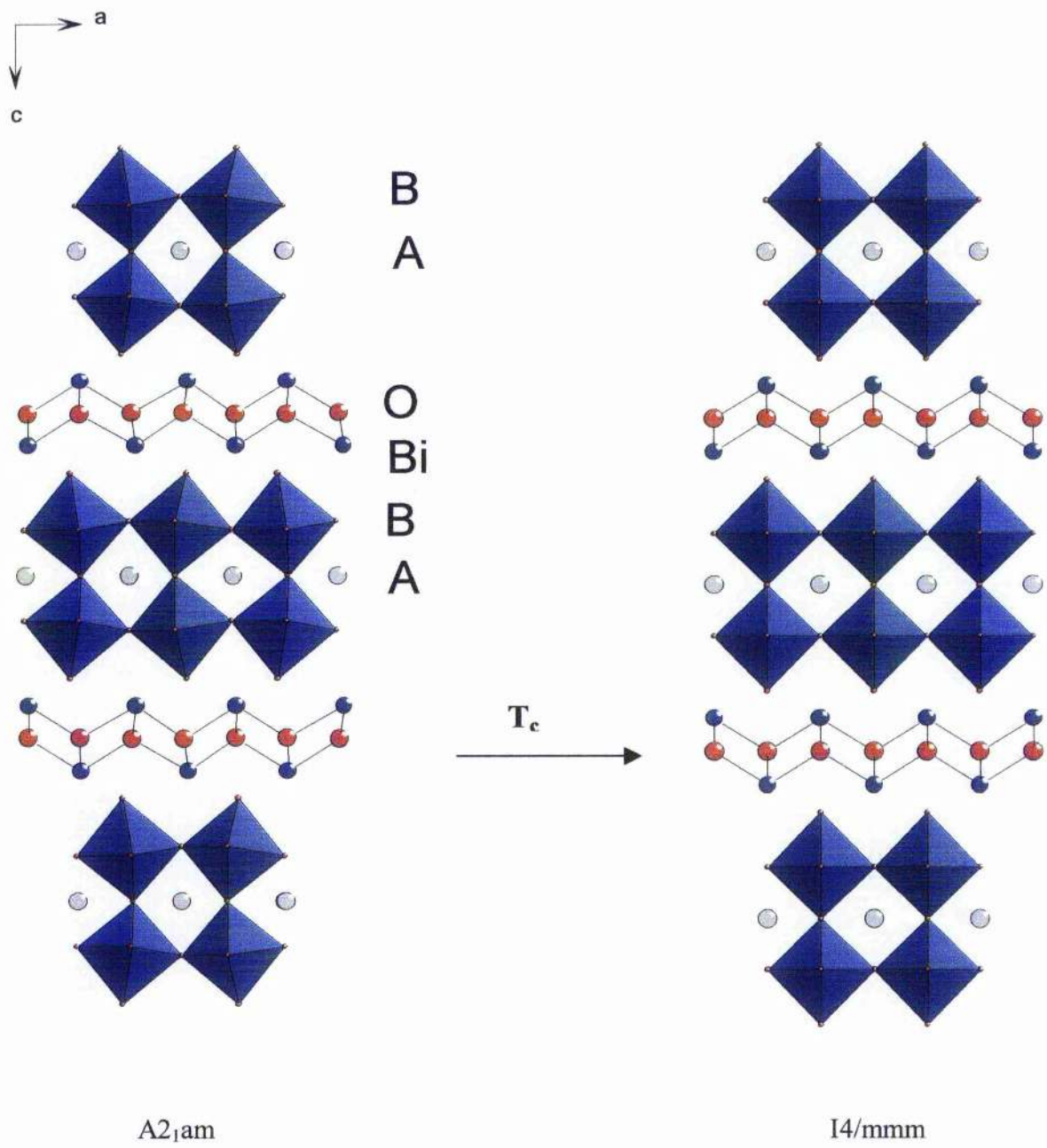


Figure 5.2: General picture showing the transition from orthorhombic $A2_1am$ to tetragonal $I4/mmm$ previously believed to occur for all “even-layer” Aurivillius materials of formula $(M_2O_2)(A_{n-1}B_nO_{3n+1})$

The orthorhombicity, defined as $2(b-a)/(b+a)$, decreases with increasing A^{2+} cation size. Therefore, the smaller the A^{2+} cation size is, the greater is the tilting (or distortion) of the AO_6 octahedra around all three axes.

This leads to higher T_c and larger P_r , which are important features for FeRAMs applications along with the fatigue-free property and a low coercive field (E_c). (cf. Chapter 3: Properties).

The literature on perovskite ferroelectrics indicates that the polarisation increases when T_c increases⁶, and that a larger dielectric constant (ϵ) at T_c is also linked to a greater polarisation.

The structural distortions responsible for the non-centrosymmetry (illustrated by the space group $A2_1am$ here) are responsible for the spontaneous ferroelectric polarisation along the a -axis, linked with the displacements of the A cations along this same axis.

Some of these materials present a certain amount of disorder Bi/A that increases as the size of the A^{2+} cation increases^{4,5}. This phenomenon is discussed in the next chapter (Chapter 6: Aurivillius phases with an odd number of perovskite layers).

The effect of the nature of the B^{5+} cation in $ABi_2B_2O_9$ has also been studied with $A = Nb$ or Ta . In the same column of the periodic table, vanadium seems to have too small an ionic size ($r(V^{5+}) = 0.54 \text{ \AA}$ for $CN = 6$) to form a stable layered perovskite structure by itself, but partial substitution of Nb^{5+} or Ta^{5+} by V^{5+} has been obtained up to 10 at.%^{7,8}, resulting in improved ferroelectric properties^{9,10}.

In the case of Nb^{5+} and Ta^{5+} , their ionic radii are the same ($r(Nb^{5+}) = r(Ta^{5+}) = 0.64 \text{ \AA}$ for $CN = 6$), therefore the increased structural distortion observed with $B = Nb$ seems to be better explained by the covalence character of the shorter $B-O$ bondlengths (less than 2 \AA) that is increased by the less extended $4d$ orbital of the Nb in comparison with the $5d$ orbital of the Ta ¹¹. The importance of covalency over structural distortion in ferroelectric oxides had been discussed in an earlier paper by Cohen¹².

All compounds of formula $ABi_2Nb_2O_9$ have a higher Curie temperature T_c than $ABi_2Ta_2O_9$ (e.g. $T_c(SrBi_2Nb_2O_9) \sim 440^\circ C$, $T_c(SrBi_2Ta_2O_9) \sim 335^\circ C$)^{13,20}, which is related to the increased structural distortion observed with $B = Nb$.

5.1.1. Variable temperature study of $\text{Sr}_{0.85}\text{Bi}_{2.1}\text{Ta}_2\text{O}_9$

This material has been studied because it has been shown that a Sr-deficient and Bi-excess compound have improved electrical properties over the stoichiometric material $\text{SrBi}_2\text{Ta}_2\text{O}_9$.¹⁴

The powder neutron diffraction data were collected at temperatures of 110, 200, 250, 300, 350, 400, 450, 500 and 550°C on HRPD; each data collection lasting approximately two hours for a total collected value of 65 μAhrs . All the refinements were carried out using a data range $0.65 < d < 2.5 \text{ \AA}$.

The original crystallographic data before refinement were taken from the work from Shimakawa et al.¹⁴ for $\text{SrBi}_2\text{Ta}_2\text{O}_9$ at room temperature in space group $A2_1am$.

At 110°C, the structure has been refined as orthorhombic with space group $A2_1am$. This confirms what was suggested before; the Aurivillius phases containing an even number of perovskite layers belong to the same space group $A2_1am$.

The results of the Rietveld refinement at 110°C are shown in Table V-I below.

Table V-I: Final parameters from the Rietveld refinement of $\text{Sr}_{0.85}\text{Bi}_{2.1}\text{Ta}_2\text{O}_9$ at 110°C: Space group $A2_1am$, $a = 5.5225(2) \text{ \AA}$, $b = 5.5246(2) \text{ \AA}$, $c = 25.0338(6) \text{ \AA}$, Cell volume = $763.77(5) \text{ \AA}^3$.

Name	x	y	z	Uiso x 100	Fractn
Sr	0	0.247(2)	0	1.6(1)	0.85
Bi(1)	0.455(2)	0.769(2)	0.2001(2)	2.6(1)	1.0
Ta	0.514(2)	0.746(2)	0.4150(2)	1.00(8)	1.0
O(1)	0.519(3)	0.298(2)	0	1.6(2)	1.0
O(2)	0.514(3)	0.692(2)	0.3414(3)	2.3(2)	1.0
O(3)	0.729(3)	0.998(2)	0.2507(4)	1.5(1)	1.0
O(4)	0.752(3)	0.986(2)	0.0703(3)	1.7(2)	1.0
O(5)	0.788(3)	0.971(2)	0.5838(3)	1.5(2)	1.0
Bi(2)	0	0.247(2)	0	1.6(1)	0.10

Final agreement factors are $\chi^2 = 5.01$, $R_{wp} = 0.076$ for 39 variable parameters.

Unlike $\text{SrBi}_2\text{Nb}_2\text{O}_9$ ⁵ or even the stoichiometric compound $\text{SrBi}_2\text{Ta}_2\text{O}_9$ ⁴, our data show no evidence for partial disorder of the Sr/Bi cations over the two sites. This is presumably due, at least in part, to the Bi-excess in $\text{Sr}_{0.85}\text{Bi}_{2.1}\text{Ta}_2\text{O}_9$ composition.

It also transforms to the undistorted tetragonal phase I4/mmm at high temperature. But unexpectedly, the refinements showed that it also presents an intermediate phase between A2₁am and I4/mmm.

Some papers point out the possibility of a second phase. In particular, a variable temperature X-ray diffraction study by Onodera et al.¹⁵ suggested an intermediate phase between A2₁am and I4/mmm for $\text{Sr}_{0.85}\text{Bi}_{2.1}\text{Ta}_2\text{O}_9$, however their results are very different from those presented here.

The literature sometimes describes the presence of two phase transitions with a 200° temperature difference for Aurivillius phases containing an even number of perovskite-like layers^{16,20}; the phase transition occurring at the higher temperature corresponds to the transition from the ferroelectric state to the paraelectric one. These studies are based on differential thermal analyses but the nature of the phase transition at the lower temperature is not known and does not seem to be related to any change of the crystallographic data (except for the small change of slope for b/a observed by Subbarao for $\text{Bi}_3\text{TiNbO}_9$)²⁰. Another study based on electron diffraction for several strontium bismuth titanate Aurivillius phases concluded the presence of a second phase transition above T_c ¹⁷.

However, a study by Jimenez et al.¹⁸ of the Young's modulus of several Aurivillius phases including $\text{SrBi}_2\text{Nb}_2\text{O}_9$ and $\text{Bi}_3\text{TiNbO}_9$ did not observe any other phase transition than the ferroelectric to paraelectric state one for any of them.

The existence of the intermediate phase can be seen in the plots of the lattice parameters versus the temperature calculated from the GSAS Rietveld refinements in space group A2₁am (Cf. Figure 5.3).

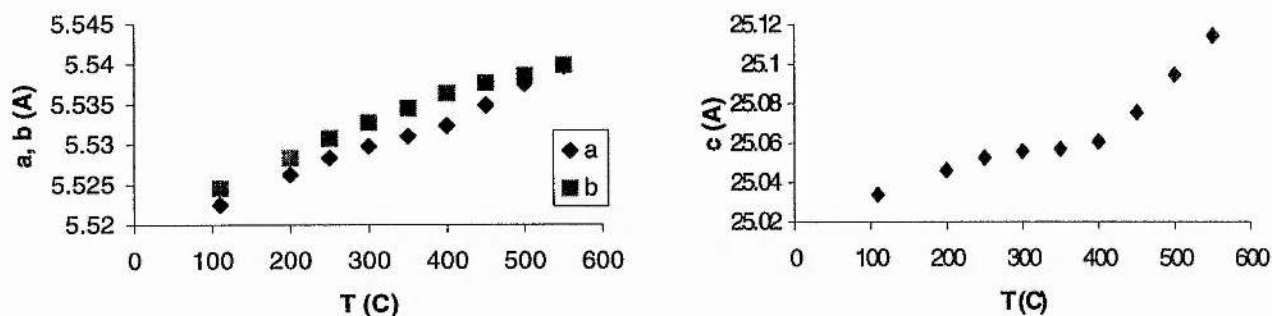


Figure 5.3: Lattice parameters for $\text{Sr}_{0.85}\text{Bi}_{2.1}\text{Ta}_2\text{O}_9$ versus the temperature

There is a change of slope in the c-parameter versus T with the transition temperature situated between 350 and 400°C. This correlates with a measured T_c for the present sample of 375°C (Cf. a.c. impedance measurements at the end of this section).

It can also be seen that the orthorhombicity ($2(b-a)/(b+a)$) (i.e. the difference between a and b) increases in the range 250°C < T < 375°C.

These results confirm the existence of an intermediate phase in the region 375°C < T < 550°C, since the material is clearly still orthorhombic, not tetragonal, in this region.

Investigation of the possible space groups for this intermediate phase was carried out. The space groups studied were the supergroups of $A2_1am$: $Amam$, $Abam$ or $F2mm$ as some older papers suggested a possible F-centered intermediate for some compounds.

The powder neutron diffraction study of this compound at 450°C proved that this intermediate phase must be A centered. The F centered option wouldn't allow the three peaks marked on the portion of the Rietveld plot shown in Figure 5.4 as they present an odd number value of (h + k) or (h + l). The $Abam$ space group was also ruled out by the presence of the reflection (033).

The final Rietveld refinement of this compound at 450°C indicates this intermediate phase to be orthorhombic with space group $Amam$.

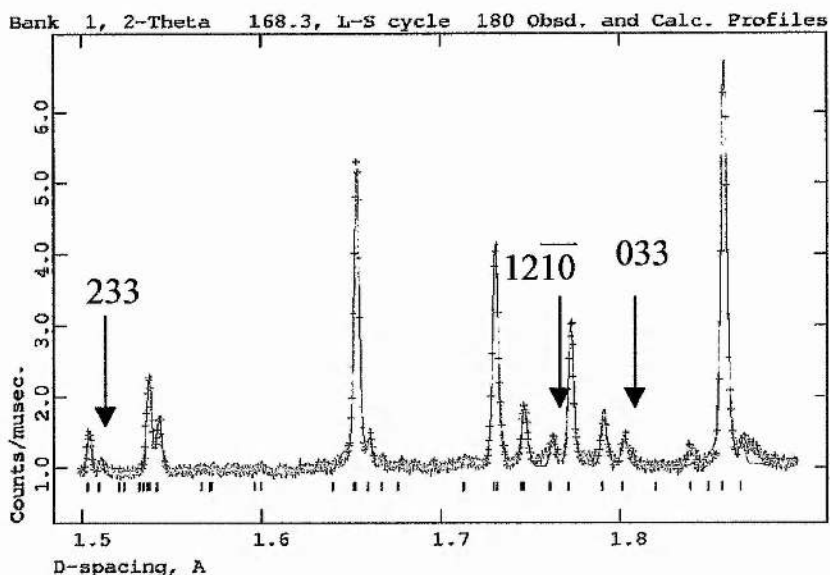


Figure 5.4: Rietveld refinement plot of $\text{Sr}_{0.85}\text{Bi}_{2.1}\text{Ta}_2\text{O}_9$ at 450°C showing the three peaks not allowed in an F-centered space group (233, 12-10, 033)

Table V-II: Final parameters from the Rietveld refinement of $\text{Bi}_{2.1}\text{Sr}_{0.85}\text{Ta}_2\text{O}_9$ at 450°C : Space group Amam , $a = 5.5350(2)$ Å, $b = 5.5376(2)$ Å, $c = 25.0755(5)$ Å, Cell volume = $768.57(4)$ Å³.

Name	x	y	z	Uiso x 100	Fractn
Sr	0.25	0.240(2)	0	3.1(1)	0.85
Bi(1)	0.75	0.760(1)	0.2001(1)	4.9(1)	1.0
Ta	0.75	0.748(1)	0.4145(1)	1.75(7)	1.0
O(1)	0.75	0.278(3)	0	3.9(2)	1.0
O(2)	0.75	0.695(2)	0.3414(2)	4.0(2)	1.0
O(3)	0	0	0.2501(4)	2.5(1)	1.0
O(4)	0	0	0.0722(2)	3.1(2)	1.0
O(5)	0	0	0.5821(3)	3.8(3)	1.0
Bi(2)	0.25	0.240(2)	0	3.1(1)	0.10

Final agreement factors are $\chi^2 = 3.62$, $R_{\text{wp}} = 0.065$ for 29 variable parameters.

Finally, the crystal structure above the point where the lattice parameters a and b merge (cf. Figure 5.3) has also been established by Rietveld refinement. The final results indicate the space group to be tetragonal, crystallising in space group $I4/mmm$. The final results of the refinement at 550°C are in the table below.

Table V-III: Final parameters from the Rietveld refinement of $\text{Sr}_{0.85}\text{Bi}_{2.1}\text{Ta}_2\text{O}_9$ at 550°C : Space group $I4/mmm$, $a = 3.91721(6) \text{ \AA}$, $c = 25.1142(5) \text{ \AA}$, Cell volume = $385.37(1) \text{ \AA}^3$.

Name	x	y	z	Uiso x 100	Fractn
Sr	0.5	0.5	0	3.38*	0.8500
Bi(1)	0.5	0.5	0	3.38*	0.1000
Ta	0	0	0.0856(2)	2.01*	1.0000
O(1)	0.5	0.5	0.5	4.17*	1.0000
O(2)	0	0.5	0.25	2.94*	1.0000
O(3)	0	0	0.1593(2)	7.55*	1.0000
O(4)	0	0.5	0.0772(2)	4.05*	1.0000
Bi(2)	0.5	0.5	0.2002(2)	5.40*	1.0000

*Refined anisotropically

Thermal parameters multiplied by 100.0 are

Name	U11	U22	U33
Sr	2.9(3)	2.9(3)	4.4(4)
Bi(1)	2.9(3)	2.9(3)	4.4(4)
Ta	1.50(1)	1.50(1)	3.1(2)
O(1)	5.50(3)	5.50(3)	1.6(4)
O(2)	2.8(2)	2.8(2)	3.2(3)
O(3)	10.0(4)	10.0(4)	2.6(3)
O(4)	4.6(2)	4.6(2)	6.5(2)
Bi(2)	5.6(2)	5.6(2)	4.9(3)

Final agreement factors are $\chi^2 = 3.17$, $R_{wp} = 0.061$ for 31 variable parameters.

In conclusion, the series of phase transitions for this sample can be summed-up like this :



The Rietveld plots at 110, 450 and 550°C are shown in the following page.

A picture along the c-axis showing the three different space groups follows in Figure 5.6.

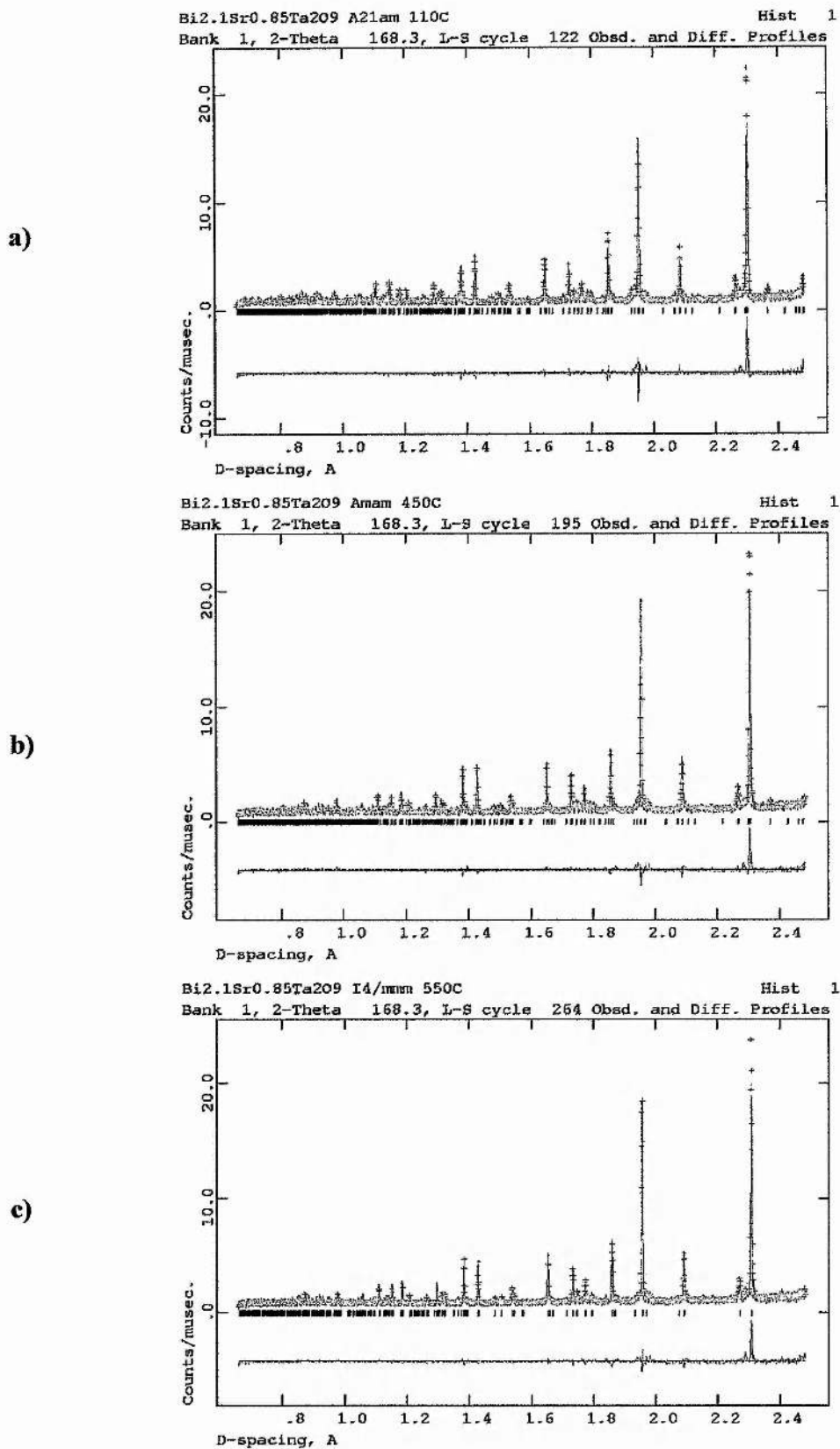


Figure 5.5: Final Rietveld plots for Sr_{0.85}Bi_{2.1}Ta₂O₉ at (a) 110°C in space group A2₁am, (b) 450°C in space group Amam and (c) 550°C in space group I4/mmm

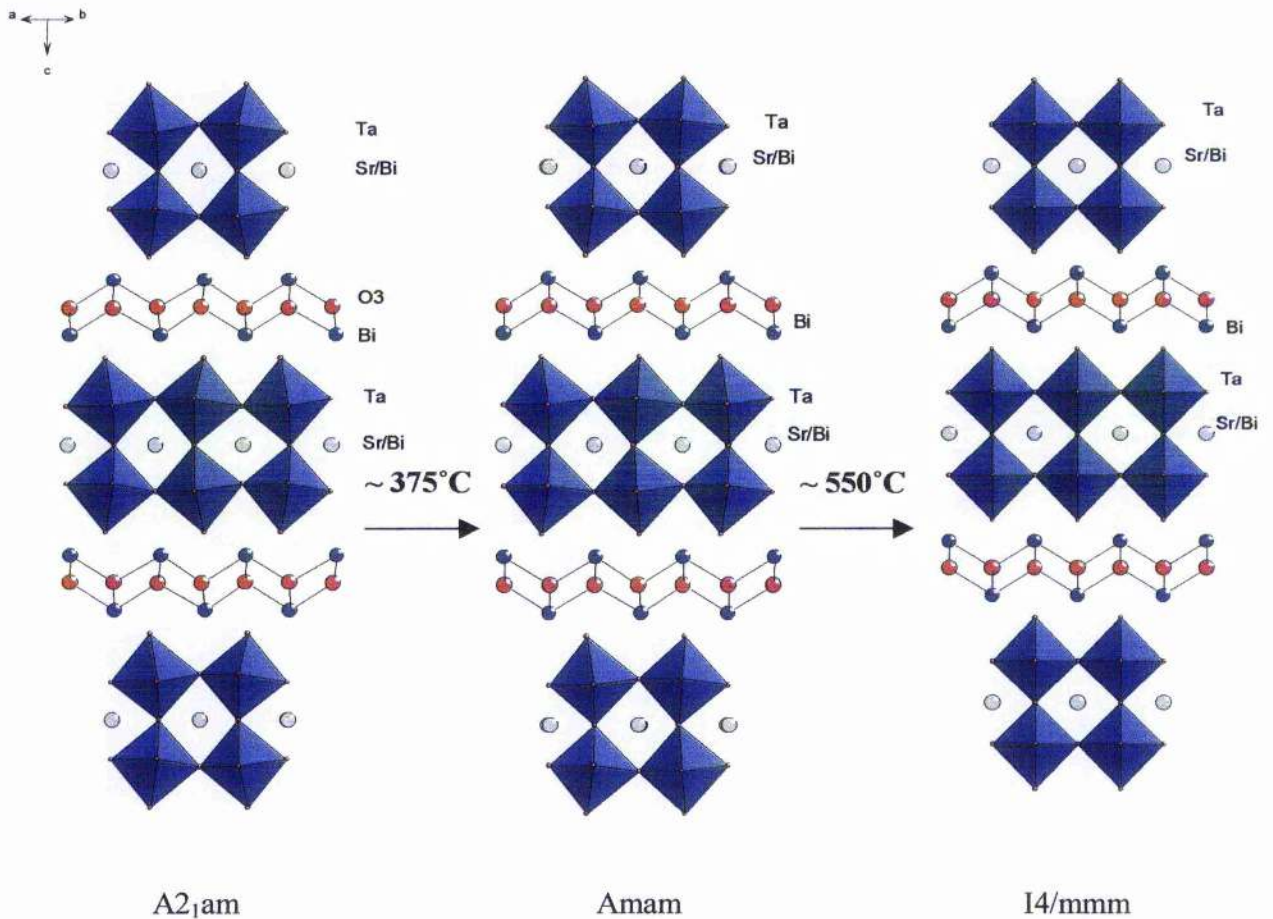
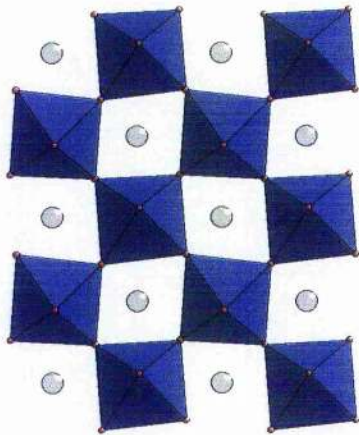


Figure 5.6: The three different space groups of $\text{Sr}_{0.85}\text{Bi}_{2.1}\text{Ta}_2\text{O}_9$ at different temperatures.

The difference between the $A2_1am$ and $Amam$ structures is firstly that the displacive mode along the polar axis (a) is lost and, secondly, that a rotational mode of the TaO_6 octahedra of the perovskite unit is also lost.

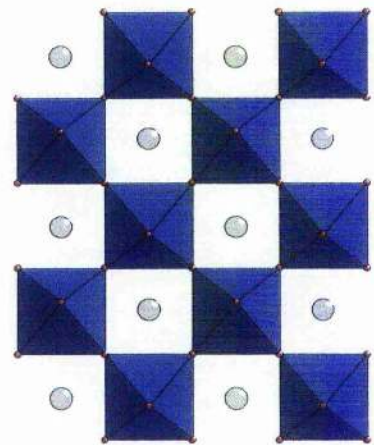
This can be seen on the c-axis projection of one octahedra layer of the structures (Cf. Figure 5.7).

Ferroelectric phase
 $\text{Sr}_{0.85}\text{Bi}_{2.1}\text{Ta}_2\text{O}_9$ at 110 °C : $A2_1am$



Tilts around all three axes.
 Displacements along a.

Intermediate paraelectric phase
 $\text{Sr}_{0.85}\text{Bi}_{2.1}\text{Ta}_2\text{O}_9$ at 450 °C : $Amam$



Tilts around a only.

~375°C



Figure 5.7: Evolution of the octahedra tilting of $\text{Sr}_{0.85}\text{Bi}_{2.1}\text{Ta}_2\text{O}_9$ with the temperature (projection on the c-axis)

From the atomic displacements, we can calculate the spontaneous polarisation P_s along the a-axis according to the following formula:

$$P_s = (a/V) \sum_i m_i q_i \Delta x_i$$

where: q_i is the charge of the ion (e.g. +3 for Bi, -2 for O), m_i its multiplicity, Δx_i is the displacement along a of the ion (e.g. for $\text{Sr}_{0.85}\text{Bi}_{2.1}\text{Ta}_2\text{O}_9$ at 110°C, O(1): $x = 0.519 \rightarrow \Delta x = 0.5 - 0.519 = -0.019$), a the unit cell parameter, and V the volume of the unit cell¹⁹.

We can consider the sum of the dipoles produced by displacements of Ta/Bi, O(1), O(2), O(4) and O(5) as the contribution of the perovskite block to the overall polarisation, and the ones of Bi in the $[\text{Bi}_2\text{O}_2]$ site and O(3) as the contribution of the $[\text{Bi}_2\text{O}_2]$ unit.

Figure 5.8 shows that the contribution of the $[\text{Bi}_2\text{O}_2]$ layer is greater than the one of the perovskite unit, and that the later increases just before T_c , both components being more or less equal to each other at $T = 350^\circ\text{C}$.

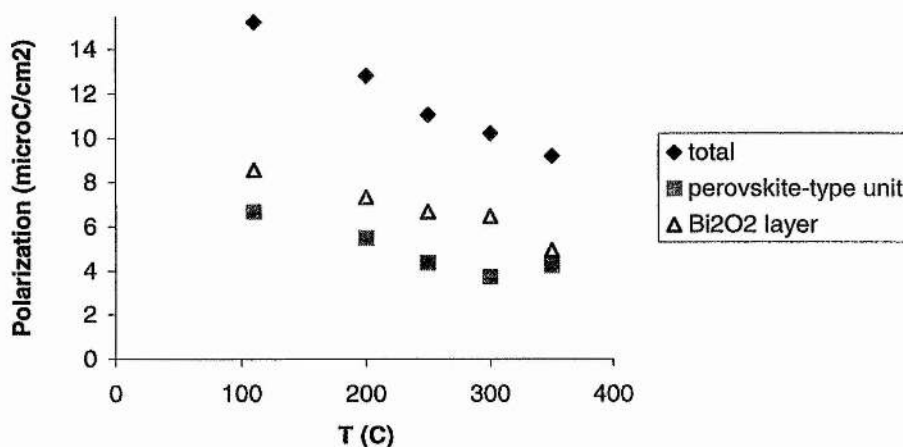


Figure 5.8: Study of the evolution of the spontaneous polarisation and its components with the temperature in $\text{Sr}_{0.85}\text{Bi}_{2.1}\text{Ta}_2\text{O}_9$

a.c. impedance spectroscopy measurements have been carried out, following the method described in Chapter 4., over a large range of temperatures.

The dielectric constant ϵ' has been calculated for each temperature according to the method described in § 4.7.1.

The data obtained from the in-house Solartron showed a single Debye-type arc.

The study of the dielectric constant ϵ' versus the temperature shows clearly the ferroelectric to paraelectric transition at $T_c \sim 375^\circ\text{C}$, as shown in Figure 5.9.

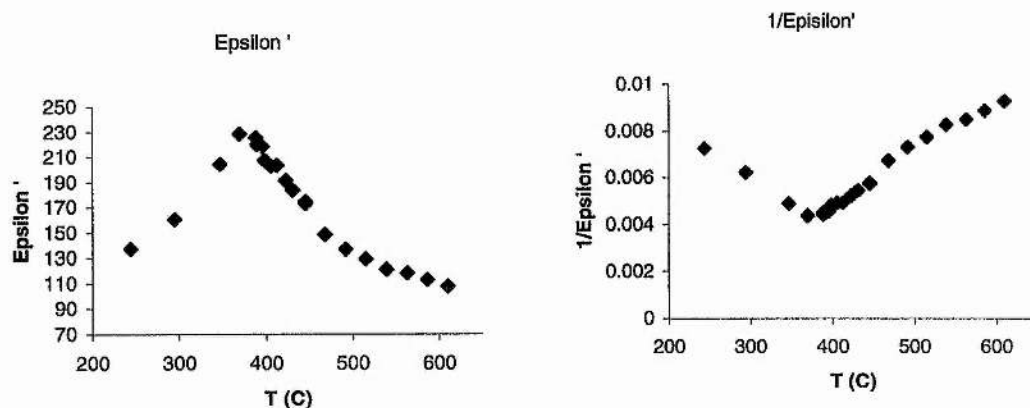


Figure 5.9: $\text{Sr}_{0.85}\text{Bi}_{2.1}\text{Ta}_2\text{O}_9$ ac impedance measurements

Note: The results in this section have been published in *Physical Review B*: “Two high temperature paraelectric phases in $\text{Sr}_{0.85}\text{Bi}_{2.1}\text{Ta}_2\text{O}_9$ “, C. H. Hervoches, J. T. S. Irvine and P. Lightfoot, *Physical Review B*, 2001, **64**, article no. 100102

5.1.2. Variable temperature study of $\text{SrBi}_2\text{Nb}_2\text{O}_9$

This temperature-related study has been carried out in order to characterise the nature of the ferroelectric to paraelectric phase transition (T_c) which is known to be at around 440°C for this material²⁰. It was particularly interesting to see if a second phase transition exists in this material as it does for $\text{Sr}_{0.85}\text{Bi}_{2.1}\text{Ta}_2\text{O}_9$.

The crystal structure of $\text{SrBi}_2\text{Nb}_2\text{O}_9$ at several temperatures in the range 20 to 700°C has been determined using powder neutron diffraction data. The data were collected

on the Polaris instrument at ISIS for approximately one hour at each temperature for a total collected value of 180 μ Ahrs.

The original crystallographic data before refinement were taken from the work from Shimakawa et al.¹⁴ for SrBi₂Ta₂O₉ at room temperature in space group A2₁am.

At each temperature (from 350°C), the two space groups orthorhombic A2₁am and tetragonal I4/mmm have been envisaged, the results of which are in Table V-IV.

Note : For the Rietveld refinement of the neutron diffraction data, all the relative occupancies have been fixed to 1 as the neutron scattering factor contrast for Bi and Sr is much smaller than that for X-rays (neutrons scattering lengths, b (x 10⁻¹⁵ m) : Bi, 8.532 ; Sr, 7.02 ; Ti, -3.438 ; Nb, 7.054 ; O, 5.803).

Table V-IV: Final lattice parameters and agreement factors from the Rietveld refinements of SrBi₂Nb₂O₉ at several temperatures in space groups A2₁am and I4/mmm.

A2 ₁ am (39var)					
T (°C)	a (Å)	b(Å)	c(Å)	χ^2	R _{wp}
20	5.5167(2)	5.5143(2)	25.0808(4)	6.761	0.0298
50	5.5186(2)	5.5162(2)	25.0891(4)	6.066	0.0267
100	5.5211(3)	5.5190(3)	25.1001(5)	5.923	0.0264
150	5.52340(3)	5.52193(3)	25.1116(5)	5.779	0.0261
200	5.5260(3)	5.5248(3)	25.1230(5)	5.813	0.0261
250	5.5287(3)	5.5278(3)	25.1338(5)	5.565	0.0257
300	5.5314(4)	5.5309(4)	25.1449(5)	5.48	0.0255
350	5.5343(4)	5.5343(4)	25.1558(5)	5.528	0.0256
400	5.5377(5)	5.5380(5)	25.1657(5)	5.317	0.025
450	5.5422(8)	5.5433(8)	25.1706(6)	6.233	0.0273
500	5.5455(8)	5.5468(8)	25.1860(6)	6.032	0.0269
550	5.5485(8)	5.5499(8)	25.2040(6)	5.81	0.0264
600	5.5515(8)	5.5526(8)	25.2228(6)	5.475	0.0257
650	5.5544(8)	5.5554(8)	25.2433(6)	5.135	0.0249
700	5.5575(9)	5.5582(9)	25.2639(6)	4.944	0.0244

I4/mmm Uaniso. (32var)					
T (°C)	a (Å)	a√2 (Å)	c (Å)	χ^2	Rwp
350	3.91347(8)	5.5345(1)	25.1577(6)	7.7	0.0302
400	3.91597(7)	5.5380(1)	25.1670(5)	5.142	0.0247
450	3.91941(5)	5.54288(7)	25.1711(4)	2.765	0.0182
500	3.92185(5)	5.54633(7)	25.1864(4)	2.467	0.0172
550	3.92395(5)	5.54930(7)	25.2042(4)	2.337	0.0168
600	3.92598(5)	5.55217(7)	25.2231(4)	2.123	0.0161
650	3.92803(5)	5.55507(7)	25.2437(4)	2.056	0.0158
700	3.93008(5)	5.55797(7)	25.2644(4)	1.959	0.0154

Note: The temperature factors of all the atoms have been refined isotropically in space group $A2_1am$ and anisotropically in $I4/mmm$. The reason for this is that it increases the number of variables refined in space group $I4/mmm$ to a number closer to the 39 variables refined in $A2_1am$ and therefore permits a better comparison of the agreement factors (that depend on the number of variables).

The analysis of the agreement factors for both space groups (Cf. Table V-IV) shows that the transition from the orthorhombic space group $A2_1am$ to the tetragonal space group $I4/mmm$ occurs somewhere between 400 and 450 °C, and are in agreement with the known transition temperature of this compound ($T_c = 440^\circ C$).

Two of the Rietveld plots at room temperature and 700°C are shown in the following page.

The results of the Rietveld refinements at two different temperatures follow in Table V-V and Table V-VI.

The complete results of the Rietveld refinement at all temperatures studied for this compound can be found in Appendix A.

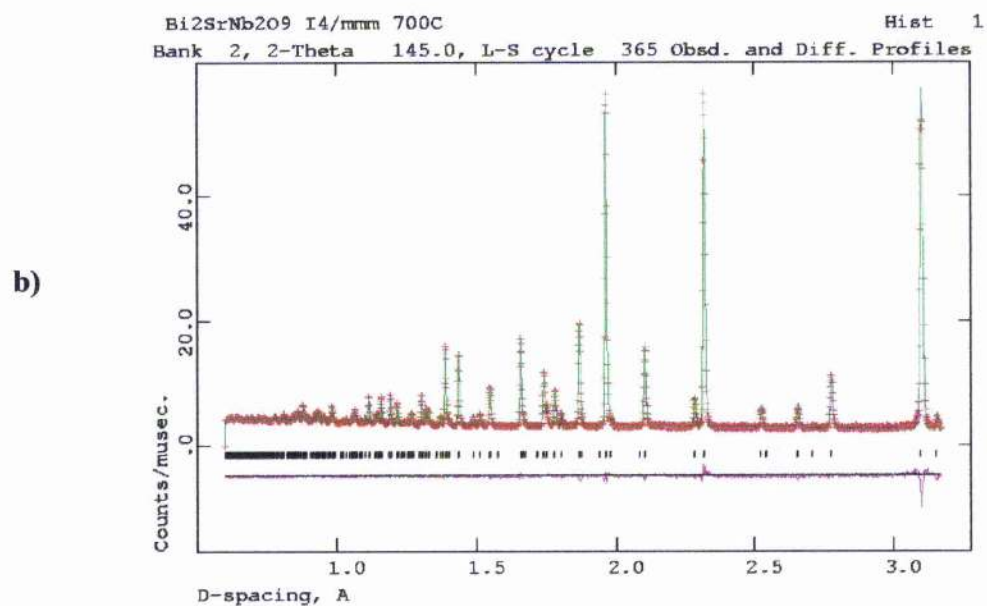
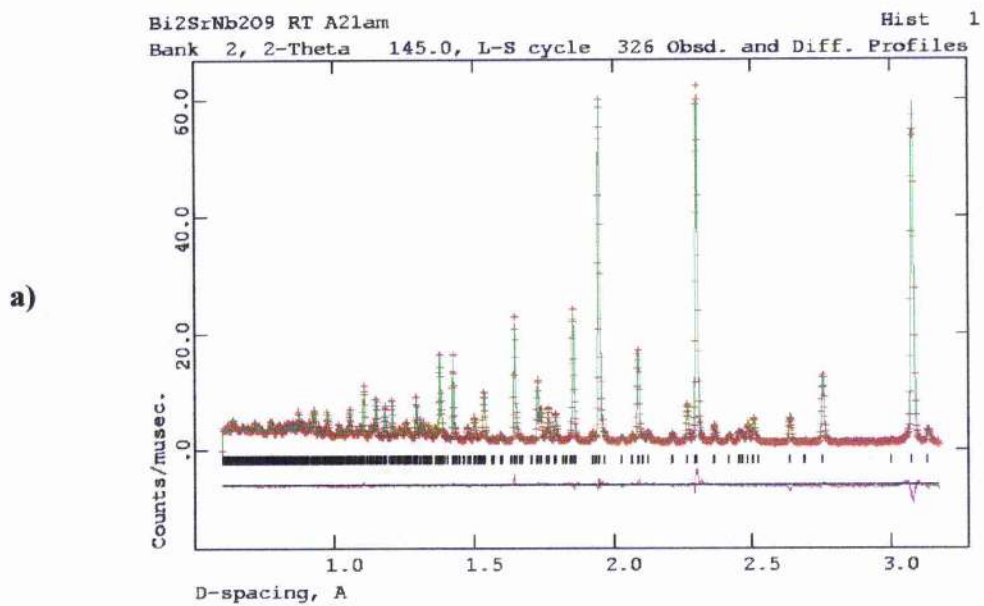


Figure 5.10: Final Rietveld plots of $\text{SrBi}_2\text{Nb}_2\text{O}_9$ at (a) room temperature in orthorhombic space group $A2_1am$ and (b) 700°C in tetragonal space group $I4/mmm$

Table V-V: Final parameters from the Rietveld refinement of SrBi₂Nb₂O₉ at 20°C: Space group A2₁am, a = 5.5167(2) Å, b = 5.5143(2) Å, c = 25.0808(4) Å, Cell volume = 762.97(4) Å³.

Atom	x	y	z	Uiso (x 100)
Sr	0.0*	0.2546(7)	0.0	0.80(4)
Bi	0.4880(9)	0.7642(5)	0.20134(6)	1.97(4)
Nb	0.5159(8)	0.7468(5)	0.41331(6)	0.11(2)
O(1)	0.542(2)	0.295(1)	0.0	0.83(7)
O(2)	0.529(1)	0.7037(6)	0.34133(8)	1.43(6)
O(3)	0.747(1)	0.9975(6)	0.2508(1)	0.58(3)
O(4)	0.754(1)	0.9748(6)	0.07019(8)	0.55(4)
O(5)	0.8124(9)	0.9632(6)	0.58447(9)	0.47(4)

*Fixed to define origin
(With all occupancy = 1)

The final agreement factors are $R_{wp} = 0.0298$, $R_p = 0.0478$, $\chi^2 = 6.761$ for 39 variable parameters.

Table V-VI: Final parameters from the Rietveld refinement of Bi₂SrNb₂O₉ at 700°C: Space group I4/mmm, a = 3.9301(5) Å, c = 25.2644(4) Å, Cell volume = 390.22(2) Å³

Name	x	y	z	U _{equiv} (x 100)
Sr	0.5	0.5	0.0	2.64*
Nb	0.0	0.0	0.08653(5)	1.01*
O(1)	0.5	0.5	0.5	3.92*
O(2)	0.0	0.5	0.25	2.46*
O(3)	0.0	0.0	0.15850(8)	6.37*
O(4)	0.0	0.5	0.07693(6)	3.70*
Bi	0.5	0.5	0.20094(6)	4.37*

*refined anisotropically
(With all occupancy = 1)

Thermal parameters multiplied by 100.0 are:

Name	U ₁₁	U ₂₂	U ₃₃
Sr	2.87(7)	2.87(7)	2.2(1)
Nb	0.96(3)	0.96(3)	1.12(5)
O(1)	4.8(1)	4.8(1)	2.2(2)
O(2)	2.25(6)	2.25(6)	2.89(9)
O(3)	9.0(2)	9.0(2)	1.04(9)
O(4)	4.63(7)	0.47(4)	5.99(8)
Bi	3.97(6)	3.97(6)	5.19(9)

The final agreement factors are $R_{wp} = 0.0154$, $R_p = 0.0279$, $\chi^2 = 1.959$ for 32 variable parameters.

Our final Rietveld refinements indicate that the crystal system is orthorhombic, crystallising in space group $A2_1am$ below T_c , and becomes tetragonal, crystallising in space group $I4/mmm$ above T_c .

A plot of the evolution of the lattice parameters a and b obtained with the Rietveld refinement in space group $A2_1am$ versus the temperature can be seen in Figure 5.11, and clearly shows the merging of a and b above T_c .

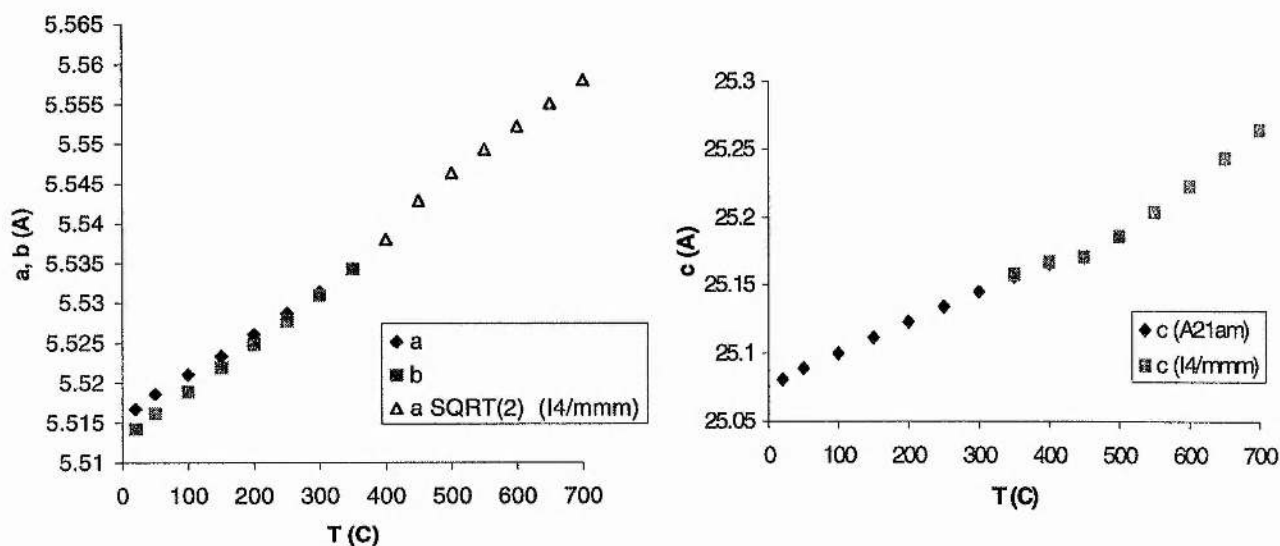
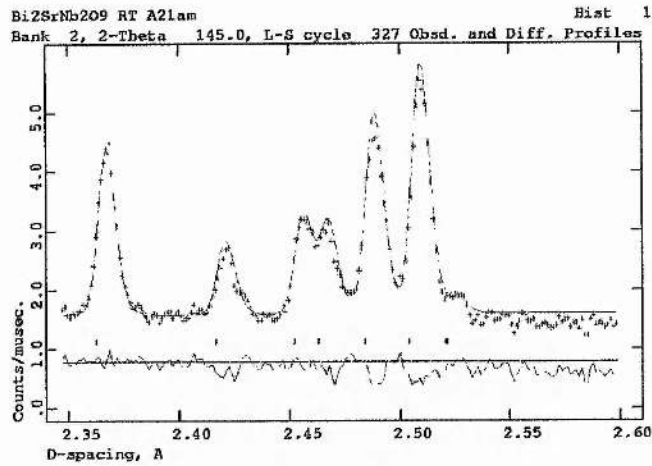


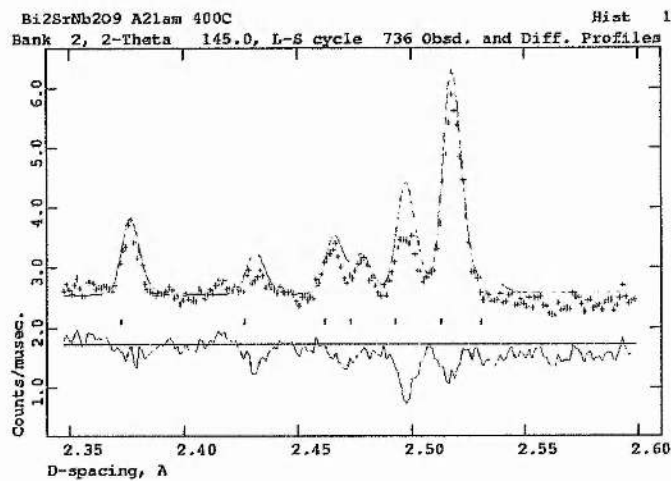
Figure 5.11: Evolution of the lattice parameters versus the temperature for $SrBi_2Nb_2O_9$ showing the merging of lattice parameters a and b above T_c

Portions of the final Rietveld plots at several temperatures, demonstrating the lack of intermediate phase for this compound, are shown in Figure 5.12.

a)



b)



c)

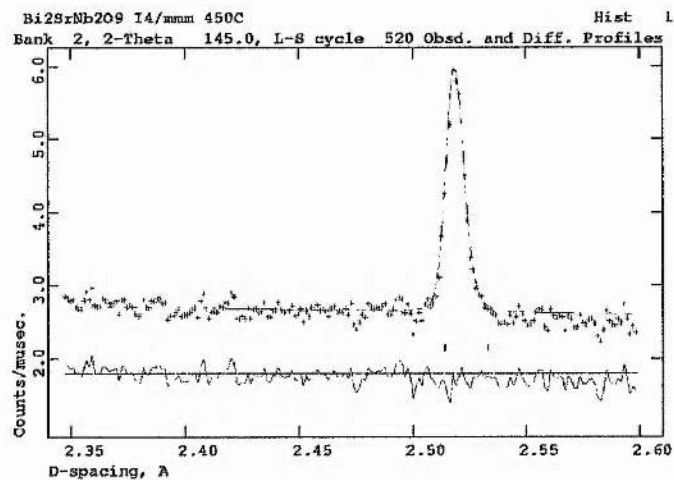


Figure 5.12: Portions of the Rietveld plots of $\text{SrBi}_2\text{Nb}_2\text{O}_9$ at (a) room temperature, (b) 400°C , and (c) 450°C , showing the non-presence of an intermediate phase between $\text{A2}_1\text{am}$ and I4/mmm

Note: The evolution of the orthorhombicity $2(a-b)/(a+b)$ versus the temperature exhibits a fairly anomalous change of slope around 150°C (Cf. Figure 5.13).

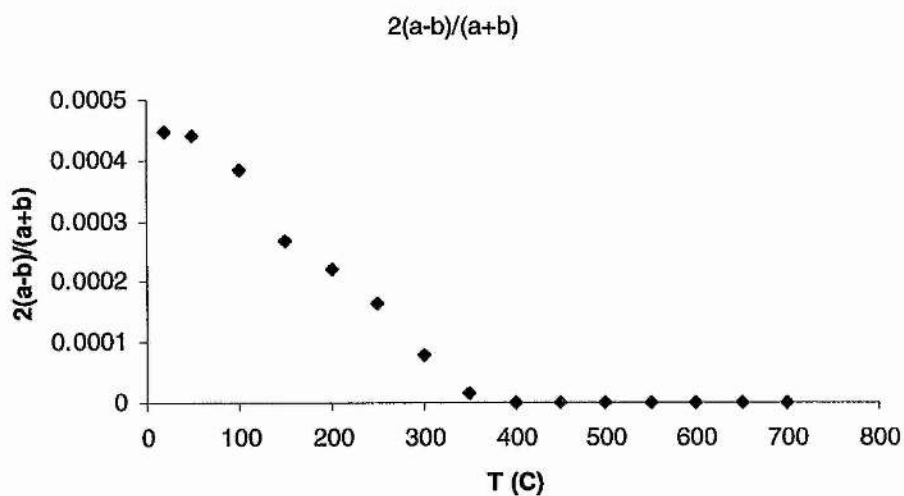


Figure 5.13: Evolution of the orthorhombicity of $\text{SrBi}_2\text{Nb}_2\text{O}_9$ with the temperature

A selection of some bondlengths at several temperatures is presented in Table V-VII.

A schematic image of the structure both below and above T_c can be seen in Figure 5.14

Table V-VII: Selection of bondlengths in SrBi₂Nb₂O₉ at several temperaturesa) Space group A2₁am

	25°C	50°C	100°C	150°C	200°C
Sr_O(1)	2.538(7)	2.535(8)	2.548(9)	2.56(1)	2.57(1)
Sr_O(1)	2.997(7)	3.000(7)	2.988(8)	2.979(9)	2.97(1)
Sr_O(1)	3.039(6)	3.028(7)	3.018(7)	3.009(8)	2.989(9)
Sr_O(1)	2.495(7)	2.508(7)	2.519(8)	2.529(8)	2.550(9)
Sr_O(4)x2	2.705(4)	2.707(4)	2.712(4)	2.709(4)	2.715(5)
Sr_O(4)x2	2.582(4)	2.582(4)	2.578(4)	2.580(5)	2.579(6)
Sr_O(5)x2	2.623(3)	2.630(3)	2.639(4)	2.649(4)	2.659(4)
Sr_O(5)x2	3.143(3)	3.137(4)	3.124(4)	3.116(4)	3.104(5)
Bi_O(2)	2.754(5)	2.760(5)	2.767(5)	2.779(6)	2.790(6)
Bi_O(2)	3.177(5)	3.174(5)	3.170(6)	3.162(6)	3.154(7)
Bi_O(2)	3.279(4)	3.278(4)	3.278(4)	3.271(4)	3.267(5)
Bi_O(2)	2.659(4)	2.663(4)	2.664(5)	2.674(5)	2.680(5)
Bi_O(3)	2.290(5)	2.290(5)	2.289(5)	2.287(6)	2.289(6)
Bi_O(3)	2.240(4)	2.244(5)	2.247(5)	2.252(5)	2.257(6)
Bi_O(3)	2.298(5)	2.296(5)	2.303(6)	2.305(6)	2.309(7)
Bi_O(3)	2.379(4)	2.379(5)	2.374(5)	2.370(6)	2.362(6)
Nb_O(1)	2.195(1)	2.194(1)	2.195(2)	2.194(2)	2.192(2)
Nb_O(2)	1.822(3)	1.822(3)	1.822(3)	1.822(3)	1.825(3)
Nb_O(4)	1.935(4)	1.940(4)	1.944(5)	1.950(5)	1.959(6)
Nb_O(4)	2.038(4)	2.035(4)	2.029(4)	2.026(5)	2.018(5)
Nb_O(5)	1.955(4)	1.952(5)	1.956(5)	1.959(5)	1.960(6)
Nb_O(5)	2.026(4)	2.025(5)	2.023(5)	2.016(5)	2.013(6)

	250°C	300°C	350°C	400°C
Sr_O(1)	2.58(2)	2.60(2)	2.65(2)	2.68(2)
Sr_O(1)	2.96(2)	2.94(1)	2.89(2)	2.87(2)
Sr_O(1)	2.973(9)	2.95(1)	2.92(1)	2.88(1)
Sr_O(1)	2.57(1)	2.59(1)	2.62(1)	2.66(2)
Sr_O(4)x2	2.716(6)	2.718(6)	2.732(8)	2.725(9)
Sr_O(4)x2	2.577(6)	2.574(7)	2.558(8)	2.560(9)
Sr_O(5)x2	2.673(5)	2.686(5)	2.715(6)	2.736(7)
Sr_O(5)x2	3.090(5)	3.075(6)	3.042(7)	3.023(8)
Bi_O(2)	2.799(7)	2.807(8)	2.829(9)	2.84(1)
Bi_O(2)	3.146(7)	3.141(8)	3.121(9)	3.11(1)
Bi_O(2)	3.263(5)	3.256(6)	3.246(6)	3.221(7)
Bi_O(2)	2.684(6)	2.694(6)	2.702(7)	2.729(8)
Bi_O(3)	2.286(7)	2.283(7)	2.279(7)	2.290(8)
Bi_O(3)	2.263(6)	2.269(7)	2.281(8)	2.289(9)
Bi_O(3)	2.318(7)	2.325(8)	2.333(8)	2.337(9)
Bi_O(3)	2.356(7)	2.349(7)	2.341(8)	2.323(8)
Nb_O(1)	2.193(2)	2.192(2)	2.189(2)	2.189(2)
Nb_O(2)	1.827(3)	1.827(4)	1.832(3)	1.831(4)
Nb_O(4)	1.964(7)	1.970(8)	1.977(10)	1.98(1)
Nb_O(4)	2.015(6)	2.009(7)	2.009(9)	2.00(1)
Nb_O(5)	1.961(7)	1.963(7)	1.963(9)	1.97(1)
Nb_O(5)	2.010(7)	2.006(8)	1.998(10)	1.998(11)

b) Space group I4/mmm

	450°C	500°C	550°C	600°C	650°C	700°C
Sr_O(1)x4	2.77144(3)	2.77317(3)	2.77465(3)	2.77608(3)	2.77754(3)	2.77899(3)
Sr_O(4)x8	2.7526(9)	2.7544(9)	2.7569(9)	2.7594(9)	2.7602(9)	2.7639(9)
Bi_O(2)x4	2.3149(8)	2.3171(7)	2.3180(8)	2.3204(8)	2.3226(8)	2.3233(8)
Bi_O(3)x4	2.9687(8)	2.9706(8)	2.9726(8)	2.9737(8)	2.9757(9)	2.9787(9)
Nb_O(1)	2.178(1)	2.181(1)	2.182(1)	2.183(1)	2.183(1)	2.186(1)
Nb_O(3)	1.818(2)	1.817(2)	1.817(2)	1.820(2)	1.820(2)	1.818(2)
Nb_O(4)x4	1.9750(2)	1.9763(2)	1.9773(2)	1.9780(2)	1.9791(2)	1.9800(2)

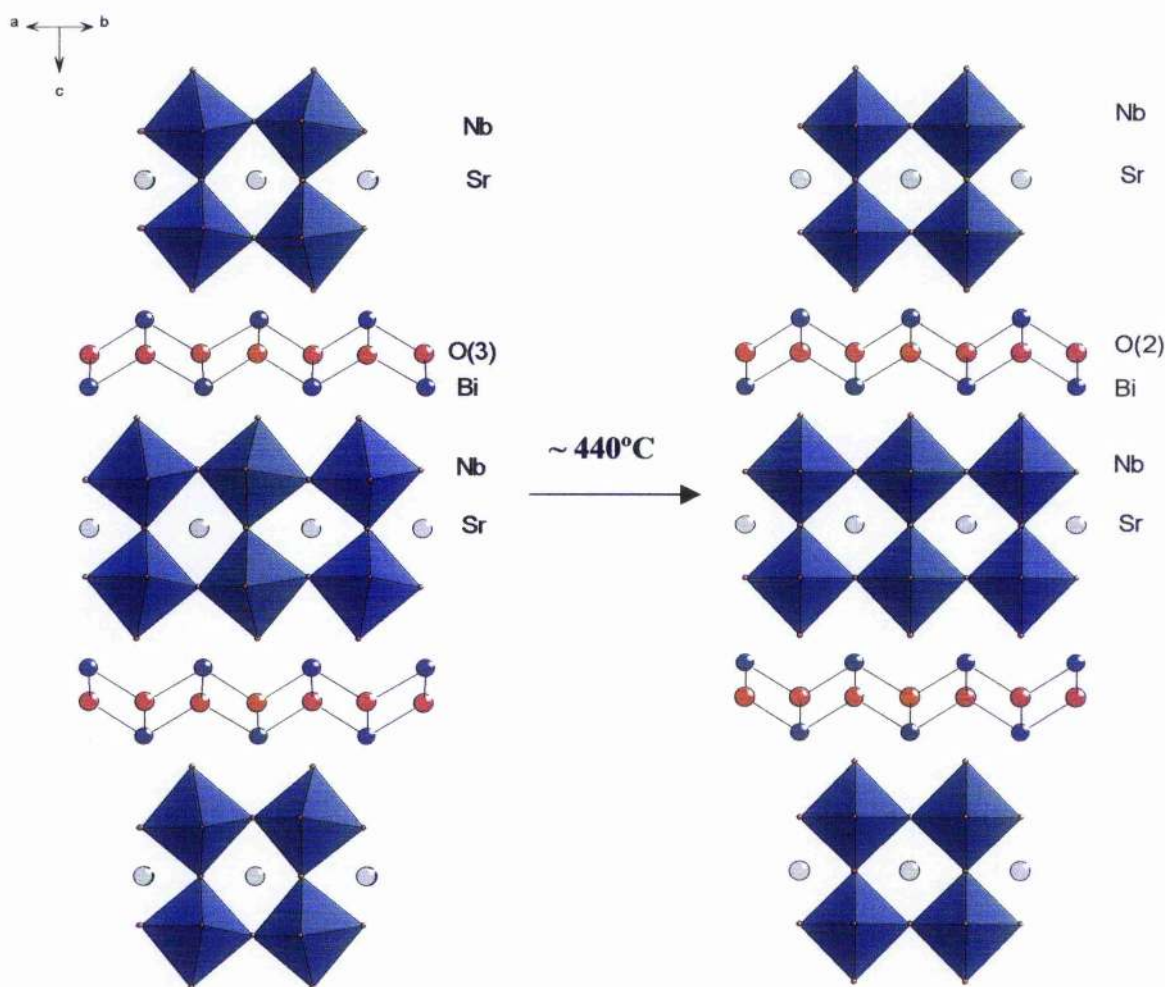


Figure 5.14: Structure of $\text{Bi}_2\text{Sr}_2\text{Nb}_2\text{O}_9$ below (orthorhombic space group $A2_1am$) and above (tetragonal space group $I4/mmm$) the phase transition

We demonstrated that this compound is orthorhombic at room temperature crystallising in the space group $A2_1am$ and transforms to the tetragonal space group $I4/mmm$ at high temperature. Contrarily to $Sr_{0.85}Bi_{2.1}Ta_2O_9$, careful inspection of the data show no “intermediate phase” for this compound, i.e. the space group $I4/mmm$ appears as soon at the transition temperature T_c .

The reason for this “intermediate phase” appearing for $Sr_{0.85}Bi_{2.1}Ta_2O_9$ and not for $SrBi_2Nb_2O_9$ is not yet understood. The differences between these two compounds that may explain this behaviour are:

1. The Bi/Sr disorder in the $[Bi_2O_2]$ layer observed only for $SrBi_2Nb_2O_9$, and that is linked to the Bi-excess / Sr-deficiency nature of $Sr_{0.85}Bi_{2.1}Ta_2O_9$.
2. The nature of the B^{5+} cation: Nb^{5+} or Ta^{5+} .

In this respect, it would be interesting to carry out a variable temperature study of the stoichiometric compound $SrBi_2Ta_2O_9$ as it was reported to present Bi/Sr disorder in the $[Bi_2O_2]$ layer.

Note: for $Sr_{0.85}Bi_{2.1}Ta_2O_9$ and $SrBi_2Ta_2O_9$, $b > a$; for $SrBi_2Nb_2O_9$, $b < a$.

(Shimakawa et al. showed that for $SrBi_2(Ta_{1-x}Nb_x)_2O_9$: with $0 < x < 0.5 \rightarrow b > a$, with $0.5 < x < 1 \rightarrow b < a$)¹¹.

5.1.3. “Solid solutions” $Bi_{2+2x/3}Sr_{1-x}Ta_2O_9$ and $Bi_2Sr_{1-x/2}Ta_{2-x}W_xO_9$

Attempts to prepare two new solid solutions based on the materials $Bi_2SrTa_2O_9$ and $Bi_2W_2O_9$ have been carried out in order to see how much A-site deficiency can be introduced. Several compositions based on $Bi_{2+2x/3}Sr_{1-x}Ta_2O_9$ (with $x = 0.2, 0.4, 0.6, 0.8$, and 1) and $Bi_2Sr_{1-x/2}Ta_{2-x}W_xO_9$ (with $x = 0.3, 1, 1.3, 1.6$, and 2) have been prepared according to the method described in Chapter 4 (§ 4.10.2.), with the starting and final temperatures being $700^\circ C$ and $850^\circ C$ for $Bi_2Sr_{1-x/2}Ta_{2-x}W_xO_9$ and $850^\circ C$ and $1000^\circ C$ for $Bi_{2+2x/3}Sr_{1-x}Ta_2O_9$.

The X-ray data collected on the Phillips diffractometer for $\text{Bi}_{2+2x/3}\text{Sr}_{1-x}\text{Ta}_2\text{O}_9$ show the non-existence of this solid solution. We seem to obtain a mixture of $\text{Bi}_2\text{SrTa}_2\text{O}_9$ and the materials introduced for reaction (Cf. Figure 5.15)

The observation of the X-ray data collected on the Phillips for $\text{Bi}_2\text{Sr}_{1-x/2}\text{Ta}_{2-x}\text{W}_x\text{O}_9$ is not more conclusive (Cf. Figure 5.16). A further heating treatment at 1000°C for the $x = 0.3$ compound gave a graph quite similar to the one of $\text{Bi}_2\text{SrTa}_2\text{O}_9$ with the presence of impurities.

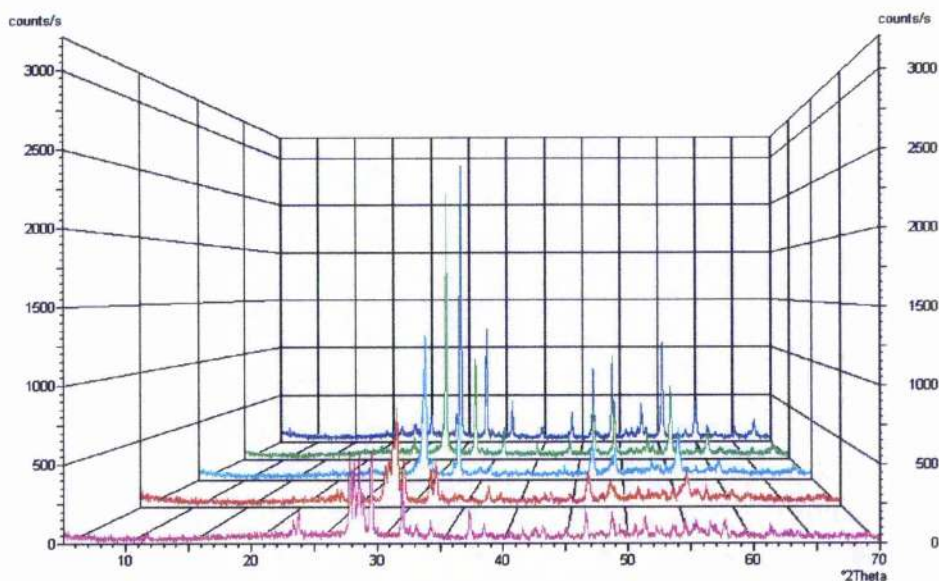


Figure 5.15: Degradation of the results obtained for the “solid solution” $\text{Bi}_{2+2x/3}\text{Sr}_{1-x}\text{Ta}_2\text{O}_9$ as x increases (blue: $x = 0.2$, green : $x = 0.4$, pale blue: $x = 0.6$, red: $x = 0.8$, pink: $x = 1$)

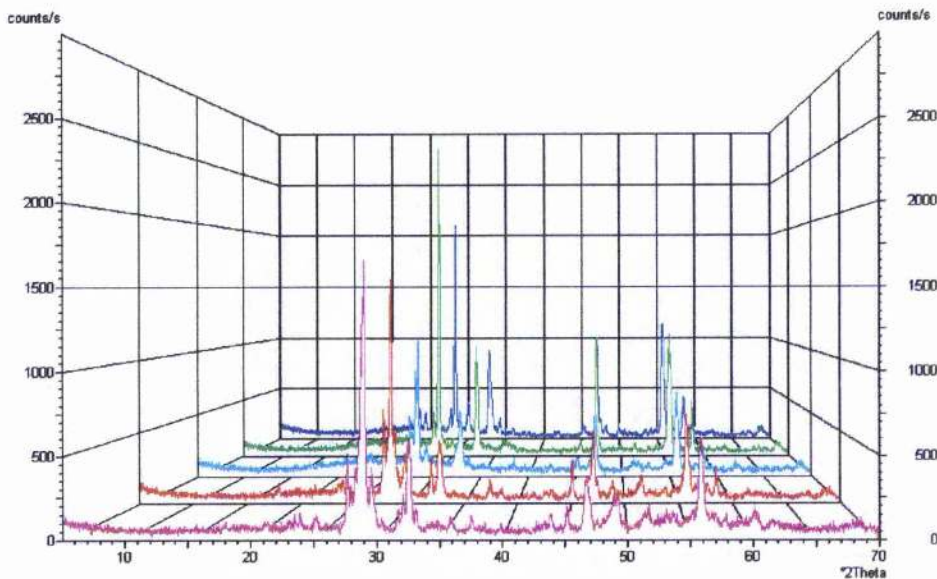


Figure 5.16: Solid solution $\text{Bi}_2\text{Sr}_{1-x/2}\text{Ta}_{2-x}\text{W}_x\text{O}_9$ with $x = 2$ (blue), $x = 1.6$ (green), $x = 1.3$ (pale blue), $x = 1$ (red), and $x = 0.3$ (pink)

5.2. $n=4$: Four perovskite layers: $\text{SrBi}_4\text{Ti}_4\text{O}_{15}$

The interest of studying this compound with four perovskite-type layers is again to compare it with the structures with two perovskite layers. In particular, the variable temperature study is interesting to establish if its thermal behaviour is similar to $\text{SrBi}_2\text{Nb}_2\text{O}_9$ (i.e. one phase transition at T_c : orthorhombic $A2_1am \rightarrow$ tetragonal $I4/mmm$) or to the more original behaviour found for $\text{Sr}_{0.85}\text{Bi}_{2.1}\text{Ta}_2\text{O}_9$ (orthorhombic $A2_1am \rightarrow$ orthorhombic $Amam \rightarrow$ tetragonal $I4/mmm$).

A study by electron diffraction suggested a similar transition sequence orthorhombic \rightarrow orthorhombic \rightarrow tetragonal²¹.

The structure of this compound has been studied at room temperature by powder X-ray diffraction on the in-house Stoe STADI/P powder diffractometer and on the high-

resolution X-ray powder diffractometer on the beamline 9.1 at the CLRC Daresbury Laboratory.

Precise neutron diffraction study was carried out on HRPD at ISIS at several temperatures: Room temperature, 200, 300, 400, 500, 550, 600, 650, 700 and 800°C. Each data collection lasting approximately 2 hours for a total collected value of 65 μ Ahrs.

5.2.1. Room temperature study

The inspection of the raw data at room temperature clearly indicated an A centred cell. Therefore, at room temperature the structure has been refined in orthorhombic space group $A2_1am$ ($\chi^2 = 6.581$, $R_{wp} = 0.1072$) rather than $I4/mmm$ ($\chi^2 = 18.97$, $R_{wp} = 0.1827$) or F centered (space group $Fmmm$) as suggested for $Bi_5FeTi_3O_{15}$ ²². The Rietveld plot shows that the F-centered version doesn't index at least two peaks, one before $d = 2.3$ and one around 2.33 \AA as it is shown in Figure 5.17.

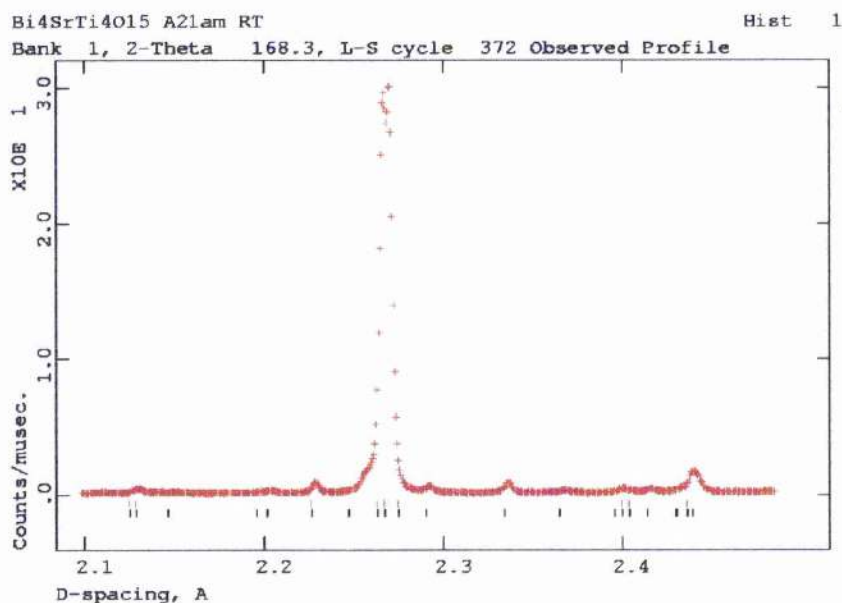


Figure 5.17: Raw neutron diffraction data for $SrBi_4Ti_4O_{15}$. The red tickmarks (above) representing the F-centered space group do not index two peaks. The black tickmarks correspond to $A2_1am$

We started the Rietveld refinements in space group $A2_1am$ with the atomic coordinates derived from the model reported by Kubel ²², but shifting the origin by $(\frac{1}{4}, \frac{1}{4}, 0)$ in accordance with the different space group.

The relative occupancy of the two cations Bi^{3+} and Sr^{2+} in the different sites have been established using powder X-ray diffraction data from the STOE and station 9.1 at Daresbury synchrotron. The choice of X-ray rather than neutron diffraction for this analysis is justified by the fact that the neutron scattering lengths for Bi and Sr are quite close (7.02 and 8.53×10^{-15} m respectively), which doesn't allow to differentiate them properly.

These refinements showed no significant occupancy of the $[M_2O_2]$ layer by Sr.

The relative occupancy of Bi and Sr in the perovskite sites are as follows :

$$Bi(1) / Sr(1) : 65.1\%(0.8) / 34.9\%(0.8), Bi(2) / Sr(2) : 67.5\%(0.4) / 32.5\%(0.4)$$

Nb : in the X-ray refinements, the positions of the oxygens atoms were not refined.

The relative occupancies in these sites were consequently fixed to these values for the refinements of the neutron data at all temperatures studied.

The results of the Rietveld refinement at room temperature is shown in the table below (Table V-VIII). The final Rietveld plot at room temperature follows in Figure 5.18.

Table V-VIII: Final parameters from the Rietveld refinement of SrBi₄Ti₄O₁₅ at room temperature: Space group A2₁am, a = 5.4507(1) Å, b = 5.4376(1) Å, c = 40.9841(8) Å, Cell volume = 1214.716(8) Å³

Atom	x	y	z	U _{iso} (x100)
Bi(1) ²	0.25 ¹	0.258(2)	0	3.3(2)
Bi(2) ²	0.255(3)	0.248(1)	0.10409(10)	4.3(1)
Bi(3)	0.245(2)	0.263(1)	0.21881(9)	3.5(1)
Ti(1)	0.277(3)	0.250(3)	0.45032(14)	1.0(1)
Ti(2)	0.268(3)	0.242(2)	0.34697(16)	1.7(2)
O(1)	0.306(3)	0.203(3)	0.5	4.5(4)
O(2)	0.580(3)	0.538(3)	0.0515(2)	2.8(2)
O(3)	0.301(3)	0.298(2)	0.40348(14)	2.6(2)
O(4)	0.523(2)	0.495(2)	0.14058(14)	1.2(2)
O(5)	0.286(3)	0.212(2)	0.30456(14)	3.2(2)
O(6)	0.510(3)	0.498(2)	0.2502(2)	2.3(2)
O(7)	0.017(4)	-0.019(2)	0.0433(2)	4.7(3)
O(8)	0.047(2)	0.016(2)	0.1479(2)	4.1(2)

1. Fixed to define origin of polar axis
2. Composition fixed at 0.67 Bi / 0.33 Sr

The final agreement factors are: $\chi^2 = 6.1$, $R_{wp} = 0.104$ for 60 variable parameters.

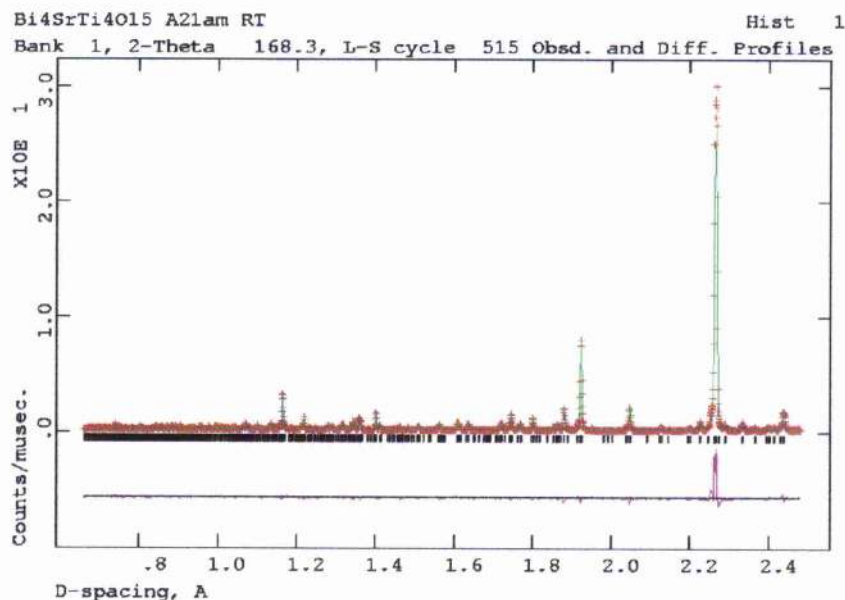


Figure 5.18: Final Rietveld plot of SrBi₄Ti₄O₁₅ at room temperature, space group A2₁am

Displacements of the Bi/Sr in the A site relative to their local environment can be seen in Figure 5.19.

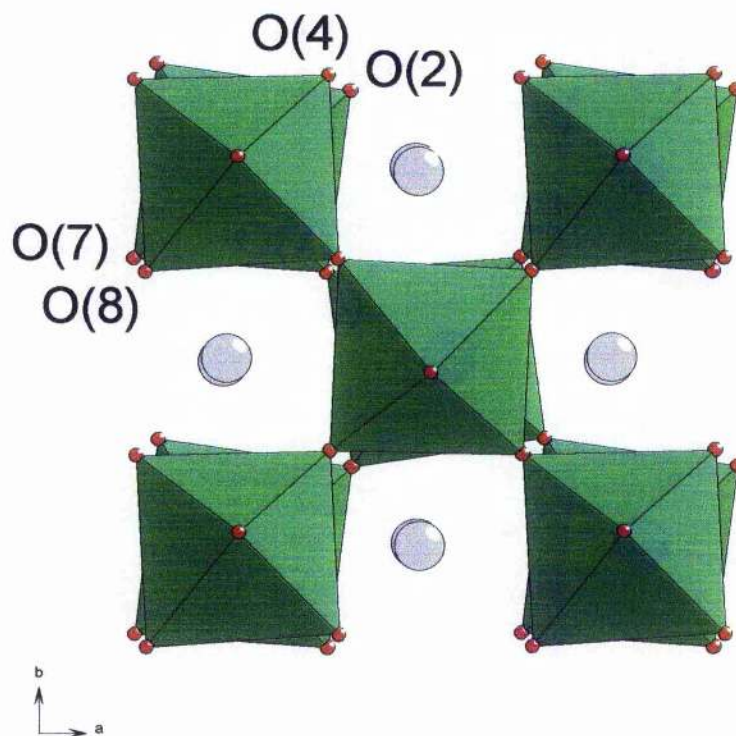


Figure 5.19: Projection of the perovskite block along the c-axis showing the rotation of the octahedra and displacements of the A-site cations along a

5.2.2. Variable temperature study

The refinements were carried out using the two space groups $A2_1am$ and $I4/mmm$ at each temperature. The resulting goodness-of-fit indices (χ^2) are given in the following table.

Table V-IX: Final parameters and agreement factors from the Rietveld refinements of SrBi₄Ti₄O₁₅ at several temperatures in space groups A2₁am and I4/mmm.

T (°C)	A2 ₁ am (60 var.)				I4/mmm anisotropic (44 var.)		
	χ^2	a	b	c	χ^2	a	c
20	6.581	5.4507(1)	5.4376(1)	40.9841(8)	16.29	3.8498(2)	40.984(2)
200	3.655	5.45674(1)	5.44679(1)	41.0814(8)	4.638	3.85518(8)	41.082(1)
300	3.564	5.46041(1)	5.45235(1)	41.1431(7)	3.643	3.85843(6)	41.1438(8)
400	3.488	5.4643(2)	5.4586(2)	41.2095(7)	2.882	3.86190(5)	41.2094(6)
500	3.542	5.4672(5)	5.4667(5)	41.2793(6)	2.394	3.86222(6)	41.2170(7)
550	3.627	5.4710(6)	5.4708(6)	41.3092(6)	2.287	3.86853(4)	41.3089(5)
600	3.672	5.4752(7)	5.4751(7)	41.3306(6)	2.311	3.87156(4)	41.3304(5)
650	3.853	5.4797(7)	5.4795(7)	41.3524(7)	2.42	3.87469(4)	41.3523(5)
700	3.955	5.4836(7)	5.4833(7)	41.3793(7)	2.622	3.87741(5)	41.3792(5)
800	3.856	5.4910(6)	5.4905(6)	41.4433(7)	2.378	3.88260(4)	41.4431(5)

Again, above 550°C, the structure is transformed from orthorhombic A2₁am to the undistorted tetragonal phase I4/mmm. This can be seen in the merging of lattice parameters a and b in Figure 5.20 and coincides approximately with the established value of T_c found in the literature for this compound (between T_c = 520°C²⁰ and T_c = 570°C²¹).

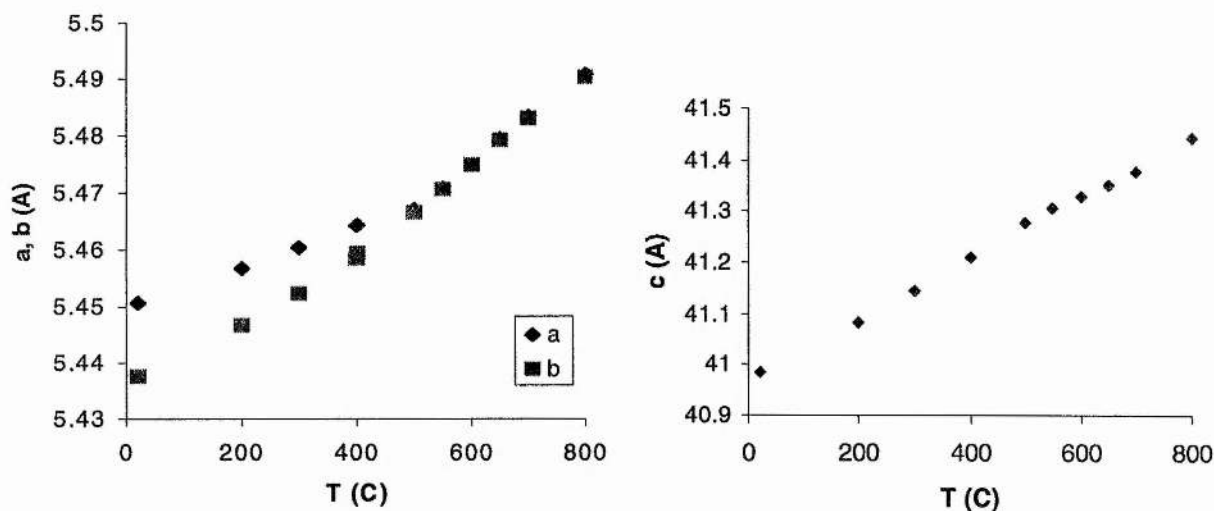


Figure 5.20: Evolution of the lattice parameters of SrBi₄Ti₄O₁₅ versus the temperature, showing the merging of a and b lattice parameters above T_c

The disappearance of the peak (1 2 26) at $d \sim 1.323 \text{ \AA}$ (characteristic of an A-centred space group) as soon as 650°C proves that the tetragonal space group $I4/mmm$ is valid at this temperature and above. This (1 2 26) peak at $d \sim 1.323 \text{ \AA}$ still exists at $T = 550^\circ\text{C}$ and $T = 600^\circ\text{C}$ (Cf. Figure 5.21 and Figure 5.22). A refinement at this temperature in the space group Amm was carried out and led to good agreement factors ($\chi^2 = 3.5$ for 67 variables) but not significantly better than the refinement in space group $A2_1am$ ($\chi^2 = 3.6$ for 60 variables).

In conclusion, these results suggest the presence of an intermediate paraelectric phase in orthorhombic space group Amm in this compound. This intermediate phase exists between $T \sim 550^\circ\text{C}$ and $T \sim 650^\circ\text{C}$. However, this is a far less pronounced phenomenon than in the case of $\text{Sr}_{0.85}\text{Bi}_{2.1}\text{Ta}_2\text{O}_9$ (Cf. § 5.1.1.).

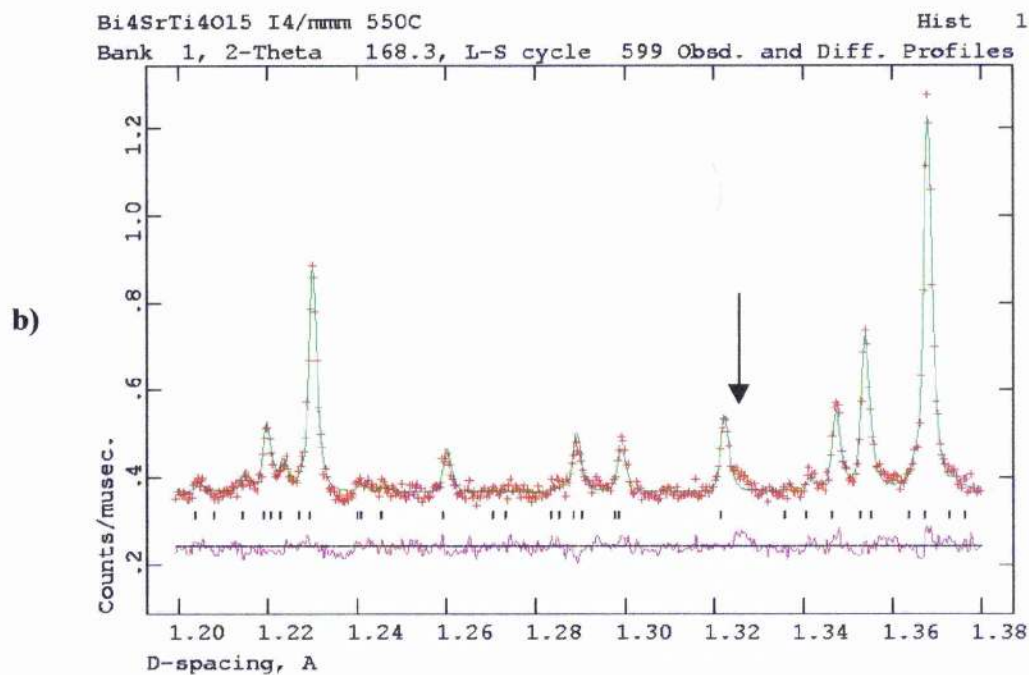
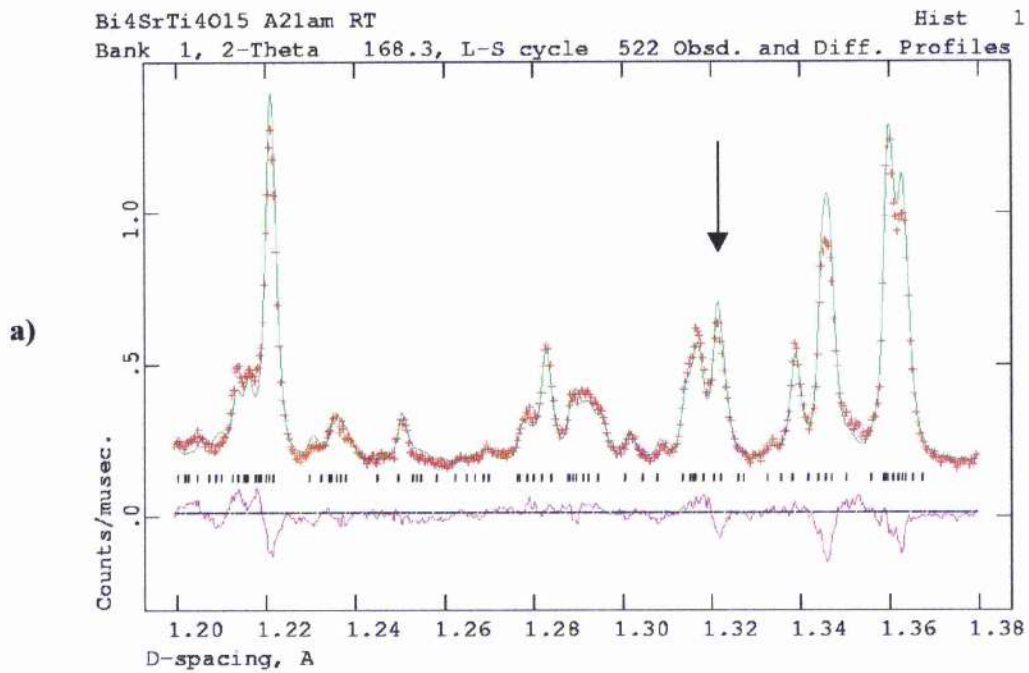


Figure 5.21: Portion of the Rietveld plot of $\text{SrBi}_4\text{Ti}_4\text{O}_{15}$ at room temperature (a) and 550°C (b) showing the (1 2 2 6) reflection due to the orthorhombic A-centred space group

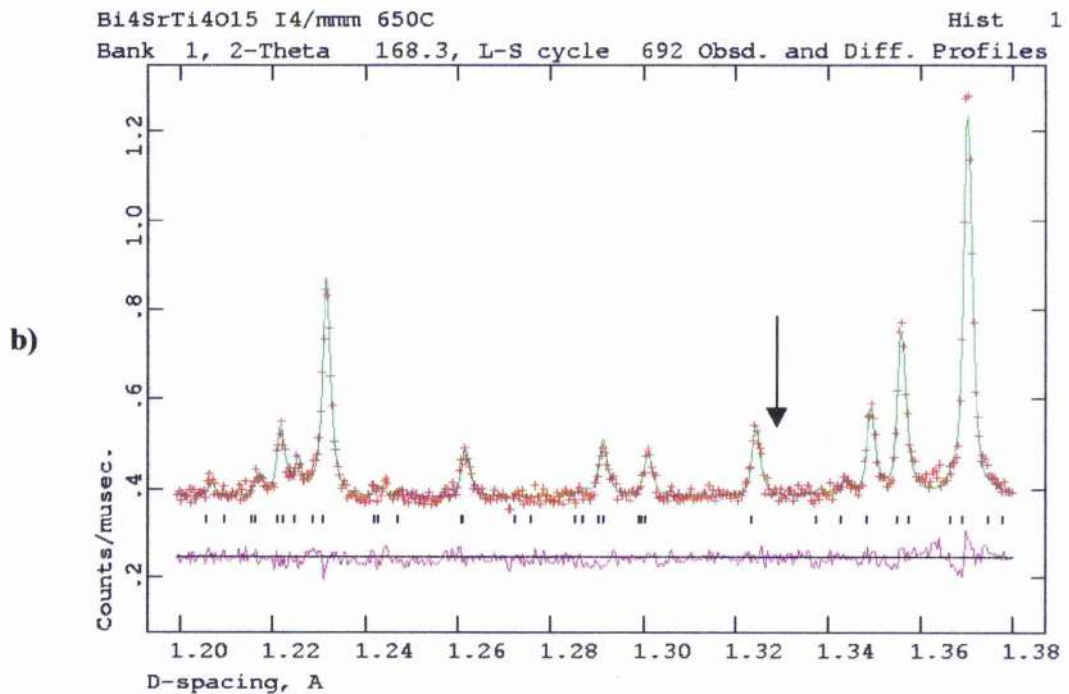
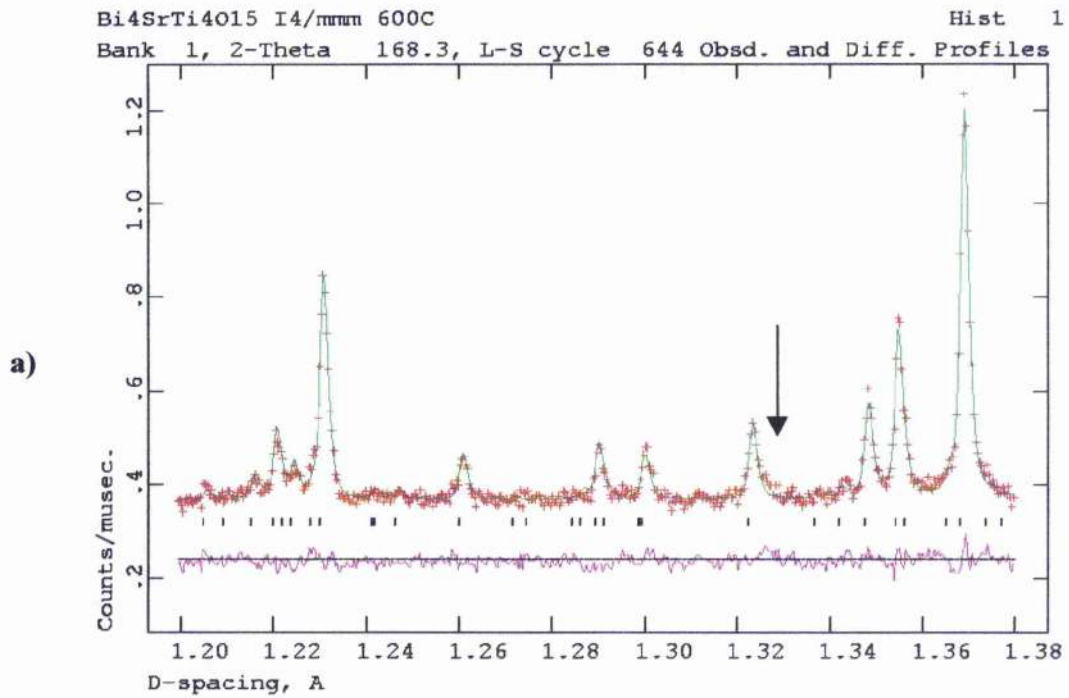


Figure 5.22: Disappearance of the (1 2 2 6) reflection between 600 (a) and 650°C (b) due to the orthorhombic A-centred \rightarrow tetragonal I-centred transition

The gradual decrease of the tiltings of the octahedra can be visualised in Figure 5.23, showing the increase of the inter-octahedral O-O-O angles with the temperature below T_c . All these angles are equal to 180° above the phase transition.

Figure 5.24 represents the evolution of the Bi(3)-O(5) bondlengths versus the temperature, and is an other indication of the reduction of the tiltings of the octahedra as the temperature increases.

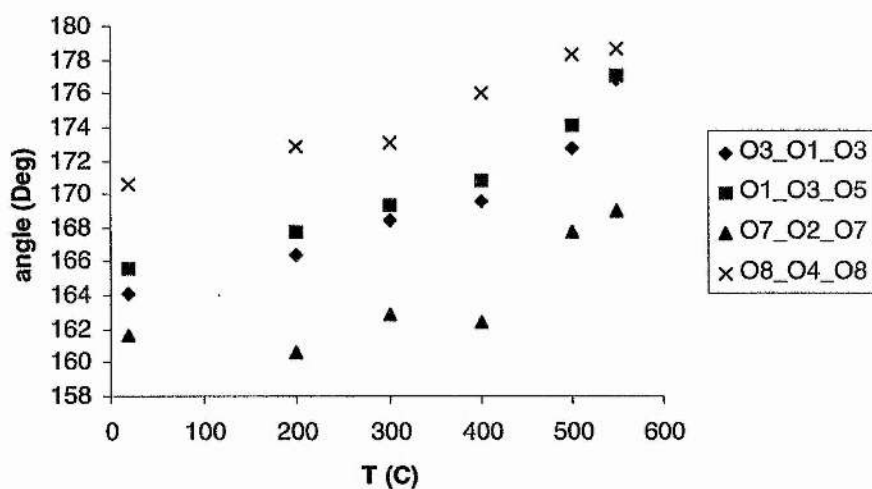


Figure 5.23: Evolution of the inter-octahedral O-O-O angles with the temperature in $\text{SrBi}_4\text{Ti}_4\text{O}_{15}$

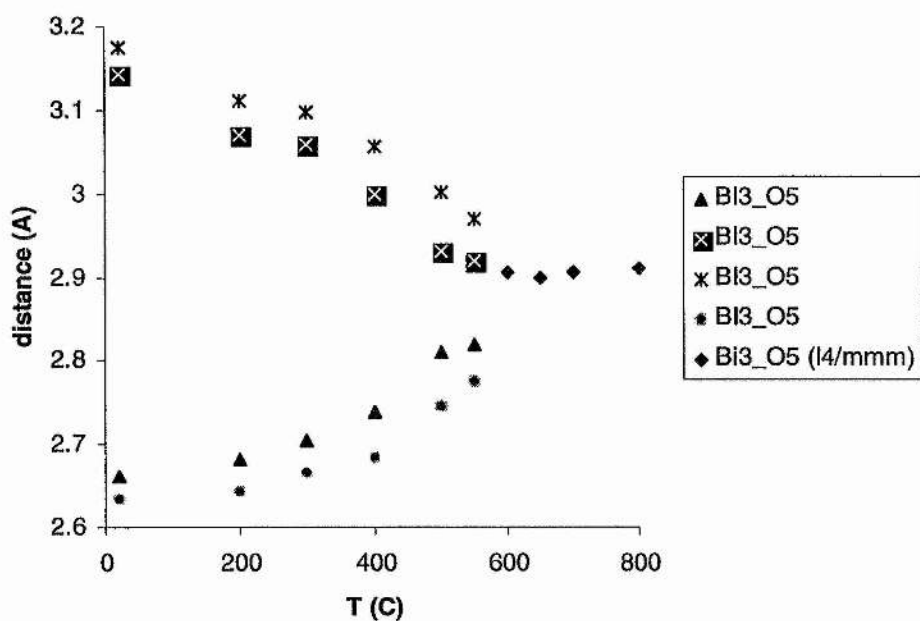


Figure 5.24: Evolution of the Bi(3)-O(5) bondlengths with the temperature in $\text{SrBi}_4\text{Ti}_4\text{O}_{15}$

The complete results of the Rietveld refinements at all temperature are in Appendix B.

A representation of the structure at different temperatures is shown in Figure 5.25.

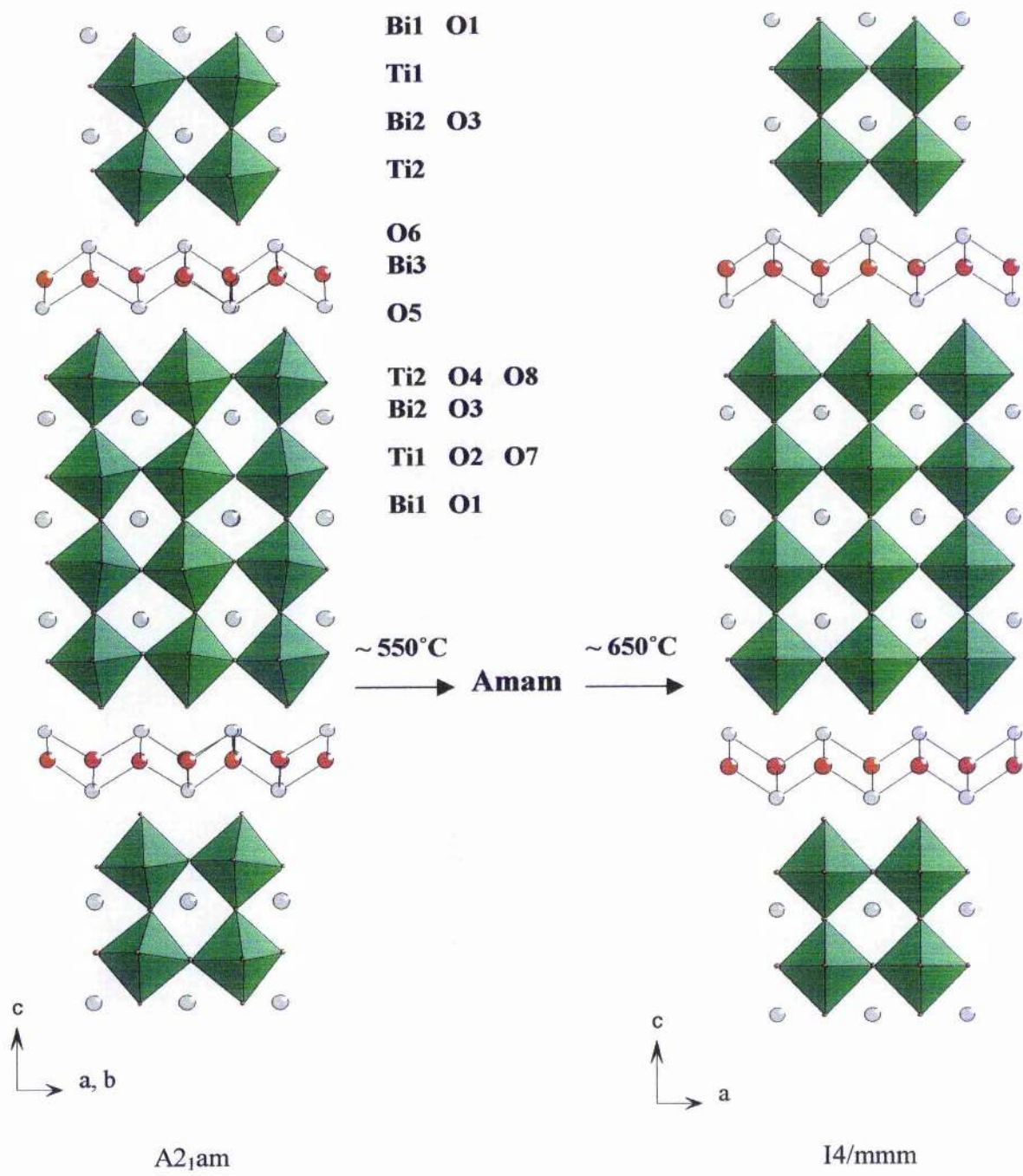


Figure 5.25: Structure of SrBi₄Ti₄O₁₅ below and above the transition temperature

Conclusion

In this chapter, temperature-dependant structural studies of several Aurivillius phases presenting an even number of perovskite-type layer have been carried out by X-ray and powder neutron diffraction. They show unexpected and interesting behaviour for many of them.

In particular, it has been demonstrated the existence of a second paraelectric phase with orthorhombic space group for some Aurivillius phases with two or four perovskite-type layers (i.e. $\text{Sr}_{0.85}\text{Bi}_{2.1}\text{Ta}_2\text{O}_9$ and $\text{SrBi}_4\text{Ti}_4\text{O}_{15}$). This behaviour, never observed before, might be present in many more compounds with this type of structure. This is however not observable for all "even-layer" Aurivillius phases (e.g. $\text{SrBi}_2\text{Nb}_2\text{O}_9$), the reason for this is not yet understood. Partial occupancy of Bi in the perovskite site and A cation in the $[\text{Bi}_2\text{O}_2]$ site is also observed for some, but not all compounds.

It has been shown that the ferroelectric phase adopts the orthorhombic space group $A2_1am$ for all compounds studied. The high temperature paraelectric phase crystallises in tetragonal space group $I4/mmm$ also for all of them, but with an intermediate paraelectric orthorhombic phase $Amam$ for $\text{Sr}_{0.85}\text{Bi}_{2.1}\text{Ta}_2\text{O}_9$ and $\text{SrBi}_4\text{Ti}_4\text{O}_{15}$.

References

- ¹ R. E. Newnham, R. W. Wolfe and J. F. Dorrian, *Mat. Res. Bull.*, 1971, **6**, 1029
- ² C. A-Paz de Araujo, J. D. Cuchiaro, L. D. McMillan, M. C. Scott and J. F. Scott, *Nature (London)*, 1995, **374**, 627
- ³ Y. Shimakawa, Y. Kubo, Y. Nakagawa, S. Goto, T. Kamiyama, H. Asano and F. Izumi, *Phys. Rev. B*, 2000, **61**, 6559
- ⁴ R. Macquart, B. J. Kennedy and Y. Shimakawa, *J. Solid State Chem*, 2001, **160**, 174

-
- ⁵ S.M. Blake, M.J. Falconer, M. McCreeedy and P. Lightfoot, *J. Mater. Chem.*, 1997, **7**(8), 1609
- ⁶ K. Singh, D. K. Bopardikar and D. V. Atkare, *Ferroelectrics*, 1988, **82**, 55
- ⁷ Y. Wu and G. Cao, *Appl. Phys. Lett.*, 1999, **75**, 2650
- ⁸ Y. Wu, M. J. Forbess, S. Seraji, S. J. Limmer, T. P. Chou and G. Cao, *J. Appl. Phys.*, 2001, **89**, 5647
- ⁹ Y. Wu and G. Cao, *J. Mater. Res.*, 2000, **15**, 1583
- ¹⁰ Y. Wu, M. J. Forbess, S. Seraji, S. J. Limmer, T. P. Chou and G. Cao, *Mater. Sci. And Engineering B*, 2001, **86**, 70
- ¹¹ Y. Shimakawa, Y. Kubo, Y. Tauchi, T. Kamiyama, H. Asano and F. Izumi, *Appl. Phys. Lett.*, 2000, **77**, 2749
- ¹² R. E. Cohen, *Nature (London)*, 1992, **358**, 136
- ¹³ E. C. Subbarao, *Integrated Ferroelectrics*, 1996, **12**, 33
- ¹⁴ Y. Shimakawa, Y. Kubo, Y. Nakagawa, T. Kamiyama, H. Asano and F. Izumi, *Appl. Phys. Lett.*, 1999, **74**, 1904
- ¹⁵ A. Onodera, T. Kubo, K. Yoshio, S. Kojima, H. Yamashita, and T. Takama, *Jpn. J. Appl. Phys.*, 2000, **Part 1 39**, 5711
- ¹⁶ R. E. Newnham and R. W. Wolfe, *Mat. Res. Bull.*, 1973, **8**, 1183
- ¹⁷ I. M. Reaney, M. Roulin, H. S. Shulman, N. Setter, *Ferroelectrics*, 1995, **165**, 295
- ¹⁸ B. Jimenez, P. Duran-Martin, R. J. Jimenez-Rioboo and R. Jimenez, *J. Phys.: Condens. Matter.*, 2000, **12**, 3883
- ¹⁹ R. L. Withers, J. G. Thompson and A. D. Rae, *J. Solid State Chem.*, 1991, **94**, 404
- ²⁰ E. C. Subbarao, *J. Phys. Chem. Solids*, 1962, **23**, 665
- ²¹ I. M. Reaney and D. Damjanovic, *J. Appl. Phys.*, 1996, **80**, 4223
- ²² F. Kubel and H. Schmid, *Ferroelectrics*, 1992, **129**, 101

Chapter 6 : Aurivillius phases with an odd number of perovskite layers

Introduction	83
6.1. Structure and phase transition in $\text{Bi}_4\text{Ti}_3\text{O}_{12}$	85
6.1.1. HRPD data	86
6.1.2. Polaris data	96
6.1.3. a.c. Impedance spectroscopy measurements	104
6.2. Solid solution $\text{Bi}_{4-x}\text{Sr}_x\text{Ti}_{3-x}\text{Nb}_x\text{O}_{12}$	105
6.2.1. X-ray results of $\text{Bi}_{4-x}\text{Sr}_x\text{Ti}_{3-x}\text{Nb}_x\text{O}_{12}$	106
6.2.2. Neutron results of $\text{Bi}_{1.8}\text{Sr}_{2.2}\text{Ti}_{0.8}\text{Nb}_{2.2}\text{O}_{12}$	114
6.3. Solid solution $\text{Bi}_{4-x}\text{La}_x\text{Ti}_3\text{O}_{12}$ ($x = 1$ and 2)	120
6.4. $\text{Bi}_2\text{Ca}_2\text{TiNb}_2\text{O}_{12}$	125
6.5. $\text{Bi}_2\text{Ln}_2\text{Ti}_3\text{O}_{12}$ ($\text{Ln} = \text{Eu}, \text{Nd}$)	126
Conclusion	128
References	128

Introduction

The literature on Aurivillius phases containing an odd number n of perovskite layers, of general formula $(\text{M}_2\text{O}_2)(\text{A}_{n-1}\text{B}_n\text{O}_{3n+1})$, includes compounds with $n = 1$ (e.g. Bi_2WO_6), $n = 3$ ($\text{Bi}_4\text{Ti}_3\text{O}_{12}$ and related compounds $\text{A}_x\text{Bi}_{4-x}\text{Ti}_{3-x}\text{B}_x\text{O}_{12}$ with $\text{A} = \text{Pb}, \text{Sr}, \text{Ba}, \dots$ $\text{B} = \text{Ti}, \text{Nb}, \text{Ta}, \dots$) and $n = 5$ ($\text{A}_2\text{Bi}_4\text{Ti}_5\text{O}_{18}$ with $\text{A} = \text{Ba}, \text{Pb}, \text{Sr}$).^{1,2,3}

The crystal space groups reported in the literature for these kind of compounds are tetragonal, $I4/mmm$, orthorhombic, $Fm\bar{3}m$ and $B2cb$, or monoclinic, $B1a1$.

The “ideal” undistorted materials crystallise in space group $I4/mmm$, the other space groups deriving from this “ideal” one are due to:

- Tilting of the BO_6 octahedra.
- Off-center displacement of the A cation in the perovskite block which is related to the ferroelectric behaviour of this family of compounds.

Essentially, the highest “ideal” symmetry of these compounds is $I4/mmm$, usually lowered down to the orthorhombic space group $B2cb$ at low temperature⁴, $B1a1$ being a very subtle variation of $B2cb$ observed only for one material ($\text{Bi}_4\text{Ti}_3\text{O}_{12}$) synthesised as a single crystal⁵. $Fm\bar{3}m$ is probably only a theoretical orthorhombic space group

deriving from I4/mmm by the distortion of the lattice parameters (with $a_0 \approx b_0 \approx a_T\sqrt{2}$, where a_0 and b_0 are the lattice parameters in the orthorhombic space group and a_T in the tetragonal one) without change of the atoms positions in the unit cell (cf. Figure 5.1. in Chapter 5). This space group, unlike B2cb, does not allow tilting of the BO_6 octahedra.

A general picture of a structure presenting three perovskite-type layers in the “ideal” parent structure I4/mmm and the distorted one B2cb can be visualised in the typical example of $\text{Bi}_4\text{Ti}_3\text{O}_{12}$ in Figure 6.2. (page 93).

A review of a series of bismuth titanate solid solutions with $n = 3$ perovskite-type layers was published in 1972 by Armstrong and Newnham⁶ for $\text{A}_x^{\text{III}}\text{Bi}_{4-x}\text{Ti}_4\text{O}_{12}$ ($\text{A}^{3+} = \text{La, Pr, Nd, Sm, Eu, Gd, Tb, Dy, Ho, Er, Tm, Yb, Lu}$), $\text{Bi}_4\text{Ti}_{3-x}\text{B}_x^{\text{IV}}\text{O}_{12}$ ($\text{B}^{4+} = \text{Ge, Sn, Hf, Zr}$) and $\text{A}_x^{\text{II}}\text{Bi}_{4-x}\text{Ti}_{4-x}\text{B}_x^{\text{V}}\text{O}_{12}$ ($\text{A}^{2+} = \text{Ca, Sr, Ba, Pb}$ and $\text{B}^{5+} = \text{Nb, Ta}$). They observed that di- and trivalent ions with an ionic radius r between 1.1 and 1.3 Å could substitute Bi in the perovskite site while ions with $0.58\text{Å} < r < 0.65\text{Å}$ substitute Ti^{4+} in the octahedral site; however they didn't observe any substitution for Bi in the $[\text{Bi}_2\text{O}_2]^{2+}$ layer.

The first report of substitution of Bi in the $[\text{Bi}_2\text{O}_2]^{2+}$ layer was by Millan et al. in 1993⁷. They reported the substitution by Pb^{2+} in $\text{Bi}_{2-x}\text{Pb}_x\text{SrNb}_2\text{O}_9$ over the range $0 \leq x \leq 2$. This study was completed later by several others reporting the substitution of Pb^{2+} for Bi^{3+} in a series of $n = 2$ and $n = 3$ Aurivillius phases^{8,9,10}

Later substitution by other p-block cations all containing a stereochemically active lone pair of electrons (Sb^{3+} and Te^{4+}) were also reported in the solid solutions $\text{Bi}_{2-x}\text{Sb}_x\text{SrNb}_2\text{O}_9$ for Sb^{3+} and $\text{Bi}_{2-x}\text{Te}_x\text{SrNb}_{2-x}\text{Ti}_x\text{O}_9$ for Te^{4+} ¹¹.

The substitution of this particular Bi by a cation that doesn't contain any active lone pair of electrons (Ba, Sr or Ca) was first reported in 1997 by Blake et al. for the $n = 2$ Aurivillius phases $\text{ABi}_2\text{Nb}_2\text{O}_9$ ¹²; the same kind of study for $\text{ABi}_2\text{Ta}_2\text{O}_9$ ¹³ recently confirmed this disorder Bi/A. Both studies found that the amount of disorder increases with the ionic radius of the A^{2+} cation and the amount of disorder found for each compound can be found in the following table.

Table VI-I: amount of disorder* Bi/A for the compounds of type $ABi_2B_2O_9$ (A = Ca, Sr, Ba ; B = Nb, Ta)

A ²⁺ cation	Ionic radius (Å)	$ABi_2Nb_2O_9$ ¹²	$ABi_2Ta_2O_9$ ¹³
Ca ²⁺	1.12	5 %	2.5 %
Sr ²⁺	1.26	10.6 %	7.5 %
Ba ²⁺	1.42	13.4 %	22 %

Note: Ionic radii are for a coordination number CN = 8

* i.e. fractional occupancy of Bi in A site

This chapter present our work on several compositions containing three perovskite-type layers. The aims of this chapter are:

1. To study the crystal structure and the nature of the phase transition in the parent phase for n = 3: $Bi_4Ti_3O_{12}$
2. To explore the possibility of Sr substitution into the $[Bi_2O_2]^{2+}$ layers. This has been studied through the solid solution $Bi_{4-x}Sr_xTi_{3-x}Nb_xO_{12}$.

6.1. Structure and phase transition in $Bi_4Ti_3O_{12}$

$Bi_4Ti_3O_{12}$ is a well known ferroelectric material and its bulk material shows a large remanent polarisation P_r ¹⁴ which makes it a good candidate for Ferroelectric memories.

This product was synthesised by traditional solid state reaction according to the method described in § 4.10.2.

Here is presented the first temperature-dependant structural study of this compound.

A first Rietveld refinement of X-ray data of $Bi_4Ti_3O_{12}$ at room temperature has been undertaken with two envisaged symmetries, Fmmm (centrosymmetric) and B2cb (not centrosymmetric), in order to judge the sensitivity of the X-ray data to octahedral

tilting, as the ferroelectric properties of this compound implies a non-centrosymmetric space group.

The final agreement factors after Rietveld refinement for this primary study are the following ones:

- Space group Fmmm: $\chi^2 = 1.014$, $R_{wp} = 0.1835$, $R_p = 0.1383$ for 22 variables.
- Space group B2cb: $\chi^2 = 0.8954$, $R_{wp} = 0.1721$, $R_p = 0.1243$ for 43 variables.

Powder neutron diffraction has been used for more detailed study of this compound as well as to analyse the nature of the structure transformations that happen above and below the ferroelectric-paraelectric phase transition temperature (T_c), which is reported to be at 675°C .¹⁵

These studies have been carried out using neutron rather than X-ray diffraction because the X-ray scattering is dominated by Bi, and the precision of oxygen atoms from X-ray refinement of this type is poor, whereas with neutron diffraction the contribution of oxygen to the overall scattering is much more significant (cf. Table of neutron scattering lengths in Appendix E).

6.1.1. HRPD data

The powder neutron diffraction data were collected at 25, 500, 650 and 800°C on HRPD, each data collection lasting approximately five hours for a total collected value of 150 μAhrs (except for the experiment at room temperature: one hour, 30 μAhrs).

All Rietveld refinements were carried out using a data range $0.65 < d < 2.5 \text{ \AA}$

Below T_c the structure has been refined in orthorhombic space group B2cb (cf. Figure 6.2), which is in agreement with both the work of Newnham et al.¹⁶ and the theory of an “all-odd layered” structure; i.e. all Aurivillius phases containing an odd number of

perovskite layers should crystallise in the same space group B2cb (Cf. Introduction in Chapter 5).

However, a precise single crystal study by Rae et al.⁵ suggests the true symmetry at room temperature to be monoclinic, B1a1. We were unable to refine our data using that model, and conclude that either the deviation from orthorhombic symmetry is too small to be detectable with powder neutron data or that the single crystalline and powder samples are genuinely different. This is possible, since the preparation conditions were different for the two samples.

The final lattice parameters after refinement are the following ones:

- At 25°C: $a = 5.44441(8) \text{ \AA}$, $b = 5.40856(7) \text{ \AA}$, $c = 32.8417(5) \text{ \AA}$, Cell volume = $967.07(3) \text{ \AA}^3$
- At 500°C: $a = 5.46209(4) \text{ \AA}$, $b = 5.43727(4) \text{ \AA}$, $c = 33.0610(3) \text{ \AA}$, Cell volume = $981.87(2) \text{ \AA}^3$
- At 650°C: $a = 5.46186(5) \text{ \AA}$, $b = 5.44845(5) \text{ \AA}$, $c = 33.1743(4) \text{ \AA}$, Cell volume = $987.22(2) \text{ \AA}^3$

Inspection of these results shows that the unit cell volume is increasing with temperature as expected, and that the orthorhombicity decreases (i.e. a and b values become more similar), though is still very significant at 650°C.

At 800°C the structure has been refined as tetragonal I4/mmm (cf. Figure 6.2) with the following lattice parameters:

- $a = 3.86334(2) \text{ \AA}$, $c = 33.2942(2) \text{ \AA}$, Cell volume = $496.928(7)$

A first Rietveld refinement in space group B2cb for the three temperatures (25, 500 and 650°C) was carried out and gave acceptable agreement factors, but careful reanalyse of these results proved it to be wrong and the acceptable agreement factors are in fact a “false minimum” as described by Rae et al.⁵

In particular, the calculation of the macroscopic spontaneous polarisation P_s gave an unacceptable value of $15.6 \mu\text{C}/\text{cm}^2$, which proved the results to be wrong.

The calculation of the spontaneous polarisation P_s along the a-axis was effectuated according to the following formula already introduced in § 5.1.1.

$$P_s = (a/V) \sum_i m_i q_i \Delta x_i$$

Where: q_i is the charge of the ion (e.g. +3 for Bi, -2 for O), m_i its multiplicity, Δx_i is the displacement along a of the ion (e.g. for the "wrong" version, O(6): $x = 0.217 \rightarrow \Delta x = 0.25 - 0.217 = 0.033$; for the "good" version, O(6): $x = 0.3556 \rightarrow \Delta x = 0.25 - 0.3556 = -0.1056$), a the unit cell parameter, and V the volume of the unit cell¹⁷.

Similarly to the work of Rae et al.⁵, a better result was obtained by changing the sign of the x and y displacements for the O(6) atom comparatively to the "ideal" value of 0.25. The calculated P_s for this version is $P_s = 34.0 \mu\text{C}/\text{cm}^2$ which is closer to the expected value.

The final atomic coordinates in both versions ("good" and "wrong due to a false minimum") are shown in Table VI-II and Table VI-V.

Table VI-II: Final Atomic Coordinates and Isotropic Temperature Factors for $\text{Bi}_4\text{Ti}_3\text{O}_{12}$ at 25°C ("false minimum" version), space group B2cb

atom	x	y	z	Uiso (x100) Å ²
Bi(1)	0.0 *	0.9982(7)	0.06639(8)	1.30(7)
Bi(2)	1.001(1)	0.0139(9)	0.21127(8)	1.80(8)
Ti(1)	0.052(2)	0.0	0.5	0.2(2)
Ti(2)	0.037(2)	1.004(2)	0.3717(2)	1.6(2)
O(1)	0.322(2)	0.265(1)	0.0069(2)	3.2(2)
O(2)	0.265(1)	0.263(1)	0.2485(2)	0.7(1)
O(3)	0.086(1)	1.0640(9)	0.4406(2)	1.4(1)
O(4)	1.052(1)	0.9453(9)	0.3193(1)	1.0(1)
O(5)	0.284(2)	0.253(2)	0.1109(2)	2.3(1)
O(6)	0.217(2)	0.201(2)	0.8756(2)	3.4(2)

* Coordinate fixed to define origin of polar axis.

Table VI-III: Final Atomic Coordinates and Isotropic Temperature Factors for $\text{Bi}_4\text{Ti}_3\text{O}_{12}$ at 500°C ("false minimum" version), space group B2cb

atom	x	y	z	Uiso (x100) Å ²
Bi(1)	0.0 *	0.9996(7)	0.06690(8)	3.38(7)
Bi(2)	1.008(1)	0.0098(8)	0.21118(7)	3.29(8)
Ti(1)	0.046(2)	0.0	0.5	1.1(2)

Ti(2)	0.023(2)	0.997(2)	0.3713(1)	2.2(1)
O(1)	0.304(2)	0.266(1)	0.0056(2)	5.1(2)
O(2)	0.258(1)	0.265(1)	0.2494(2)	2.3(1)
O(3)	0.070(1)	1.0522(8)	0.4406(1)	3.1(1)
O(4)	1.050(1)	0.949(1)	0.3188(1)	3.1(1)
O(5)	0.278(1)	0.257(1)	0.1122(2)	3.0(1)
O(6)	0.219(1)	0.213(1)	0.8755(2)	3.3(2)

* Coordinate fixed to define origin of polar axis.

Table VI-IV: Final Atomic Coordinates and Isotropic Temperature Factors for $\text{Bi}_4\text{Ti}_3\text{O}_{12}$ at 650°C (“false minimum” version), space group B2cb

atom	x	y	z	Uiso (x100) Å ²
Bi(1)	0.0 *	0.9997(7)	0.06733(7)	4.69(7)
Bi(2)	1.006(1)	0.0111(8)	0.21114(5)	3.64(7)
Ti(1)	0.023(3)	0.0	0.5	2.6(2)
Ti(2)	0.021(2)	0.994(2)	0.3708(1)	2.3(1)
O(1)	0.297(2)	0.274(1)	0.0044(2)	5.9(2)
O(2)	0.257(2)	0.259(1)	0.2498(2)	3.0(1)
O(3)	0.050(1)	1.041(1)	0.4408(1)	4.9(1)
O(4)	1.048(1)	0.959(1)	0.3183(1)	3.9(1)
O(5)	0.282(2)	0.264(1)	0.1131(2)	3.8(2)
O(6)	0.230(1)	0.221(1)	0.8772(2)	3.6(2)

* Coordinate fixed to define origin of polar axis.

Table VI-V: Final Atomic Coordinates and Isotropic Temperature Factors for $\text{Bi}_4\text{Ti}_3\text{O}_{12}$ at 25°C (“good version”), space group B2cb, a = 5.44441(8) Å, b = 5.40856(7) Å, c = 32.8417(5) Å, Cell volume = 967.07(3) Å³

Name	x	y	z	Uiso x 100
Bi(1)	0.0	0.9987(6)	0.06676(7)	1.38(6)
Bi(2)	0.9975(8)	0.0179(6)	0.21138(7)	1.44(7)

Ti(1)	0.041(2)	0.0	0.5	0.52(18)
Ti(2)	0.047(2)	1.002(2)	0.3716(2)	0.75(13)
O(1)	0.324(2)	0.259(2)	0.0079(2)	3.41(17)
O(2)	0.269(2)	0.2434(9)	0.2499(2)	1.41(10)
O(3)	0.0864(9)	1.0609(8)	0.4408(2)	1.66(11)
O(4)	1.0564(9)	0.9471(9)	0.3189(2)	1.38(12)
O(5)	0.289(2)	0.228(1)	0.1120(2)	1.00(10)
O(6)	0.3556(9)	0.293(1)	0.8756(2)	1.35(12)

The final agreement factors are : $\chi^2 = 2.294$, $R_{wp} = 0.0690$, $R_p = 0.0637$ for 50 variable parameters.

Table VI-VI: Final Atomic Coordinates and Isotropic Temperature Factors for $\text{Bi}_4\text{Ti}_3\text{O}_{12}$ at 500°C (“good version”), space group B2cb, a = 5.46209(4) Å, b = 5.43727(4) Å, c = 33.0610(3) Å, Cell volume = 981.87(2) Å³

Name	x	y	z	Uiso x 100
Bi(1)	0.0	0.9984(6)	0.06698(6)	3.70(6)
Bi(2)	1.0076(8)	0.0125(6)	0.21129(5)	3.04(6)
Ti(1)	0.037(2)	0.0	0.5	1.7(2)
Ti(2)	0.035(2)	0.998(2)	0.37103(9)	1.65(11)
O(1)	0.314(2)	0.265(2)	0.0059(2)	5.2(2)
O(2)	0.272(2)	0.2460(9)	0.2500(2)	2.75(8)
O(3)	0.0716(8)	1.0516(8)	0.4408(1)	3.6(1)
O(4)	1.050(1)	0.9520(8)	0.31830(9)	3.3(1)
O(5)	0.278(1)	0.2281(9)	0.1123(2)	2.4(1)
O(6)	0.3373(8)	0.283(1)	0.8761(2)	2.8(2)

The final agreement factors are: $\chi^2 = 4.649$, $R_{wp} = 0.0434$, $R_p = 0.0403$ for 50 variable parameters.

Table VI-VII: Final Atomic Coordinates and Isotropic Temperature Factors for $\text{Bi}_4\text{Ti}_3\text{O}_{12}$ at 650°C (“good version”), space group B2cb, a = 5.46186(5) Å, b = 5.44845(5) Å, c = 33.1743(4) Å, Cell volume = 987.22(2) Å³

Name	x	y	z	Uiso x 100
Bi(1)	0.0	0.9985(7)	0.06739(7)	5.16(8)
Bi(2)	1.007(2)	0.0114(7)	0.21115(5)	3.62(7)
Ti(1)	0.029(4)	0.0	0.5	2.7(2)
Ti(2)	0.021(2)	0.994(2)	0.3706(1)	1.8(1)

O(1)	0.307(2)	0.272(2)	0.0041(2)	5.6(2)
O(2)	0.269(2)	0.248(2)	0.2503(2)	3.3(1)
O(3)	0.052(2)	1.041(2)	0.4408(2)	5.3(2)
O(4)	1.046(2)	0.960(2)	0.3177(1)	4.1(2)
O(5)	0.265(2)	0.231(2)	0.1126(2)	3.2(2)
O(6)	0.316(2)	0.277(2)	0.8772(2)	3.4(2)

The final agreement factors are : $\chi^2 = 5.202$, $R_{wp} = 0.0463$, $R_p = 0.0446$ for 50 variable parameters.

Table VI-VIII: Final Atomic Coordinates and Anisotropic Temperature Factors for $\text{Bi}_4\text{Ti}_3\text{O}_{12}$ at 800°C , space group $I4/mmm$, $a = 3.86334(2) \text{ \AA}$, $c = 33.2942(2) \text{ \AA}$, Cell volume =

atom	x	y	z	$U_{11} (\text{\AA}^2)$	$U_{22} (\text{\AA}^2)$	$U_{33} (\text{\AA}^2)$
Bi(1)	0.5	0.5	0.06752(7)	0.064(1)	0.064(1)	0.082(2)
Bi(2)	0.5	0.5	0.21147(5)	0.052(1)	0.052(1)	0.044(1)
Ti(1)	0.5	0.5	0.5	0.026(2)	0.026(2)	0.041(3)
Ti(2)	0.5	0.5	0.37074(8)	0.025(1)	0.025(1)	0.027(2)
O(1)	0.5	0	0	0.016(2)	0.145(4)	0.129(4)
O(2)	0.5	0	0.25	0.035(1)	0.035(1)	0.037(2)
O(3)	0.5	0.5	0.4411(1)	0.089(1)	0.089(1)	0.043(2)
O(4)	0.5	0.5	0.3183(1)	0.103(2)	0.103(2)	0.022(2)
O(5)	0.5	0	0.11768(7)	0.022(1)	0.061(1)	0.072(2)

Note: O(5) corresponds to the O(5) and O(6) positions in B2cb.

The final agreement factors are: $\chi^2 = 3.688$, $R_{wp} = 0.0386$, $R_p = 0.0360$ for 38 variable parameters.

The structure at 800°C corresponds to the ideal undistorted tetragonal structure $I4/mmm$ (cf. Figure 6.2) whereas below the Curie Temperature the structure is distorted in the orthorhombic system B2cb (cf. Figure 6.2). The transformation from the orthorhombic to the tetragonal system after the transition temperature can be seen, for example, by the merging of a doublet at $d \sim 2.28 \text{ \AA}$, corresponding to the (208) and (028) reflections (cf. Rietveld plot in Figure 6.1).

A picture along the c-axis showing the two different space groups is in Figure 6.2.

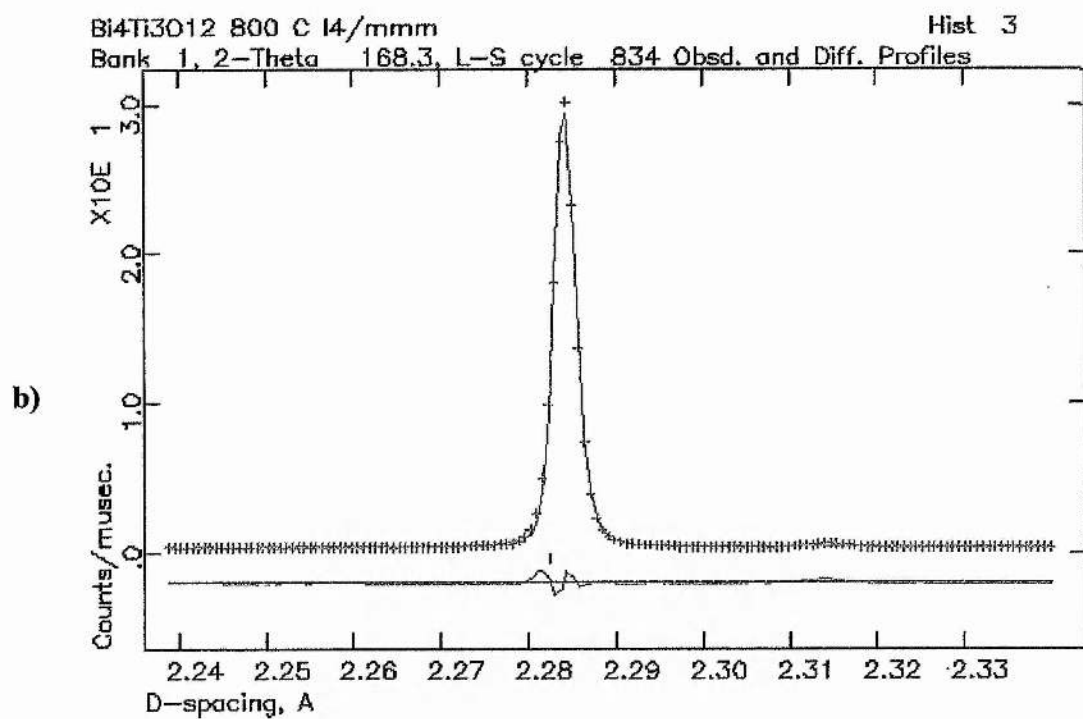
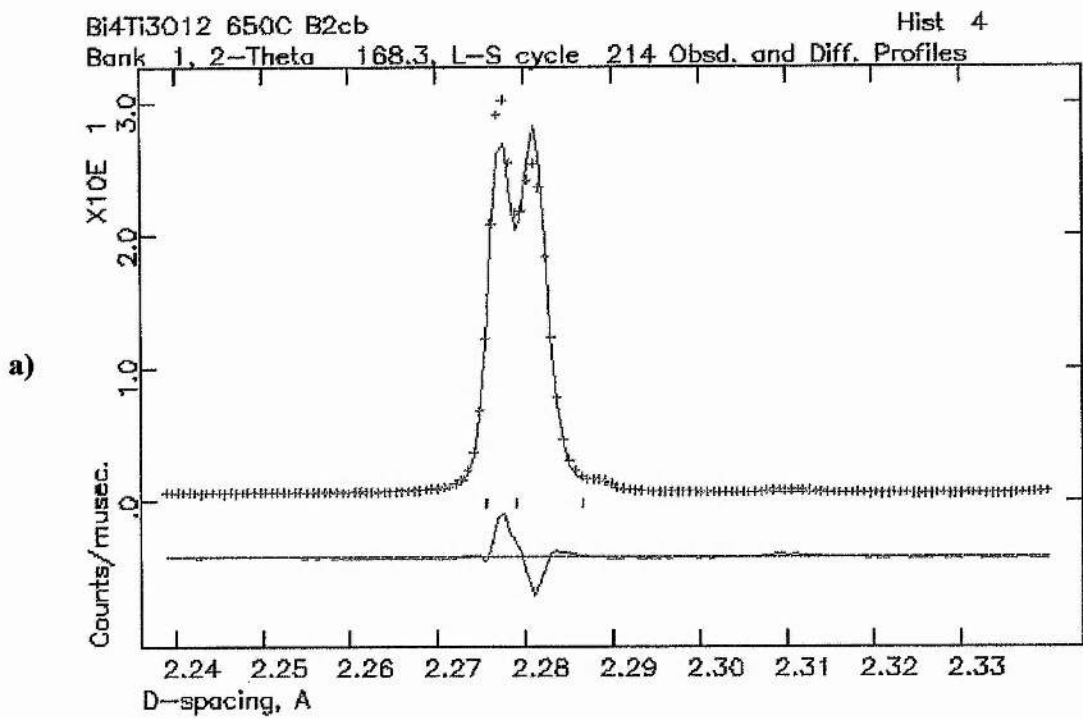


Figure 6.1: Merging of a doublet above T_c , demonstrating the transition from orthorhombic (a) to tetragonal (b)

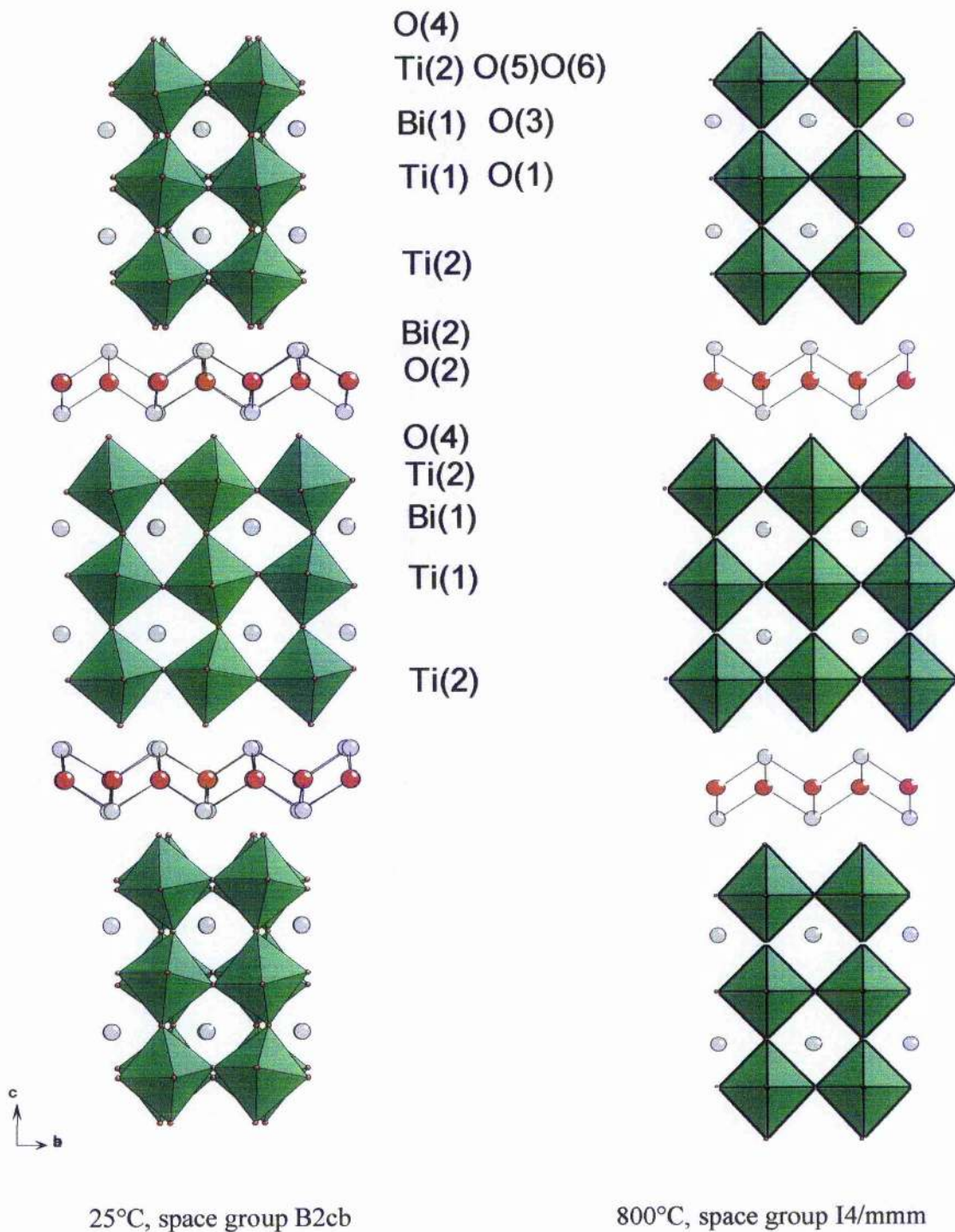


Figure 6.2: Representation of the structure of $\text{Bi}_4\text{Ti}_3\text{O}_{12}$ below and above T_c in space group B2cb and I4/mmm

The tetragonal unit cell has approximately half the volume of the orthorhombic cell, being related by $a_{\text{orth}} \sim b_{\text{orth}} \sim \sqrt{2} a_{\text{tet}}$; $c_{\text{orth}} \sim c_{\text{tet}}$.

The gradual decrease of orthorhombic distortion with increasing temperature, and the eventual change to tetragonal symmetry above T_c can be linked with the cationic displacements from ideal positions as well as the degree of tilting of the octahedra.

The following table presents the evolution of some selected bond-lengths and angles versus the temperature (Table VI-IX).

Table VI-IX: Selected Bond Lengths (Å) and Angles (°) for $\text{Bi}_4\text{Ti}_3\text{O}_{12}$ ("good version") from HRPD data

bond	T = 25 °C	T = 500 °C	T = 650 °C	T = 800 °C
Bi(1)-O(1)	2.973(6)	3.020(5)	3.072(7)	2.964(2) x 4
Bi(1)-O(1)	3.327(6)	3.285(5)	3.258(6)	
Bi(1)-O(1)	2.524(6)	2.602(6)	2.661(7)	
Bi(1)-O(1)	2.934(6)	2.907(6)	2.874(7)	
Bi(1)-O(3)	2.427(5)	2.474(5)	2.521(7)	2.7470(3) x 4
Bi(1)-O(3)	3.087(5)	3.044(5)	2.985(7)	
Bi(1)-O(3)	2.288(4)	2.370(4)	2.469(6)	
Bi(1)-O(3)	3.218(4)	3.145(4)	3.038(6)	
Bi(1)-O(5)	2.495(6)	2.471(5)	2.439(7)	2.554(2) x 4
Bi(1)-O(5)	2.389(5)	2.436(5)	2.463(7)	
Bi(1)-O(6)	3.135(5)	3.046(5)	2.934(6)	
Bi(1)-O(6)	2.332(6)	2.390(5)	2.418(6)	
Bi(2)-O(2)	2.296(6)	2.311(6)	2.324(7)	2.3189(8) x 4
Bi(2)-O(2)	2.452(5)	2.413(5)	2.398(7)	
Bi(2)-O(2)	2.272(6)	2.294(5)	2.305(8)	
Bi(2)-O(2)	2.192(6)	2.240(6)	2.257(7)	
Bi(2)-O(4)	3.259(5)	3.209(5)	3.159(6)	2.907(1) x 4
Bi(2)-O(4)	2.545(5)	2.593(4)	2.635(6)	
Bi(2)-O(4)	2.606(5)	2.690(5)	2.698(7)	
Bi(2)-O(4)	3.206(6)	3.127(6)	3.100(8)	
Bi(2)-O(6)	3.199(5)	3.282(4)	3.363(5)	
Ti(1)-O(1) x 2	2.034(8)	1.989(10)	1.971(13)	1.93167(1)
Ti(1)-O(1) x 2	1.851(8)	1.897(9)	1.916(11)	
Ti(1)-O(3) x 2	1.986(4)	1.987(4)	1.982(4)	1.960(3)
Ti(2)-O(3)	2.307(6)	2.333(5)	2.350(5)	2.344(4)
Ti(2)-O(4)	1.757(5)	1.763(4)	1.769(4)	1.744(3)
Ti(2)-O(5)	2.056(8)	2.053(8)	2.035(10)	1.9697(7) x 4
Ti(2)-O(5)	1.950(8)	1.947(8)	1.945(11)	
Ti(2)-O(6)	2.018(8)	2.043(8)	2.049(11)	
Ti(2)-O(6)	1.893(9)	1.894(8)	1.916(10)	
Ti(1)-O(1)-Ti(1)	161.9(4)	165.2(4)	165.9(7)	180.0
Ti(1)-O(3)-Ti(2)	158.5(3)	161.5(3)	164.9(4)	180.0
Ti(2)-O(5)-Ti(2)	148.0(4)	147.4(3)	146.9(4)	157.4(2)
Ti(2)-O(6)-Ti(2)	155.6(4)	158.4(4)	159.3(5)	180.0

Inspection of the bond lengths and angles shown in Table VI-IX reveals several things:

- For Bi(1) in the perovskite site, the coordination number is twelve. This consists in the tetragonal symmetry $I4/mmm$ of three symmetry-equivalent sets of four lengths. In the orthorhombic symmetry $B2cb$ these lengths become inequivalent and the range of bond lengths gradually increases as the temperature decreases.
- For Bi(2) in the $[Bi_2O_2]$ layer site, the coordination number is eight, consisting of a trigonal anti-prism of four oxygens from within the $[Bi_2O_2]$ layer and four oxygens from the apices of the perovskite blocks. In the tetragonal structure they are, respectively “short” (2.32 Å) and “long” (2.91 Å). As the temperature is lowered, a similar effect as for Bi(1) is observed on the bond lengths. The distortion of the structure is so dramatic that an additional atom, O(6), enters the coordination sphere at ~ 3.20 Å.
- Octahedral tilts increase as temperature is lowered, particularly for the Ti(2) octahedron, as manifested in the Ti(2)-O(6)-Ti(2) bond angle.

A measure of the tendency of the structure to distort may also be found in the bond valence sums (BVS)¹⁸. This method is described in Chapter 4: Experimental techniques and instruments.

For optimum bonding satisfaction (i.e. no strain), the BVS for a metal site would be equal to its oxidation state, i.e. 4 for Ti and 3 for Bi, in this case.

Bond valence sum analysis of the coordination environments around each metal site has been done, they are written in the following table.

Table VI-X: Bond valence sums for Bi₄Ti₃O₁₂

Metal site	25°C	500°C	650°C	800°C
Bi(1)	3.03	2.74	2.58	2.22
Bi(2)	3.08	2.90	2.82	2.70
Ti(1)	4.18	4.11	4.11	4.27
Ti(2)	4.04	3.97	3.92	4.08

Of particular significance is the change in the Bi environment in perovskite site (Bi(1)) on passing through the phase transition:

A more satisfactory coordination of Bi in the perovskite block happens below the transition temperature with a nearly optimal 3.03 at room temperature.

This can be linked with off-centre displacement of this Bi that reduces the strain on this atom.

The non-centrosymmetry that results from this gives rise to ferroelectricity.

6.1.2. Polaris data

In addition to the very precise study of this compound on HRPD at 25, 500, 650 and 800°C, we also carried out another series of Neutron powder diffraction studies on Polaris for a much larger number of temperatures between 20 and 810°C.

This was done essentially in order to see if an intermediate phase between orthorhombic B2cb and tetragonal I4/mmm could exist in this composition as it does with Sr_{0.85}Bi_{2.1}Ta₂O₉ and SrBi₄Ti₄O₁₅ (Cf. Chapter 5).

The powder neutron diffraction data were collected at several temperatures: room temperature, 100, 150, 200, 250, 300, 350, 400, 450, 500, 550, 580, 610, 640, 670, 700, 730, 770 and 810°C, on Polaris. Each data collection lasting approximately fifty minutes for a total collected value of 150 μAhrs (except for the 730, 770 and 810°C experiment: approximately 35 minutes, 100 μAhrs).

The results of this study can be summed-up in the graph below showing the evolution of the lattice parameters (data obtained from the Rietveld refinements of the data obtained on Polaris) versus the temperature (cf. Figure 6.3). The complete results are in Appendix C.

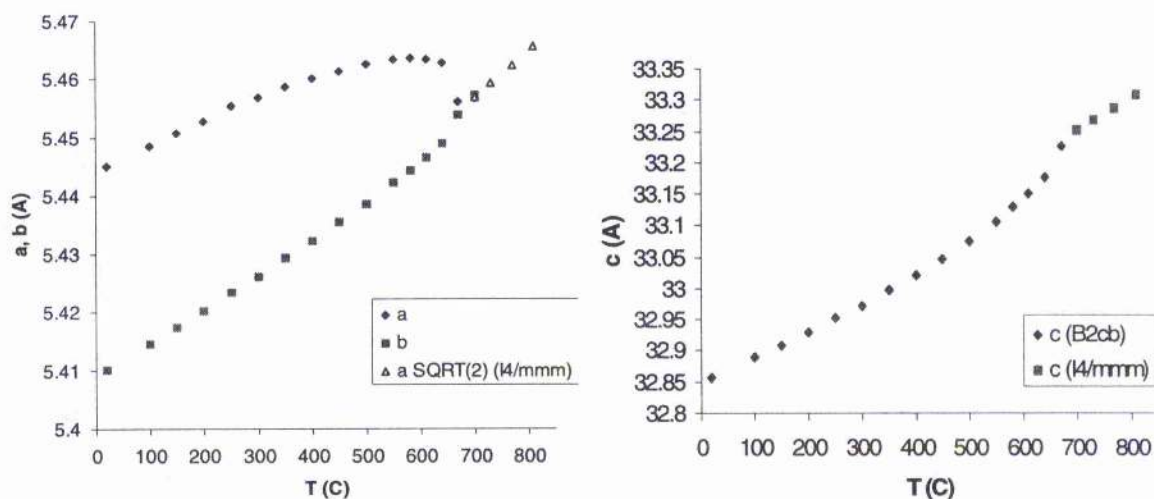


Figure 6.3: Evolution of the lattice parameters versus the temperature for $\text{Bi}_4\text{Ti}_3\text{O}_{12}$ from the Polaris data

It can be seen in this plot that the phase transition is preceded by a sudden decrease of the a-parameter, the difference between a and b is still very significant at 640°C. This could be an indication of the transition being of the first order kind.

The rapid transition at T_c can also be seen in the sudden change of some Bi-O distances within the structure and Ti-O-Ti angles.

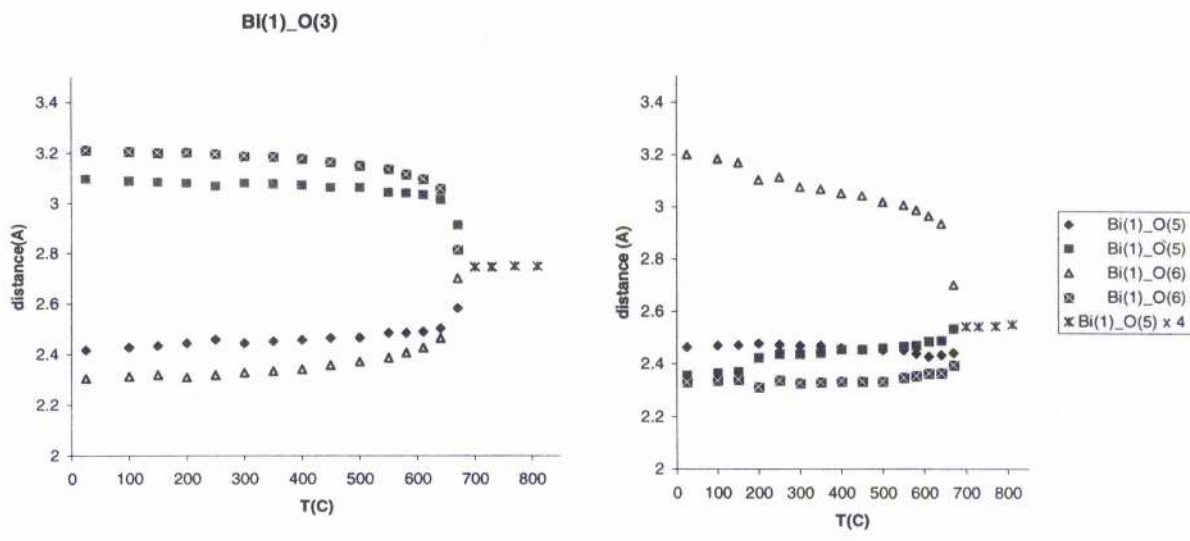


Figure 6.4: Evolution of Bi(1)-O distances with the temperature in $\text{Bi}_4\text{Ti}_3\text{O}_{12}$

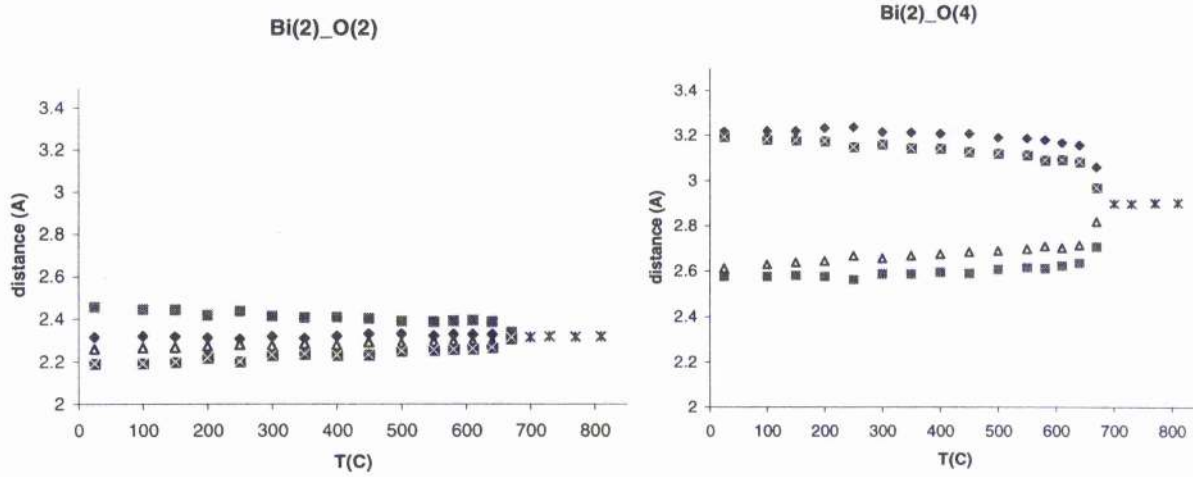


Figure 6.5: Evolution of Bi(2)-O distances with the temperature in $\text{Bi}_4\text{Ti}_3\text{O}_{12}$

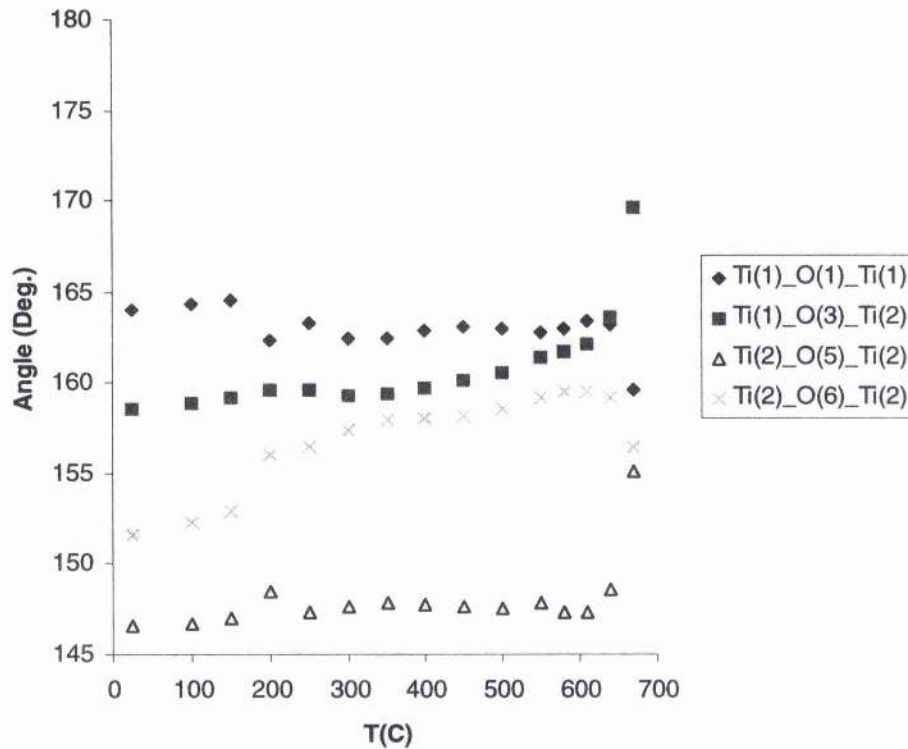


Figure 6.6: Evolution of some Ti-O-Ti angles with the temperature in $\text{Bi}_4\text{Ti}_3\text{O}_{12}$

According to the Landau theory of phase transitions, the Landau order parameter Q is related to the change in some macroscopic properties through the phase transition, and is scaled so that it is assigned a value of 0 in the high temperature form (at $T = T_c$ in our case), and 1 in the low temperature form (at $T = 0 \text{ K}$)¹⁹.

If there is no change in the translational symmetry of the lattice, no extra reflections will appear in the diffraction pattern. Transitions of this type are called “zone centre transitions”, and in general in this case $\epsilon \propto Q$ where ϵ is the “spontaneous strain” and in our case can be expressed by the value of the orthorhombicity defined by:

$$\text{Orthorhombicity} = 2 \times (a-b)/(a+b)$$

On the other hand, if there is change in the lattice type or formation of a superlattice, the transition is called “zone boundary transition”, and $\epsilon \propto Q^2$; this is the case for this compound.

Therefore, for our purpose, $\epsilon = (a-b)/(a+b) \propto Q^2$.

In order to define the order of the transition, we should plot Q versus $(T_c-T)/T_c$, i.e. in our case $Q = B \times ((a-b)/(a+b))^{1/2}$ versus $(T_c-T)/T_c$, where B is a constant to determine. Here, B was determined to be approximately 17 so that the scale ($Q = 0$ at T_c and 1 at $T = 0$ K) is respected.

If for $\text{Bi}_4\text{Ti}_3\text{O}_{12}$, we define Q by $Q = 17 \times ((a-b)/(a+b))^{1/2}$, we obtain the plot shown in Figure 6.7.

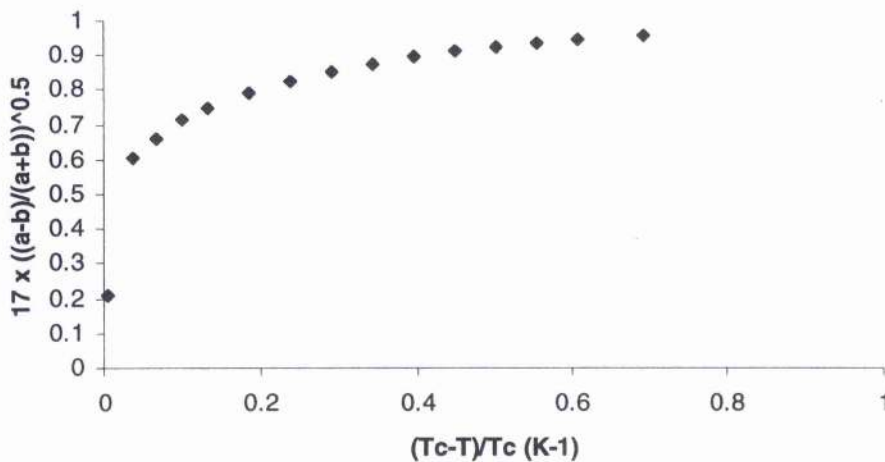


Figure 6.7: variation of the Landau order parameter Q with the reduced temperature t , where $Q = 17 \times ((a-b)/(a+b))^{1/2}$, and $t = (T_c-T)/T_c$

If Q^2 is directly proportional to the reduced temperature, then the transition is of the second order. This clearly is not the case here (Cf. Figure 6.8), therefore the transition is of a lower order, i.e. the change during the phase transition is more abrupt.

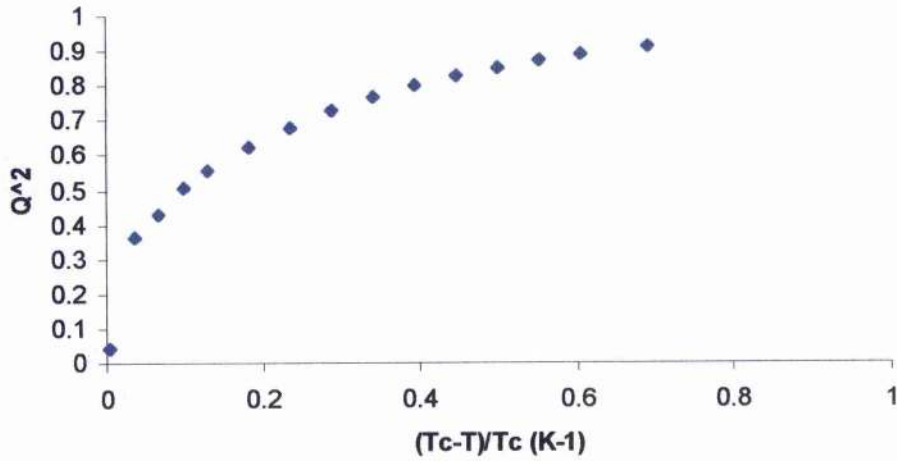


Figure 6.8: plot of Q^2 versus the reduced temperature

More precisely, $Q = [(T_c - T)/T_c]^\beta$

where β is the “critical exponent” ; it is equal to $1/2$ for a second order transition, and equal to $1/4$ for a tricritical transition (i.e. intermediate between second and first order). We calculated the value for our data as $\beta \approx 1/6$. The comparison between the observed data and the function $y = x^\beta$, where $\beta \approx 1/6$, can be seen in the following graph.

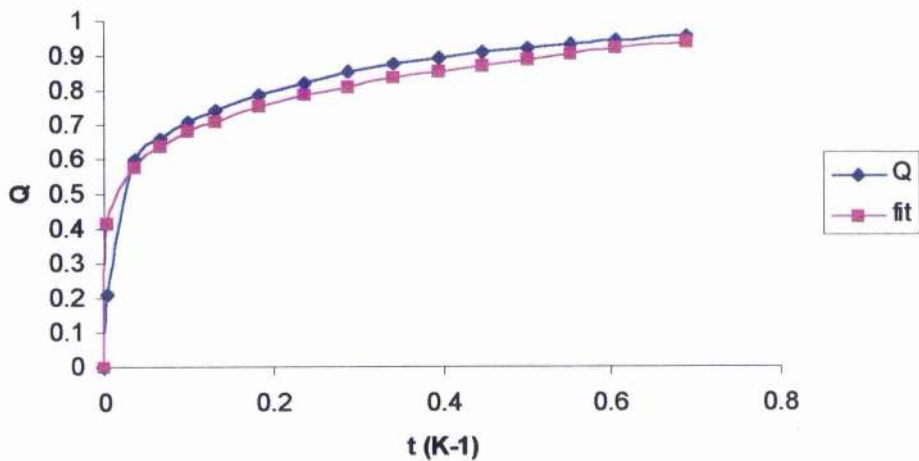


Figure 6.9: fitting of $Q = [(T_c - T)/T_c]^\beta$ with $\beta \approx 1/6$ (in pink), and data (in blue)

It indicates the transition to be close to first order.

The DTA measurements effectuated with this material also seem to indicate a transition close to first order around 670°C (Cf. Figure 6.10).

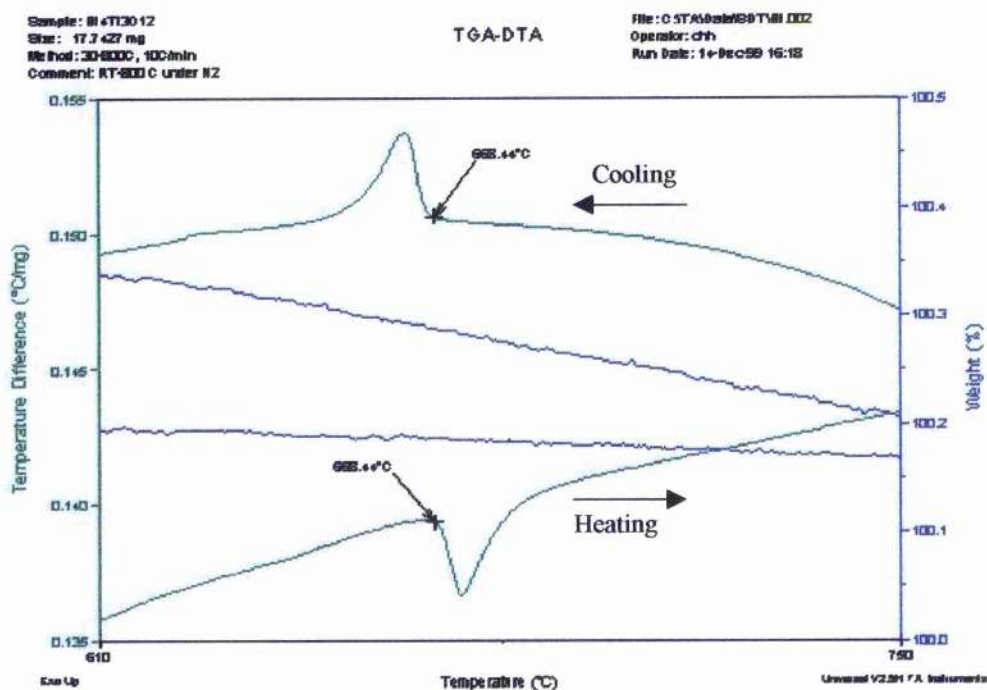


Figure 6.10: DTA measurements of Bi₄Ti₃O₁₂, showing a transition (endothermic when T increases) looking like first order around T ~ 670°C

Another interesting thing to look at is the evolution of the anisotropically refined thermal parameter versus the temperature. If we plot the U_{ij} parameters versus the temperature of the Bi and Ti atoms for the compounds above T_c and draw a median line this theoretical line should pass through zero at absolute zero ($T = 0$ K). If it doesn't it means that the position of the atom is actually displaced or split. This is an indication that the transition is of the "order-disorder" rather than "displacive" type.

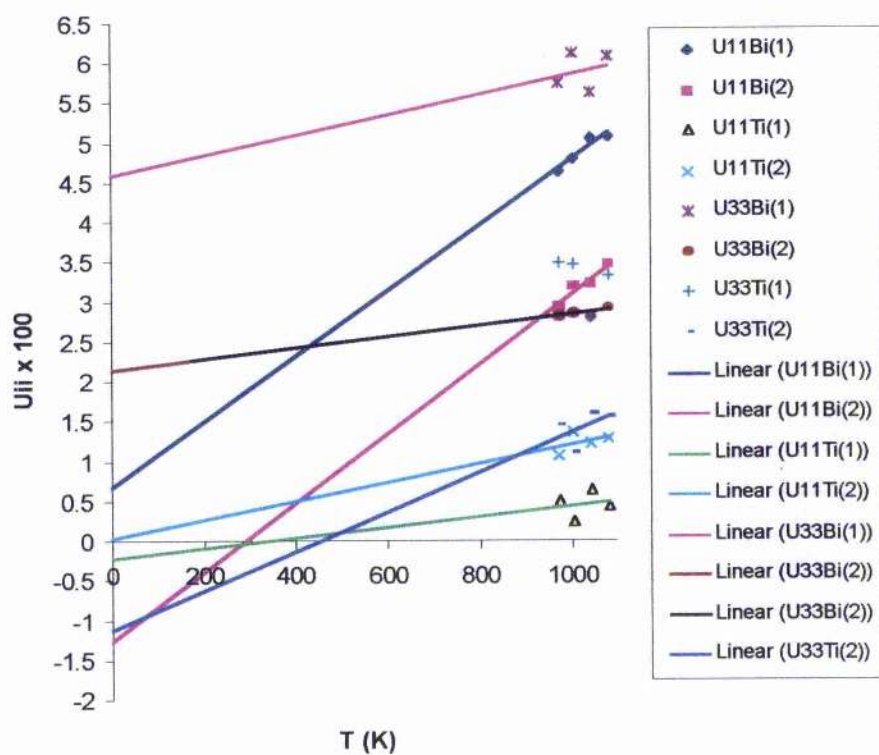


Figure 6.11: U_{ij} versus T

In this plot (Figure 6.11), it can be seen that most of the temperature factors data extrapolate towards zero at $T = 0$ K. Exceptions are $U_{33}\text{Bi}(1)$, $U_{33}\text{Bi}(2)$ and $U_{33}\text{Ti}(1)$. This seems to indicate a disorder of the Bi atoms in both sites along the c-axis, above T_c .

6.1.3. a.c. Impedance spectroscopy measurements

Ferroelectric measurements of $\text{Bi}_4\text{Ti}_3\text{O}_{12}$ have been carried out. The results confirm the phase transition temperature T_c at 675°C and are presented here below (ϵ' designates the dielectric constant ϵ') in Figure 6.12.

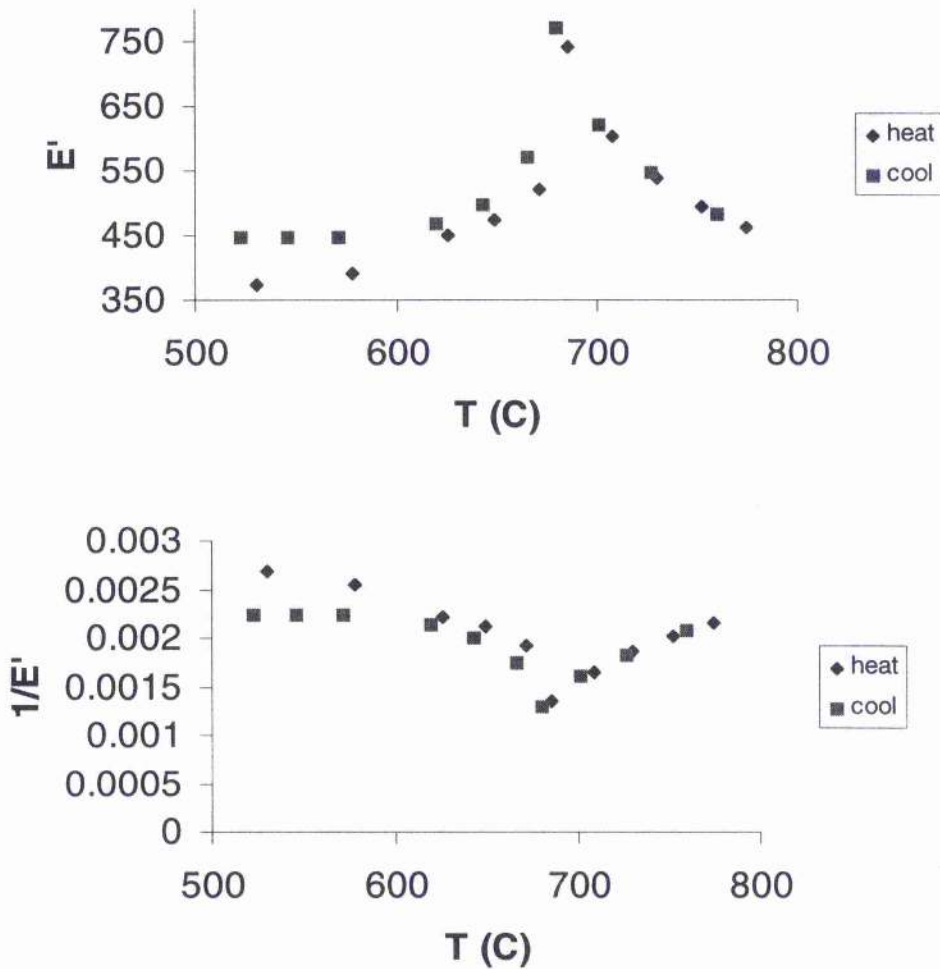


Figure 6.12: ac impedance measurements for $\text{Bi}_4\text{Ti}_3\text{O}_{12}$

Note: The results in this section have been published in *Chemistry of Materials*: "A variable-temperature powder neutron diffraction study of ferroelectric $\text{Bi}_4\text{Ti}_3\text{O}_{12}$ ", C. H. Hervoches and P. Lightfoot, *Chem. Mater.*, 1999, **11**, 3359

6.2. Solid solution $\text{Bi}_{4-x}\text{Sr}_x\text{Ti}_{3-x}\text{Nb}_x\text{O}_{12}$

We first synthesised the compound $\text{Bi}_2\text{Sr}_2\text{TiNb}_2\text{O}_{12}$ by traditional solid state reaction according to the method described in § 4.10.2. Its structure was investigated by X-ray diffraction and compared to previous studies realised by different groups^{10, 20}.

Rietveld refinement of $\text{Bi}_2\text{Sr}_2\text{TiNb}_2\text{O}_{12}$ indicated that disorder between Bi and Sr occurs in Bi_2O_2 layers whereas it was previously assumed not to be possible. For example, A. Castro et al. claimed that the replacement of Bi in these layers could only be possible for cations possessing stereochemically active lone pairs of electrons.¹¹

The results of the Rietveld refinement of $\text{Bi}_2\text{Sr}_2\text{TiNb}_2\text{O}_{12}$, obtained from the X-ray data on the Stoe, follows in Table VI-XI.

Table VI-XI: Rietveld refinement of $\text{Bi}_2\text{Sr}_2\text{TiNb}_2\text{O}_{12}$, space group $I4/mmm$, $a = 3.8911(2) \text{ \AA}$, $c = 33.181(2) \text{ \AA}$, Cell volume = $502.37(3) \text{ \AA}^3$

Name	x	y	z	Uiso x 100	Fractn
Bi(1)	0.5	0.5	0.06346(12)	3.49(8)	0.139(3)
Sr(1)	0.5	0.5	0.21308(8)	3.49(8)	0.139(3)
Ti(1)	0.5	0.5	0.5	1.18(14)	0.506(12)
Nb(1)	0.5	0.5	0.37217(13)	1.18(14)	0.753(6)
O(1)	0.5	0.0	0.0	2.50	1.0
O(2)	0.5	0.0	0.25	2.50	1.0
O(3)	0.5	0.5	0.3273(8)	2.50	1.0
O(4)	0.5	0.0	0.1141(6)	2.50	1.0
O(5)	0.5	0.5	0.4448(7)	2.50	1.0
Bi(2)	0.5	0.5	0.21308(8)	3.49(8)	0.861(3)
Sr(2)	0.5	0.5	0.06346(12)	3.49(8)	0.861(3)
Nb(2)	0.5	0.5	0.5	1.18(14)	0.494(12)
Ti(2)	0.5	0.5	0.37217(13)	1.18(14)	0.247(6)

The final agreement factors are: $\chi^2 = 1.121$, $R_{wp} = 0.1431$, $R_p = 0.1107$ for 22 variable parameters.

The final Rietveld plot of this compound $\text{Bi}_2\text{Sr}_2\text{TiNb}_2\text{O}_{12}$ is presented in Figure 6.13.

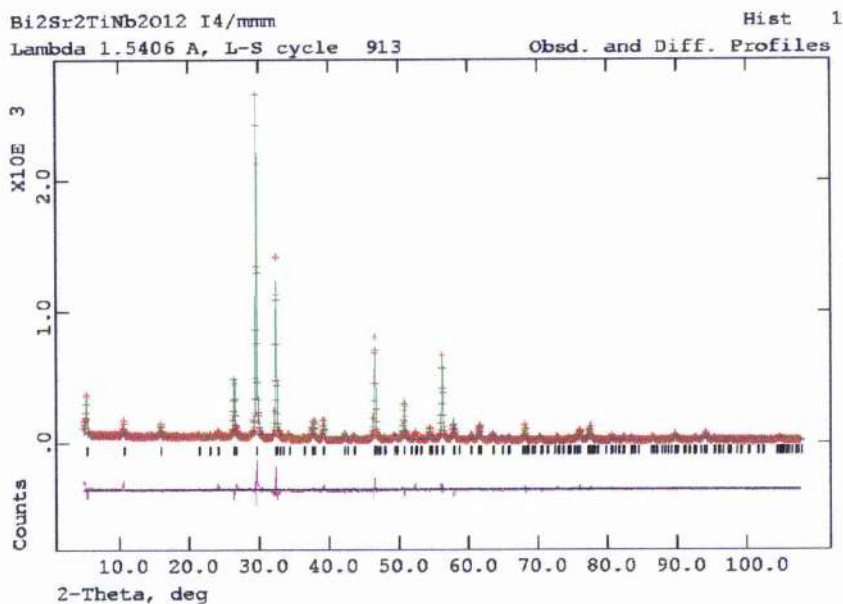


Figure 6.13: Final Rietveld plot of Bi₂Sr₂TiNb₂O₁₂ in space group I4/mmm

In order to explore this Bi/Sr disorder phenomenon further, several compounds with different proportions of Bi and Sr were prepared in order to see if a solid solution could exist and the effect on Bi/Sr disorder.

Several compounds of general formula Bi_{4-x}Sr_xTi_{3-x}Nb_xO₁₂ were synthesised (with x = 0.2, 0.5, 0.7, 0.8, 1, 1.2, 1.4, 1.5, 1.7, 1.8, 2, 2.1, 2.2, 2.3, 2.4, 2.5, 2.6, 2.7 and 2.8).

This solid solution has been analysed in detail by a combination of powder X-ray and neutron diffraction.

6.2.1. X-ray results of Bi_{4-x}Sr_xTi_{3-x}Nb_xO₁₂

X-ray powder diffraction data were collected on the Stoe STADI/P transmission diffractometer using CuK_{α1} radiation over the range 4° < 2θ < 120°, the entire run lasting about 14 hours.

In the products containing a low percentage of Bi (i.e. From x = 2.6 to x = 2.8), an impurity appears on the X-ray patterns indicating that we reached the limit of the solid

solution. This is in agreement with a previous study of the same solid solution $\text{Bi}_{4-x}\text{Sr}_x\text{Ti}_{3-x}\text{Nb}_x\text{O}_{12}$ by Armstrong et al.⁶, that observed the limit to be at $x = 2.6$.

The peaks corresponding to this impurity are correlated with the following compound: $\text{Sr}_5\text{Nb}_4\text{O}_{15}$ (PDF n° 28-1248).

A neutron analysis of $\text{Bi}_{1.8}\text{Sr}_{2.2}\text{Ti}_{0.8}\text{Nb}_{2.2}\text{O}_{12}$ has also been carried out, the result of which is described later in this report.

All these compounds have been studied and the structures refined by the Rietveld method with two envisaged space groups: B2cb and I4/mmm. The result of this study is summed-up in the following table.

Table VI-XII: Final parameters, agreement factors and relative occupancy of Bi(1) and Sr(2) for $\text{Bi}_{4-x}\text{Sr}_x\text{Ti}_{3-x}\text{Nb}_x\text{O}_{12}$ ($0.2 < x < 2.7$) in space groups B2cb and I4/mmm

a) Space group B2cb

$\text{Bi}_{4-x}\text{Sr}_x\text{Ti}_{3-x}\text{Nb}_x\text{O}_{12}$ B2cb (30 variables)							
x	a	b	c	χ^2	R_{wp}	Frac Bi(1)	Frac Sr(2)
0.2	5.4508(3)	5.4190(3)	32.902(2)	1.43	0.1627	0.901(4)	0.001(4)
0.5	5.4551(2)	5.4369(2)	32.9938(8)	2.244	0.1085	0.792(2)	0.042(2)
0.8	5.4578(3)	5.4514(3)	33.067(2)	1.246	0.1673	0.678(4)	0.078(4)
1	5.4654(9)	5.4621(9)	33.128(2)	1.404	0.1894	0.577(4)	0.077(4)
1.2	5.4637(7)	5.4680(6)	33.117(2)	1.096	0.2376	0.503(5)	0.103(5)

b) Space group I4/mmm

$\text{Bi}_{4-x}\text{Sr}_x\text{Ti}_{3-x}\text{Nb}_x\text{O}_{12}$ I4/mmm (22 variables)							
x	a	$a\sqrt{2}$	c	χ^2	R_{wp}	Frac Bi(1)	Frac Sr(2)
1	3.8635(2)	5.4638(3)	33.127(2)	1.432	0.1916	0.554(4)	0.054(4)
1.2	3.8651(2)	5.4661(3)	33.117(2)	1.065	0.2345	0.463(5)	0.063(5)
1.4	3.8708(2)	5.4741(3)	33.118(2)	1.178	0.2282	0.386(4)	0.086(4)
1.7	3.88224(9)	5.4903(1)	33.158(2)	3.388	0.158	0.264(3)	0.114(3)
1.8	3.8873(3)	5.4975(4)	33.132(4)	2.332	0.2191	0.212(5)	0.112(5)
2	3.8910(2)	5.5027(3)	33.179(2)	1.354	0.1573	0.197(4)	0.197(4)
2.1	3.8944(2)	5.5075(3)	33.201(2)	1.771	0.2139	0.176(5)	0.226(5)
2.2	3.8952(1)	5.5087(2)	33.206(2)	7.949	0.2057	0.110(4)	0.210(4)
2.3	3.8972(3)	5.5115(4)	33.264(3)	1.682	0.2466	0.114(5)	0.264(5)
2.4	3.8986(2)	5.5135(3)	33.372(2)	5.211	0.2233	0.054(4)	0.254(4)
2.5	3.9071(2)	5.5255(3)	33.585(2)	0.998	0.1655	0.007(3)	0.257(3)
2.6	3.9054(2)	5.5231(3)	33.633(3)	2.9	0.2382	0.010(5)	0.310(5)
2.7	3.9041(2)	5.5212(3)	33.667(2)	11.54	0.2717	0	0.35
2.8	3.9044(3)	5.5216(4)	33.682(3)	13.59	0.3531	0	0.4

In this table, Frac Bi(1) corresponds to the relative occupancy of Bi located in the perovskite site ($x,y,z \sim 0.5,0.5,0.065$), Frac Sr(2) corresponds to the relative occupancy of Sr located in the Bi_2O_2 layer ($x,y,z \sim 0.5,0.5,0.21$).

According to these results, the solid solution can be separated into three regions corresponding to three different types of behaviour in the evolution of (i) the lattice parameters, and (ii) the disorder Bi/Sr for this material: $0 < x < 1.2$, $1.2 < x < 2.5$, and $x > 2.5$.

The comparison of the agreement factors shows that the “transformation point” from B2cb to I4/mmm occurs around $x = 1.2$ (i.e. for $\text{Bi}_{2.8}\text{Sr}_{1.2}\text{Ti}_{1.8}\text{Nb}_{1.2}\text{O}_{12}$)

The evolution of the lattice parameters versus x shows clearly that the solid solution transforms from orthorhombic B2cb in favour of the non-distorted tetragonal space group I4/mmm at $x = 1.2$ (cf. Figure 6.14). This is proved both by the merging of lattice parameters a and b and by the change of slope in the evolution of the parameter c . There is an other phenomenon occurring around $2.0 < x < 2.5$ and it is described later in this section.

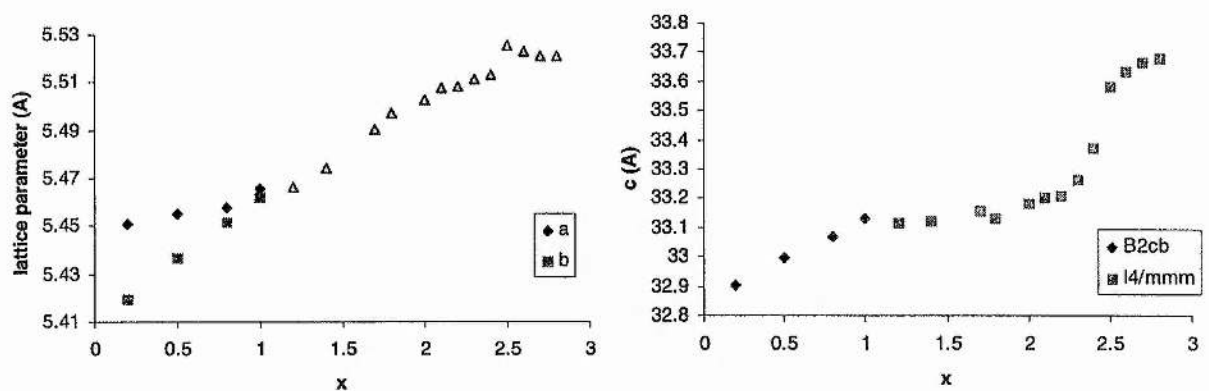


Figure 6.14: Evolution of the lattice parameters of the solid solution $\text{Bi}_{4-x}\text{Sr}_x\text{Ti}_{3-x}\text{Nb}_x\text{O}_{12}$ versus x

It appears that the variation of the lattice parameters after the phase transition from B2cb to I4/mmm doesn't follow the same behaviour before and after $x = 2.0$ (cf. Figure 6.14).

This frontier is also confirmed by the introduction of Bi cation into the perovskite site (or "Sr site") and of Sr into the "Bi site" (i.e. Bi_2O_2 layers): cf. Figure 6.15.

The evolution of the relative occupancy of Bi(1) in the perovskite site (or "A" site) and of Sr(2) in the Bismuth ("M") site in the $[\text{M}_2\text{O}_2]$ layers has also been studied. The results are shown in the two plots below.

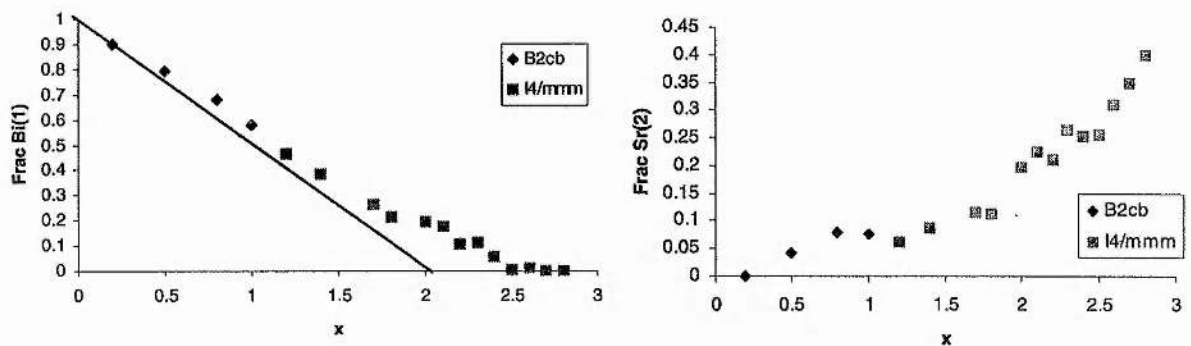


Figure 6.15: evolution of the relative occupancy of Bi(1) in the perovskite site and Sr(2) in the $[\text{M}_2\text{O}_2]$ site of the solid solution $\text{Bi}_{4-x}\text{Sr}_x\text{Ti}_{3-x}\text{Nb}_x\text{O}_{12}$ versus x . The expected line for a non-disordered system is shown.

From Figure 6.14, we can see a breaking point in the region $2.2 < x < 2.5$, where the parameter c increases dramatically. This is presumably due to all the extra Sr going into the (Bi_2O_2) layer site after this point (this frontier can also be seen in Figure 6.15). The plateau in both a and c after $x = 2.5$ suggests that the solid solution limit is reached after this value.

From these observations we can say that the disorder between Bi and Sr atoms occurs even for compounds with a small amount of Sr in the structure. It means that even if all the Sr atoms present could be in their ideal site, i.e. the perovskite site, in fact some of them are going into the $[\text{Bi}_2\text{O}_2]$ sites whatever the composition of the member of the series is.

The Bi atoms are present in the perovskite sites only when their amount in the compound starts to be significant, i.e. when $x \leq 2.6$. When x is superior to this value, i.e. for $\text{Bi}_{1.2}\text{Sr}_{2.8}\text{Ti}_{0.2}\text{Nb}_{2.8}\text{O}_{12}$ and $\text{Bi}_{1.3}\text{Sr}_{2.7}\text{Ti}_{0.3}\text{Nb}_{2.7}\text{O}_{12}$, all of the Bi present in the structure goes into the $[\text{Bi}_2\text{O}_2]$ layers.

The perovskite sites are therefore completely occupied by the Sr atoms when x is superior or equal to 2.5; at the same time some of the Sr atoms occupy all the $[\text{Bi}_2\text{O}_2]$ sites left vacant by the lack of Bi.

Earlier suppositions that cations without lone pair, such as Sr^{2+} , would not be able to occupy the $[\text{M}_2\text{O}_2]$ sites are therefore invalid.

This partial disordering can be linked with the size of the atoms as geometrical tolerance factor argument. This is discussed in the next section.

As an example, in Table VI-XIII is presented the Rietveld refinement results of $\text{Bi}_{3.5}\text{Sr}_{0.5}\text{Ti}_{2.5}\text{Nb}_{0.5}\text{O}_{12}$.

Table VI-XIII: Rietveld refinement of $\text{Bi}_{3.5}\text{Sr}_{0.5}\text{Ti}_{2.5}\text{Nb}_{0.5}\text{O}_{12}$, space group B2cb, $a = 5.4551(2) \text{ \AA}$, $b = 5.4369(2) \text{ \AA}$, $c = 32.9938(7) \text{ \AA}$, Cell volume = $978.55(4) \text{ \AA}^3$

Name	x	y	z	$U_{\text{iso}} \times 100 (\text{ \AA}^2)$	Fractn
Bi(1)	0.0	0.9907(7)	0.06650(5)	2.98(5)	0.792(2)
Bi(2)	1.005(2)	0.0156(6)	0.21171(4)	2.98(5)	0.958(2)
Ti(1)	0.035(4)	0.0	0.5	2.1(2)	0.883(9)
Ti(2)	0.034(3)	1.012(2)	0.3714(2)	2.1(2)	0.808(5)
O(1)	0.206229	0.169951	0.018410	2.50	1.0
O(2)	0.245181	0.217193	0.244172	2.50	1.0
O(3)	0.112506	1.007776	0.443196	2.50	1.0
O(4)	1.038831	0.934611	0.319976	2.50	1.0
O(5)	0.196049	0.274279	0.114765	2.50	1.0
O(6)	0.123246	0.160957	0.867278	2.50	1.0
Sr(1)	1.005(3)	0.0156(6)	0.21172(4)	2.98(5)	0.042(2)
Sr(2)	-0.037(9)	0.9907(7)	0.06651(5)	2.98(5)	0.208(2)
Nb(1)	0.034(3)	1.012(2)	0.3714(2)	2.1(2)	0.192(5)
Nb(2)	0.035(4)	0.0	0.5	2.1(2)	0.117(9)

The final agreement factors are: $\chi^2 = 2.244$, $R_{\text{wp}} = 0.1085$, $R_p = 0.0809$ for 30 variable parameters.

Note: the positions of the oxygens were not refined due to their poor scattering factors with X-rays.

The final Rietveld plot of $\text{Bi}_{3.5}\text{Sr}_{0.5}\text{Ti}_{2.5}\text{Nb}_{0.5}\text{O}_{12}$ is presented in the following figure (Figure 6.16).

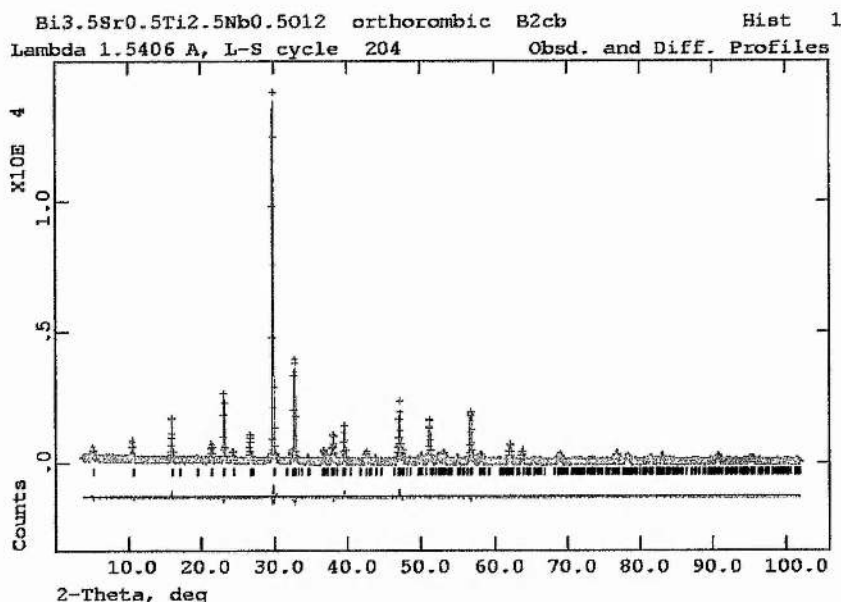


Figure 6.16: Final Rietveld plot of $\text{Bi}_{3.5}\text{Sr}_{0.5}\text{Ti}_{2.5}\text{Nb}_{0.5}\text{O}_{12}$ in space group B2cb

The relative occupancies by Nb and Ti in the B sites of the perovskite layers (i.e. the centre of the octahedra) has been studied for all compounds of the solid solution, and the results can be seen in Figure 6.17. They show that the Ti exhibit a slight preference for the inner site (labelled “Ti1/Nb2” in Figure 6.19), and the Nb for the outer site (labelled “Nb1/Ti2” in Figure 6.19). This is in accordance with recent studies on several Aurivillius and Dion-Jacobson phases.^{21,22}

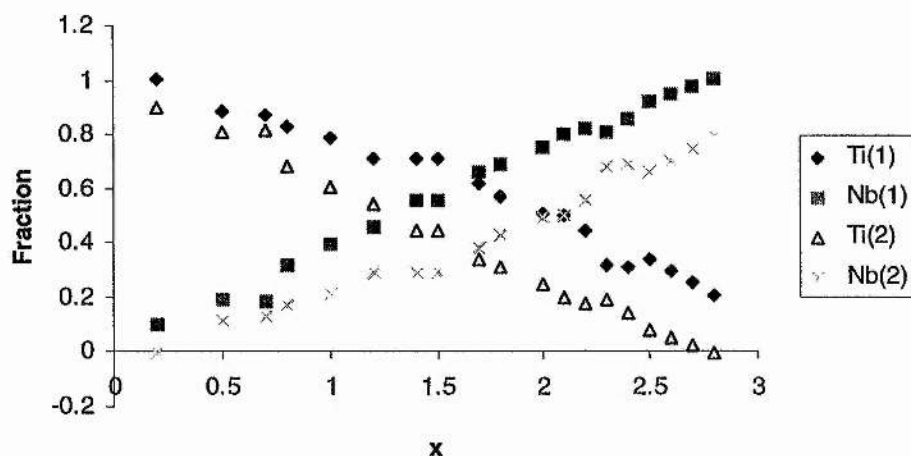


Figure 6.17: Occupancies Nb/Ti in the B sites for $\text{Bi}_{4-x}\text{Sr}_x\text{Ti}_{3-x}\text{Nb}_x\text{O}_{12}$ versus x

a.c impedance spectroscopy measurements on $\text{Bi}_{3.8}\text{Sr}_{0.2}\text{Ti}_{2.8}\text{Nb}_{0.2}\text{O}_{12}$ have been carried out, the results are presented here below and show the T_c to be about 600°C , which is significantly lower than that of $\text{Bi}_4\text{Ti}_3\text{O}_{12}$ ($T_c = 675^\circ\text{C}$). The calculated value of ϵ' at T_c ($\epsilon' \sim 550$) is also lower than that of $\text{Bi}_4\text{Ti}_3\text{O}_{12}$.

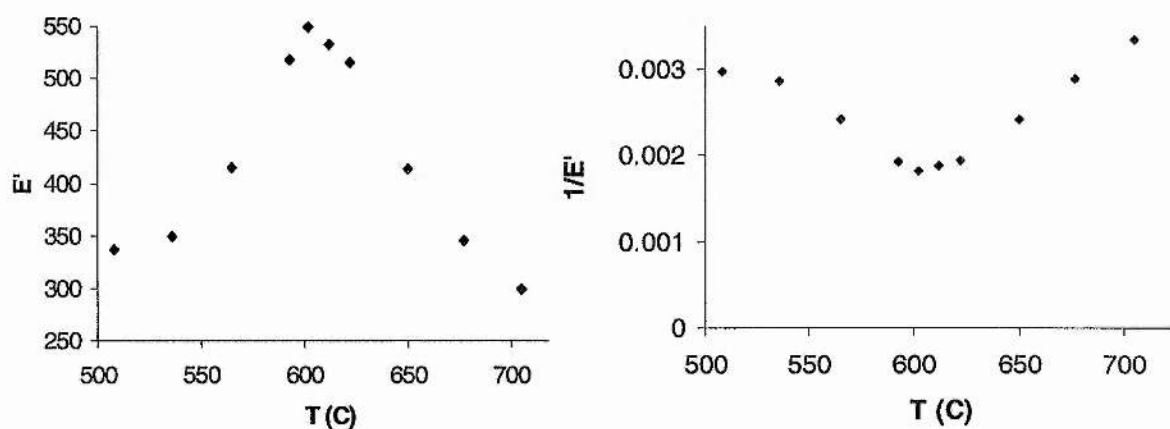


Figure 6.18: a.c. impedance measurements for $\text{Bi}_{3.8}\text{Sr}_{0.2}\text{Ti}_{2.8}\text{Nb}_{0.2}\text{O}_{12}$

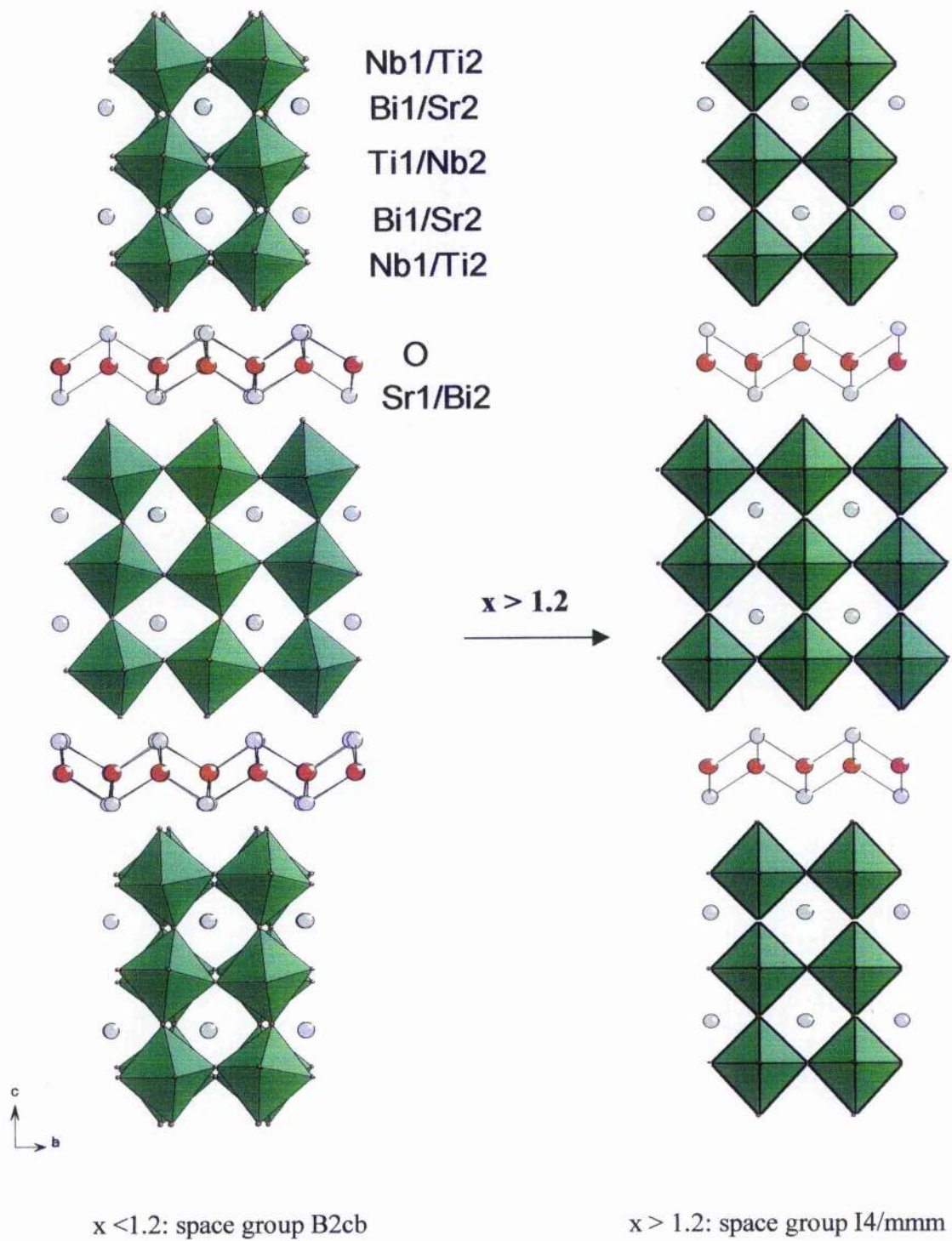


Figure 6.19: The two different space groups of $\text{Bi}_{4-x}\text{Sr}_x\text{Ti}_{3-x}\text{Nb}_x\text{O}_{12}$ at room temperature according to the value of x

6.2.2. Neutron results of $\text{Bi}_{1.8}\text{Sr}_{2.2}\text{Ti}_{0.8}\text{Nb}_{2.2}\text{O}_{12}$

A precise neutron diffraction study of this compound has been undertaken in order to have better information on the positions of the atoms for one member of the solid solution, especially the position of the oxygens.

The powder neutron diffraction data were collected at room temperature on HRPD. The data collection lasting approximately five hours for a total collected value of 206 μAhrs .

The structure has been refined by Rietveld refinement as tetragonal $I4/mmm$.

In the refinement done with the neutron data, as the relative scattering for Bi and Sr are lower than with X-rays, it was not useful to refine the occupancy of these atoms with these data as the results would be more reliable with X-rays.

On the contrary, the relative scattering of Nb and Ti are higher with neutrons than with X-rays. Therefore the relative occupancy of Nb/Ti in the B sited refined with the neutron data are of better quality than with X-rays.

Similarly, scattering of oxygens is more significant with neutrons than with X-rays, that is why we could refine the positions of the oxygen atoms in this case.

We could also allow the Bi and Sr in the M site to occupy slightly different positions. This "splitting model" led to marked improvement of the agreement factors ("non-splitting" model: $R_{wp} = 0.167$ for 31 variables, "splitting" model: $R_{wp} = 0.161$ for 32 variables).

The results of this refinement are shown on the next page.

Table VI-XIV: Rietveld refinement of $\text{Bi}_{1.8}\text{Sr}_{2.2}\text{Ti}_{0.8}\text{Nb}_{2.2}\text{O}_{12}$, space group $I4/mmm$, $a = 3.9012(1)\text{\AA}$, $c = 33.292(1)\text{\AA}$, Cell volume = $506.68(3)\text{\AA}^3$

Name	x	y	z	U_{iso} (x100)	Fractn
Bi1	0.5	0.5	0.0637(2)	2.56(14)	0.11
Sr1	0.5	0.5	0.0637(2)	2.56(14)	0.89
Bi2	0.5	0.5	0.2150(2)	2.07(16)	0.79
Sr2	0.5	0.5	0.1913(10)	2.07(16)	0.21
Ti1	0.5	0.5	0.5	1.12(13)	0.36(1)
Nb1	0.5	0.5	0.5	1.12(13)	0.64(1)
Ti2	0.5	0.5	0.3720(2)	1.12(13)	0.22(1)
Nb2	0.5	0.5	0.3720(2)	1.12(13)	0.78(1)
O1	0.5	0.5	0	7.6 *	1
O2	0.5	0	0.25	2.8 *	1
O3	0.5	0.5	0.4417(2)	3.0 *	1
O4	0.5	0.5	0.3204(2)	4.0 *	1
O5	0.5	0	0.1193(2)	1.9 *	1

Note: The relative Bi/Sr occupancy values were fixed according to X-ray refinement

* Refined anisotropically

Thermal parameters multiplied by 100.0 are

Name	U11 (x100)	U22 (x100)	U33 (x100)
O1	0.3(5)	17(1)	4.5(7)
O2	0.3(3)	0.3(3)	7.6(7)
O3	2.9(3)	2.9(3)	3.3(5)
O4	4.8(4)	4.8(4)	2.2(6)
O5	0.3(3)	1.2(3)	4.3(4)

The oxygens were refined anisotropically as they are usually more anisotropic, this is especially true for the O(1), the large value of U_{22} is explained by strain at this site (middle of the three octahedra in the perovskite layers) requiring large displacements of this oxygen around the c-axis.

Final agreement factors are: $\chi^2 = 55.30$, $R_{\text{wp}} = 0.161$ for 32 variable parameters.

The final Rietveld plot taken from the neutron diffraction data of this compound is presented on the following page.

Some selected bond-lengths for this compound are presented in Table VI-XV.

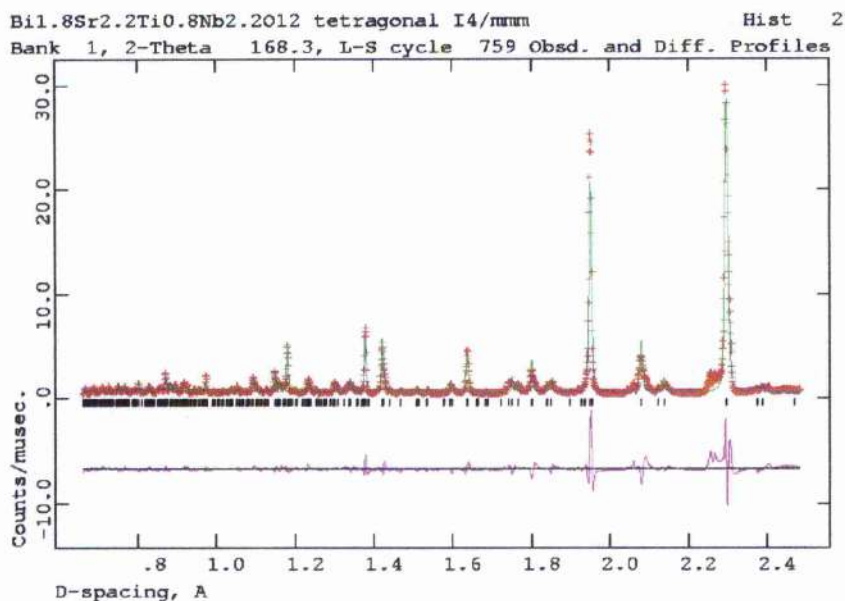


Figure 6.20: Final Rietveld plot of Bi_{1.8}Sr_{2.2}Ti_{0.8}Nb_{2.2}O₁₂ in tetragonal space group I4/mmm

Table VI-XV: Selected bond lengths for Bi_{1.8}Sr_{2.2}Ti_{0.8}Nb_{2.2}O₁₂ in space group I4/mmm established from Neutron diffraction.

Vector	Length (Å)
Bi1/Sr1 – O1 (x 4)	2.881(4)
Bi1/Sr1 – O3 (x 4)	2.7643(5)
Bi1/Sr1 – O5 (x 4)	2.688(5)
Bi2 – O2 (x 4)	2.271(4)
Bi2 – O4 (x 4)	3.001(5)
Sr2 – O2 (x4)	2.76(2)
Sr2 – O4 (x 4)	2.786(5)
Sr2 – O5 (x 4)	3.09(3)
Bi2 – Sr2	0.79(3)*
Ti1/Nb1 – O1 (x 4)	1.95061(3)
Ti1/Nb1 – O3 (x 2)	1.942(8)
Ti2/Nb2 – O3	2.32(1)
Ti2/Nb2 – O4	1.72(1)
Ti2/Nb2 – O5 (x 4)	1.973(1)

* Bi-Sr distance in the split M site

Our refinements show that the Bi and Sr cations in the fluorite sites do not occupy exactly the same position. The difference is about 0.8 Å, leading to a more regular coordination around the Sr than around the Bi, i.e. The difference in distance between the cation and the two different kinds of oxygen are less important with the Sr. (Cf. Figure 6.21)

Unlike the Bi^{3+} , the Sr^{2+} doesn't have any lone pair so that it is displaced in order to find more similar bond-lengths with the two kinds of Oxygen.

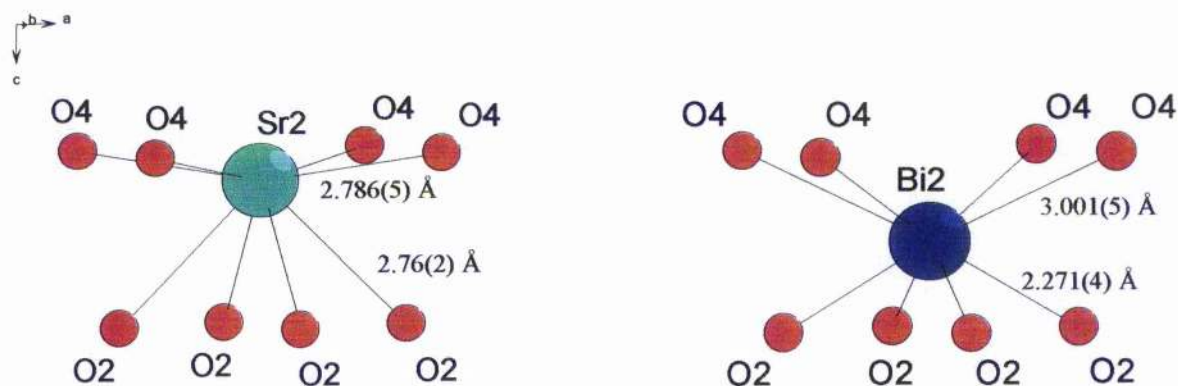
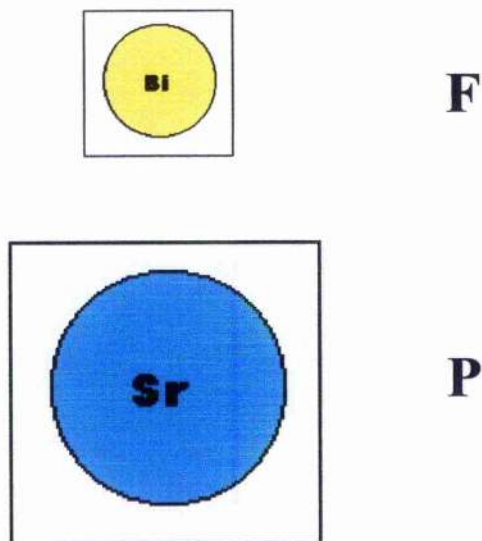


Figure 6.21: local environments of cations occupying the M site in $\text{Bi}_{1.8}\text{Sr}_{2.2}\text{Ti}_{0.8}\text{Nb}_{2.2}\text{O}_{12}$ obtained from neutron Rietveld refinement. The distances are: $\text{Sr}(2)\text{-O}(2) = 2.76(2) \text{ \AA}$, $\text{Sr}(2)\text{-O}(4) = 2.786(5) \text{ \AA}$, $\text{Bi}(2)\text{-O}(2) = 2.271(4) \text{ \AA}$, $\text{Bi}(2)\text{-O}(4) = 3.001(5) \text{ \AA}$

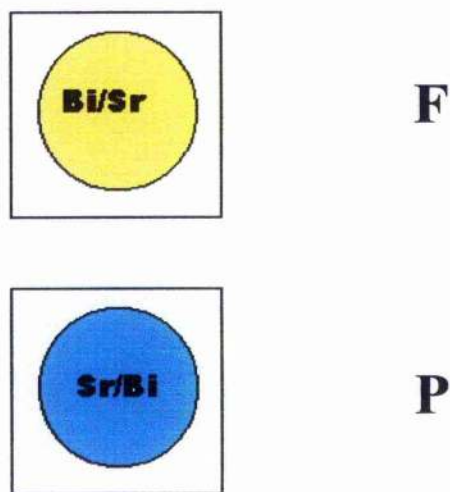
In conclusion, our study of the solid solution $\text{Bi}_{4-x}\text{Sr}_x\text{Ti}_{3-x}\text{Nb}_x\text{O}_{12}$ ($0 < x < 2.8$) shows partial substitution of the non-lone pair cation Sr^{2+} for Bi^{3+} into the $[\text{Bi}_2\text{O}_2]$ layer, the maximum amount of substitution being about 30 % at $x = 2.6$.

The neutron study of $\text{Bi}_{1.8}\text{Sr}_{2.2}\text{Ti}_{0.8}\text{Nb}_{2.2}\text{O}_{12}$ gives a precise picture of the relative position of the Sr^{2+} and Bi^{3+} in the $[\text{M}_2\text{O}_2]$ layers, demonstrating that the absence of lone pair electron for Sr^{2+} doesn't prevent its presence in the $[\text{M}_2\text{O}_2]$ layers but induces a more isotropic coordination environment illustrated by the displacement of $\sim 0.8 \text{ \AA}$ when $M = \text{Sr}$ compared with $M = \text{Bi}$.

The Bi/Sr disorder can be linked with the size of the atoms as a tolerance factor argument ($r(\text{Bi}^{3+}) = 1.17 \text{ \AA}$ for CN = 8 ; $r(\text{Sr}^{2+}) = 1.26 \text{ \AA}$ for CN = 8). The structure is much more equilibrated, and therefore stable, with a certain Bi/Sr disorder in the fluorite and perovskite sites. It can be visualised in the following schematic drawing.



(i) Ordered structure – block size mismatch



(ii) Disordered structure – block size compatible

Figure 6.22: Rationalisation of cation disorder in $\text{Bi}_{2-x}\text{Sr}_{2+x}\text{Ti}_{1-x}\text{Nb}_{2+x}\text{O}_{12}$, Consider an intergrowth of fluorite (F) and perovskite (P) blocks

As the size of the A cation increases, the perovskite block $[A_{n-1}B_nO_{3n+1}]$ becomes “too wide”, i.e the values of the lattice parameters a and b are too large comparatively to the fluorite block $[M_2O_2]$ and cation disorder occurs to stabilise the structure (Cf. Figure 6.22)

Moreover, in previous work it has been shown that in $Bi_2AB_2O_9$ (with A = Ba, Sr or Ca and B = Nb or Ta) the disorder in the two sites increases with the atom radius of the cation introduced to substitute Bi.^{12,13}

Note: The fact that no disorder was observed in the “even-layers” compound $SrBi_4Ti_4O_{15}$ (Cf. Chapter 5) is also in agreement with this “size-mismatch” theory as the perovskite layer $[A_{n-1}B_nO_{3n+1}]$ is more narrow in this case.

A table summing-up the relations between the amount of disorder Bi/A with the lattice parameters and the number of perovskite layers for different Sr-containing products follows.

Product	$SrBi_4Ti_4O_{15}$ (n = 4)		$Bi_2Sr_2TiNb_2O_{12}$ (n = 3)	$Bi_2SrNb_2O_9$ (n = 2)	
Lattice	a	b	$a\sqrt{2}$	a	b
parameters	5.451	5.438	5.503	5.520	5.515
disorder	none		~ 20 %	~ 10 %	

Note: Part of the results in this section have been published in the *Journal of Solid State Chemistry*, “Cation disorder in three-layer Aurivillius phases: Structural studies of $Bi_{2-x}Sr_{2+x}Ti_{1-x}Nb_{2+x}O_{12}$ ($0 < x < 0.8$) and $Bi_{4-x}La_xTi_3O_{12}$ ($x = 1$ and 2)”, C. H. Hervoches and P. Lightfoot, *J. Solid State Chem.*, 2000, **153**, 66.

6.3. Solid solution $\text{Bi}_{4-x}\text{La}_x\text{Ti}_3\text{O}_{12}$ ($x = 1$ and 2)

The partial substitution of La for Bi in $\text{Bi}_4\text{Ti}_3\text{O}_{12}$ has been shown to produce more effective ferroelectric properties²³, and more recently, B. H. Park et al. have demonstrated that $\text{Bi}_{3.25}\text{La}_{0.75}\text{Ti}_3\text{O}_{12}$ possesses a larger P_r than $\text{SrBi}_2\text{Ta}_2\text{O}_9$ and, in its thin film form, better physical properties (less fatigue) than $\text{Bi}_4\text{Ti}_3\text{O}_{12}$.²⁴

Two members of this promising solid solution $\text{Bi}_{4-x}\text{La}_x\text{Ti}_3\text{O}_{12}$ had been studied: $\text{Bi}_2\text{La}_2\text{Ti}_3\text{O}_{12}$ and $\text{Bi}_3\text{LaTi}_3\text{O}_{12}$.

X-ray powder diffraction data for the samples $\text{Bi}_2\text{La}_2\text{Ti}_3\text{O}_{12}$ and $\text{Bi}_3\text{LaTi}_3\text{O}_{12}$ were collected at room temperature on the Stoe STADI/P transmission diffractometer using $\text{CuK}_{\alpha 1}$ radiation over the range $4^\circ < 2\theta < 120^\circ$, the entire run lasting about 14 hours.

Rietveld refinement of X-ray data obtained on the Stoe for samples $\text{Bi}_2\text{La}_2\text{Ti}_3\text{O}_{12}$ and $\text{Bi}_3\text{LaTi}_3\text{O}_{12}$ at room temperature have been carried out.

The final Rietveld plots of these two compounds are presented on the following page.

For both of them the crystal system is tetragonal with space group $I4/mmm$. The structure type is the same as the ideal structure for $\text{Bi}_4\text{Ti}_3\text{O}_{12}$ shown in Figure 6.24 with “normal” site for La corresponding to the atom labelled Bi1/La2 in Figure 6.24.

The complete results of the Rietveld refinements are shown in Table VI-XVI and Table VI-XVII.

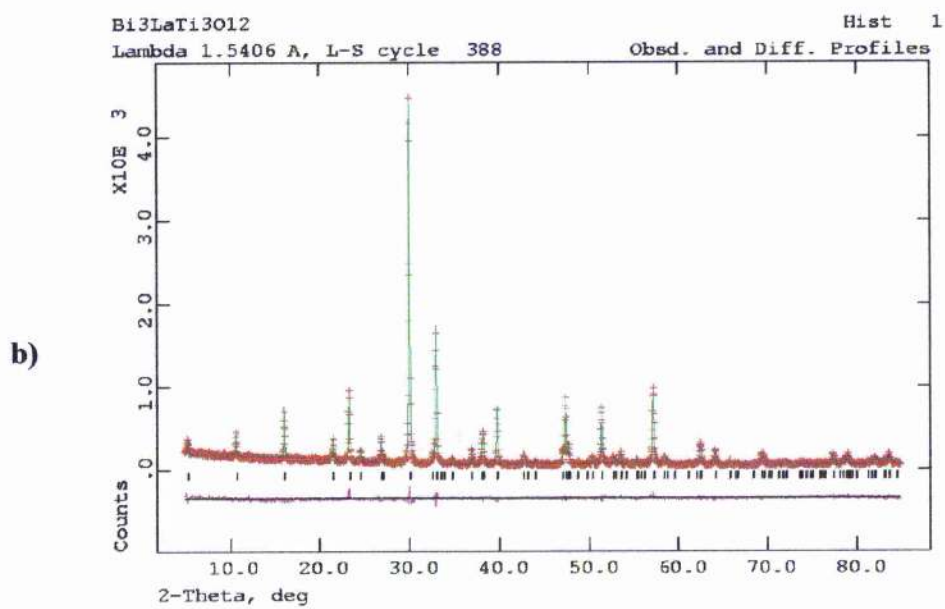
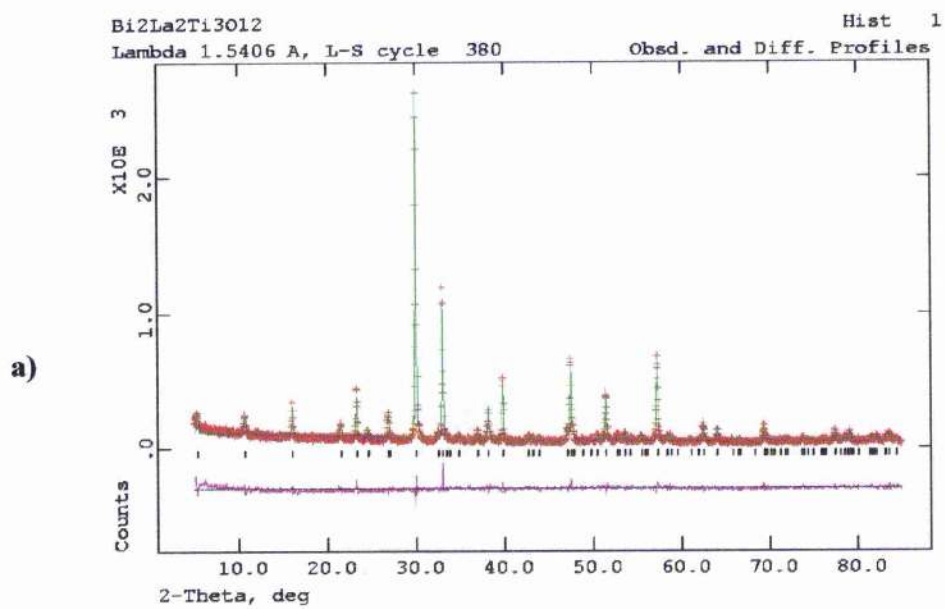


Figure 6.23: Final Rietveld plots of (a)Bi₂La₂Ti₃O₁₂ and (b)Bi₃LaTi₃O₁₂ in tetragonal space group I4/mmm

The lattice parameters are very similar, but the differences obtained in Bi and La proportion indicates clearly the presence of two different structures (cf. Table VI-XVI and Table VI-XVII).

Table VI-XVI: Rietveld refinement of $\text{Bi}_2\text{La}_2\text{Ti}_3\text{O}_{12}$, space group $I4/mmm$, $a = 3.8237(2)\text{\AA}$, $c=32.912(2)\text{\AA}$, Cell volume = $481.19(4)\text{\AA}^3$

Name	x	y	z	Uiso x 100	Fractn
Bi(1)	0.5	0.5	0.0669(2)	2.25(11)	0.173(9)
La(2)	0.5	0.5	0.0669(2)	2.25(11)	0.827(9)
Ti(1)	0.5	0.5	0.5	3.1(9)	1.0
Ti(2)	0.5	0.5	0.3681(4)	1.3(5)	1.0
O(1)	0.5	0.0	0.0	2.50	1.0
O(2)	0.5	0.0	0.25	2.50	1.0
O(3)	0.5	0.5	0.3245(14)	2.50	1.0
O(4)	0.5	0.0	0.1164(9)	2.50	1.0
O(5)	0.5	0.5	0.442(2)	2.50	1.0
Bi(2)	0.5	0.5	0.2116(2)	2.25(11)	0.827(9)
La(1)	0.5	0.5	0.2116(2)	2.25(11)	0.173(9)

Final agreement factors are: $\chi^2 = 1.485$, $R_{wp} = 0.1350$, $R_p = 0.1072$ for 24 variable parameters.

Table VI-XVII: Rietveld refinement of $\text{Bi}_3\text{LaTi}_3\text{O}_{12}$, space group $I4/mmm$, $a=3.8271(1)\text{\AA}$, $c=32.873(2)\text{\AA}$, Cell volume = $481.49(3)\text{\AA}^3$

Name	x	y	z	Uiso x 100	Fractn
Bi(1)	0.5	0.5	0.06709(8)	2.39(7)	0.564(6)
La(2)	0.5	0.5	0.06709(8)	2.39(7)	0.436(6)
Ti(1)	0.5	0.5	0.5	2.1(5)	1.0
Ti(2)	0.5	0.5	0.3706(3)	2.6(4)	1.0
O(1)	0.5	0.0	0.0	2.50	1.0
O(2)	0.5	0.0	0.25	2.50	1.0
O(3)	0.5	0.5	0.3185(9)	2.50	1.0
O(4)	0.5	0.0	0.1167(6)	2.50	1.0
O(5)	0.5	0.5	0.4399(7)	2.50	1.0
Bi(2)	0.5	0.5	0.21122(7)	2.39(7)	0.936(6)
La(1)	0.5	0.5	0.21122(7)	2.39(7)	0.064(6)

Final agreement factors are: $\chi^2 = 1.432$, $R_{wp} = 0.1041$, $R_p = 0.0806$ for 24 variable parameters.

For these compounds as well, disorder between Bi and La cations is observed, the amount of which is indicated below:

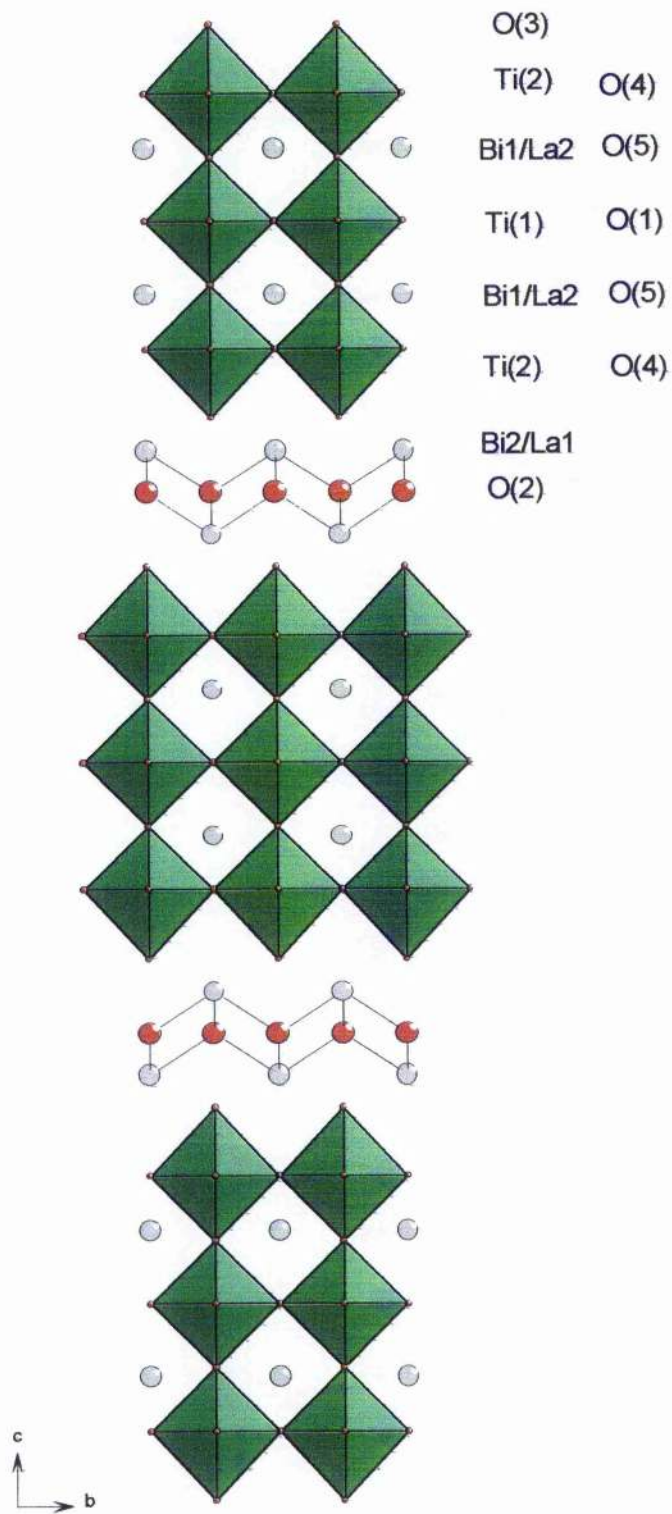


Figure 6.24: Structure of $\text{Bi}_{4-x}\text{La}_x\text{Ti}_3\text{O}_{12}$ for $x=1$ and $x=2$, space group $I4/mmm$

6.4. $\text{Bi}_2\text{Ca}_2\text{TiNb}_2\text{O}_{12}$

The compound of proposed formula $\text{Bi}_2\text{Ca}_2\text{TiNb}_2\text{O}_{12}$ has been prepared by the traditional solid state method as described in Chapter 4 (§ 4.10.2.). The X-ray pattern obtained after treatment at 1000°C is shown in Figure 6.25.

An attempt to eliminate the last impurities by a further heating treatment at 1100°C for 24 hours decomposed the sample (Cf. Figure 6.26).

No later study of this compound has been done.

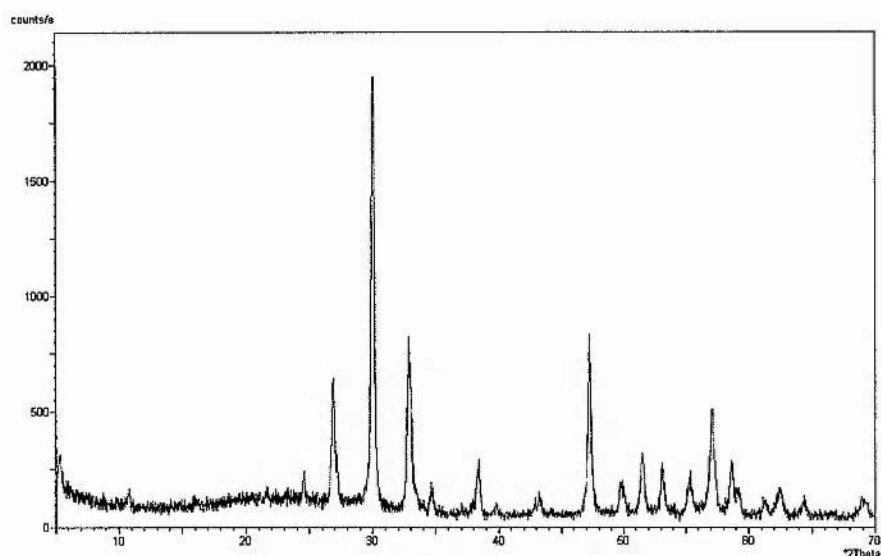


Figure 6.25: X-ray raw data of $\text{Bi}_2\text{Ca}_2\text{TiNb}_2\text{O}_{12}$ obtained after last heating treatment at 1000°C (data obtained on the Phillips diffractometer)

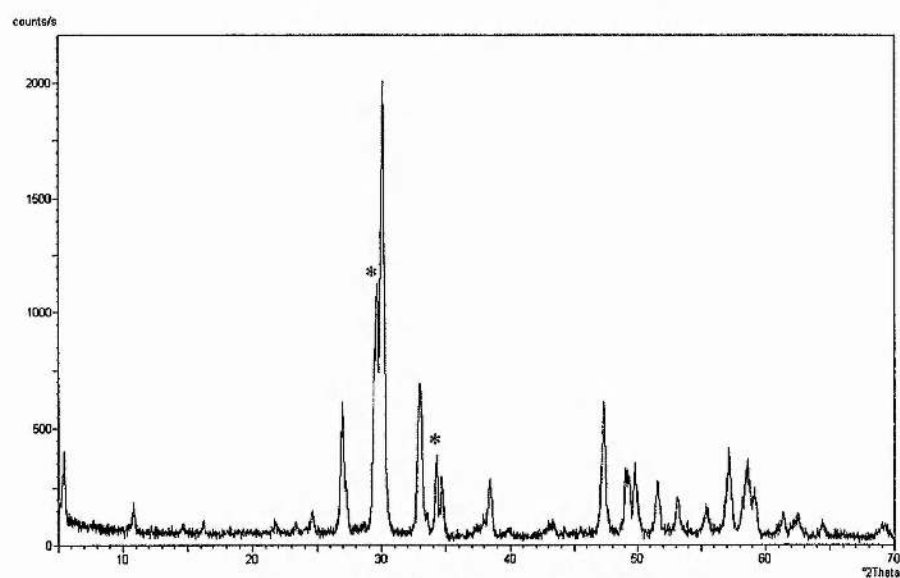


Figure 6.26: X-ray raw data of $\text{Bi}_2\text{Ca}_2\text{TiNb}_2\text{O}_{12}$ obtained after a further heating treatment at 1100°C for 24 hours (data obtained on the Phillips diffractometer) (* = impurity)

6.5. $\text{Bi}_2\text{Ln}_2\text{Ti}_3\text{O}_{12}$ (Ln = Eu, Nd)

Two compounds of the type $\text{Bi}_2\text{Ln}_2\text{Ti}_3\text{O}_{12}$, where Ln is a Lanthanide cation, have been synthesised. They are $\text{Bi}_2\text{Nd}_2\text{Ti}_3\text{O}_{12}$ and $\text{Bi}_2\text{Eu}_2\text{Ti}_3\text{O}_{12}$.

The synthesis was effectuated by by the traditional solid state method as described in Chapter 4 (§ 4.10.2.). Powder X-ray diffraction data of these two materials, collected for approximately 14 hours on the Stoe diffractometer are shown in Figure 6.27 and Figure 6.28.

The reaction seems to be completed for both of them. Unfortunately, it has not been possible to carry out a complete study of these materials due to lack of time.

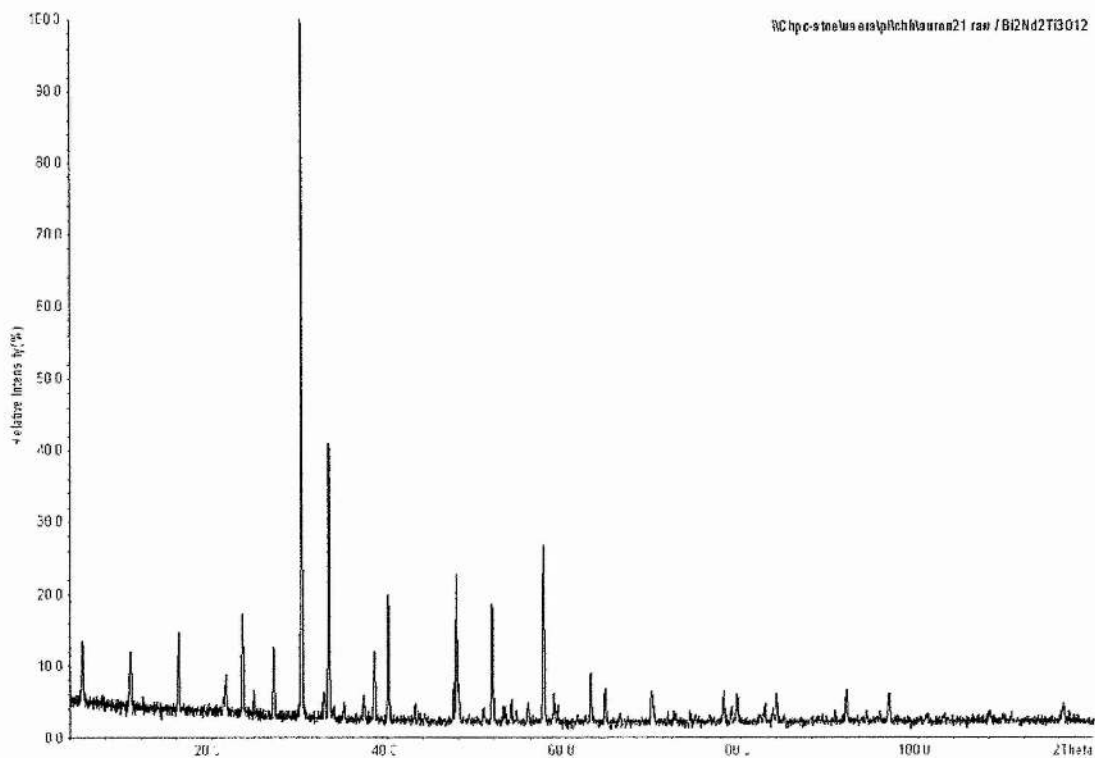


Figure 6.27: X-ray raw data of $\text{Bi}_2\text{Nd}_2\text{Ti}_3\text{O}_{12}$ obtained on the Stoe diffractometer

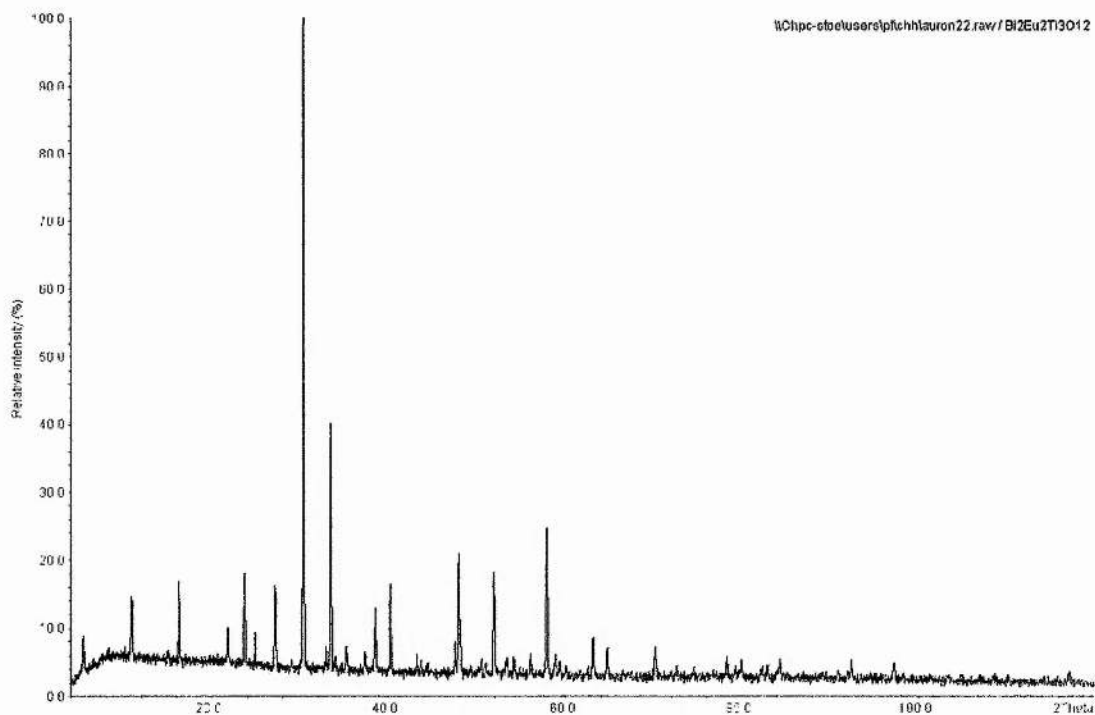


Figure 6.28: X-ray raw data of $\text{Bi}_2\text{Eu}_2\text{Ti}_3\text{O}_{12}$ obtained on the Stoe diffractometer

Conclusion

In this chapter, the existence of the phase transition scheme was confirmed as: Orthorhombic space group B2cb in the ferroelectric phase, and tetragonal space group I4/mmm in the paraelectric phase for the Aurivillius phase with three perovskite-type layers studied at different temperatures ($\text{Bi}_4\text{Ti}_3\text{O}_{12}$). No “intermediate phase” was found with this compound.

We have also demonstrated the possibility, as well as the widespread existence, of substitution of Bi in the $[\text{Bi}_2\text{O}_2]$ site by different kinds of A cations. The degree of disorder is linked with the size of the A cation, or more exactly by the size matching of the fluorite-like and perovskite-like layers, rather than the presence of an electronic lone pair as previously thought; the structure is stabilised by a more isotropic coordination environment for the cation with no electronic lone pair.

References

- ¹ E.C. Subbarao, *Phys. Rev.*, 1961, **122**, 804
- ² R. E. Newnham, R. W. Wolfe and J. F. Dorrian, *Mater. Res. Bull.*, 1971, **6**, 1029
- ³ E. C. Subbarao, *Integrated Ferroelectrics*, 1996, **12**, 33
- ⁴ V. K. Yanovskii and V. I. Voronkova, *Neorganicheskie Materialy (English translation)*, 1986, **22**, 2029
- ⁵ A. D. Rae, J. G. Thompson, R. L. Withers and A. C. Willis, *Acta Cryst.*, 1990, **B46**, 474
- ⁶ R. A. Armstrong and R. E. Newnham, *Mater. Res. Bull.*, 1972, **7**, 1025
- ⁷ P. Millan, A. Castro and J. B. Torrance, *Mater. Res. Bull.*, 1993, **28**, 117
- ⁸ T. Rentschler, M. Karus, A. Wellm and A. Reller, *Solid State Ionics*, 1996, **90**, 49
- ⁹ T. Rentschler, *Mater. Res. Bull.*, 1997, **32**, 351
- ¹⁰ M. T. Montero, P. Millan, P. Duran-Martin, B. Jimenez and A. Castro, *Mater. Res. Bull.*, 1998, **33**, 1103

-
- ¹¹ A. Castro, P. Millan, M. J. Martinez-Lope and J. B. Torrance, *Solid State Ionics*, 1993, **63-65**, 897
- ¹² S. M. Blake, M. J. Falconer, M. McCreedy and P. Lightfoot, *J. Mater. Chem.*, 1997, **7**, 1609
- ¹³ R. Macquart, B. J. Kennedy and Y. Shimakawa, *J. Solid State Chem.*, 2001, **160**, 174
- ¹⁴ S. E. Cummins and L. E. Cross, *J. Appl. Phys.*, 1968, **39**, 2268
- ¹⁵ E.C. Subbarao, *Phys. Rev.*, 1961, **122**, 804
- ¹⁶ R. E. Newnham, R. W. Wolfe and J. F. Dorrian, *Mater. Res. Bull.*, 1971, **6**, 1029
- ¹⁷ R. L. Withers, J. G. Thompson and A. D. Rae, *J. Solid State Chem.*, 1991, **94**, 404
- ¹⁸ A. S. Wills and I. D. Brown, Program VaList, CEA, France (1999).
- ¹⁹ A. Putnis, "*Introduction to Mineral Sciences*", Cambridge University Press, 1992
- ²⁰ T. Rentschler, *Mater. Res. Bull.*, 1997, **33**, 351
- ²¹ Y. S. Hong, S. J. Kim and J. H. Choy, *J. Mater. Chem.*, 2000, **10**, 1209
- ²² Y. S. Hong, C. H. Han and K. Kim, *J. Solid State Chem.*, 2001, **158**, 290
- ²³ T. Takenaka and K. Sakata, *Ferroelectrics*, 1981, **38**, 769
- ²⁴ B. H. Park, B. S. Kang, S. D. Bu, T. W. Noh, J. Lee and W. Jo, *Nature (London)*, 1999, **401**, 682
- ²⁵ I. D. Brown, *Acta Cryst.*, 1992, **B48**, 553

Chapter 7 : Sillen and Bipox phases

7.1. Sillen phases	130
7.1.1. $\text{Bi}_2\text{MO}_4\text{Cl}$ (M = Er, Yb, Lu)	130
7.1.2. $\text{Bi}_5\text{TeO}_{8.5}\text{I}_2$	137
7.2. Bipox phases: $\text{Bi}_4\text{MO}_8\text{Cl}$ (M = Ta, Nb)	140
Conclusion	148
References:	148

7.1. Sillen phases

This family of Bismuth oxyhalides has been described in Chapter 2: "Structure of the Sillen, Aurivillius, and Bipox phases".

The work presented here contains two different kinds of new materials, both belonging to the Sillen phases, and both presenting a triple fluorite-like layer (i.e. $[\text{Bi}_3\text{O}_{4+n}]$) and a single halide layer. Therefore, the symbol X_1^3 (see Chapter 2) applies to both of them.

A complete structural study of each compound prepared and a discussion follows.

7.1.1. $\text{Bi}_2\text{MO}_4\text{Cl}$ (M = Er, Yb, Lu)

These three compounds are part of a larger family of layered oxychlorides with the same global formula: $\text{Bi}_2\text{MO}_4\text{Cl}$. This family belonging itself to the X_1^3 structure type of the Sillen phases (see Chapter 2).

The first members of this family studied were $\text{Bi}_2\text{LaO}_4\text{Cl}$, $\text{Bi}_2\text{NdO}_4\text{Cl}$ and $\text{Bi}_2\text{YO}_4\text{Cl}$ ¹. The aim of the work presented here was to extend the members of this group, particularly to see if this family could accommodate Lanthanides of smaller ionic size than La^{III} , Nd^{III} and Y^{III} (ionic radii are: La^{3+} : 1.160 Å, Nd^{3+} : 1.109 Å, Y^{3+} : 1.019 Å, Er^{3+} : 1.004 Å, Yb^{3+} : 0.985 Å, Lu^{3+} : 0.977 Å, Sc^{3+} : 0.870 Å for CN = 8)².

Our results clearly show that it does as Er^{III} , Yb^{III} and Lu^{III} can all fit in the $\text{Bi}_2\text{MO}_4\text{Cl}$ type of structure. But attempts to synthesise $\text{Bi}_2\text{ScO}_4\text{Cl}$, which should be the next compound with a smaller cation in this family, were unsuccessful, probably because of the much smaller ionic size of Sc^{III} ($r(\text{Sc}^{3+}) = 0.870 \text{ \AA}$ for CN = 8).

These phases are obtained almost pure except for a small unexpected peak at $2\theta \approx 28^\circ$ which occurs in each sample. This corresponds to the strongest peak of $\beta\text{-Bi}_2\text{O}_3$, and is due to the excess of Bi_2O_3 introduced in the reaction in order to minimise the effects of its volatility.

The peaks sometimes appearing at $2\theta \approx 21.4^\circ$ and $2\theta \approx 23.8^\circ$ are due to the Vaseline used in the X-ray run with the STOE diffractometer.

The Rietveld refinements of these three compounds were realised using the powder X-ray diffraction data obtained on the STOE diffractometer collected over the range $4 < 2\theta < 120^\circ$ in 0.02° step for a total time of 14 hours.

For all of these three compounds the refinement started using the coordinates of $\text{Bi}_2\text{LaO}_4\text{Cl}$ ¹ in the tetragonal space group $P4/mmm$.

Final convergence were achieved at $\chi^2 = 2.614, 0.627, 0.908$, $R_{\text{wp}} = 0.281, 0.343, 0.204$ respectively for $\text{Bi}_2\text{ErO}_4\text{Cl}$, $\text{Bi}_2\text{YbO}_4\text{Cl}$ and $\text{Bi}_2\text{LuO}_4\text{Cl}$ for 19 variable parameters.

Nb: The relatively high value of the χ^2 for $\text{Bi}_2\text{ErO}_4\text{Cl}$ is significantly reduced when the crystallographic data of Bi_2O_3 is introduced as a second phase for the Rietveld refinement. The final agreement factors become then: $\chi^2 = 0.975$, $R_{\text{wp}} = 0.171$ for 26 variables.

For all of these products the crystal system is tetragonal, crystallising in space group $P4/mmm$, a schematic image of the structure can be seen in Figure 7.2.

The refinement plots are shown in the following page (Figure 7.1).

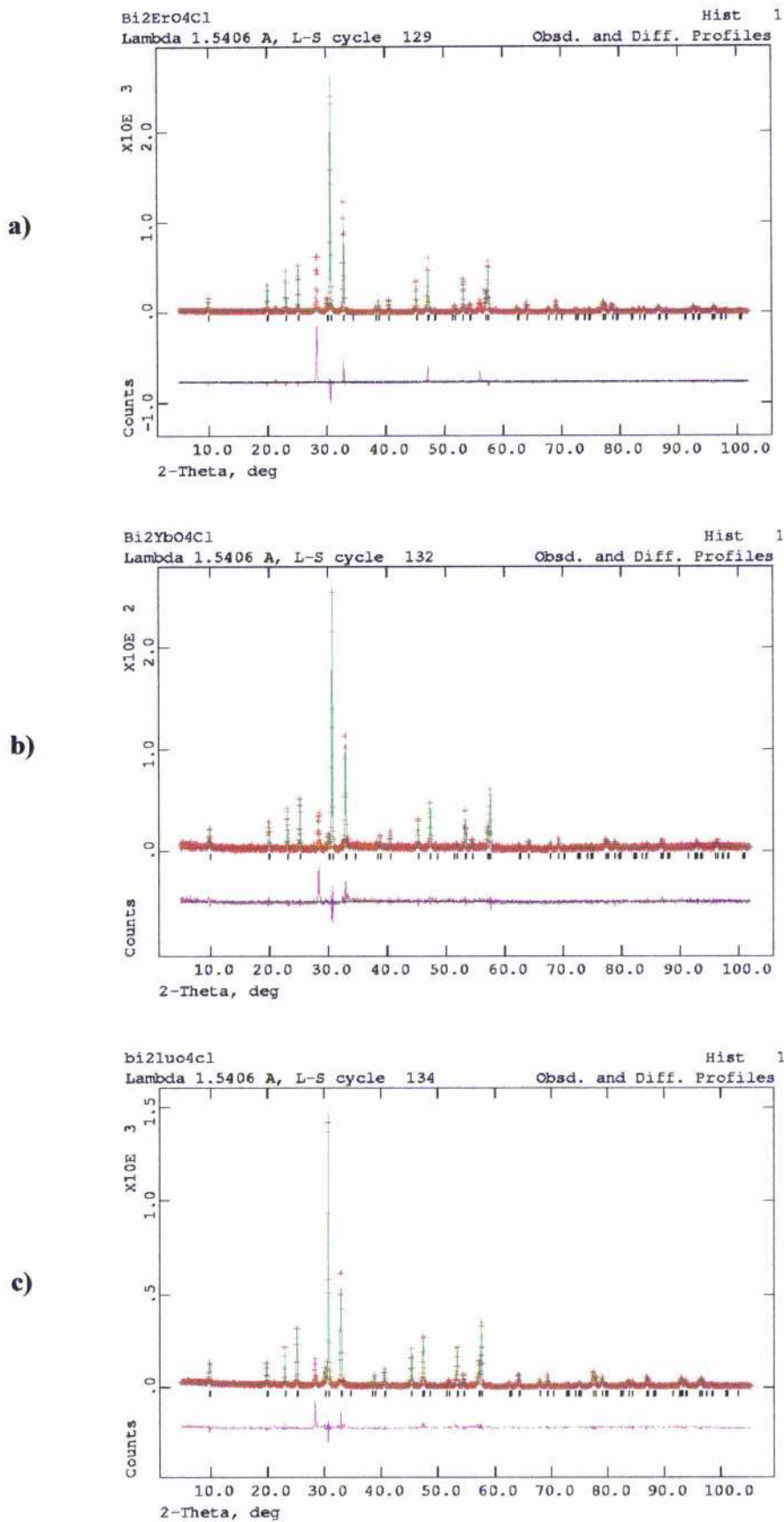


Figure 7.1: Rietveld plots of a) Bi₂ErO₄Cl, b) Bi₂YbO₄Cl and c) Bi₂LuO₄Cl

The final results of Rietveld refinements are shown in the tables below.

Table VII-I: Final parameters from the Rietveld refinement of Bi₂ErO₄Cl: Space group P4/mmm, a = 3.83895(8) Å, c = 8.8764(2) Å, Cell volume = 130.816(8) Å³.

Name	x	y	z	U _{iso} x 100 (Å ²)
Bi	0.0	0.0	0.2194(2)	2.40*
Er	0.5	0.5	0.5	2.10*
O	0.0	0.5	0.349(2)	3.3(5)
Cl	0.5	0.5	0.0	3.9(5)

*Refined anisotropically

Thermal parameters multiplied by 100.0 are

Name	U ₁₁	U ₂₂	U ₃₃
Bi	2.37(8)	2.37(8)	2.47(2)
Er	1.8(2)	1.8(2)	2.7(3)

Table VII-II: Final parameters from the Rietveld refinement of Bi₂YbO₄Cl: Space group P4/mmm, a = 3.8288(3) Å, c = 8.8664(9) Å, Cell volume = 129.98(2) Å³.

Name	x	y	z	U _{iso} x 100
Bi	0.0	0.0	0.2198(5)	3.27*
Yb	0.5	0.5	0.5	3.77*
O	0.0	0.5	0.356(4)	7.2(18)
Cl	0.5	0.5	0.0	4.6(15)

Thermal parameters multiplied by 100.0 are:

Name	U ₁₁	U ₂₂	U ₃₃
Bi	2.7(3)	2.7(3)	4.4(5)
Yb	2.8(5)	2.8(5)	5.7(9)

Table VII-III: Final parameters from the Rietveld refinement of Bi₂LuO₄Cl: Space group P4/mmm, a = 3.8197(1) Å, c = 8.8471(4) Å, Cell volume = 129.080(7)Å³.

Name	x	y	z	Uiso x 100
Bi	0.0	0.0	0.2205(3)	1.52*
Lu	0.5	0.5	0.5	1.33*
O	0.0	0.5	0.350(2)	3.0(6)
Cl	0.5	0.5	0.0	4.0(7)

* = refined anisotropically

Thermal parameters multiplied by 100.0 are:

Name	U ₁₁	U ₂₂	U ₃₃
Bi	1.30(9)	1.30(9)	1.9(2)
Lu	1.0(2)	1.0(2)	2.0(3)

Table VII-IV: selected bond distances of Bi₂MO₄Cl (M=Er, Lu, Yb):

	Bi ₂ ErO ₄ Cl	Bi ₂ YbO ₄ Cl	Bi ₂ LuO ₄ Cl
Bi-O (x 4)	2.231(11)	2.261(20)	2.228(9)
M-O (x 8)	2.346(12)	2.303(20)	2.325(9)
Bi-Cl (x 4)	3.344(2)	3.336(3)	3.332(2)

A Schematic picture of the structure can be seen in Figure 7.2.

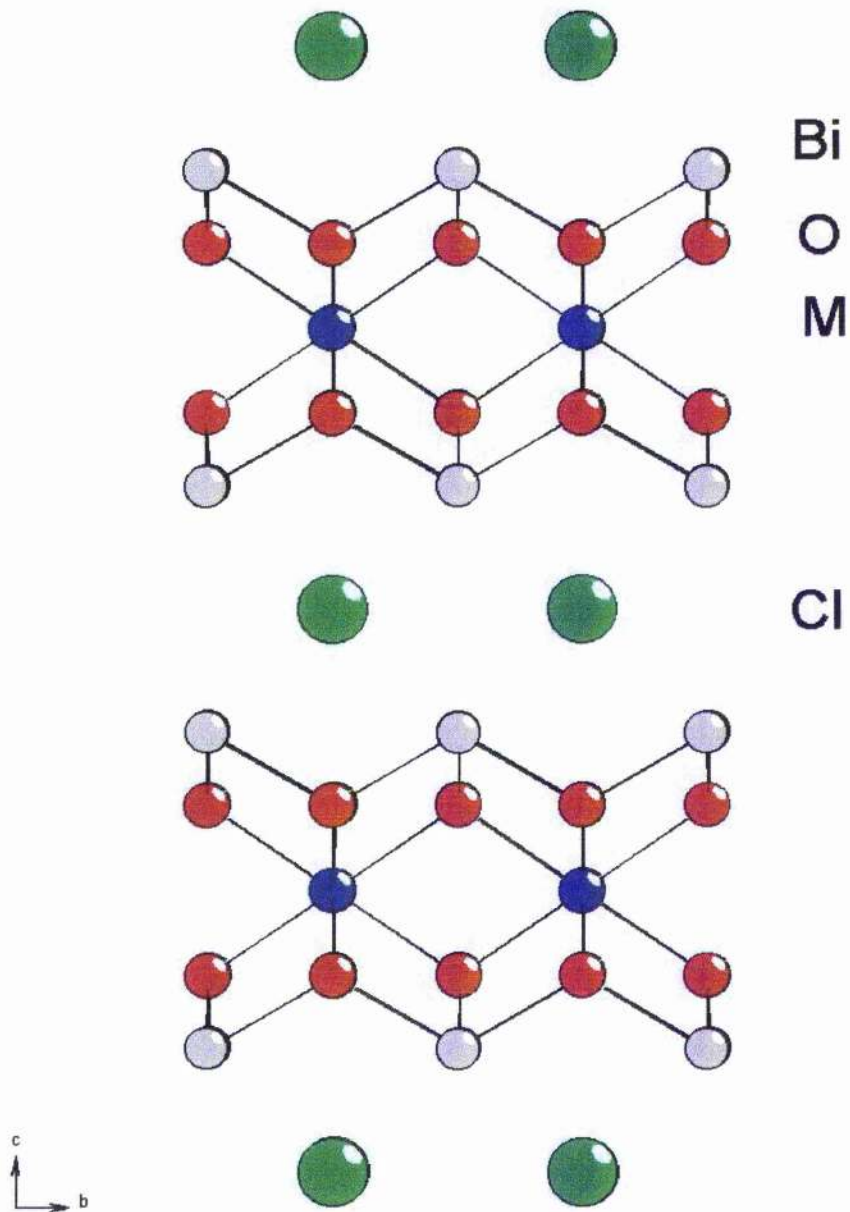


Figure 7.2: $\text{Bi}_2\text{MO}_4\text{Cl}$ (M=Er, Lu, Yb), view along the a axis.

All the patterns obtained for these three products are very similar except for the positions of the peaks: the lowest values of 2θ are obtained for $\text{Bi}_2\text{ErO}_4\text{Cl}$, the highest for $\text{Bi}_2\text{YbO}_4\text{Cl}$ (cf. plots in Figure 7.1.). This is an indication of the increase in the cell

volume (and decrease of the 2θ values) with the ionic radius of the cations introduced in the structure (cf. Table VII-V and plots in Figure 7.1.).

The lattice parameters obtained are indicated in the table below as well as the $\text{Bi}_2\text{MO}_4\text{Cl}$ products previously known¹ for comparison.

Table VII-V: $\text{Bi}_2\text{MO}_4\text{Cl}$ samples, all in tetragonal space group $P4/mmm$

M ionic r (Å)	Sample	a (Å)	c (Å)	Volume (Å ³)
1.160	$\text{Bi}_2\text{LaO}_4\text{Cl}$	3.9547(1)	9.1275(3)	142.751
1.109	$\text{Bi}_2\text{NdO}_4\text{Cl}$	3.909(2)	9.002(3)	137.553
1.019	$\text{Bi}_2\text{YO}_4\text{Cl}$	3.849(1)	8.894(3)	131.763
1.004	$\text{Bi}_2\text{ErO}_4\text{Cl}$	3.8392(2)	8.8762(4)	130.831(9)
0.985	$\text{Bi}_2\text{YbO}_4\text{Cl}$	3.8288(3)	8.8664(9)	129.98(2)
0.977	$\text{Bi}_2\text{LuO}_4\text{Cl}$	3.8197(1)	8.8471(4)	129.080(7)

The evolution of the lattice parameters versus the ionic radius clearly indicates an increase in the cell volume with the ionic radius of the cations introduced in the structure as shown in these two plots of the lattice parameters versus the ionic radii (Figure 7.3.).

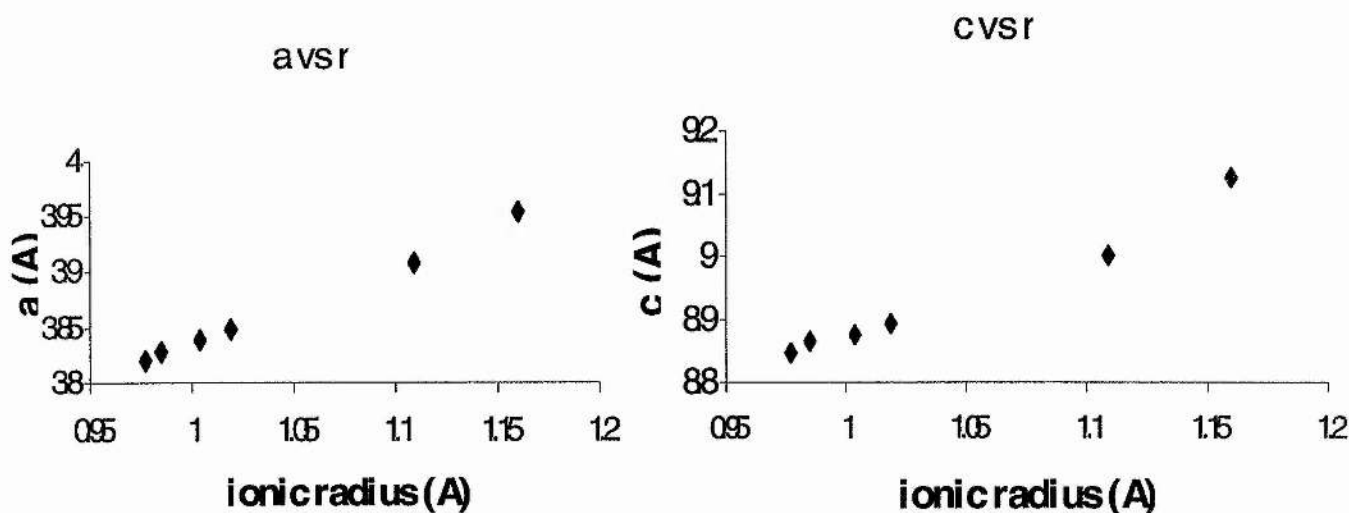


Figure 7.3: Lattice parameters versus ionic radii.

7.1.2. $\text{Bi}_5\text{TeO}_{8.5}\text{I}_2$

This product was synthesised by annealing stoichiometric mixtures of BiOI , Bi_2O_3 and TeO_2 in evacuated silica ampoules at 400°C for 96 hours in Moscow State University, Russia by D.O. Charkin and co-workers.

As in the $\text{Bi}_2\text{MO}_4\text{Cl}$ compound described in the previous section, this compound belongs to the X_1^3 structure type that present a triple metal-oxygen layer. The first two representatives of this particular series were $\text{Bi}_5\text{NdO}_8\text{Cl}$ ³ and $\text{Bi}_3\text{O}_4\text{Br}$ ⁴ discovered in the 1980's.

In this type of compound, an octahedral interstice is present in the middle of the triple metal-oxygen layer, this is clearly seen in Figure 7.2 of $\text{Bi}_2\text{MO}_4\text{Cl}$ (between the two ions M^{2+} in the fluorite-type layer). This interstice permits the introduction of an additional oxygen and thus allows the presence of a tetravalent metal atom such as Ce^{IV} (i.e. $\text{Bi}_5\text{CeO}_{8.5}\text{Cl}_2$)⁴ and Te^{IV} (i.e. $\text{Bi}_5\text{TeO}_{8.5}\text{Br}_2$)⁵.

The structure of $\text{Bi}_5\text{TeO}_{8.5}\text{I}_2$ was solved using X-ray and neutron data collected respectively on the STOE machine and HRPD at room temperature. Neutron data were collected over the range $0.72\text{-}2.3 \text{ \AA}$ for approximately 4 hours for a total collected value of $127 \mu\text{Amps}$.

The Rietveld refinement started from the atomic coordinates of $\text{Bi}_5\text{TeO}_{8.5}\text{Br}_2$, but the final crystal structure differs significantly from this model.

The final agreement factors are $R_{\text{wp}} = 0.112$, $\chi^2 = 9.493$ for 24 variable parameters.

$\text{Bi}_5\text{TeO}_{8.5}\text{I}_2$ adopts a distorted, non-centrosymmetric version of the X_1^3 structure type, space group $\text{Cmm}2$, $a = 5.6878(3) \text{ \AA}$, $b = 5.7230(3) \text{ \AA}$, $c = 9.7260(6) \text{ \AA}$, consisting of single halogen layers sandwiched between triple fluorite layers, in which there is partial ordering of the Bi/Te cations.

There is a slight difference in the position of Bi(3) and Te that appeared evident as the refinement done with the Bi and Te occupying the same position led to very large

thermal factor values. In the final version of the refinement, these two atoms are separated by 0.98 Å.

The final Rietveld plot can be seen in Figure 7.4., the final positions of the atoms in the structure and some interatomic distances are presented in the two tables below, and a representation of the unit cell can be seen in Figure 7.5.

Table VII-VI: Final parameters from the Rietveld refinement of $\text{Bi}_5\text{TeO}_{8.5}\text{I}_2$: Space group $\text{Cmm}2$, $a = 5.6878(3)$ Å, $b = 5.7230(3)$ Å, $c = 9.7260(6)$ Å, Cell volume = $316.59(5)$ Å³.

Name	x	y	z	Uiso x 100	Occupancy
Bi1	0	0	0	4.9(2)	1
Bi2	0	0.5	0.245(2)	0.7(1)	1
Bi3	0	0.5	0.698(2)	2.1(2)	0.5
Te	0.5	0	0.800(3)	2.1(2)	0.5
I	0	0	0.4948(8)	0.9(2)	1
O1	0.25	0.25	0.131(2)	3.54(8)	1
O2	0.25	0.25	0.8024(7)	3.54(8)	1
O3	0.5	0	0	3.54(8)	0.25

Note: The position of the extra oxygen O(3) was not refined due to its small scattering power.

Table VII-VII: Selected interatomic distances for $\text{Bi}_5\text{TeO}_{8.5}\text{I}_2$.

Vector	Length	Vector	Length	Vector	Length
Bi1_Bi2 x 2	3.727(6)	Bi2_I x 2	3.752(6)	Bi3_O3	2.92(3)
Bi1_Bi2 x 2	3.713(6)	Bi2_I x 2	3.738(6)	Te_O2 x 4	2.0174(4)
Bi1_Te x 2	3.44(2)	Bi2_O1 x 4	2.305(6)	Te_O3	1.95(3)
Bi1_Te x 2	3.45(2)	Bi2_O3	2.39(1)		
Bi1_O1 x 4	2.384(6)	Bi3_Te *	0.98(1)		
Bi1_O2 x 4	2.786(5)	Bi3_I x 2	3.48(1)		
Bi1_O3 x 2	2.8439(1)	Bi3_I x 2	3.41(1)		
Bi1_O3 x 2	2.8615(1)	Bi3_O2 x 4	2.256(9)		

* Split cation site.

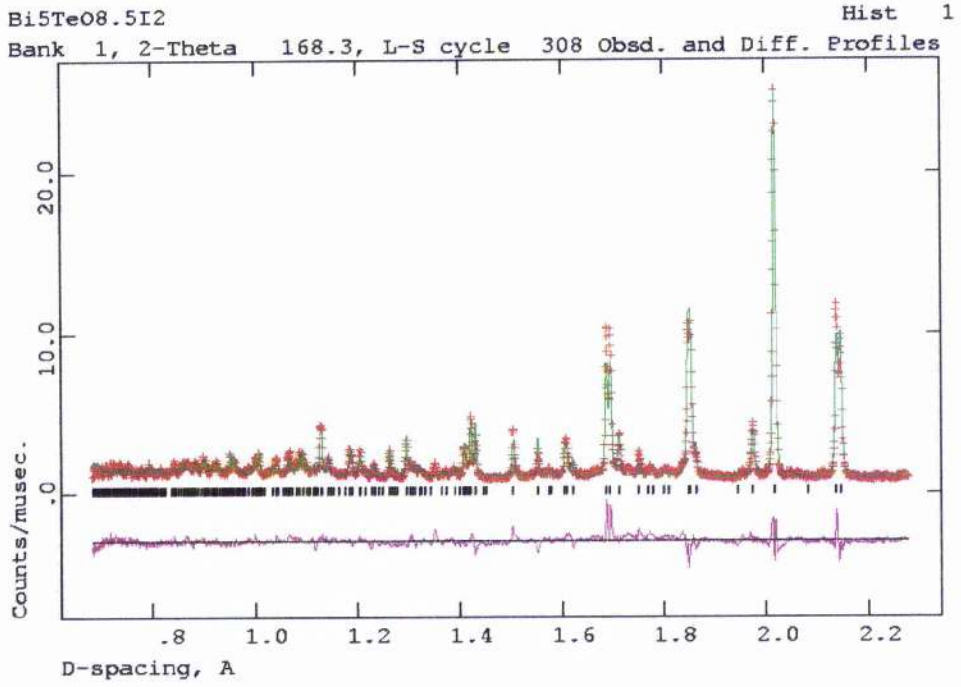


Figure 7.4: Rietveld plot of Bi₅TeO_{8.5}I₂

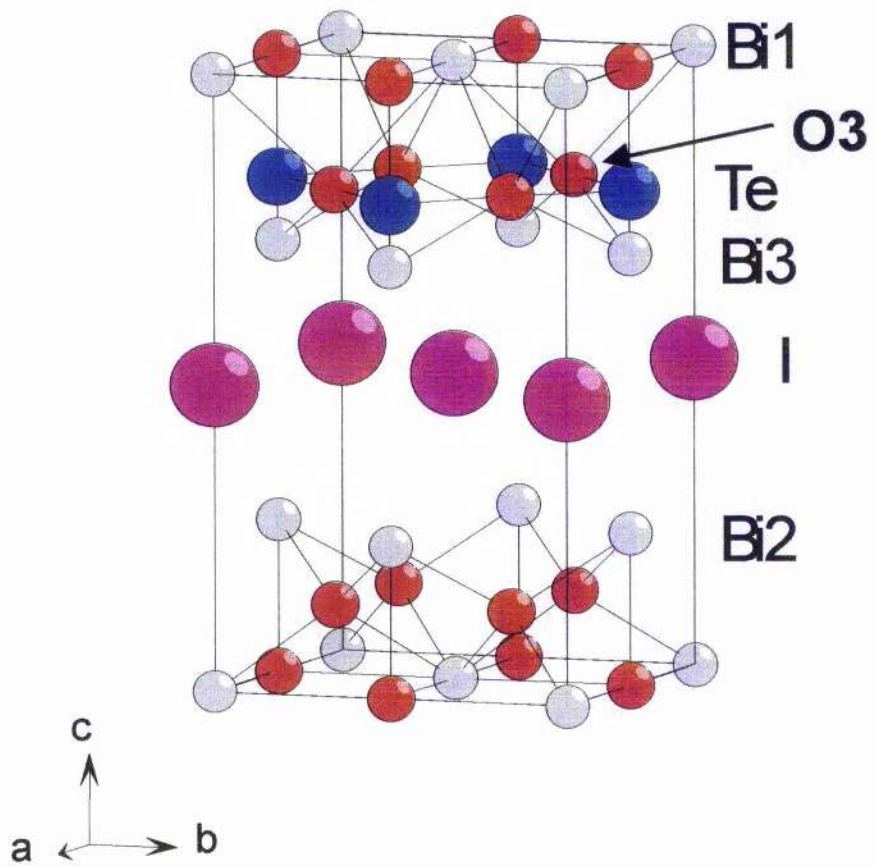


Figure 7.5: The unit cell of Bi₅TeO_{8.5}I₂

This structure is the unique case so far of a X_1^3 Sillen phase presenting a “mixed” Bi-Te layer.

Note: The work described here has been published in *Solid State Sciences*: “**The crystal structures of BiTeO_3I , NdTeO_3X ($\text{X} = \text{Cl, Br}$) and $\text{Bi}_5\text{TeO}_{8.5}\text{I}_2$: some crystal chemistry peculiarities of layered $\text{Bi}(\text{Ln})\text{-Te}$ oxyhalides**”, P. S. Berdonosov, D. O. Charkin, A. M. Kusainova, C. H. Hervoches and P Lightfoot, *Solid State Sci.*, 2000, **2(5)**, 553

7.2. Bipox phases: $\text{Bi}_4\text{MO}_8\text{Cl}$ ($M = \text{Ta, Nb}$)

The Bipox family is structurally related to both the Sillen and Aurivillius phases by regular intergrowth of Sillen block-Aurivillius block, and is described better in Chapter 2.

Because of its structural similarities with the Aurivillius family, it was interesting to see if the ferroelectric properties observed in the former were also present in this one.

The two products described in this section constitute two of the simplest members of this family, and can be designated by the symbol A_1X_1 (see Chapter 2, § 2.3.).

They have been synthesised at Moscow State University by A. M. Kusainova and co-workers by heating stoichiometric quantities of BiOCl , Bi_2O_3 and Nb_2O_5 in air at 720°C for 24 hours. Non-linear optical and dielectric characterisation have been realised by the same research group and a paper has been published containing this information together with the structural data obtained, which are described thereafter.

The crystal structures of $\text{Bi}_4\text{TaO}_8\text{Cl}$ at 50°C and that of $\text{Bi}_4\text{NbO}_8\text{Cl}$ at room temperature have been determined using powder neutron diffraction data collected on HRPD at ISIS. The data were collected for approximately four hours each for a total collected value of $160 \mu\text{Ahrs}$.

The Rietveld refinement of $\text{Bi}_4\text{TaO}_8\text{Cl}$ at 50°C and $\text{Bi}_4\text{NbO}_8\text{Cl}$ at room temperature started from the crystal data established by Ackerman⁶ using single X-ray diffraction.

The possibility that the material may crystallise in a higher, tetragonal “parent structure” symmetry represented by the structure of $\text{PbBi}_3\text{WO}_8\text{Cl}$ described by Ackerman in the same paper has also been tested. This “parent structure” of space group $P4/mmm$ is related to the actual lower symmetry $P2_1cn$ by the following relations: $a \approx b \approx \sqrt{2} a_p$, $c \approx 2 c_p$, $V \approx 4 V_p$, where the subscript p designs the “parent structure”. This possibility is proved to be wrong by the presence of the peaks (131) at 1.74 \AA , (135) at 1.66 \AA – the doubling of the c -parameter would not allow an odd value for the Miller index l – and (124) which would not be allowed in the smaller cell.

The possibility of a C-centred supercell was also tested but was invalidated by the presence of the peak (124) at 2.32 \AA .

These results confirm the orthorhombic space group $P2_1cn$, but the atomic positions differ from the structure proposed by Ackerman, leading to a better structural description. The better quality of this neutron refinement can be seen by bond valence sum analysis in the table below, which shows a particular improvement on the unusual bond valence sum values in the Ackerman model (5.23 for Bi(3) and 1.20 for O(8)).

Table VII-VIII: Bond valence sum analysis for $\text{Bi}_4\text{TaO}_8\text{Cl}$ and $\text{Bi}_4\text{NbO}_8\text{Cl}$

Atom	$\text{Bi}_4\text{TaO}_8\text{Cl}$ Present Work	$\text{Bi}_4\text{NbO}_8\text{Cl}$ Ackerman	$\text{Bi}_4\text{NbO}_8\text{Cl}$ Present Work
M(1)	4.84	5.26	4.89
Bi(1)	2.91	3.20	2.88
Bi(2)	3.16	2.90	3.34
Bi(3)	2.73	5.23	2.77
Bi(4)	3.39	3.39	3.15
Cl(1)	0.75	0.85	0.74
O(1)	2.34	2.54	2.48
O(2)	2.38	2.79	2.65
O(3)	2.15	2.85	2.00
O(4)	2.10	2.51	1.95
O(5)	1.94	2.15	2.19
O(6)	1.69	3.27	1.46
O(7)	1.76	1.82	1.77
O(8)	1.83	1.20	1.81

The final Rietveld plots are in Figure 7.6.

The structural parameters obtained are in Table VII-IX and Table VII-X. A picture of the structure is shown on Figure 7.7.

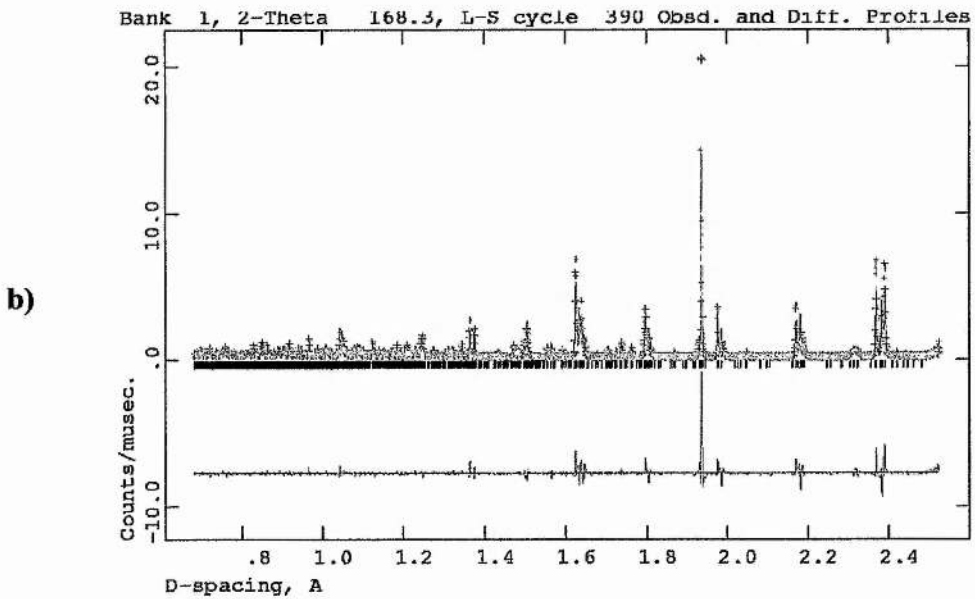
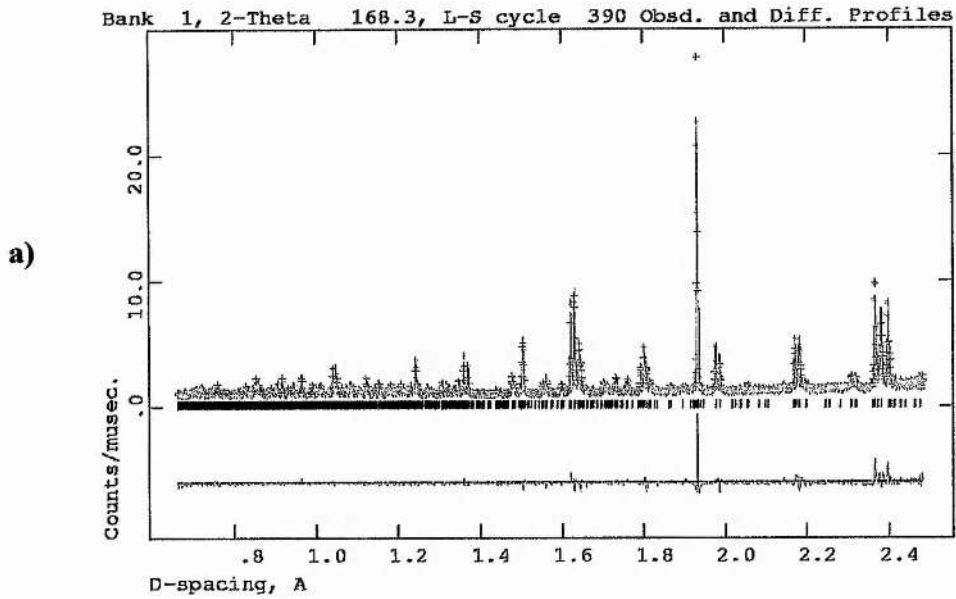


Figure 7.6: Rietveld plots of a) $\text{Bi}_4\text{TaO}_8\text{Cl}$ at 50°C and b) $\text{Bi}_4\text{NbO}_8\text{Cl}$ at room temperature

Table VII-IX: Refined structural parameters for Bi₄TaO₈Cl at 50°C, in the true polar space group P2₁cn (first line), a = 5.4472(1) Å, b = 5.4901(1) Å, c = 28.8125(6) Å and centrosymmetric space group Pmcn (second line)

Atom	x ¹	y	z	U _{iso} (x100)
Ta(1)	0.014(4)	0.243(1)	0.2516(6)	0.6(1)
	0.25	0.241(2)	0.2460(3)	0.5(1)
Bi(1)	0.0 ²	0.814(2)	0.1569(4)	2.2(3)
	0.25	0.785(1)	0.1563(2)	1.0(2)
Bi(2)	0.004(3)	0.253(2)	0.4327(4)	1.5(3)
	0.25	0.250(1)	0.4311(2)	0.3(1)
Bi(3)	0.031(2)	0.779(2)	0.3425(4)	2.7(3)
	0.25	0.817(2)	0.3383(4)	7.2(4)
Bi(4)	0.023(3)	0.254(2)	0.0681(4)	0.6(2)
	0.25	0.253(2)	0.0666(3)	2.7(2)
Cl(1)	0.521(4)	0.238(2)	-0.0011(6)	2.0(1)
	0.75	0.236(2)	0.0027(3)	2.4(1)
O(1)	0.771(4)	0.516(3)	0.3947(5)	0.6(4)
	0.017(2)	0.514(2)	0.3951(3)	0.7(2)
O(2) ³	0.263(5)	0.495(3)	0.3978(5)	1.2(4)
	-	-	-	-
O(3)	0.767(5)	-0.016(3)	0.3918(5)	1.4(4)
	0.004(3)	-0.011(2)	0.3940(3)	3.6(3)
O(4) ⁴	0.267(6)	0.004(3)	0.3940(5)	1.4(4)
	-	-	-	-
O(5)	0.432(3)	0.687(2)	0.3171(4)	0.2(2)
	0.75	0.700(5)	0.318(1)	10.2(8)
O(6)	0.589(5)	0.744(5)	0.1818(10)	8.6(7)
	0.75	0.705(12)	0.182(2)	21.7(20)
O(7)	0.299(4)	0.024(3)	0.2358(5)	2.4(4)
	0.502(4)	-0.011(4)	0.2400(5)	10.1(4)
O(8) ⁵	-0.200(5)	-0.055(3)	0.2590(7)	4.3(4)
	-	-	-	-

1. There is a shift of $\Delta x = 0.25$ between the two settings
2. Fixed to define origin of polar axis
3. Equivalent to O(1) in Pmcn
4. Equivalent to O(3) in Pmcn
5. Equivalent to O(7) in Pmcn

For P2₁cn Convergence was achieved with the following agreement factors : $\chi^2 = 3.65$ and $R_{wp} = 0.065$ for 68 variables ; for Pmcn $\chi^2 = 5.55$, $R_{wp} = 0.080$.

Our Rietveld refinement of $\text{Bi}_4\text{NbO}_8\text{Cl}$ at 25°C leads to the final structure described in the table below ; This structure is very similar to the one of $\text{Bi}_4\text{TaO}_8\text{Cl}$.

Table VII-X: Refined structural parameters for $\text{Bi}_4\text{NbO}_8\text{Cl}$ at 25°C , space group $\text{P2}_1\text{cn}$, $a = 5.4589(2)$ Å, $b = 5.5044(2)$ Å, $c = 28.6998(9)$ Å.

Atom	x	y	z	U_{iso} (x100)
Nb(1)	-0.003(4)	0.248(2)	0.2483(5)	-0.6(1)
Bi(1)	0.0 ¹	0.832(2)	0.1570(4)	1.2(2)
Bi(2)	0.006(4)	0.251(2)	0.4313(4)	0.1(2)
Bi(3)	0.025(3)	0.743(2)	0.3425(4)	1.6(2)
Bi(4)	0.016(4)	0.249(2)	0.0670(4)	0.9(2)
Cl(1)	0.509(5)	0.254(2)	-0.0002(5)	1.7(1)
O(1)	0.772(6)	0.516(4)	0.394(1)	0.9(9)
O(2)	0.264(6)	0.496(3)	0.395(1)	0.3(7)
O(3)	0.768(6)	0.003(4)	0.395(1)	1.2(8)
O(4)	0.269(6)	0.006(3)	0.395(1)	-0.3(7)
O(5)	0.420(5)	0.712(3)	0.3196(7)	2.0(6)
O(6)	0.589(5)	0.701(3)	0.1856(7)	1.9(6)
O(7)	0.301(6)	0.061(1)	0.240(1)	3.9(8)
O(8)	-0.221(7)	-0.048(4)	0.2624(9)	3.6(7)

1. Fixed to define origin of polar axis

The final agreement factors for this compound are $R_{\text{wp}} = 0.179$ and $\chi^2 = 27.5$ for 68 variables.

Note: The high value of the agreement factors for this compound are due to a systemic broadening of the (0kl) reflection. This would suggest that the actual symmetry is actually lower than $\text{P2}_1\text{cn}$. Attempts to refine the structure in the monoclinic space group P2_111 were unsuccessful due to the large number of atomic coordinates (83) to refine with this structure.

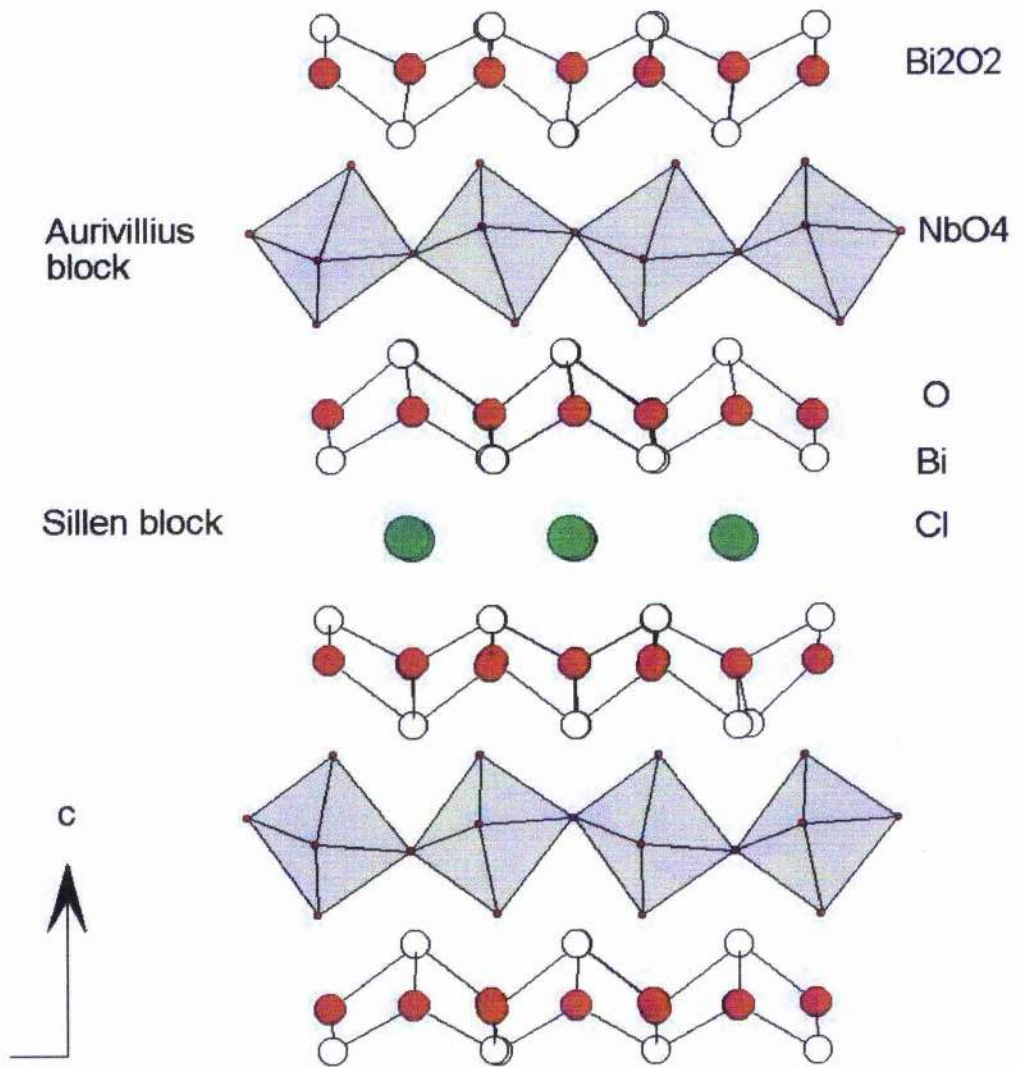


Figure 7.7: Representation of the crystal structure of $\text{Bi}_4\text{NbO}_8\text{Cl}$

It can be noted that, in the present study, the TaO_6 or NbO_6 octahedra are more regular (i.e. the metal is more central) than in related Aurivillius phases such as $\text{Bi}_2\text{ANb}_2\text{O}_9$ ($A = \text{Ca}, \text{Sr}, \text{Ba}$) described in a previous chapter (see Chapter 5).

Dielectric characterisations of the two compounds were performed at the Karpov Institute of Physical Chemistry, Moscow. The dielectric constant was measured between 300 and 1000 K with a.c. bridges in the frequency range 10^3 - 10^6 Hz.

The results near the phase transition are presented in Figure 7.8 and clearly demonstrate ferroelectric properties for both of them.

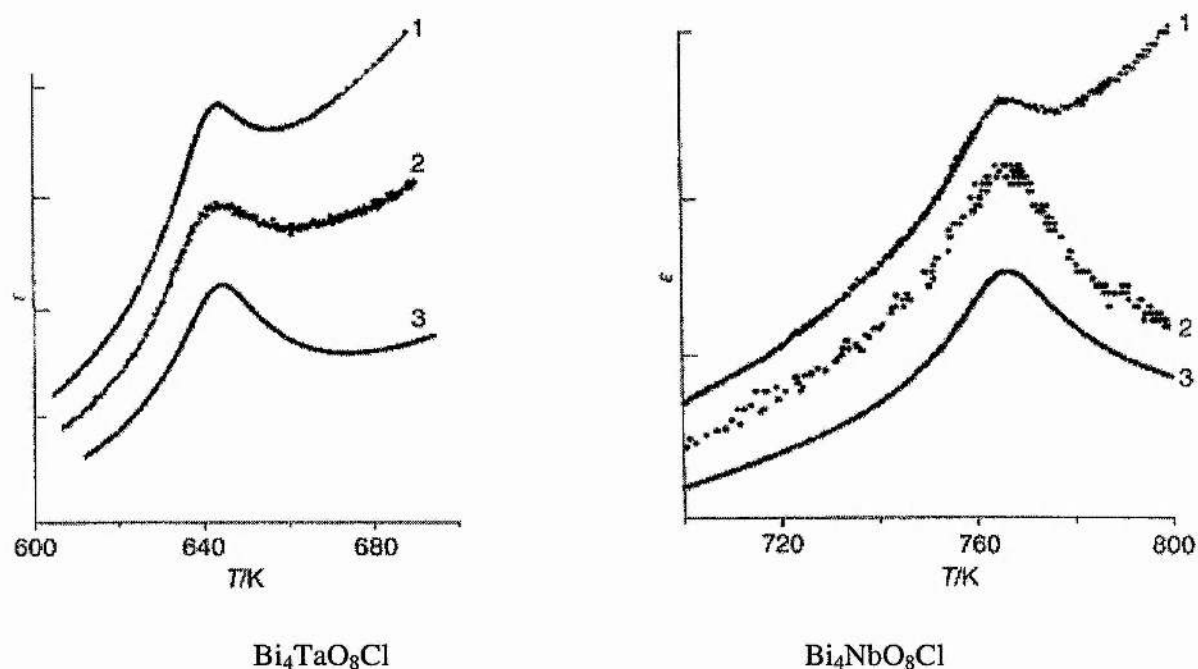


Figure 7.8: Measurement of the dielectric constant versus the temperature by a.c. impedance spectroscopy at frequency 10 (1), 100 (2) and 1000 kHz (3).

Note: for ease of comparison, the scale of ϵ' is arbitrary

Note: The work described in this section has been published in the Journal of Materials Chemistry: “**Dielectric properties and structure of $\text{Bi}_4\text{NbO}_8\text{Cl}$ and $\text{Bi}_4\text{TaO}_8\text{Cl}$** “, A. M. Kusainova, S. Yu. Stefanovich, V. A. Dolgikh, A. V. Mosunov, C. H. Hervoches and P. Lightfoot, *J. Mater. Chem*, 2001, **11**, 1141

Additionally, the crystal structure of $\text{Bi}_4\text{TaO}_8\text{Cl}$ has also been studied at several temperatures until 750°C by neutron diffraction on HRPD by P. Lightfoot et al. and should be published soon.

Conclusion

In the Sillen family, we extended the numbers of materials belonging to the $\text{Bi}_2\text{MO}_4\text{Cl}$ type, with M = Lanthanide cation, and proved that in this family, the smaller introducible Lanthanide is Lu^{3+} .

We also solved the unusual structure of a X_1^3 Sillen phase (i.e. $\text{Bi}_5\text{TeO}_{8.5}\text{I}_2$) presenting the unique known case of a "mixed" Bi-Te layer for these phases.

In the Bipox family, two materials presenting ferroelectric properties have been studied and their crystal structures solved. One of them presenting a significant improvement over the previous crystallographic data reported in the literature, the other being entirely new.

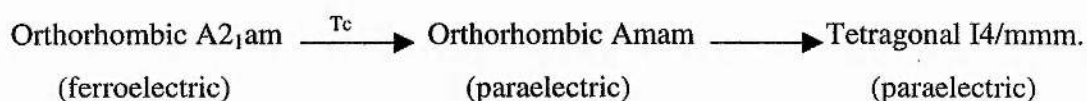
References:

-
- ¹ C. J. Milne, P. Lightfoot, J. D. Jorgensen and S. Short, *J. Mater. Chem.*, 1995, **5**, 1419
 - ² R. D. Shannon, *Acta Cryst.*, 1976, **A32**, 751
 - ³ B. Z. Nurgaliev, B. A. Popovkin and S. Y. Stefanovich, *Zh. Neorg. Khim*, 1983, **28**, 2207
 - ⁴ B. Aurivillius, *Chem. Scripta*, 1984, **24**, 125
 - ⁵ V. A. Dolgikh L. N. Kholodkovskaya and B. A. Popovkin, *Russ. J. Inorg. Chem.*, 1996, **41**, 932
 - ⁶ J. F. Ackerman, *J. Solid State Chem.*, 1986, **62**, 92

CONCLUSION

In this thesis, several structural features in the Aurivillius, Sillen and Bipox phases have been revealed, particularly, the sequence of the phases transition(s) in the Aurivillius phases. They are of importance to understand the physical properties observed in these materials.

In the Aurivillius phases studied containing an even number ($n = 2$ or 4) of perovskite-type layers, the presence of two phases transitions have been demonstrated to occur for $\text{Sr}_{0.85}\text{Bi}_{2.1}\text{Ta}_2\text{O}_9$ ($n = 2$) and $\text{SrBi}_4\text{Ti}_4\text{O}_{15}$ ($n = 4$). The sequence of these phases transitions can be presented as follows:



This phase transition sequence is not observed in $\text{SrBi}_2\text{Nb}_2\text{O}_9$ ($n = 2$), which presents only one phase transition from the orthorhombic space group $A2_1am$ to the tetragonal $I4/mmm$ at T_c .

Similarly, no “intermediate” phase is observed for $\text{Bi}_4\text{Ti}_3\text{O}_{12}$, the Aurivillius phase studied containing an odd number ($n = 3$) of perovskite-type layers. That seems to make the presence of an intermediate phase the “privilege” of the “even-layer” compounds. The “odd-layer” present one phase transition, at T_c , from the orthorhombic space group $B2cb$ to the tetragonal $I4/mmm$.

The nature of the phase transition in $\text{Bi}_4\text{Ti}_3\text{O}_{12}$ has been defined as close to first order, and an indication that the transition in this material is of the “order-disorder” rather than “displacive” type has been given.

In the “odd-layer” compounds, the major interest of the studies carried out concern the atom-ordering scheme. In the solid solutions $\text{Bi}_{4-x}\text{Sr}_x\text{Ti}_{3-x}\text{Nb}_x\text{O}_{12}$ and $\text{Bi}_{4-x}\text{La}_x\text{Ti}_3\text{O}_{12}$, the presence of Bi in the A site ($A = \text{Sr}$ and La), and the related presence of the A cation in the $[\text{Bi}_2\text{O}_2]$ site has been demonstrated. The absence of a lone pair of electrons for the A cations studied implies the displacement of this cation in the $[\text{Bi}_2\text{O}_2]$ site relative to the position occupied by the Bi in this same site, in order to find a more isotropic coordination environment.

The observation of disorder Bi/A has been rationalised in terms of “size matching” between the fluorite and the perovskite sites, i.e. the structure is more stable with the fluorite and the perovskite layers of similar width, thus allowing Bi/A disorder to occur.

Ti/Nb disorder in the B site has also been studied for $\text{Bi}_{4-x}\text{Sr}_x\text{Ti}_{3-x}\text{Nb}_x\text{O}_{12}$, and shows a preference of the Ti for the middle octahedra of the three perovskite layers, the Nb being preferentially present in the two outer ones.

In the Sillen family, the crystal structure of three new members of the X_1^3 structure type phases with the formula $\text{Bi}_2\text{MO}_4\text{Cl}$ ($M = \text{Er}, \text{Yb}, \text{Lu}$) has been solved. They crystallise in the tetragonal space group $P4/mmm$. Lu^{3+} has been defined as the smallest Lanthanide cation able to be accommodated in the structure.

In the same structure-type, $\text{Bi}_5\text{TeO}_{8.5}\text{I}_2$ crystallises in the orthorhombic space group $Cmm2$, with a unique case of a “mixed” Bi-Te layer.

Two members of the Bipox family, $\text{Bi}_4\text{MO}_8\text{Cl}$ ($M = \text{Nb}, \text{Ta}$), presenting ferroelectric properties have been characterised. They crystallise in the orthorhombic space group $P2_1cn$.

APPENDICES

- Appendix A: Final atomic coordinates for $\text{SrBi}_2\text{Nb}_2\text{O}_9$ at several temperatures (Polaris data)
- Appendix B: Final atomic coordinates for $\text{SrBi}_4\text{Ti}_4\text{O}_{15}$ at several temperatures (HRPD data)
- Appendix C.1: Final atomic coordinates for $\text{Bi}_4\text{Ti}_3\text{O}_{12}$ at several temperatures (Polaris data)
- Appendix C.2: Selected bondlengths and angles for $\text{Bi}_4\text{Ti}_3\text{O}_{12}$ (Polaris data)
- Appendix D: Final atomic coordinates for the solid solution $\text{Bi}_{4-x}\text{Sr}_x\text{Ti}_{3-x}\text{Nb}_x\text{O}_{12}$ at room temperature (data obtained on the Stoe diffractometer)
- Appendix E: Neutron scattering lengths

Appendix A: Final atomic coordinates for SrBi₂Nb₂O₉ at several temperatures (Polaris data)

25°C space group A2₁am

constants are

a = 5.51672(19) b = 5.51426(19) c = 25.0808(4)

Alpha = 90 Beta = 90 Gamma = 90

Cell volume = 762.97(4)

Name	x	y	z	Uiso (x100)	Fractn
Sr	.000000	.2546(6)	.000000	.801(34)	1.0000
Bi	.4880(9)	.7642(5)	.20134(5)	1.969(40)	1.0000
Nb	.5159(8)	.7468(5)	.41331(5)	.115(18)	1.0000
O(1)	.5417(12)	.2949(10)	.000000	.826(67)	1.0000
O(2)	.5292(10)	.7037(6)	.34133(8)	1.432(54)	1.0000
O(3)	.7477(10)	.9975(5)	.25076(11)	.577(28)	1.0000
O(4)	.7544(10)	.9748(5)	.07019(7)	.551(35)	1.0000
O(5)	.8124(9)	.9632(6)	.58447(9)	.466(38)	1.0000

50°C space group A2₁am

constants are

a = 5.51863(20) b = 5.51620(20) c = 25.0891(4)

Alpha = 90 Beta = 90 Gamma = 90

Cell volume = 763.76(4)

Name	x	y	z	Uiso (x100)	Fractn
Sr	.000000	.2543(7)	.000000	.89(4)	1.0000
Bi	.4889(9)	.7637(5)	.20138(6)	2.09(4)	1.0000
Nb	.5159(9)	.7470(5)	.41332(5)	.146(18)	1.0000
O(1)	.5423(14)	.2930(11)	.000000	.959(72)	1.0000
O(2)	.5293(10)	.7037(6)	.34138(8)	1.515(57)	1.0000
O(3)	.7486(11)	.9970(6)	.25074(11)	.628(29)	1.0000
O(4)	.7537(11)	.9750(6)	.07026(8)	.601(37)	1.0000
O(5)	.8113(10)	.9646(6)	.58441(9)	.587(41)	1.0000

100°C space group A2₁am

constants are

a = 5.52105(21) b = 5.51893(21) c = 25.1001(5)

Alpha = 90 Beta = 90 Gamma = 90

Cell volume = 764.81(4)

Name	x	y	z	Uiso (x100)	Fractn
Sr	.000000	.2541(7)	.000000	1.05(4)	1.0000
Bi	.4885(10)	.7635(6)	.20136(6)	2.24(4)	1.0000
Nb	.5136(10)	.7466(5)	.41331(5)	.186(18)	1.0000
O(1)	.5400(15)	.2912(12)	.000000	1.186(77)	1.0000
O(2)	.5277(11)	.7036(7)	.34139(9)	1.607(60)	1.0000
O(3)	.7470(12)	.9977(6)	.25070(11)	.754(31)	1.0000
O(4)	.7511(12)	.9760(6)	.07030(8)	.712(39)	1.0000
O(5)	.8075(11)	.9653(6)	.58430(10)	.711(44)	1.0000

150°C space group A2₁am

constants are

a = 5.52340(23) b = 5.52193(23) c = 25.1116(5)

Alpha = 90 Beta = 90 Gamma = 90

Cell volume = 765.90(5)

Name	x	y	z	Uiso (x100)	Fractn
Sr	.000000	.2530(8)	.000000	1.18(4)	1.0000
Bi	.4896(11)	.7626(6)	.20142(6)	2.43(5)	1.0000
Nb	.5132(11)	.7469(6)	.41331(5)	.247(19)	1.0000
O(1)	.5379(17)	.2907(13)	.000000	1.473(85)	1.0000
O(2)	.5269(12)	.7043(7)	.34142(9)	1.833(65)	1.0000
O(3)	.7471(13)	.9975(7)	.25057(12)	.872(33)	1.0000
O(4)	.7507(13)	.9772(7)	.07040(8)	.859(42)	1.0000
O(5)	.8049(12)	.9661(7)	.58420(10)	.842(48)	1.0000

200°C space group $A2_1am$

constants are

$a = 5.52603(25)$ $b = 5.52482(26)$ $c = 25.1230(5)$

Alpha = 90 Beta = 90 Gamma = 90

Cell volume = 767.01(5)

Name	x	y	z	Uiso (x100)	Fractn
Sr	.000000	.2523(9)	.000000	1.35(4)	1.0000
Bi	.4897(13)	.7616(6)	.20141(6)	2.58(5)	1.0000
Nb	.5110(13)	.7472(6)	.41335(6)	.290(19)	1.0000
O(1)	.5358(20)	.2875(15)	.000000	1.72(9)	1.0000
O(2)	.5251(14)	.7044(8)	.34140(9)	1.93(7)	1.0000
O(3)	.7460(15)	.9983(7)	.25054(13)	1.00(4)	1.0000
O(4)	.7478(15)	.9789(8)	.07059(9)	.99(5)	1.0000
O(5)	.8013(14)	.9671(8)	.58405(11)	1.00(5)	1.0000

250°C space group $A2_1am$

constants are

$a = 5.52871(28)$ $b = 5.52780(28)$ $c = 25.1338(5)$

Alpha = 90 Beta = 90 Gamma = 90

Cell volume = 768.13(6)

Name	x	y	z	Uiso (x100)	Fractn
Sr	.000000	.251184	.000000	1.48	1.0000
Bi	.489789	.761155	.201399	2.76	1.0000
Nb	.508514	.747377	.413342	.35	1.0000
O(1)	.533763	.285612	.000000	1.95	1.0000
O(2)	.523583	.704770	.341350	2.04	1.0000
O(3)	.744355	.998716	.250425	1.11	1.0000
O(4)	.745687	.980349	.070711	1.13	1.0000
O(5)	.796957	.968241	.583888	1.14	1.0000

300°C space group A2₁am

constants are

a = 5.53137(31) b = 5.53093(32) c = 25.1449(5)

Alpha = 90 Beta = 90 Gamma = 90

Cell volume = 769.27(6)

Name	x	y	z	Uiso (x100)	Fractn
Sr	.000000	.2501(10)	.000000	1.68(4)	1.0000
Bi	.4901(18)	.7604(7)	.20139(7)	2.98(5)	1.0000
Nb	.5053(17)	.7476(6)	.41336(6)	.396(20)	1.0000
O(1)	.5305(26)	.2827(18)	.000000	2.24(11)	1.0000
O(2)	.5226(18)	.7057(10)	.34137(10)	2.28(8)	1.0000
O(3)	.7429(20)	.9992(9)	.25028(15)	1.30(4)	1.0000
O(4)	.7428(21)	.9823(10)	.07081(10)	1.27(5)	1.0000
O(5)	.7921(20)	.9690(9)	.58369(11)	1.31(6)	1.0000

350°C space group A2₁am

constants are

a = 5.5343(4) b = 5.5343(4) c = 25.1558(5)

Alpha = 90 Beta = 90 Gamma = 90

Cell volume = 770.48(8)

Name	x	y	z	Uiso (x100)	Fractn
Sr	.000000	.2481(12)	.000000	1.77(5)	1.0000
Bi	.4862(23)	.7589(8)	.20135(7)	3.17(5)	1.0000
Nb	.4952(22)	.7487(7)	.41343(6)	.445(21)	1.0000
O(1)	.5221(33)	.2788(20)	.000000	2.41(12)	1.0000
O(2)	.5146(24)	.7060(11)	.34134(11)	2.47(9)	1.0000
O(3)	.7366(23)	.9992(11)	.25006(16)	1.42(5)	1.0000
O(4)	.7347(28)	.9852(12)	.07098(10)	1.43(6)	1.0000
O(5)	.7807(27)	.9693(12)	.58336(12)	1.55(7)	1.0000

400°C space group A2₁am

constants are

a = 5.5377(5) b = 5.5380(5) c = 25.1657(5)

Alpha = 90 Beta = 90 Gamma = 90

Cell volume = 771.78(9)

Name	x	y	z	Uiso (x100)	Fractn
Sr	.000000	.2457(14)	.000000	1.86(7)	1.0000
Bi	.4867(25)	.7566(9)	.20133(8)	3.40(5)	1.0000
Nb	.4912(25)	.7482(7)	.41339(6)	.508(23)	1.0000
O(1)	.5170(37)	.2735(24)	.000000	2.92(14)	1.0000
O(2)	.5136(29)	.7089(12)	.34133(11)	2.75(10)	1.0000
O(3)	.7357(25)	1.0012(13)	.25012(17)	1.64(5)	1.0000
O(4)	.7328(32)	.9887(14)	.07118(11)	1.62(6)	1.0000
O(5)	.7746(31)	.9710(14)	.58304(12)	1.72(8)	1.0000

450°C space group I4/mmm

constants are

a = 3.91941(5) b = A c = 25.1711(4)

Alpha = 90 Beta = 90 Gamma = 90

Cell volume = 386.672(9)

Name	x	y	z	Ueq (x100)	Fractn
Sr	.500000	.500000	.000000	1.95*	1.0000
Nb	.000000	.000000	.08656(4)	.66*	1.0000
O(1)	.500000	.500000	.500000	3.50*	1.0000
O(2)	.000000	.500000	.250000	1.87*	1.0000
O(4)	.000000	.000000	.15878(7)	5.72*	1.0000
O(5)	.000000	.500000	.07680(5)	3.37*	1.0000
Bi	.500000	.500000	.20105(6)	3.60*	1.0000

Thermal parameters multiplied by 100.0 are

Name	U11	U22	U33
Sr	2.22(6)	2.22(6)	1.40(9)
Nb	.628(22)	.628(22)	.72(5)
O(1)	4.41(10)	4.41(10)	1.67(12)
O(2)	1.72(5)	1.72(5)	2.16(8)
O(4)	8.24(11)	8.24(11)	.67(9)
O(5)	4.41(7)	.32(4)	5.37(7)
Bi	3.22(5)	3.22(5)	4.35(8)

500°C space group I4/mmm

constants are

a = 3.92185(5) b = A c = 25.1864(4)

Cell volume = 387.390(9)

Name	x	y	z	Ueq (x100)	Fractn
Sr	.500000	.500000	.000000	2.04*	1.0000
Nb	.000000	.000000	.08658(4)	0.74*	1.0000
O(1)	.500000	.500000	.500000	3.59*	1.0000
O(2)	.000000	.500000	.250000	1.97*	1.0000
O(4)	.000000	.000000	.15871(7)	5.77*	1.0000
O(5)	.000000	.500000	.07680(5)	3.37*	1.0000
Bi	.500000	.500000	.20099(6)	3.77*	1.0000

Thermal parameters multiplied by 100.0 are

Name	U11	U22	U33
Sr	2.32(5)	2.32(5)	1.49(9)
Nb	.695(22)	.695(22)	.83(5)
O(1)	4.47(10)	4.47(10)	1.83(12)
O(2)	1.81(5)	1.81(5)	2.30(8)
O(4)	8.25(11)	8.25(11)	.83(9)
O(5)	4.31(7)	.37(4)	5.43(7)
Bi	3.43(5)	3.43(5)	4.44(8)

550°C space group I4/mmm

constants are

a = 3.92395(5) b = A c = 25.2042(4)

Cell volume = 388.078(9)

Name	x	y	z	Ueq (x100)	Fractn
Sr	.500000	.500000	.000000	2.23*	1.0000
Nb	.000000	.000000	.086594	.79*	1.0000
O(1)	.500000	.500000	.500000	3.69*	1.0000
O(2)	.000000	.500000	.250000	2.05*	1.0000
O(4)	.000000	.000000	.158703	5.92*	1.0000
O(5)	.000000	.500000	.076846	3.48*	1.0000
Bi	.500000	.500000	.201026	3.94*	1.0000

Thermal parameters multiplied by 100.0 are

Name	U11	U22	U33
Sr	2.47	2.47	1.75
Nb	.75	.75	.86
O(1)	4.58	4.58	1.90
O(2)	1.87	1.87	2.41
O(4)	8.46	8.46	.86
O(5)	4.35	.41	5.68
Bi	3.58	3.58	4.66

600°C space group I4/mmm

constants are

a = 3.92598(5) b = A c = 25.2231(4)

Cell volume = 388.771(9)

Name	x	y	z	Ueq (x100)	Fractn
Sr	.500000	.500000	.000000	2.35*	1.0000
Nb	.000000	.000000	.08654(4)	.86*	1.0000
O(1)	.500000	.500000	.500000	3.72*	1.0000
O(2)	.000000	.500000	.250000	2.23*	1.0000
O(4)	.000000	.000000	.15869(7)	6.14*	1.0000
O(5)	.000000	.500000	.07689(5)	3.54*	1.0000
Bi	.500000	.500000	.20095(6)	4.12*	1.0000

Thermal parameters multiplied by 100.0 are

Name	U11	U22	U33
Sr	2.62(6)	2.62(6)	1.81(10)
Nb	.821(22)	.821(22)	.93(5)
O(1)	4.61(10)	4.61(10)	1.95(12)
O(2)	2.00(6)	2.00(6)	2.69(8)
O(4)	8.75(12)	8.75(12)	.92(9)
O(5)	4.43(7)	.40(4)	5.79(7)
Bi	3.74(5)	3.74(5)	4.86(8)

650°C space group I4/mmm

constants are

a = 3.92803(5) b = A c = 25.2437(4)

Cell volume = 389.496(9)

Name	x	y	z	Ueq (x100)	Fractn
Sr	.500000	.500000	.000000	2.53*	1.0000
Nb	.000000	.000000	.08648(4)	.96*	1.0000
O(1)	.500000	.500000	.500000	3.93*	1.0000
O(2)	.000000	.500000	.250000	2.34*	1.0000
O(4)	.000000	.000000	.15859(7)	6.24*	1.0000
O(5)	.000000	.500000	.07683(5)	3.62*	1.0000
Bi	.500000	.500000	.20089(6)	4.24*	1.0000

Thermal parameters multiplied by 100.0 are

Name	U11	U22	U33
Sr	2.89(6)	2.89(6)	1.82(10)
Nb	.910(23)	.910(23)	1.05(5)
O(1)	4.77(10)	4.77(10)	2.26(13)
O(2)	2.13(6)	2.13(6)	2.75(9)
O(4)	8.77(12)	8.77(12)	1.16(9)
O(5)	4.50(7)	.45(4)	5.91(7)
Bi	3.82(5)	3.82(5)	5.07(8)

700°C space group I4/mmm

constants are

a = 3.93008(5) b = A c = 25.2644(4)

Cell volume = 390.222(9)

Name	x	y	z	Ueq (x100)	Fractn
Sr	.500000	.500000	.000000	2.64*	1.0000
Nb	.000000	.000000	.08653(4)	1.01*	1.0000
O(1)	.500000	.500000	.500000	3.92*	1.0000
O(2)	.000000	.500000	.250000	2.46*	1.0000
O(4)	.000000	.000000	.15850(7)	6.37*	1.0000
O(5)	.000000	.500000	.07693(5)	3.70*	1.0000
Bi	.500000	.500000	.20094(6)	4.37*	1.0000

Thermal parameters multiplied by 100.0 are

Name	U11	U22	U33
Sr	2.87(6)	2.87(6)	2.19(11)
Nb	.956(23)	.956(23)	1.13(5)
O(1)	4.79(11)	4.79(11)	2.18(13)
O(2)	2.25(6)	2.25(6)	2.89(9)
O(4)	9.03(12)	9.03(12)	1.04(9)
O(5)	4.63(7)	.48(4)	5.99(8)
Bi	3.97(5)	3.97(5)	5.19(8)

Appendix B: Final atomic coordinates for SrBi₄Ti₄O₁₅ at several temperatures (HRPD data)

At 200°C, space group A2₁am

Lattice constants are

a = 5.45672(10) b = 5.44672(10) c = 41.0808(8)

Alpha = 90 Beta = 90 Gamma = 90

Cell volume = 1220.97(4)

Name	x	y	z	Uiso (x100)	fractn
Sr1	.2500000	.253(4)	.0000000	3.10(22)	.350
Sr2	.253(7)	.2482(32)	.10366(18)	6.23(24)	.325
Bi4	.2500000	.253(4)	.0000000	3.10(22)	.650
Bi5	.253(7)	.2482(32)	.10367(18)	6.23(24)	.675
Bi6	.244(4)	.2594(20)	.21835(13)	4.52(19)	1.000
Ti7	.272(5)	.248(5)	.45059(20)	.87(22)	1.000
Ti8	.264(6)	.246(4)	.34721(24)	1.62(22)	1.000
O9	.301(5)	.217(5)	.5000000	3.66(49)	1.000
O10	.559(5)	.5397(27)	.0545(4)	3.31(37)	1.000
O11	.293(5)	.2941(31)	.40433(22)	3.09(27)	1.000
O12	.505(4)	.4910(27)	.14197(26)	1.41(28)	1.000
O13	.278(4)	.215(4)	.30387(22)	4.21(34)	1.000
O14	.494(5)	.4981(26)	.2495(4)	2.90(25)	1.000
O15	-.008(5)	-.0260(33)	.04340(31)	4.21(41)	1.000
O16	.014(4)	.002(4)	.1459(4)	4.83(44)	1.000

The final agreement factors are: $\chi^2 = 3.595$, $R_{wp} = 0.0668$, $R_p = 0.0698$ for 60variables.

At 300°C, space group A2₁am

Lattice constants are

a = 5.46040(10) b = 5.45236(10) c = 41.1428(7)

Alpha = 90 Beta = 90 Gamma = 90

Cell volume = 1224.91(4)

Name	x	y	z	Uiso (x100)	Fractn
Sr1	.2500000	.251(4)	.0000000	4.61(26)	.350
Sr2	.252(7)	.2487(32)	.10456(17)	6.20(25)	.325
Bi4	.2500000	.251(4)	.0000000	4.61(26)	.650
Bi5	.252(7)	.2487(32)	.10456(17)	6.20(25)	.675
Bi6	.242(5)	.2600(20)	.21829(13)	4.63(20)	1.000
Ti7	.270(6)	.245(6)	.45007(20)	1.01(21)	1.000
Ti8	.265(7)	.239(4)	.34677(22)	1.25(22)	1.000
O9	.296(6)	.218(7)	.5000000	4.39(56)	1.000
O10	.556(6)	.5391(28)	.05166(34)	3.08(37)	1.000
O11	.287(6)	.2906(34)	.40349(23)	3.99(31)	1.000
O12	.504(5)	.4940(29)	.14076(27)	1.64(26)	1.000
O13	.279(5)	.222(4)	.30348(22)	4.36(34)	1.000
O14	.495(7)	.4976(29)	.2503(4)	3.64(27)	1.000
O15	-.005(7)	-.023(4)	.04410(31)	4.73(46)	1.000
O16	.017(6)	.006(5)	.14672(34)	4.78(48)	1.000

The final agreement factors are: $\chi^2 = 3.533$, $R_{wp} = 0.0652$, $R_p = 0.0679$ for 60variables.

At 400°C, space group A2₁am

Lattice constants are

a = 5.46440(13) b = 5.45943(13) c = 41.2174(8)

Alpha = 90 Beta = 90 Gamma = 90

Cell volume = 1229.62(5)

Name	x	y	z	Uiso (x100)	Fractn
Sr1	.250000	.254(5)	.000000	5.00(30)	.3500
Sr2	.253(9)	.252(4)	.10401(21)	6.86(26)	.3250
Bi4	.250000	.2538(55)	.000000	5.00(30)	.6500
Bi5	.253(9)	.2518(43)	.10401(21)	6.86(26)	.6750
Bi6	.251(6)	.2584(32)	.21822(16)	6.27(25)	1.0000
Ti7	.273(7)	.245(8)	.44992(24)	1.18(27)	1.0000
Ti8	.268(8)	.244(5)	.34753(26)	1.25(27)	1.0000
O9	.291(8)	.2196(88)	.500000	5.05(66)	1.0000
O10	.554(7)	.5387(30)	.05470(39)	3.36(38)	1.0000
O11	.281(7)	.2830(52)	.40390(27)	4.98(38)	1.0000
O12	.496(6)	.4899(29)	.14292(31)	1.94(33)	1.0000
O13	.278(6)	.2270(63)	.30333(25)	4.81(38)	1.0000
O14	.497(9)	.5014(44)	.25187(47)	5.06(33)	1.0000
O15	-.006(7)	-.0218(41)	.04445(37)	5.03(47)	1.0000
O16	.000(6)	-.0052(37)	.14392(31)	2.68(37)	1.0000

The final agreement factors are: $\chi^2 = 2.179$, $R_{wp} = 0.0728$, $R_p = 0.0740$ for 60variables.

At 500°C, space group A2₁am

Lattice constants are

a = 5.4671(5) b = 5.4668(5) c = 41.2792(6)

Alpha = 90 Beta = 90 Gamma = 90

Cell volume = 1233.73(17)

Name	x	y	z	Uiso (x100)	Fractn
Sr1	.250000	.249(6)	.000000	6.53(36)	.3500
Sr2	.246(17)	.252(4)	.10540(16)	6.68(26)	.3250
Bi4	.250000	.2490(56)	.000000	6.53(36)	.6500
Bi5	.246(17)	.2516(41)	.10540(16)	6.68(26)	.6750
Bi6	.237(11)	.2651(28)	.21803(14)	6.13(25)	1.0000
Ti7	.270(11)	.247(7)	.44964(26)	1.95(30)	1.0000
Ti8	.265(12)	.236(4)	.34714(22)	.46(25)	1.0000
O9	.270(14)	.2264(76)	.500000	5.10(65)	1.0000
O10	.539(13)	.5365(42)	.05003(33)	4.02(51)	1.0000
O11	.264(14)	.2717(51)	.40290(26)	5.93(36)	1.0000
O12	.499(12)	.4919(33)	.14305(21)	1.56(29)	1.0000
O13	.247(15)	.2428(50)	.30321(25)	6.27(29)	1.0000
O14	.495(11)	.5012(36)	.25571(25)	3.83(29)	1.0000
O15	-.007(15)	-.0176(58)	.04847(40)	7.26(66)	1.0000
O16	-.001(13)	-.0005(47)	.14411(27)	4.33(45)	1.0000

The final agreement factors are: $\chi^2 = 3.562$, $R_{wp} = 0.0635$, $R_p = 0.0682$ for 60variables.

At 550°C, space group Amam

Lattice constants are

a = 5.4710(6) b = 5.4708(6) c = 41.3092(6)

Alpha = 90 Beta = 90 Gamma = 90

Cell volume = 1236.41(20)

Name	x	y	z	Uiso (x100)	Fractn
Sr1	.250000	.243(4)	.000000	6.26(31)	.3500
Sr2	.250000	.248(4)	.10485(19)	8.00(26)	.3250
Bi4	.250000	.2433(44)	.000000	6.26(31)	.6500
Bi5	.250000	.2476(38)	.10485(19)	8.00(26)	.6750
Bi6	.250000	.2620(28)	.21822(14)	6.74(25)	1.0000
Ti7	.250000	.248(5)	.45038(24)	2.24(23)	1.0000
Ti8	.250000	.220(4)	.34751(21)	.81(28)	1.0000
O9	.250000	.222(6)	.500000	6.00*	1.0000
O10	.500000	.500000	.05002(50)	7.36*	1.0000
O11	.250000	.253(5)	.40333(24)	6.73*	1.0000
O12	.500000	.500000	.14358(28)	1.87*	1.0000
O13	.250000	.263(5)	.30354(24)	6.68*	1.0000
O14	.500000	.500000	.25360(59)	5.68*	1.0000
O15	.000000	.000000	.04891(54)	8.66*	1.0000
O16	.000000	.000000	.14392(36)	4.60*	1.0000

Thermal parameters multiplied by 100.0 are

Name	U11	U22	U33	U12	U13	U23
O9	1.7(16)	12.3(28)	4.0(8)	.00	.00	.00
O10	2.8(11)	11.2(21)	8.1(17)	4.1(10)	.00	.00
O11	3.0(15)	11.3(22)	5.8(6)	.00	.00	-.1(16)
O12	1.3(9)	1.9(10)	2.5(8)	3.2(5)	.00	.00
O13	5.9(25)	9.2(30)	5.0(6)	.00	.00	1.3(13)
O14	3.5(16)	3.5(15)	10.0(11)	-1.5(7)	.00	.00
O15	7.5(19)	9.5(25)	9.0(19)	3.2(12)	.00	.00
O16	6.7(17)	3.4(14)	3.6(11)	-2.1(7)	.00	.00

The final agreement factors are: $\chi^2 = 3.447$, $R_{wp} = 0.0623$, $R_p = 0.0668$ for 63 variables.

At 600°C, space group Amam

Lattice constants are

a = 5.47465(21) b = 5.47574(21) c = 41.3301(6)

Alpha = 90 Beta = 90 Gamma = 90

Cell volume = 1238.98(7)

Name	x	y	z	Uiso (x100)	Fractn
Sr1	.250000	.244(5)	.000000	6.52(33)	.3500
Sr2	.250000	.254(4)	.10502(20)	8.47(29)	.3250
Bi4	.250000	.2436(47)	.000000	6.52(33)	.6500
Bi5	.250000	.2539(37)	.10503(20)	8.47(29)	.6750
Bi6	.250000	.2556(29)	.21844(15)	7.33(27)	1.0000
Ti7	.250000	.2478(57)	.45021(28)	2.74(25)	1.0000
Ti8	.250000	.2137(27)	.34732(20)	.10(23)	1.0000
O9	.250000	.245(8)	.500000	7.51*	1.0000
O10	.500000	.500000	.04813(68)	7.81*	1.0000
O11	.250000	.245(5)	.40312(26)	7.06*	1.0000
O12	.500000	.500000	.14497(38)	3.37*	1.0000
O13	.250000	.264(5)	.30403(25)	6.60*	1.0000
O14	.500000	.500000	.25176(76)	7.00*	1.0000
O15	.000000	.000000	.04941(65)	8.23*	1.0000
O16	.000000	.000000	.14260(34)	4.00*	1.0000

Thermal parameters multiplied by 100.0 are

Name	U11	U22	U33	U12	U13	U23
O9	1.4(13)	16.8(30)	4.3(8)	.00	.00	.00
O10	3.1(11)	10.9(21)	9.4(16)	4.2(10)	.00	.00
O11	3.7(16)	11.3(23)	6.2(6)	.00	.00	.2(16)
O12	.6(6)	3.7(11)	5.8(9)	4.7(5)	.00	.00
O13	6.8(25)	8.2(29)	4.8(6)	.00	.00	1.7(12)
O14	4.1(17)	4.5(19)	12.4(11)	-2.9(8)	.00	.00
O15	4.8(15)	12.1(22)	7.8(15)	2.5(11)	.00	.00
O16	5.1(15)	5.7(15)	1.2(6)	-1.9(6)	.00	.00

The final agreement factors are: $\chi^2 = 3.417$, $R_{wp} = 0.0614$, $R_p = 0.0653$ for 63 variables.

At 650°C, space group I4/mmm

Lattice constants are

a = 3.87469(4) b = A c = 41.3523(5)

Alpha = 90 Beta = 90 Gamma = 90

Cell volume = 620.831(12)

Name	x	y	z	Ueq (x100)	Fractn
Sr1	.000000	.000000	.000000	5.88*	.3500
Sr2	.000000	.000000	.10369(24)	9.29*	.3250
Bi4	.000000	.000000	.000000	5.88*	.6500
Bi5	.000000	.000000	.10370(24)	9.29*	.6750
Bi6	.000000	.000000	.21845(15)	7.39*	1.0000
Ti7	.000000	.000000	.45093(27)	3.28*	1.0000
Ti8	.000000	.000000	.34813(23)	1.85*	1.0000
O9	.000000	.000000	.500000	6.56*	1.0000
O10	.000000	.500000	.04907(31)	9.69*	1.0000
O11	.000000	.000000	.40522(22)	6.20*	1.0000
O12	.000000	.500000	.14439(15)	3.59*	1.0000
O13	.000000	.000000	.30444(25)	6.62*	1.0000
O14	.000000	.500000	.250000	4.62*	1.0000

Thermal parameters multiplied by 100.0 are

Name	U11	U22	U33
Sr1	5.54(41)	5.54(41)	6.6(6)
Sr2	7.26(34)	7.26(34)	13.3(7)
Bi4	5.54(41)	5.54(41)	6.6(6)
Bi5	7.26(34)	7.26(34)	13.3(7)
Bi6	7.50(31)	7.50(31)	7.2(4)
Ti7	2.71(35)	2.71(35)	4.4(5)
Ti8	1.01(32)	1.01(32)	3.5(5)
O9	8.42(66)	8.42(66)	2.84(66)
O10	5.74(41)	11.81(59)	11.51(59)
O11	7.14(40)	7.14(40)	4.31(47)
O12	1.45(27)	5.84(36)	3.48(31)
O13	6.58(42)	6.58(42)	6.71(64)
O14	2.57(25)	2.57(25)	8.73(65)

The final agreement factors are: $\chi^2 = 2.420$, $R_{wp} = 0.0520$, $R_p = 0.0528$ for 44 variables.

At 700°C, space group I4/mmm
 Lattice constants are
 a = 3.87741(5) b = A c = 41.3792(5)
 Alpha = 90 Beta = 90 Gamma = 90
 Cell volume = 622.108(13)

Name	x	y	z	Ueq (x100)	Fractn
Sr1	.000000	.000000	.000000	3.76*	.3500
Sr2	.000000	.000000	.10813(33)	13.43*	.3250
Bi4	.000000	.000000	.000000	3.76*	.6500
Bi5	.000000	.000000	.10813(33)	13.43*	.6750
Bi6	.000000	.000000	.21455(20)	10.89*	1.0000
Ti7	.000000	.000000	.44645(36)	3.97*	1.0000
Ti8	.000000	.000000	.35106(24)	2.41*	1.0000
O9	.000000	.000000	.500000	19.47*	1.0000
O10	.000000	.500000	.04783(24)	8.06*	1.0000
O11	.000000	.000000	.40320(18)	3.85*	1.0000
O12	.000000	.500000	.14332(17)	6.20*	1.0000
O13	.000000	.000000	.30875(32)	8.81*	1.0000
O14	.000000	.500000	.250000	3.10*	1.0000

Thermal parameters multiplied by 100.0 are

Name	U11	U22	U33
Sr1	4.36(26)	4.36(26)	2.6(4)
Sr2	8.77(34)	8.77(34)	22.8(12)
Bi4	4.36(26)	4.36(26)	2.6(4)
Bi5	8.77(34)	8.77(34)	22.8(12)
Bi6	9.72(39)	9.72(39)	13.2(7)
Ti7	.97(30)	.97(30)	10.0(9)
Ti8	2.49(37)	2.49(37)	2.2(6)
O9	20.13(162)	20.13(162)	18.2(27)
O10	4.55(34)	10.65(45)	9.0(6)
O11	4.59(24)	4.59(24)	2.4(4)
O12	4.23(35)	8.88(45)	5.5(4)
O13	6.35(37)	6.35(37)	13.7(11)
O14	.83(19)	.83(19)	7.6(6)

The final agreement factors are: $\chi^2 = 2.622$, $R_{wp} = 0.0538$, $R_p = 0.0539$ for 44 variables.

At 800°C, space group I4/mmm

Lattice constants are

a = 3.88260(4) b = A c = 41.4431(5)

Alpha = 90 Beta = 90 Gamma = 90

Cell volume = 624.737(12)

Name	x	y	z	Ueq (x100)	Fractn
Sr1	.000000	.000000	.000000	6.11*	.3500
Sr2	.000000	.000000	.10387(28)	10.41*	.3250
Bi4	.000000	.000000	.000000	6.11*	.6500
Bi5	.000000	.000000	.10388(28)	10.41*	.6750
Bi6	.000000	.000000	.21843(16)	9.10*	1.0000
Ti7	.000000	.000000	.45112(31)	3.51*	1.0000
Ti8	.000000	.000000	.34782(25)	2.27*	1.0000
O9	.000000	.000000	.500000	7.15*	1.0000
O10	.000000	.500000	.04937(30)	9.74*	1.0000
O11	.000000	.000000	.40519(24)	7.32*	1.0000
O12	.000000	.500000	.14425(17)	4.11*	1.0000
O13	.000000	.000000	.30491(24)	6.33*	1.0000
O14	.000000	.500000	.250000	5.31*	14

Thermal parameters multiplied by 100.0 are

Name	U11	U22	U33
Sr1	5.5(4)	5.5(4)	7.4(6)
Sr2	8.3(4)	8.3(4)	14.6(7)
Bi4	5.5(4)	5.5(4)	7.4(6)
Bi5	8.3(4)	8.3(4)	14.6(7)
Bi6	9.6(4)	9.6(4)	8.0(5)
Ti7	2.2(4)	2.2(4)	6.1(6)
Ti8	1.9(4)	1.9(4)	3.0(6)
O9	9.11(73)	9.11(73)	3.23(72)
O10	5.52(43)	11.41(58)	12.30(66)
O11	8.35(48)	8.35(48)	5.25(57)
O12	2.21(32)	6.02(40)	4.08(35)
O13	6.02(41)	6.02(41)	6.94(66)
O14	2.71(28)	2.71(28)	10.53(75)

The final agreement factors are: $\chi^2 = 2.378$, $R_{wp} = 0.0509$, $R_p = 0.0511$ for 44 variables.

Appendix C.1: Final atomic coordinates for Bi₄Ti₃O₁₂ at several temperatures (Polaris data)

At 25°C space group B2cb

Lattice constants are

$$a = 5.44512(11) \quad b = 5.41013(11) \quad c = 32.8564(7)$$

Cell volume = 967.912(35)

Name	x	y	z	Uiso (x100)
Bi1	.000000	.9981(4)	.06690(4)	.486(27)
Bi2	.9992(4)	.0180(4)	.21141(4)	.702(28)
Ti3	.0440(7)	.000000	.500000	-.36(7)
Ti4	.0474(6)	1.0016(9)	.37154(7)	-.22(5)
O5	.3222(6)	.2543(6)	.00818(9)	1.978(68)
O6	.2712(6)	.2425(5)	.24983(9)	.495(35)
O7	.0866(5)	1.0608(4)	.44110(7)	.503(46)
O8	1.0558(6)	.9475(5)	.31880(6)	.710(57)
O9	.2900(5)	.2270(5)	.11220(6)	.082(33)
O10	.3597(5)	.2953(5)	.87592(7)	.321(45)

The final agreement factors are: $\chi^2 = 3.924$, $R_{wp} = 0.020$, $R_p = 0.0356$ for 47 variables.

At 100°C space group B2cb

Lattice constants are

$$a = 5.44855(13) \quad b = 5.41467(13) \quad c = 32.8886(8)$$

Cell volume = 970.28(4)

Name	x	y	z	Uiso (x100)
Bi1	.000000	.9973(4)	.06696(5)	.556(30)
Bi2	1.0003(5)	.0164(5)	.21148(5)	1.041(34)
Ti3	.0405(8)	.000000	.500000	-.53(7)
Ti4	.0478(6)	.9999(9)	.37156(8)	-.61(5)
O5	.3228(8)	.2565(8)	.00812(11)	2.447(87)
O6	.2698(7)	.2449(6)	.25007(11)	.681(42)
O7	.0846(6)	1.0591(5)	.44108(8)	.526(53)
O8	1.0540(7)	.9489(6)	.31884(7)	.663(63)
O9	.2885(6)	.2250(5)	.11247(7)	-.006(35)
O10	.3570(6)	.2922(6)	.87621(8)	.309(49)

The final agreement factors are: $\chi^2 = 3.675$, $R_{wp} = 0.0218$, $R_p = 0.0385$ for 47 variables.

At 150°C space group B2cb

Lattice constants are

a = 5.45070(14) b = 5.41737(13) c = 32.9077(8)

Cell volume = 971.72(4)

Name	x	y	z	Uiso (x100)
Bi1	.000000	.9978(5)	.06691(6)	.84(4)
Bi2	1.0007(6)	.0165(5)	.21146(5)	1.14(4)
Ti3	.0408(9)	.000000	.500000	-.54(8)
Ti4	.0468(7)	.9964(10)	.37158(8)	-.46(5)
O5	.3222(9)	.2569(9)	.00783(13)	2.71(10)
O6	.2712(8)	.2451(7)	.24987(11)	.69(5)
O7	.0835(6)	1.0575(5)	.44140(8)	.35(5)
O8	1.0523(8)	.9491(7)	.31872(8)	1.32(8)
O9	.2862(7)	.2256(6)	.11246(8)	-.05(4)
O10	.3561(7)	.2918(7)	.87602(10)	.75(6)

The final agreement factors are: $\chi^2 = 3.901$, $R_{wp} = 0.0225$, $R_p = 0.0397$ for 47 variables.

At 200°C space group B2cb

Lattice constants are

a = 5.45285(13) b = 5.42030(13) c = 32.9282(8)

Cell volume = 973.23(4)

Name	x	y	z	Uiso (x100)
Bi1	.000000	.9974(5)	.06721(5)	.925(35)
Bi2	1.0010(6)	.0147(5)	.21137(5)	1.444(38)
Ti3	.0391(9)	.000000	.500000	-.58(7)
Ti4	.0465(7)	1.0013(10)	.37167(8)	-.68(5)
O5	.3206(9)	.2579(9)	.00779(12)	2.60(9)
O6	.2694(8)	.2454(7)	.25040(12)	.98(5)
O7	.0828(6)	1.0571(6)	.44095(9)	.95(6)
O8	1.0530(7)	.9498(6)	.31890(7)	.85(7)
O9	.2844(7)	.2245(6)	.11240(8)	.24(4)
O10	.3537(6)	.2908(6)	.87630(8)	.40(5)

The final agreement factors are: $\chi^2 = 3.550$, $R_{wp} = 0.0215$, $R_p = 0.0392$ for 47 variables.

At 250°C space group B2cb

Lattice constants are

a = 5.45531(14) b = 5.42360(13) c = 32.9524(8)

Cell volume = 974.98(4)

Name	x	y	z	Uiso (x100)
Bi1	.000000	.9972(5)	.06709(6)	1.25(4)
Bi2	1.0017(6)	.0143(6)	.21140(6)	1.54(4)
Ti3	.0406(9)	.000000	.500000	-.61(7)
Ti4	.0448(7)	.9956(10)	.37148(8)	-.45(5)
O5	.3205(9)	.2592(9)	.00768(13)	2.91(11)
O6	.2709(9)	.2454(7)	.24999(12)	1.07(5)
O7	.0816(7)	1.0562(6)	.44139(9)	.92(7)
O8	1.0515(9)	.9501(7)	.31870(8)	1.44(9)
O9	.2826(8)	.2248(6)	.11247(8)	.21(4)
O10	.3520(7)	.2886(8)	.87618(10)	1.00(7)

The final agreement factors are: $\chi^2 = 3.528$, $R_{wp} = 0.0212$, $R_p = 0.0388$ for 47 variables.

At 300°C space group B2cb

Lattice constants are

a = 5.45677(14) b = 5.42621(14) c = 32.9723(8)

Cell volume = 976.30(4)

Name	x	y	z	Uiso(x100)
Bi1	.000000	.9968(6)	.06724(6)	1.40(4)
Bi2	1.0024(6)	.0130(6)	.21130(6)	1.72(4)
Ti3	.0378(10)	.000000	.500000	-.43(8)
Ti4	.0448(8)	.9939(10)	.37152(8)	-.60(5)
O5	.3199(10)	.2606(9)	.00747(13)	2.90(10)
O6	.2698(9)	.2457(8)	.25036(12)	1.20(6)
O7	.0797(7)	1.0564(7)	.44104(10)	1.37(7)
O8	1.0517(9)	.9512(7)	.31862(8)	1.26(8)
O9	.2809(8)	.2244(7)	.11244(9)	.32(4)
O10	.3500(7)	.2863(8)	.87642(10)	.92(7)

The final agreement factors are: $\chi^2 = 3.352$, $R_{wp} = 0.0209$, $R_p = 0.0390$ for 47 variables.

At 350°C space group B2cb

Lattice constants are

a = 5.45859(14) b = 5.42940(14) c = 32.9969(9)

Cell volume = 977.92(4)

Name	x	y	z	Uiso(x100)
Bi1	.000000	.9972(6)	.06731(7)	1.57(4)
Bi2	1.0047(7)	.0136(6)	.21127(6)	1.86(5)
Ti3	.0368(11)	.000000	.500000	-.28(8)
Ti4	.0453(8)	.9924(10)	.37149(8)	-.64(5)
O5	.3192(10)	.2631(10)	.00726(14)	3.06(11)
O6	.2698(10)	.2460(8)	.25039(13)	1.31(6)
O7	.0789(7)	1.0558(7)	.44109(10)	1.46(8)
O8	1.0512(9)	.9519(8)	.31849(9)	1.55(9)
O9	.2806(9)	.2242(7)	.11264(9)	.38(4)
O10	.3489(8)	.2853(8)	.87653(11)	1.16(7)

The final agreement factors are: $\chi^2 = 3.329$, $R_{wp} = 0.0206$, $R_p = 0.0386$ for 47 variables.

At 400°C space group B2cb

Lattice constants are

a = 5.46008(14) b = 5.43236(14) c = 33.0210(9)

Cell volume = 979.44(4)

Name	x	y	z	Uiso(x100)
Bi1	.000000	.9968(6)	.06733(7)	1.84(5)
Bi2	1.0046(7)	.0123(7)	.21133(6)	1.95(5)
Ti3	.0378(12)	.000000	.500000	-.45(8)
Ti4	.0427(9)	.9916(11)	.37151(9)	-.37(6)
O5	.3181(11)	.2633(10)	.00714(14)	3.06(12)
O6	.2715(11)	.2464(8)	.25029(14)	1.33(6)
O7	.0773(8)	1.0545(8)	.44118(11)	1.67(9)
O8	1.0503(10)	.9520(9)	.31850(9)	1.80(10)
O9	.2778(9)	.2234(7)	.11265(9)	.42(5)
O10	.3458(8)	.2843(9)	.87675(12)	1.36(8)

The final agreement factors are: $\chi^2 = 3.162$, $R_{wp} = 0.0204$, $R_p = 0.0386$ for 47 variables.

At 450°C space group B2cb

Lattice constants are

a = 5.46136(15) b = 5.43552(15) c = 33.0473(9)

Cell volume = 981.02(5)

Name	x	y	z	Uiso(x100)
Bi1	.000000	.9975(7)	.06745(7)	2.13(5)
Bi2	1.0056(8)	.0132(7)	.21117(6)	2.10(5)
Ti3	.0373(13)	.000000	.500000	-.40(9)
Ti4	.0418(10)	.9906(11)	.37152(9)	-.31(6)
O5	.3178(11)	.2649(11)	.00686(15)	3.14(12)
O6	.2718(12)	.2485(9)	.25053(14)	1.45(7)
O7	.0748(9)	1.0535(9)	.44106(11)	1.98(9)
O8	1.0491(11)	.9527(9)	.31842(9)	1.86(11)
O9	.2761(10)	.2238(8)	.11265(10)	.65(5)
O10	.3443(9)	.2841(10)	.87693(12)	1.53(9)

The final agreement factors are: $\chi^2 = 3.100$, $R_{wp} = 0.0203$, $R_p = 0.0388$ for 47 variables.

At 500°C space group B2cb

Lattice constants are

a = 5.46241(15) b = 5.43862(15) c = 33.0742(9)

Cell volume = 982.57(5)

Name	x	y	z	Uiso(x100)
Bi1	.000000	.9975(7)	.06751(8)	2.24(5)
Bi2	1.0077(9)	.0116(7)	.21121(6)	2.37(5)
Ti3	.0343(15)	.000000	.500000	.03(10)
Ti4	.0422(11)	.9915(12)	.37135(9)	-.37(6)
O5	.3163(12)	.2652(11)	.00671(15)	3.18(12)
O6	.2720(12)	.2477(9)	.25072(15)	1.61(7)
O7	.0720(9)	1.0531(9)	.44110(12)	2.21(10)
O8	1.0501(12)	.9543(10)	.31825(10)	2.06(11)
O9	.2749(11)	.2236(8)	.11274(11)	.76(6)
O10	.3405(9)	.2829(10)	.87730(13)	1.71(10)

The final agreement factors are: $\chi^2 = 2.914$, $R_{wp} = 0.0197$, $R_p = 0.0372$ for 47 variables.

At 550°C space group B2cb

Lattice constants are

a = 5.46322(15) b = 5.44217(15) c = 33.1065(9)

Cell volume = 984.31(5)

Name	x	y	z	Uiso(x100)
Bi1	.000000	.9986(8)	.06740(8)	2.64(6)
Bi2	1.0090(9)	.0119(8)	.21123(6)	2.39(6)
Ti3	.0330(16)	.000000	.500000	.04(10)
Ti4	.0417(12)	.9920(13)	.37137(10)	-.09(7)
O5	.3152(13)	.2671(11)	.00665(16)	3.25(13)
O6	.2714(13)	.2477(9)	.25067(15)	1.57(7)
O7	.0694(10)	1.0509(11)	.44128(12)	2.68(11)
O8	1.0496(12)	.9560(11)	.31831(10)	2.18(12)
O9	.2743(12)	.2232(9)	.11296(11)	.89(6)
O10	.3372(10)	.2812(11)	.87748(13)	1.86(11)

The final agreement factors are: $\chi^2 = 2.873$, $R_{wp} = 0.0196$, $R_p = 0.0373$ for 47 variables.

At 580°C space group B2cb

Lattice constants are

a = 5.46341(15) b = 5.44427(15) c = 33.1282(8)

Cell volume = 985.37(5)

Name	x	y	z	Uiso(x100)
Bi1	.000000	.9982(8)	.06747(8)	2.92(7)
Bi2	1.0104(10)	.0120(8)	.21108(6)	2.48(6)
Ti3	.0318(18)	.000000	.500000	.19(10)
Ti4	.0392(14)	.9901(13)	.37134(9)	-.02(7)
O5	.3154(13)	.2694(11)	.00610(16)	3.24(13)
O6	.2731(14)	.2475(10)	.25071(16)	1.57(7)
O7	.0657(11)	1.0499(11)	.44131(12)	2.74(12)
O8	1.0476(14)	.9566(12)	.31799(10)	2.51(13)
O9	.2710(13)	.2241(9)	.11272(12)	1.06(7)
O10	.3340(11)	.2796(11)	.87766(14)	2.15(12)

The final agreement factors are: $\chi^2 = 2.694$, $R_{wp} = 0.0190$, $R_p = 0.0328$ for 47 variables.

At 610°C space group B2cb

Lattice constants are

a = 5.46322(16) b = 5.44655(16) c = 33.1498(8)

Cell volume = 986.39(5)

Name	x	y	z	Uiso(x100)
Bi1	.000000	.9989(8)	.06748(9)	3.15(7)
Bi2	1.0094(11)	.0121(8)	.21108(7)	2.54(6)
Ti3	.0333(20)	.000000	.500000	.09(11)
Ti4	.0354(15)	.9890(14)	.37123(10)	.05(8)
O5	.3138(14)	.2704(12)	.00609(16)	3.22(14)
O6	.2725(16)	.2472(10)	.25075(17)	1.65(8)
O7	.0620(12)	1.0496(12)	.44132(12)	2.91(12)
O8	1.0475(15)	.9591(14)	.31786(11)	2.74(14)
O9	.2668(14)	.2237(10)	.11293(12)	1.25(7)
O10	.3288(12)	.2786(12)	.87794(15)	2.38(14)

The final agreement factors are: $\chi^2 = 2.689$, $R_{wp} = 0.0190$, $R_p = 0.0363$ for 47 variables.

At 640°C space group B2cb

Lattice constants are

a = 5.46274(18) b = 5.44887(18) c = 33.1750(8)

Cell volume = 987.48(5)

Name	x	y	z	Uiso(x100)
Bi1	.000000	.9999(9)	.06763(9)	3.45(7)
Bi2	1.0093(13)	.0088(9)	.21110(7)	2.49(6)
Ti3	.0302(23)	.000000	.500000	.33(12)
Ti4	.0319(18)	.9925(17)	.37123(10)	.35(8)
O5	.3113(14)	.2729(12)	.00582(17)	3.10(14)
O6	.2711(18)	.2471(12)	.25038(18)	1.75(8)
O7	.0549(14)	1.0474(14)	.44141(13)	3.23(13)
O8	1.0452(17)	.9579(15)	.31791(11)	2.64(14)
O9	.2656(16)	.2253(11)	.11339(14)	1.45(8)
O10	.3231(14)	.2781(14)	.87842(16)	2.64(16)

The final agreement factors are: $\chi^2 = 2.652$, $R_{wp} = 0.0189$, $R_p = 0.0349$ for 47 variables.

At 670°C space group B2cb

Lattice constants are

a = 5.4561(5) b = 5.4538(5) c = 33.2264(8)

Cell volume = 988.70(13)

Name	x	y	z	Uiso(x100)
Bi1	.000000	1.0049(15)	.06827(11)	4.41(8)
Bi2	1.0006(25)	-.0073(12)	.21085(7)	2.98(7)
Ti3	.0093(39)	.000000	.500000	.88(14)
Ti4	.0105(27)	1.0005(20)	.37135(11)	.60(9)
O5	.2963(23)	.2867(17)	.00596(16)	1.94(12)
O6	.2548(26)	.2487(24)	.24875(22)	1.68(9)
O7	.0107(36)	1.0355(19)	.44164(15)	4.76(18)
O8	1.0154(32)	.9585(15)	.31745(13)	3.20(16)
O9	.2453(25)	.2394(21)	.11616(19)	2.71(18)
O10	.2794(27)	.2723(20)	.88243(19)	2.83(19)

The final agreement factors are: $\chi^2 = 2.885$, $R_{wp} = 0.0198$, $R_p = 0.0353$ for 47 variables.

At 700°C space group I4/mmm

Lattice constants are

a = 3.85864(7) b = A c = 33.2515(7)

Alpha = 90 Beta = 90 Gamma = 90

Cell volume = 495.085(16)

Name	x	y	z	Uequiv(x100)
Bi1	.500000	.500000	.06746(9)	5.01*
Bi2	.500000	.500000	.21136(6)	2.89*
Ti3	.500000	.500000	.500000	1.50*
Ti4	.500000	.500000	.37068(10)	1.19*
O5	.500000	.000000	.000000	8.23*
O6	.500000	.000000	.250000	1.91*
O7	.500000	.500000	.31831(9)	5.96*
O8	.500000	.000000	.11719(9)	3.66*
O9	.500000	.500000	.44155(11)	5.62*

Thermal parameters multiplied by 100.0 are

Name	U11	U22	U33
Bi1	4.64(9)	4.64(9)	5.75(18)
Bi2	2.93(8)	2.93(8)	2.82(12)
Ti3	.50(19)	.50(19)	3.49(35)
Ti4	1.07(13)	1.07(13)	1.44(20)
O5	.79(18)	13.71(50)	10.18(43)
O6	2.14(10)	2.14(10)	1.46(15)
O7	8.89(20)	8.89(20)	.10(15)
O8	1.35(11)	5.13(16)	4.49(17)
O9	7.21(18)	7.21(18)	2.43(19)

The final agreement factors are: $\chi^2 = 2.249$, $R_{wp} = 0.0175$, $R_p = 0.0318$ for 36 variables.

At 730°C space group I4/mmm

Lattice constants are

a = 3.86034(7) b = A c = 33.2680(7)

Alpha = 90 Beta = 90 Gamma = 90

Cell volume = 495.769(17)

Name	x	y	z	Uequiv(x100)
Bi1	.500000	.500000	.06737(10)	5.24*
Bi2	.500000	.500000	.21123(7)	3.08*
Ti3	.500000	.500000	.500000	1.31*
Ti4	.500000	.500000	.37076(11)	1.29*
O5	.500000	.000000	.000000	8.20*
O6	.500000	.000000	.250000	1.89*
O7	.500000	.500000	.31829(9)	6.06*
O8	.500000	.000000	.11709(9)	3.73*
O9	.500000	.500000	.44165(12)	5.59*

Thermal parameters multiplied by 100.0 are

Name	U11	U22	U33
Bi1	4.80(9)	4.80(9)	6.13(19)
Bi2	3.19(9)	3.19(9)	2.86(13)
Ti3	.23(19)	.23(19)	3.46(36)
Ti4	1.37(15)	1.37(15)	1.12(21)
O5	.41(17)	14.14(53)	10.04(44)
O6	2.17(11)	2.17(11)	1.35(15)
O7	9.06(21)	9.06(21)	.05(16)
O8	1.46(11)	5.07(17)	4.66(18)
O9	6.99(18)	6.99(18)	2.81(20)

The final agreement factors are: $\chi^2 = 1.579$, $R_{wp} = 0.0180$, $R_p = 0.0321$ for 36 variables.

At 770°C space group I4/mmm

Lattice constants are

a = 3.86253(7) b = A c = 33.2877(7)

Alpha = 90 Beta = 90 Gamma = 90

Cell volume = 496.625(17)

Name	x	y	z	Uequiv(x100)
Bi1	.500000	.500000	.06757(10)	5.24*
Bi2	.500000	.500000	.21137(7)	3.10*
Ti3	.500000	.500000	.500000	1.35*
Ti4	.500000	.500000	.37069(11)	1.36*
O5	.500000	.000000	.000000	8.19*
O6	.500000	.000000	.250000	2.02*
O7	.500000	.500000	.31844(10)	6.19*
O8	.500000	.000000	.11730(9)	3.82*
O9	.500000	.500000	.44163(12)	5.53*

Thermal parameters multiplied by 100.0 are

Name	U11	U22	U33
Bi1	5.05(10)	5.05(10)	5.62(19)
Bi2	3.24(9)	3.24(9)	2.82(13)
Ti3	.64(21)	.64(21)	2.79(35)
Ti4	1.23(14)	1.23(14)	1.61(23)
O5	.55(18)	13.60(53)	10.42(46)
O6	2.16(11)	2.16(11)	1.72(17)
O7	9.16(22)	9.16(22)	.26(17)
O8	1.49(12)	5.21(18)	4.75(19)
O9	6.99(18)	6.99(18)	2.61(21)

The final agreement factors are: $\chi^2 = 1.526$, $R_{wp} = 0.0177$, $R_p = 0.0326$ for 36 variables.

At 810°C space group I4/mmm

Lattice constants are

a = 3.86488(8) b = A c = 33.3083(8)

Alpha = 90 Beta = 90 Gamma = 90

Cell volume = 497.536(18)

Name	x	y	z	Uequiv(x100)
Bi1	.500000	.500000	.06737(10)	5.41*
Bi2	.500000	.500000	.21131(7)	3.28*
Ti3	.500000	.500000	.500000	1.39*
Ti4	.500000	.500000	.37077(12)	1.38*
O5	.500000	.000000	.000000	8.48*
O6	.500000	.000000	.250000	2.18*
O7	.500000	.500000	.31841(10)	6.06*
O8	.500000	.000000	.11725(10)	3.86*
O9	.500000	.500000	.44149(13)	5.73*

Thermal parameters multiplied by 100.0 are

Name	U11	U22	U33
Bi1	5.07(10)	5.07(10)	6.09(21)
Bi2	3.46(10)	3.46(10)	2.92(14)
Ti3	.43(21)	.43(21)	3.33(38)
Ti4	1.28(16)	1.28(16)	1.56(24)
O5	.68(20)	14.16(58)	10.59(49)
O6	2.41(12)	2.41(12)	1.72(18)
O7	8.97(23)	8.97(23)	.23(17)
O8	1.43(12)	5.15(19)	5.01(20)
O9	7.13(19)	7.13(19)	2.93(22)

The final agreement factors are: $\chi^2 = 1.567$, $R_{wp} = 0.0180$, $R_p = 0.0323$ for 36 variables.

Appendix C.2: Selected bondlengths and angles for Bi₄Ti₃O₁₂ (Polaris data)

Space group B2cb

vector\T(C)	25	100	150	200	250
Bi(1)_O(1)	2.956(9)	2.954(9)	2.949(8)	2.979(5)	2.985(5)
Bi(1)_O(1)	3.321(8)	3.316(8)	3.309(7)	3.327(4)	3.312(5)
Bi(1)_O(1)	2.560(9)	2.563(8)	2.571(8)	2.558(5)	2.559(5)
Bi(1)_O(1)	2.974(10)	2.973(9)	2.978(8)	2.957(5)	2.935(6)
Bi(1)_O(3)	2.416(9)	2.427(9)	2.433(8)	2.444(4)	2.458(4)
Bi(1)_O(3)	3.098(9)	3.088(8)	3.083(8)	3.079(4)	3.068(4)
Bi(1)_O(3)	2.305(9)	2.313(9)	2.318(8)	2.309(4)	2.319(4)
Bi(1)_O(3)	3.213(9)	3.206(8)	3.202(7)	3.2031(34)	3.1973(34)
Bi(1)_O(5)	2.464(11)	2.470(10)	2.471(10)	2.477(4)	2.472(4)
Bi(1)_O(5)	2.357(11)	2.364(10)	2.369(9)	2.423(4)	2.437(4)
Bi(1)_O(6)	3.200(10)	3.183(10)	3.169(9)	3.102(4)	3.113(5)
Bi(1)_O(6)	2.331(10)	2.337(9)	2.340(8)	2.313(4)	2.339(4)
Bi(2)_O(2)	2.316(12)	2.320(11)	2.318(11)	2.315(5)	2.310(5)
Bi(2)_O(2)	2.456(10)	2.447(9)	2.444(9)	2.420(4)	2.439(4)
Bi(2)_O(2)	2.261(12)	2.267(11)	2.268(11)	2.274(4)	2.283(5)
Bi(2)_O(2)	2.193(11)	2.194(11)	2.200(10)	2.222(5)	2.203(5)
Bi(2)_O(4)	3.218(9)	3.219(8)	3.220(8)	3.233(4)	3.236(4)
Bi(2)_O(4)	2.575(10)	2.576(9)	2.580(9)	2.576(4)	2.564(5)
Bi(2)_O(4)	2.612(11)	2.630(10)	2.638(9)	2.646(4)	2.668(5)
Bi(2)_O(4)	3.195(11)	3.183(11)	3.179(10)	3.176(4)	3.149(6)
Bi(2)_O(6)	3.119(9)	3.147(9)	3.164(8)	3.2329(34)	3.233(4)
Ti(1)_O(1)x2	1.993(15)	1.993(15)	1.989(14)	2.036(6)	2.021(7)
Ti(1)_O(1)x2	1.883(14)	1.884(14)	1.888(13)	1.855(6)	1.867(6)
Ti(1)_O(3)x2	1.992(8)	1.992(7)	1.990(7)	1.9831(31)	1.9574(29)
Ti(2)_O(3)	2.322(12)	2.328(11)	2.328(10)	2.310(4)	2.350(4)
Ti(2)_O(4)	1.747(10)	1.746(10)	1.746(9)	1.760(4)	1.757(4)
Ti(2)_O(5)	2.002(18)	2.008(17)	2.010(16)	2.052(5)	2.020(6)
Ti(2)_O(5)	2.028(16)	2.018(16)	2.014(15)	1.953(5)	1.939(5)
Ti(2)_O(6)	2.063(16)	2.063(15)	2.056(14)	2.024(5)	2.053(6)
Ti(2)_O(6)	1.873(18)	1.876(17)	1.880(16)	1.895(5)	1.925(6)
Ti(1)_O(1)_Ti(1)	164.0(5)	164.3(5)	164.5(4)	162.35(26)	163.33(28)
Ti(1)_O(3)_Ti(2)	158.6(5)	158.9(5)	159.2(5)	159.66(19)	159.58(19)
Ti(2)_O(5)_Ti(2)	146.6(6)	146.7(6)	147.0(6)	148.44(23)	147.28(24)
Ti(2)_O(6)_Ti(2)	151.6(7)	152.2(6)	152.9(6)	156.05(22)	156.45(26)

vector\T(C)	300	350	400	450	500
Bi(1)_O(1)	2.997(5)	3.008(6)	3.011(6)	3.022(6)	3.025(6)
Bi(1)_O(1)	3.327(5)	3.330(5)	3.326(5)	3.328(5)	3.324(5)
Bi(1)_O(1)	2.566(5)	2.568(5)	2.576(5)	2.582(6)	2.592(6)
Bi(1)_O(1)	2.946(5)	2.940(6)	2.940(6)	2.936(6)	2.937(6)
Bi(1)_O(3)	2.444(5)	2.451(5)	2.456(5)	2.464(6)	2.465(6)
Bi(1)_O(3)	3.079(4)	3.076(5)	3.072(5)	3.063(5)	3.061(6)
Bi(1)_O(3)	2.328(4)	2.333(4)	2.341(5)	2.356(5)	2.371(5)
Bi(1)_O(3)	3.188(4)	3.185(4)	3.177(4)	3.164(5)	3.149(5)
Bi(1)_O(5)	2.469(5)	2.470(5)	2.461(5)	2.453(5)	2.451(6)
Bi(1)_O(5)	2.437(4)	2.441(4)	2.454(5)	2.454(5)	2.460(5)
Bi(1)_O(6)	3.075(4)	3.068(5)	3.051(5)	3.042(5)	3.019(5)
Bi(1)_O(6)	2.329(4)	2.332(5)	2.334(5)	2.334(5)	2.335(6)
Bi(2)_O(2)	2.320(5)	2.313(6)	2.323(6)	2.332(6)	2.333(6)
Bi(2)_O(2)	2.415(4)	2.409(5)	2.412(5)	2.405(5)	2.393(6)
Bi(2)_O(2)	2.276(5)	2.287(5)	2.281(5)	2.293(6)	2.287(6)
Bi(2)_O(2)	2.233(5)	2.239(5)	2.234(6)	2.236(6)	2.254(6)
Bi(2)_O(4)	3.216(4)	3.214(5)	3.209(5)	3.209(5)	3.192(6)
Bi(2)_O(4)	2.588(5)	2.587(5)	2.596(5)	2.592(5)	2.608(6)
Bi(2)_O(4)	2.657(5)	2.670(5)	2.676(6)	2.685(6)	2.690(6)
Bi(2)_O(4)	3.161(5)	3.146(5)	3.144(6)	3.130(6)	3.124(7)
Bi(2)_O(6)	3.251(4)	3.264(4)	3.278(4)	3.287(5)	3.309(5)
Ti(1)_O(1)x2	2.029(7)	2.022(7)	2.013(8)	2.008(8)	2.013(9)
Ti(1)_O(1)x2	1.864(6)	1.873(7)	1.882(7)	1.887(8)	1.884(8)
Ti(1)_O(3)x2	1.9811(34)	1.981(4)	1.977(4)	1.980(4)	1.980(4)
Ti(2)_O(3)	2.325(4)	2.329(4)	2.333(4)	2.331(5)	2.337(5)
Ti(2)_O(4)	1.760(4)	1.763(4)	1.764(4)	1.767(4)	1.768(4)
Ti(2)_O(5)	2.020(6)	2.011(6)	2.011(6)	2.003(7)	2.004(7)
Ti(2)_O(5)	1.938(5)	1.935(5)	1.931(6)	1.933(6)	1.944(7)
Ti(2)_O(6)	2.054(6)	2.057(6)	2.062(6)	2.064(7)	2.049(7)
Ti(2)_O(6)	1.917(6)	1.925(6)	1.927(7)	1.934(7)	1.940(8)
Ti(1)_O(1)_Ti(1)	162.47(30)	162.45(32)	162.89(32)	163.07(35)	163.0(4)
Ti(1)_O(3)_Ti(2)	159.31(21)	159.36(22)	159.73(23)	160.15(25)	160.58(27)
Ti(2)_O(5)_Ti(2)	147.68(25)	147.82(26)	147.76(27)	147.67(29)	147.48(30)
Ti(2)_O(6)_Ti(2)	157.43(25)	157.90(26)	158.02(28)	158.09(30)	158.58(30)

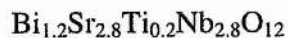
vector\T(C)	550	580	610	640	670
Bi(1)_O(1)	3.024(7)	3.047(7)	3.044(7)	3.051(7)	3.043(8)
Bi(1)_O(1)	3.327(6)	3.321(6)	3.322(6)	3.323(6)	3.351(8)
Bi(1)_O(1)	2.586(6)	2.598(6)	2.599(7)	2.607(7)	2.610(8)
Bi(1)_O(1)	2.936(7)	2.917(7)	2.921(7)	2.921(7)	2.955(7)
Bi(1)_O(3)	2.483(7)	2.484(7)	2.488(8)	2.502(9)	2.582(12)
Bi(1)_O(3)	3.043(6)	3.039(7)	3.033(7)	3.013(8)	2.913(12)
Bi(1)_O(3)	2.385(6)	2.405(6)	2.425(7)	2.463(8)	2.699(20)
Bi(1)_O(3)	3.136(6)	3.115(6)	3.096(6)	3.057(8)	2.814(19)
Bi(1)_O(5)	2.452(6)	2.439(6)	2.428(7)	2.433(7)	2.441(10)
Bi(1)_O(5)	2.467(6)	2.470(6)	2.485(6)	2.487(7)	2.532(12)
Bi(1)_O(6)	3.007(6)	2.987(6)	2.964(7)	2.935(7)	2.701(11)
Bi(1)_O(6)	2.350(6)	2.355(6)	2.364(7)	2.366(7)	2.396(11)
Bi(2)_O(2)	2.325(7)	2.330(7)	2.331(7)	2.330(8)	2.337(12)
Bi(2)_O(2)	2.390(6)	2.395(7)	2.397(7)	2.390(8)	2.344(12)
Bi(2)_O(2)	2.296(6)	2.297(6)	2.296(7)	2.296(8)	2.309(11)
Bi(2)_O(2)	2.259(7)	2.262(7)	2.264(7)	2.271(8)	2.318(12)
Bi(2)_O(4)	3.187(6)	3.180(7)	3.168(7)	3.159(8)	3.062(10)
Bi(2)_O(4)	2.617(6)	2.613(7)	2.625(7)	2.637(8)	2.710(10)
Bi(2)_O(4)	2.699(7)	2.711(8)	2.705(8)	2.717(9)	2.822(18)
Bi(2)_O(4)	3.116(7)	3.094(8)	3.096(8)	3.087(9)	2.974(17)
Bi(2)_O(6)	3.329(5)	3.343(5)	3.362(6)	3.381(6)	3.537(8)
Ti(1)_O(1)x2	2.008(10)	2.004(11)	1.988(11)	1.982(13)	1.961(20)
Ti(1)_O(1)x2	1.892(9)	1.895(10)	1.910(10)	1.918(11)	1.958(17)
Ti(1)_O(3)x2	1.974(4)	1.972(4)	1.970(4)	1.966(4)	1.949(5)
Ti(2)_O(3)	2.342(5)	2.345(5)	2.351(5)	2.350(5)	2.343(6)
Ti(2)_O(4)	1.768(5)	1.777(5)	1.778(5)	1.781(5)	1.806(6)
Ti(2)_O(5)	2.006(8)	1.995(9)	1.990(9)	2.003(10)	1.960(16)
Ti(2)_O(5)	1.943(7)	1.946(8)	1.942(9)	1.945(10)	1.994(17)
Ti(2)_O(6)	2.042(8)	2.052(9)	2.055(9)	2.037(11)	1.955(18)
Ti(2)_O(6)	1.941(8)	1.945(9)	1.952(10)	1.944(11)	1.981(17)
Ti(1)_O(1)_Ti(1)	162.8(4)	163.0(5)	163.4(5)	163.2(5)	159.6(7)
Ti(1)_O(3)_Ti(2)	161.42(30)	161.73(31)	162.08(34)	163.6(4)	169.6(6)
Ti(2)_O(5)_Ti(2)	147.86(32)	147.29(32)	147.32(34)	148.6(4)	155.1(4)
Ti(2)_O(6)_Ti(2)	159.21(32)	159.46(34)	159.5(4)	159.2(4)	156.5(5)

Space group I4/mmm

vector\T(C)	700	730	770	810
Bi(1)_O(1)x4	2.9586(23)	2.9579(25)	2.9647(25)	2.9615(26)
Bi(1)_O(3)x4	2.7448(4)	2.7461(5)	2.7484(5)	2.7488(5)
Bi(1)_O(5)x4	2.5411(25)	2.5419(27)	2.5436(27)	2.5483(29)
Bi(2)_O(2)x4	2.3179(12)	2.3214(12)	2.3202(12)	2.3227(13)
Bi(2)_O(4)x4	2.9014(14)	2.9010(14)	2.9058(15)	2.9067(16)
Ti(1)_O(1)x4	1.92932(3)	1.93017(4)	1.93127(4)	1.93244(4)
Ti(1)_O(3)x2	1.944(4)	1.941(4)	1.943(4)	1.949(4)
Ti(2)_O(3)	2.356(5)	2.358(5)	2.361(5)	2.355(5)
Ti(2)_O(4)	1.742(5)	1.746(5)	1.739(5)	1.744(5)
Ti(2)_O(5)x4	1.9710(8)	1.9721(8)	1.9722(8)	1.9732(9)

Appendix D: Final atomic coordinates for the solid solution

$\text{Bi}_{4-x}\text{Sr}_x\text{Ti}_{3-x}\text{Nb}_x\text{O}_{12}$ at room temperature (data obtained on the Stoe diffractometer)

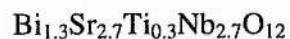


Lattice constants are

$$a = 3.90435(23) \text{ b} = A \text{ c} = 33.6822(28)$$

$$\text{Cell volume} = 513.45(6)$$

Name	x	y	z	Uiso (x100)	Fractn
Bi(1)	.500000	.500000	.06498(32)	2.91(18)	-.002(8)
Sr(1)	.500000	.500000	.21515(22)	2.91(18)	.398(8)
Ti(1)	.500000	.500000	.500000	1.46(24)	.204(31)
Nb(1)	.500000	.500000	.37163(27)	1.46(24)	1.002(15)
O(1)	.500000	.000000	.000000	2.50	1.0000
O(2)	.500000	.000000	.250000	2.50	1.0000
O(3)	.500000	.500000	.3355(20)	2.50	1.0000
O(4)	.500000	.000000	.1248(13)	2.50	1.0000
O(5)	.500000	.500000	.4473(16)	2.50	1.0000
Bi(2)	.500000	.500000	.21515(22)	2.91(18)	.602(8)
Sr(2)	.500000	.500000	.06498(32)	2.91(18)	1.002(8)
Nb(2)	.500000	.500000	.500000	1.46(24)	.796(31)
Ti(2)	.500000	.500000	.37163(27)	1.46(24)	-.002(15)

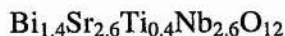


Lattice constants are

$$a = 3.90410(14) \text{ b} = A \text{ c} = 33.6667(18)$$

$$\text{Cell volume} = 513.15(4)$$

Name	x	y	z	Uiso (x100)	Fractn
Bi(1)	.500000	.500000	.06438(23)	2.48(12)	-.016(6)
Sr(1)	.500000	.500000	.21529(15)	2.48(12)	.334(6)
Ti(1)	.500000	.500000	.500000	.50(15)	.256(21)
Nb(1)	.500000	.500000	.37173(18)	.50(15)	.978(10)
O(1)	.500000	.000000	.000000	2.50	1.0000
O(2)	.500000	.000000	.250000	2.50	1.0000
O(3)	.500000	.500000	.3349(14)	2.50	1.0000
O(4)	.500000	.000000	.1222(9)	2.50	1.0000
O(5)	.500000	.500000	.4489(12)	2.50	1.0000
Bi(2)	.500000	.500000	.21530(15)	2.48(12)	.666(6)
Sr(2)	.500000	.500000	.06437(23)	2.48(12)	1.016(6)
Nb(2)	.500000	.500000	.500000	.50(15)	.744(21)
Ti(2)	.500000	.500000	.37173(18)	.50(15)	.022(10)



Lattice constants are

$$a = 3.90543(17) \text{ b} = A \text{ c} = 33.6324(22)$$

$$\text{Cell volume} = 512.97(5)$$

Name	x	y	z	Uiso (x100)	Fractn
Bi(1)	.500000	.500000	.06395(24)	3.70(14)	.002(6)
Sr(1)	.500000	.500000	.21520(15)	3.70(14)	.302(6)
Ti(1)	.500000	.500000	.500000	1.53(19)	.300(22)
Nb(1)	.500000	.500000	.37183(20)	1.53(19)	.950(11)
O(1)	.500000	.000000	.000000	2.50	1.0000
O(2)	.500000	.000000	.250000	2.50	1.0000
O(3)	.500000	.500000	.3322(14)	2.50	1.0000
O(4)	.500000	.000000	.1202(9)	2.50	1.0000
O(5)	.500000	.500000	.4443(11)	2.50	1.0000
Bi(2)	.500000	.500000	.21520(15)	3.70(14)	.698(6)
Sr(2)	.500000	.500000	.06395(24)	3.70(14)	.998(6)
Nb(2)	.500000	.500000	.500000	1.53(19)	.700(22)
Ti(2)	.500000	.500000	.37182(20)	1.53(19)	.050(11)



Lattice constants are

$$a = 3.90721(12) \text{ b} = A \text{ c} = 33.5848(16)$$

$$\text{Cell volume} = 512.716(33)$$

Name	x	y	z	Uiso (x100)	Fractn
Bi(1)	.500000	.500000	.06305(14)	4.15(9)	-.006(3)
Sr(1)	.500000	.500000	.21494(8)	4.15(9)	.244(3)
Ti(1)	.500000	.500000	.500000	1.64(13)	.338(12)
Nb(1)	.500000	.500000	.37239(11)	1.64(13)	.919(6)
O(1)	.500000	.000000	.000000	2.50	1.0000
O(2)	.500000	.000000	.250000	2.50	1.0000
O(3)	.500000	.500000	.3267(7)	2.50	1.0000
O(4)	.500000	.000000	.1178(5)	2.50	1.0000
O(5)	.500000	.500000	.4424(7)	2.50	1.0000
Bi(2)	.500000	.500000	.21495(8)	4.15(9)	.756(3)
Sr(2)	.500000	.500000	.06305(14)	4.15(9)	1.006(3)
Nb(2)	.500000	.500000	.500000	1.64(13)	.662(12)
Ti(2)	.500000	.500000	.37238(11)	1.64(13)	.081(6)

$\text{Bi}_{1.6}\text{Sr}_{2.4}\text{Ti}_{0.6}\text{Nb}_{2.4}\text{O}_{12}$ I4/mmm (tetragonal)

Lattice constants are

a = 3.89874(15) b = A c = 33.3704(19)

Cell volume = 507.24(4)

Name	x	y	z	Uiso (x100)	Fractn
Bi(1)	.500000	.500000	.06390(17)	2.90(10)	.029(4)
Sr(1)	.500000	.500000	.21460(11)	2.90(10)	.229(4)
Ti(1)	.500000	.500000	.500000	.39(13)	.312(16)
Nb(1)	.500000	.500000	.37245(15)	.39(13)	.856(8)
O(1)	.500000	.000000	.000000	2.50	1.0000
O(2)	.500000	.000000	.250000	2.50	1.0000
O(3)	.500000	.500000	.3304(11)	2.50	1.0000
O(4)	.500000	.000000	.1177(7)	2.50	1.0000
O(5)	.500000	.500000	.4380(10)	2.50	1.0000
Bi(2)	.500000	.500000	.21461(11)	2.90(10)	.771(4)
Sr(2)	.500000	.500000	.06390(17)	2.90(10)	.971(4)
Nb(2)	.500000	.500000	.500000	.39(13)	.688(16)
Ti(2)	.500000	.500000	.37245(15)	.39(13)	.144(8)

$\text{Bi}_{1.7}\text{Sr}_{2.3}\text{Ti}_{0.7}\text{Nb}_{2.3}\text{O}_{12}$

Lattice constants are

a = 3.89737(21) b = A c = 33.2649(26)

Cell volume = 505.28(5)

Name	x	y	z	Uiso (x100)	Fractn
Bi(1)	.500000	.500000	.06387(20)	4.53(14)	.067(5)
Sr(1)	.500000	.500000	.21401(13)	4.53(14)	.217(5)
Ti(1)	.500000	.500000	.500000	2.85(24)	.315(19)
Nb(1)	.500000	.500000	.37243(21)	2.85(24)	.808(9)
O(1)	.500000	.000000	.000000	2.50	1.0000
O(2)	.500000	.000000	.250000	2.50	1.0000
O(3)	.500000	.500000	.3274(12)	2.50	1.0000
O(4)	.500000	.000000	.1179(8)	2.50	1.0000
O(5)	.500000	.500000	.4357(12)	2.50	1.0000
Bi(2)	.500000	.500000	.21402(13)	4.53(14)	.783(5)
Sr(2)	.500000	.500000	.06386(20)	4.53(14)	.933(5)
Nb(2)	.500000	.500000	.500000	2.85(24)	.685(19)
Ti(2)	.500000	.500000	.37243(21)	2.85(24)	.192(9)

$\text{Bi}_{1.8}\text{Sr}_{2.2}\text{Ti}_{0.8}\text{Nb}_{2.2}\text{O}_{12}$ I4/mmm (tetragonal)

Lattice constants are

$$a = 3.89532(9) \text{ b} = a \text{ c} = 33.2066(13)$$

Cell volume = 503.861(26)

Name	x	y	z	Uiso (x100)	Fractn
Bi(1)	.500000	.500000	.06352(13)	2.36(8)	.083(4)
Sr(1)	.500000	.500000	.21359(9)	2.36(8)	.183(4)
Ti(1)	.500000	.500000	.500000	.22(11)	.441(14)
Nb(1)	.500000	.500000	.37261(13)	.22(11)	.821(7)
O(1)	.500000	.000000	.000000	2.50	1.0000
O(2)	.500000	.000000	.250000	2.50	1.0000
O(3)	.500000	.500000	.3270(10)	2.50	1.0000
O(4)	.500000	.000000	.1159(7)	2.50	1.0000
O(5)	.500000	.500000	.4413(9)	2.50	1.0000
Bi(2)	.500000	.500000	.21360(9)	2.36(8)	.817(4)
Sr(2)	.500000	.500000	.06351(13)	2.36(8)	.917(4)
Nb(2)	.500000	.500000	.500000	.22(11)	.559(14)
Ti(2)	.500000	.500000	.37261(13)	.22(11)	.179(7)

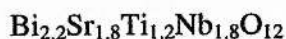
$\text{Bi}_{1.9}\text{Sr}_{2.1}\text{Ti}_{0.9}\text{Nb}_{2.1}\text{O}_{12}$

Lattice constants are

$$a = 3.89448(13) \text{ b} = a \text{ c} = 33.2013(18)$$

Cell volume = 503.56(4)

Name	x	y	z	Uiso (x100)	Fractn
Bi(1)	.500000	.500000	.06336(15)	2.13(10)	.138(5)
Sr(1)	.500000	.500000	.21284(11)	2.13(10)	.188(5)
Ti(1)	.500000	.500000	.500000	.24(16)	.497(17)
Nb(1)	.500000	.500000	.37243(17)	.24(16)	.799(9)
O(1)	.500000	.000000	.000000	2.50	1.0000
O(2)	.500000	.000000	.250000	2.50	1.0000
O(3)	.500000	.500000	.3231(11)	2.50	1.0000
O(4)	.500000	.000000	.1139(9)	2.50	1.0000
O(5)	.500000	.500000	.4412(11)	2.50	1.0000
Bi(2)	.500000	.500000	.21285(11)	2.13(10)	.812(5)
Sr(2)	.500000	.500000	.06336(15)	2.13(10)	.862(5)
Nb(2)	.500000	.500000	.500000	.24(16)	.503(17)
Ti(2)	.500000	.500000	.37243(17)	.24(16)	.201(9)

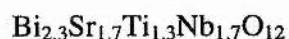


Lattice constants are

$$a = 3.88730(23) \quad b = A \quad c = 33.1324(31)$$

$$\text{Cell volume} = 500.67(6)$$

Name	x	y	z	Uiso (x100)	Fractn
Bi(1)	.500000	.500000	.06339(20)	4.32(15)	.212(5)
Sr(1)	.500000	.500000	.21258(14)	4.32(15)	.112(5)
Ti(1)	.500000	.500000	.500000	1.23(25)	.573(19)
Nb(1)	.500000	.500000	.37178(24)	1.23(25)	.686(10)
O(1)	.500000	.000000	.000000	2.50	1.0000
O(2)	.500000	.000000	.250000	2.50	1.0000
O(3)	.500000	.500000	.322123	2.50	1.0000
O(4)	.500000	.000000	.113634	2.50	1.0000
O(5)	.500000	.500000	.441887	2.50	1.0000
Bi(2)	.500000	.500000	.21258(14)	4.32(15)	.888(5)
Sr(2)	.500000	.500000	.06338(20)	4.32(15)	.788(5)
Nb(2)	.500000	.500000	.500000	1.23(25)	.427(19)
Ti(2)	.500000	.500000	.37178(24)	1.23(25)	.314(10)

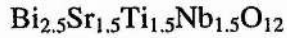


Lattice constants are

$$a = 3.88224(9) \quad b = A \quad c = 33.1579(12)$$

$$\text{Cell volume} = 499.749(24)$$

Name	x	y	z	Uiso (x100)	Fractn
Bi(1)	.500000	.500000	.06414(10)	2.64(7)	.264(3)
Sr(1)	.500000	.500000	.21252(7)	2.64(7)	.114(3)
Ti(1)	.500000	.500000	.500000	.63(13)	.616(11)
Nb(1)	.500000	.500000	.37206(13)	.63(13)	.658(6)
O(1)	.500000	.000000	.000000	2.50	1.0000
O(2)	.500000	.000000	.250000	2.50	1.0000
O(3)	.500000	.500000	.322123	2.50	1.0000
O(4)	.500000	.000000	.113634	2.50	1.0000
O(5)	.500000	.500000	.441887	2.50	1.0000
Bi(2)	.500000	.500000	.21253(7)	2.64(7)	.886(3)
Sr(2)	.500000	.500000	.06414(10)	2.64(7)	.736(3)
Nb(2)	.500000	.500000	.500000	.63(13)	.384(11)
Ti(2)	.500000	.500000	.37206(13)	.63(13)	.342(6)

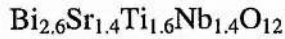


Lattice constants are

$$a = 3.87078(13) \text{ b} = A \text{ c} = 33.1179(17)$$

$$\text{Cell volume} = 496.203(34)$$

Name	x	y	z	Uiso (x100)	Fractn
Bi(1)	.500000	.500000	.064424	5.56	.3858
Sr(1)	.500000	.500000	.212408	5.56	.0858
Ti(1)	.500000	.500000	.500000	4.36	.7091
Nb(1)	.500000	.500000	.372045	4.36	.5546
O(1)	.500000	.000000	.000000	2.50	1.0000
O(2)	.500000	.000000	.250000	2.50	1.0000
O(3)	.500000	.500000	.322123	2.50	1.0000
O(4)	.500000	.000000	.113634	2.50	1.0000
O(5)	.500000	.500000	.441887	2.50	1.0000
Bi(2)	.500000	.500000	.212410	5.56	.9142
Sr(2)	.500000	.500000	.064420	5.56	.6142
Nb(2)	.500000	.500000	.500000	4.36	.2909
Ti(2)	.500000	.500000	.372050	4.36	.4454

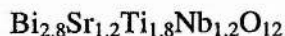


Lattice constants are

$$a = 3.87078(13) \text{ b} = A \text{ c} = 33.1179(17)$$

$$\text{Cell volume} = 496.203(34)$$

Name	x	y	z	Uiso (x100)	Fractn
Bi(1)	.500000	.500000	.06442(14)	5.56(13)	.386(4)
Sr(1)	.500000	.500000	.21241(11)	5.56(13)	.086(4)
Ti(1)	.500000	.500000	.500000	4.36(26)	.709(16)
Nb(1)	.500000	.500000	.37205(24)	4.36(26)	.555(8)
O(1)	.500000	.000000	.000000	2.50	1.0000
O(2)	.500000	.000000	.250000	2.50	1.0000
O(3)	.500000	.500000	.322123	2.50	1.0000
O(4)	.500000	.000000	.113634	2.50	1.0000
O(5)	.500000	.500000	.441887	2.50	1.0000
Bi(2)	.500000	.500000	.21241(11)	5.56(13)	.914(4)
Sr(2)	.500000	.500000	.06442(14)	5.56(13)	.614(4)
Nb(2)	.500000	.500000	.500000	4.36(26)	.291(16)
Ti(2)	.500000	.500000	.37205(24)	4.36(26)	.445(8)



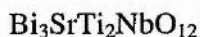
Lattice constants are

$$a = 3.86511(14) \text{ b} = A \text{ c} = 33.1169(18)$$

Cell volume = 494.73(4)

Name	x	y	z	Uiso (x100)	Fractn
Bi(1)	.500000	.500000	.06508(14)	3.85(12)	.463(5)
Sr(1)	.500000	.500000	.21219(12)	3.85(12)	.063(5)
Ti(1)	.500000	.500000	.500000	2.95(27)	.713(19)
Nb(1)	.500000	.500000	.37206(28)	2.95(27)	.457(9)
O(1)	.500000	.000000	.000000	2.50	1.0000
O(2)	.500000	.000000	.250000	2.50	1.0000
O(3)	.500000	.500000	.322123	2.50	1.0000
O(4)	.500000	.000000	.113634	2.50	1.0000
O(5)	.500000	.500000	.441887	2.50	1.0000
Bi(2)	.500000	.500000	.21219(12)	3.85(12)	.937(5)
Sr(2)	.500000	.500000	.06507(14)	3.85(12)	.537(5)
Nb(2)	.500000	.500000	.500000	2.95(27)	.287(19)
Ti(2)	.500000	.500000	.37207(28)	2.95(27)	.543(9)

Orthorhombic space group B2cb

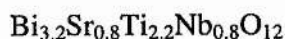


Lattice constants are

$$a = 5.4654(8) \text{ b} = 5.4621(9) \text{ c} = 33.1275(17)$$

Cell volume = 988.95(22)

Name	x	y	z	Uiso (x100)	Fractn
Bi(1)	.000000	.9893(26)	.06521(12)	4.15(11)	.577(4)
Bi(2)	1.003(6)	.0022(22)	.21192(11)	4.15(11)	.923(4)
Ti(1)	-.005(18)	.000000	.500000	3.07(28)	.786(17)
Ti(2)	.008(12)	1.001(6)	.37141(27)	3.07(28)	.607(9)
O(1)	.206229	.169951	.018410	2.50	1.0000
O(2)	.245181	.217193	.244172	2.50	1.0000
O(3)	.112506	1.007776	.443196	2.50	1.0000
O(4)	1.038831	.934611	.319976	2.50	1.0000
O(5)	.196049	.274279	.114765	2.50	1.0000
O(6)	.123246	.160957	.867278	2.50	1.0000
Sr(1)	1.003(6)	.0022(22)	.21193(11)	4.15(11)	.077(4)
Sr(2)	.023(16)	.9893(26)	.06522(12)	4.15(11)	.423(4)
Nb(1)	.008(12)	1.001(6)	.37141(27)	3.07(28)	.393(9)
Nb(2)	-.005(18)	.000000	.500000	3.07(28)	.214(17)

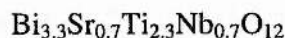


Lattice constants are

$$a = 5.45775(30) \text{ b} = 5.45142(28) \text{ c} = 33.0667(10)$$

$$\text{Cell volume} = 983.82(8)$$

Name	x	y	z	Uiso (x100)	Fractn
Bi(1)	.000000	.9896(13)	.06608(8)	2.27(8)	.678(4)
Bi(2)	1.0148(31)	.0127(11)	.21202(7)	2.27(8)	.922(4)
Ti(1)	.049(5)	.000000	.500000	.98(26)	.830(15)
Ti(2)	.035(5)	1.0128(33)	.37173(19)	.98(26)	.685(8)
O(1)	.206229	.169951	.018410	2.50	1.0000
O(2)	.245181	.217193	.244172	2.50	1.0000
O(3)	.112506	1.007776	.443196	2.50	1.0000
O(4)	1.038831	.934611	.319976	2.50	1.0000
O(5)	.196049	.274279	.114765	2.50	1.0000
O(6)	.123246	.160957	.867278	2.50	1.0000
Sr(1)	1.0148(31)	.0127(11)	.21202(7)	2.27(8)	.078(4)
Sr(2)	.0928(70)	.9896(13)	.06608(8)	2.27(8)	.322(4)
Nb(1)	.035(5)	1.0128(33)	.37173(19)	.98(26)	.315(8)
Nb(2)	.049(5)	.000000	.500000	.98(26)	.170(15)

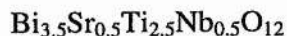


Lattice constants are

$$a = 5.45748(18) \text{ b} = 5.44683(18) \text{ c} = 33.0479(9)$$

$$\text{Cell volume} = 982.38(5)$$

Name	x	y	z	Uiso (x100)	Fractn
Bi(1)	.000000	.9892(10)	.06619(7)	2.99(7)	.760(3)
Bi(2)	.9945(27)	.0151(8)	.21195(6)	2.99(7)	.990(3)
Ti(1)	.027(5)	.000000	.500000	.59(23)	.873(12)
Ti(2)	.011(5)	1.0148(28)	.37164(18)	.59(23)	.814(6)
O(1)	.206229	.169951	.018410	2.50	1.0000
O(2)	.245181	.217193	.244172	2.50	1.0000
O(3)	.112506	1.007776	.443196	2.50	1.0000
O(4)	1.038831	.934611	.319976	2.50	1.0000
O(5)	.196049	.274279	.114765	2.50	1.0000
O(6)	.123246	.160957	.867278	2.50	1.0000
Sr(1)	.9945(27)	.0151(8)	.21195(6)	2.99(7)	.010(3)
Sr(2)	-.0765(90)	.9892(10)	.06620(7)	2.99(7)	.240(3)
Nb(1)	.011(5)	1.0148(28)	.37164(18)	.59(23)	.186(6)
Nb(2)	.027(5)	.000000	.500000	.59(23)	.127(12)

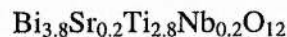


Lattice constants are

$$a = 5.45507(12) \quad b = 5.43690(12) \quad c = 32.9938(7)$$

Cell volume = 978.55(4)

Name	x	y	z	Uiso (x100)	Fractn
Bi(1)	.000000	.9907(7)	.06650(5)	2.98(5)	.792(2)
Bi(2)	1.0049(21)	.0156(6)	.21171(4)	2.98(5)	.958(2)
Ti(1)	.0355(34)	.000000	.500000	2.13(19)	.883(9)
Ti(2)	.0341(27)	1.0125(22)	.37138(14)	2.13(19)	.808(5)
O(1)	.206229	.169951	.018410	2.50	1.0000
O(2)	.245181	.217193	.244172	2.50	1.0000
O(3)	.112506	1.007776	.443196	2.50	1.0000
O(4)	1.038831	.934611	.319976	2.50	1.0000
O(5)	.196049	.274279	.114765	2.50	1.0000
O(6)	.123246	.160957	.867278	2.50	1.0000
Sr(1)	1.0049(21)	.0156(6)	.21172(4)	2.98(5)	.042(2)
Sr(2)	-.0370(91)	.9907(7)	.06651(5)	2.98(5)	.208(2)
Nb(1)	.0341(27)	1.0125(22)	.37138(14)	2.13(19)	.192(5)
Nb(2)	.0355(34)	.000000	.500000	2.13(19)	.117(9)



Lattice constants are

$$a = 5.45081(24) \quad b = 5.41900(24) \quad c = 32.9024(16)$$

Cell volume = 971.87(8)

Name	x	y	z	Uiso (x100)	Fractn
Bi(1)	.000000	.9894(15)	.06664(9)	2.67(7)	.901(4)
Bi(2)	1.007(5)	.0135(15)	.21160(8)	2.67(7)	.999(4)
Ti(1)	.038(8)	.000000	.500000	2.5(5)	1.003(18)
Ti(2)	.054(5)	1.020(5)	.37150(32)	2.5(5)	.899(9)
O(1)	.206229	.169951	.018410	2.50	1.0000
O(2)	.245181	.217193	.244172	2.50	1.0000
O(3)	.112506	1.007776	.443196	2.50	1.0000
O(4)	1.038831	.934611	.319976	2.50	1.0000
O(5)	.196049	.274279	.114765	2.50	1.0000
O(6)	.123246	.160957	.867278	2.50	1.0000
Sr(1)	1.007(5)	.0135(15)	.21161(8)	2.67(7)	.001(4)
Sr(2)	-.005(81)	.9894(15)	.06664(9)	2.67(7)	.099(4)
Nb(1)	.054(5)	1.020(5)	.37150(32)	2.5(5)	.101(9)
Nb(2)	.038(8)	.000000	.500000	2.5(5)	-.003(18)

Appendix E: Neutron scattering lengths

Isotope	Natural abundance (%)	bound coherent scattering length (fm)
Bi	100	8.532
Nb	100	7.054
Ti	---	-3.438
46Ti	8.2	4.93
47Ti	7.4	3.63
48Ti	73.8	-6.08
49Ti	5.4	1.04
50Ti	5.2	6.18
Ta	---	6.91
180Ta	0.012	7.(2.)
181Ta	99.988	6.91
O	---	5.803
16O	99.762	5.803
17O	0.038	5.78
18O	0.2	5.84
Sr	---	7.02
84Sr	0.56	7.(1.)
86Sr	9.86	5.67
87Sr	7	7.40
88Sr	82.58	7.15
La	---	8.24
138La	0.09	8.(2.)
139La	99.91	8.24